Mixed metal oxide as catalysts for acetin synthesis from glycerol

A

Thesis

Submitted for the partial fulfilment

of the requirements for the award of degree of

Doctor of Philosophy

By

Km Abida

(Registration No.901509004)

Under the Supervision of

Dr. Amjad Ali

(Professor)

SCHOOL OF CHEMISTRY AND BIOCHEMISTRY

Thapar Institute of Engineering & Technology

Patiala-147004 (Punjab), India

(Deemed to be University)

2021

DEDICATED TO

MY

BELOVED PARENTS

ACKNOWLEDGEMENTS

The Doctorate of Philosophy is a journey of lifetime where not only intellectual, but spiritual as well as emotional grooming of the being is accomplished. This realization is incomplete without the surrounding aura of the magnificent people around you, who contribute in one way or the other to nurture you into a better person. This day has arrived after immense waiting that I got the opportunity to express my gratitude towards everyone who stood by my side in the course of this realization.

First and foremost, I am deeply indebted to my supervisor, ***Dr. Amjad Ali****, who has guided me through the ups and downs in this entire journey of never-ending learning. The deep understanding, motivation and personal attention of my supervisor has provided a smooth base throughout the tenure of PhD. He helped me to bestow a better shape to my complete work into a dissertation.* ***Dr. Amjad Ali,*** *like a father has always motivated me towards a better understanding of the concepts and problems through his solution-oriented techniques. His noble thoughts and conviction have led me to perform well throughout my journey.*

I take the privilege to thank ***Dr. Prakash Gopalan*** *(Director), Thapar Institute of Engineering & Technology, Patiala for providing me resources in the institution and needful help during various stages of my work. I am thankful to* ***Dr. Rafat Siddique*** *(Dean R&SP) and* ***Dr. Susheel Mittal*** *(HSCBC) for their whole-hearted support and blessings. I thank my IRB Committee members,* ***Dr. Ranjana Prakash****,* ***Dr. Manmohan Chhibber****, and* ***Dr. N. Das*** *for their helpful suggestions and comments during my progress presentations. I whole-heartedly thank* ***Dr. Bhupendra Chudasama*** *for his valuable suggestions and help in VSM characterization of the samples.*

My sincere thanks to ***Mr. Chander Thakur*** *and office staff* ***Mr. Mayank Sharma*** *and all the teaching and non-teaching staff members of the department for their invaluable cooperation and help during the entire tenure of my studies in the department.*

A special word of thanks goes to ***Mr. Vijay*** *and* ***Mr. Ashwani*** *for their valuable official and technical support.* ***Mrs. Era, Mr. Ghanshyam Maurya, Mr. Mukesh Aggarwal*** *and* ***Mr. Pardeep Bhatia*** *of SAI Labs, TIET, Patiala for their help and services in carrying out the characterizations. I would be failing in my duties if I do not mention the Defence Research &*

*Technology (**DST**), and the Council of Scientific & Industrial Research (**CSIR**), New Delhi for providing me the financial support in the form of project Fellowship throughout my Ph.D. work.*

*I specially thank my brother **Mr. Savidh Khan** for their constant moral support, I cannot forget the motivation and passion for research instilled in me by **Mr. Savidh Khan**, which gave me the courage to begin this journey. Their blessings and zeal for hard work have always enlightened my path.*

*This journey of dissertation would have been terrible without the unlimited support, valuable discussions and suggestions from my colleagues and friends **Avneet Kaur, Himmat Singh, Sidharth Sharma, Aayush Gupta**, **Imran Khan**, **Parmandeep Kaur**, **Sonia Rani**, **Himani** and **Garima,** without their help this work could never be completed. I would like to thank **Priyanka Gautam**, **Meenakshi Budhiraja, Sunil Dutt**, **Priya Kamboj**, **Paramjeet Kaur**, **Pooja Soam,** and **Arkham Belgami** for creating a conductive environment in the holy place of work (Heterogeneous catalysis Lab).*

*I whole-heartedly with immense gratitude dedicate my thesis to my loving and caring parents without whom I could not reach this point in my life. Parents can never be thanked in words. Prayers and sacraments of my father **Chhote Khan** and Mother **Jaitun** have always enlightened my path of life. Love and support of my brothers **Dr. Ameeruddin, Subedar Sameeruddin, Mr. Savidh Khan** and **Dr. Avidh Khan** and my sisters **Mrs. Samila, Mrs. Amina, Mrs. Mojbhar** and **Mrs. Sajida Khan** have always motivated me to keep on moving.*

*Rather than thanking, I profoundly apologize to my brother's son **Victor (Anas Sameer)** and daughter **Falak Chahat** for not being with them, when they needed me the most. I lost all their childhood.*

I whole-heartedly thank every person who is not mentioned above, but contributed to my thesis in one or the other way.

Above all! I thank the Almighty Allah, who always empowered me with His heavenly blessings, and made me feel His presence every time I felt low!!!

Abida 17/08/21

Km Abida

Certificate

This is to certify that thesis entitled "**Mixed metal oxide as catalysts for acetin synthesis from glycerol**", being submitted by **Km Abida**, School of Chemistry and Biochemistry, Thapar Institute of Engineering and Technology, Patiala for the award of degree Doctor of Philosophy, is a record bonafide of the research work carried out by her. Km Abida has worked under my guidance and supervision and has fulfilled the requirements for the submission of the thesis, which to my knowledge has reached the requisite standard.

The results embodied in the thesis have not been submitted in a part or full to any other University or Institute for the award of any degree or diploma.

17/8/21

(Supervisor)
Dr. Amjad Ali
Professor
School of Chemistry and Biochemistry
Thapar Institute of Engineering and Technology, Patiala
Punjab (INDIA)

Susheel Mittal
19.8.21

(Head)
Dr. Susheel Mittal
Senior Professor and Head
School of Chemistry and Biochemistry
Thapar Institute of Engineering and Technology, Patiala
Punjab (INDIA)

Candidate's Declaration

I, hereby declare that the work presented in the thesis entitled "**Mixed metal oxide as catalysts for acetin synthesis from glycerol**" in the fulfillment of the requirement for the award of the degree of Philosophy, School of Chemistry and Biochemistry, Thapar Institute of Engineering and Technology, Patiala is an authentic record of my work carried out under the supervision of **Dr. Amjad Ali**, Professor, School of Chemistry and Biochemistry, Thapar Institute of Engineering and Technology, Patiala, India. The matter embodied in the thesis has not been submitted in part or full to any other University or Institute for the award of any degree in India or abroad.

Abida 17/08/21

Km Abida

(901509004)

TABLE OF CONTENTS

LIST OF ABBREVIATIONS

Abbreviations	Description
AcA	Acetic acid
AcAn	Acetic anhydride
GL	Glycerol
MA	Monoacetin
DA	Diacetin
TA	Triacetin
BD	Biodiesel
TOF	Turn over frequency
SZ	Siliceous zirconia
SSZ	Sulphated siliceous zirconia($SO_4^{2-}/SiZrO_4$)
MNPs	Magnetic nano particles
S	sulphonic acid
AC	Activated carbon
TEOS	Tetraethoxysilane
XRD	X-ray diffraction
JCPDS	Joint Committee for Powder Diffraction Standards
FTIR	Fourier transform infrared
BET	Brunauer- Emmett-Teller
BJH	Barret-Joyner-Halenda
NH_3-TPD	Ammonia Temperature Programmed Desorption
SEM	Scanning electron microscopy
EDX	Energy Dispersive X-ray spectroscopy
HRTEM	High-resolution transmission electron microscopy
XPS	X-ray photoelectron spectroscopy
VSM	Vibrating-samples magnetometer
HPLC	High performance liquid chromatography
^{1}H-NMR	Proton nuclear magnetic resonance
D_2O	Deuterium oxide
DRIFT	Diffuse reflectance infrared fourier transform
H_C	Coercivity

M_R	**Retentivety**
M_S	**Saturation magnetization**
emu	**Electromagnetic**
eV	**Electron volt**
mmol g^{-1}	**Millimole per gram**
mL	**Milliliter**
min	**Minute**
h^{-1}	**Per hour**
Mol	**Mole**
mg	**Milligram**
nm	**Nanometer**
v/v	**Volume by volume**
cm	**Centimeter**
kJ mol^{-1}	**Kilo joule per mole**
kJ K-1 mol-1	**Kilo joule per mole per kelvin**
LAS	**Lewis acidic sites**
BAS	**Brønsted acidic sites**
ESI	**Electronic supplementary information**
NR	**Note reported**
PR	**Present report**

LIST OF SYMBOLS

Symbols	Description
Å	**Angstrom**
C	**Celsius**
%	**percentage**
µ	**Micro**
θ	**Theta**
o	**Degree**
K	**Kelvin**
h	**hours**
g	**Gram**
X	**Conversion**
B	**Brønsted acidic sites**
L	**Lewis acidic sites**
t	**Time**
R	**Gas constant**
T	**Temperature**
k	**Rate constant**
$\Delta G^{\ddagger}$	**Gibb's free energy of activation**
$\Delta H^{\ddagger}$	**Enthalpy**
$\Delta S^{\ddagger}$	**Entropy**
E_a	**Activation energy**
k_B	**Boltzmann's constant**
h	**Planck's constant**

LIST OF FIGURES

LIST OF TABLES

LIST OF SCHEMES

ABSTRACT

In the present thesis four different heterogeneous acidic catalysts *viz.*, $SO_4^{2-}/SiZrO_4$, $Fe_3O_4@SiO_2@SO_4^{2-}$, $Nb@Fe_3O_4$ and $Ce/TiZrO_4@SO_4^{2-}$ were synthesized by chemical method. The prepared catalysts were employed for the glycerol acetylation with acetic acid to yield the diacetin or triacetin as exclusive products. The structural property of all the prepared catalysts was determined with the help of powder X-ray diffraction pattern, and FTIR analysis. X-ray photoelectron spectroscopy also revealed that the active species was incorporated over the matrix to impart the Brønsted as well as Lewis acidity to the catalyst which is vital for the acetylation activity. The surface morphology and elemental distribution were studied by SEM-EDX, and HRTEM analysis. The BET analysis of the catalysts reveals the surface porosity and pore size of the prepared samples. The acidic strength of the catalysts was quantified by the NH_3-TPD analysis while nature (Brønsted versus Lewis) of those sites was determined by analysing the FTIR of pyridine adsorbed catalyst samples. The reaction parameters were optimized to obtain a specific acetin as an exclusive product.

Under the optimized reaction parameters of 9:1 AcA/GL molar ratio, 3 wt% catalyst, 80 °C reaction temperature, and 40 min of reaction duration, a 93 % triacetin yield was obtained during $SO_4^{2-}/SiZrO_4$ catalyzed glycerol acetylation. The catalyst was recovered from the reaction mixture and reused during six consecutive reaction runs while retaining 54 % triacetin selectivity in the last cycle. A plausible mechanism suggests the heterogeneous catalyst-assisted protonation of carbonyl group of acetic acid to initiate the stepwise acetylation of the hydroxyl groups of glycerol.

A magnetic catalyst was prepared by embedding magnetite (Fe_3O_4) within the silica shell on which sulphate ions were anchored ($Fe_3O_4@SiO_2@SO_4^{2-}$). The catalyst was successfully employed for glycerol acetylation with acetic acid to obtain 100 % selectivity towards triacetin within 45 min of reaction duration at 80 °C. The catalyst was successfully isolated from the reaction medium magnetically and reused for 6 consecutive reaction cycles while retaining 90 % glycerol conversion levels and 50 % triacetin selectivity in the last reaction cycles.

In another approach, niobium oxide was incorporated over magnetic Fe_3O_4 nanoparticles, to impart the acetylation activity to the catalyst. The prepared catalyst ($Nb@Fe_3O_4$) in 7 wt% amount was found to yield 92 % triacetin within 80 min of reaction duration. The glycerol acetylation with acetic acid was found to follow the pseudo first-order kinetic equation. The thermodynamic parameters *viz.*, enthalpy ($\Delta H^{\ddagger}$), entropy ($\Delta S^{\ddagger}$), and Gibbs free energy ($\Delta G^{\ddagger}$)

of the reaction were also determined to suggest the endothermic and unspontaneous nature of the reaction. Upon completion of the reaction, the catalyst was recovered from the reaction mixture under the influence of an external magnetic field and reused during seven consecutive reaction cycles.

To prepare diacetin molecule as an exclusive product, $Ce/TiZrO_4@SO_4^{2-}$ was prepared and employed as a heterogeneous acid catalyst for the acetylation of glycerol with acetic acid. The prepared catalyst, $Ce/TiZrO_4@SO_4^{2-}$, demonstrated almost 96 % diacetin selectivity in 60 min by employing acetic acid to glycerol molar ratio of 6:1 at 120 °C reaction temperature. The catalyst was recycled in five successive reaction cycles while retaining ~36 % activity during the last cycle.

Keywords: Acetylation, Acetic acid, Glycerol, Monoacetin, Diacetin, Triacetin, XRD, HR-TEM, XPS, NH_3-TPD, HPLC, Magnetic catalysts, Leaching, and Kinetics study.

Introduction and literature review

Overview of the Chapter

The increased demand for renewable and eco-friendly energy sources (*e.g.*, biodiesel), has been encouraged in the recent past. Biodiesel production, *via* triglyceride transesterification, has also resulted in the overproduction of the side product, glycerol. To address the issue of glycerol mitigation, it has been employed as a versatile substrate for the synthesis of value-added chemicals such as mono-, di-, and tri-acetin. Triacetin has versatile applications, such as, in the fuel industry to improve the viscosity as well as cold flow property of biofuel, in food, beverage, pharmaceutical, and cosmetic industries, and could also be used as a plasticizer. Acetins could be synthesized via acetylation of glycerol with acetic acid or acetic anhydride in presence of homogeneous or heterogeneous acidic catalysts. This chapter describes in detail various roots of glycerol production reported in the literature. Different methods of glycerol acetylation to produce acetins in presence of heterogeneous catalysts have also been elaborated. In addition, the most influential operating conditions to attain the maximum triacetin selectivity during the glycerol acetylation have also been examined in light of literature reports.

1.1. Introduction

In 1779, Carl W. Scheele, a Swedish chemist, discovered a new transparent, syrupy liquid by heating olive oil and litharge (PbO) [1]. This new colorless, odorless, sweet-tasting, nontoxic and high boiling (290 °C) compound was called glycerol ($CH_2OH.CHOH.CH_2OH$). Today, the name glycerol (GL) refers to the pure chemical substance and is commercially known as propane-1,2,3-triol or glycerin and can be derived from natural and petrochemical feed stocks [2]. It is polyhydric alcohol with three hydrophilic hydroxyl groups attached to three carbon atoms [3]. Glycerol has multiple applications, such as in food, paint, cosmetic and pharmaceutical industries. The pie chart indicating the distribution of glycerol applications is shown in **Fig. 1.1** [4-7].

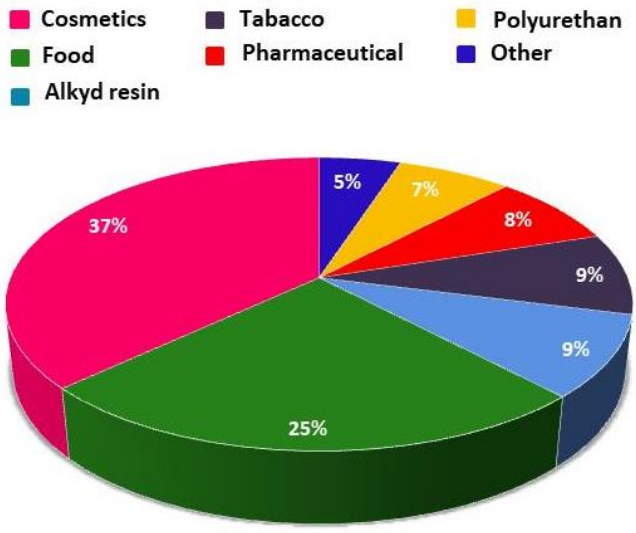

Fig. 1.1. Percentage distribution of industrial applications of glycerol.

1.2. Glycerol production

At industrial scale GL is mainly produced *via* three roots, namely (i) High-pressure splitting (ii) Saponification, and (iii) Transesterification [8-10].

1.2.1. High-pressure splitting

High-pressure splitting processing is employed to yield high-quality fatty acids from triglyceride (vegetable oils or animal fats) at industrial scale [8,11]. In this process, raw oils and water, fed from the two opposite directions, are mixed together in a reactor to obtain the tiny drops of water

into the oil (**Fig. 1.2**). The fatty acids are produced by heating triglyceride at high temperature (up to 270 °C) and under high pressure (from 70 to 80 bars) for 3 h [12]. The crude GL obtained in this process has the impurities of water, inorganic salts, fats, and GL-oligomers [13]. Such GL could be purified through a multistep process, involving the chemical, evaporation and distillation, to obtain the technical grade (88–99 %) purity [14-16].

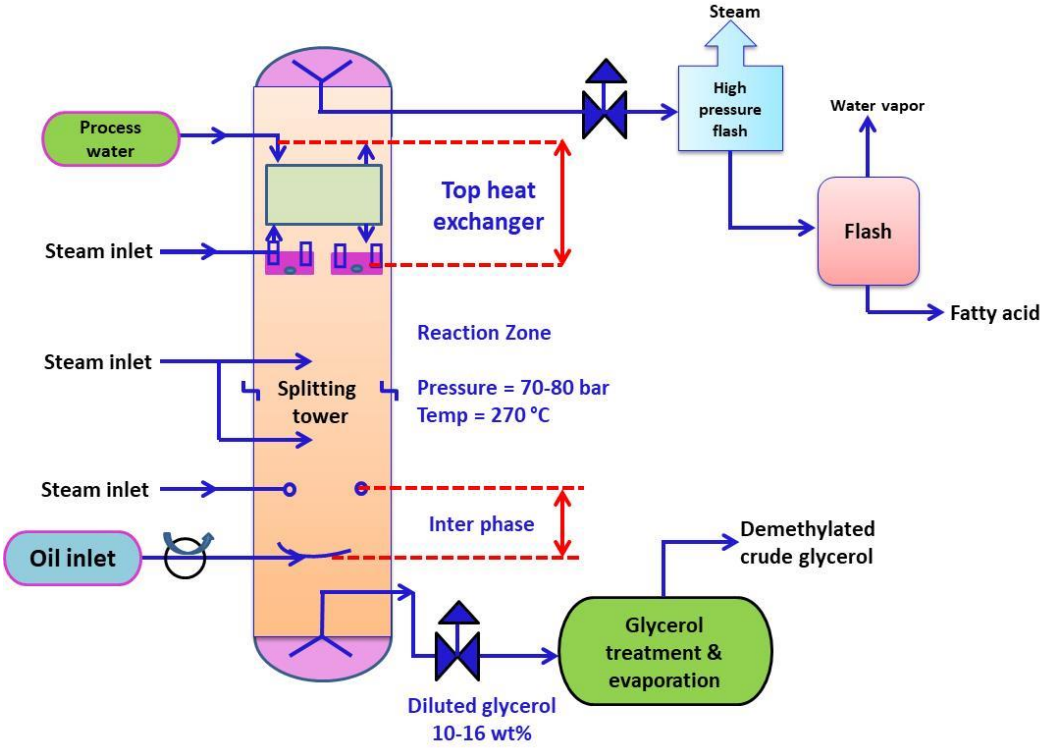

Fig. 1.2. Flow diagram for the high-pressure splitting process.

1.2.2. Saponification

In saponification reaction, tri-glycerides (vegetable oils or animal fats) are treated with aqueous NaOH or KOH to obtain the sodium or potassium salts of fatty acids (soap) and GL as a by-product [9]. After the completion of the reaction, brine was added to separate the top layer of the crude soap from the bottom GL layer as shown in **Fig. 1.3**. The GL thus obtained usually contain water, mono-, di-glycerides, alkali, brine and soap as impurities [17,18].

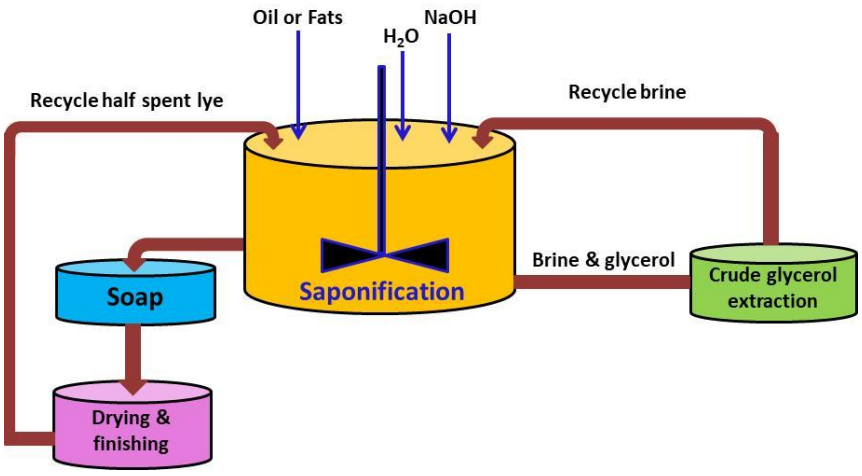

Fig. 1.3. Flow diagram for the saponification process.

1.2.3. Transesterification

During the past two decades, biodiesel (BD) production has increased manifold as it is considered a renewable and eco-friendly alternate to conventional diesel fuel. At industrial scale, BD is produced via transesterification of animal fat or vegetable oils with alcohol (*e.g.*, methanol) using alkali (*e.g.*, NaOH) as a catalyst (**Fig. 1.4**) [19]. The reaction yielded fatty acid methyl esters (BD) as the main product and GL as a by-product [20]. In this reaction, approximately 10 wt% of crude GL (with respect to BD) is formed which usually contains the moisture, alkali, mono- and di-glycerides, fatty acids, alcohol, and BD as impurities. Hence, such GL is unfit for the pharma, food, and cosmetic industries [21].

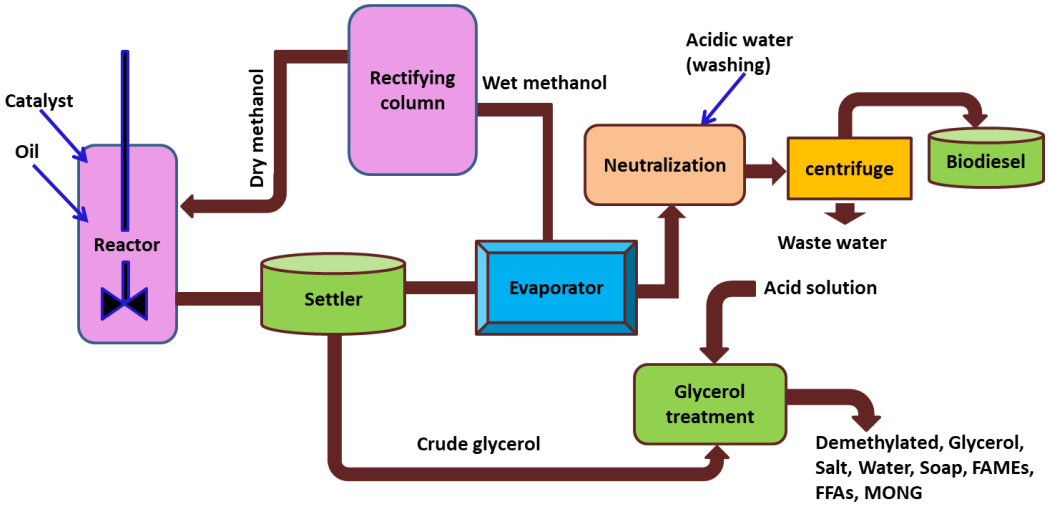

Fig. 1.4. Flow diagram for biodiesel production *via* transesterification reaction.

During the past five years, Indonesia, US, Brazil, Germany, Argentina, France, and Spain has become the major BD producing nations, as shown in **Fig. 1.5** [22,23]. The feedstock employed for the BD production varies from one geographical region to another, *e.g.*, soybean oil, palm oil, and rapeseed oil have been used as feedstock for the BD production in America, Indonesia, and Europe, respectively [22,24-26].

The ever-increasing demand of BD fuel has caused the GL overproduction (2.2 million tones/year) of the GL. Hence, it has become inevitable to find the suitable application of this low-cost and nontoxic chemical for the long run sustainability of the biodiesel industry [22].

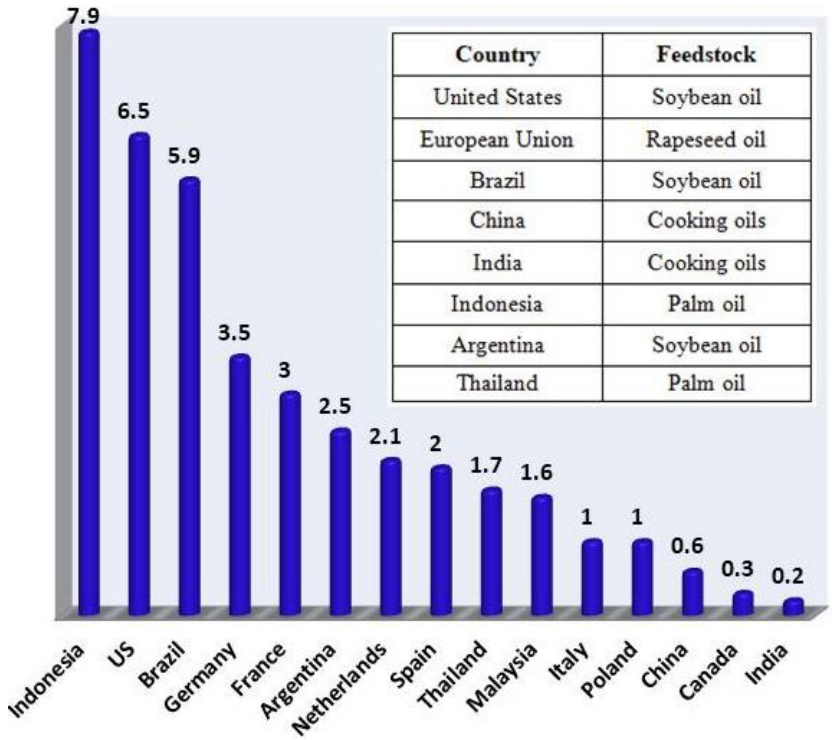

Country	Feedstock
United States	Soybean oil
European Union	Rapeseed oil
Brazil	Soybean oil
China	Cooking oils
India	Cooking oils
Indonesia	Palm oil
Argentina	Soybean oil
Thailand	Palm oil

Fig. 1.5. Plot of biodiesel production (billion liters) in various countries.

The worldwide GL production from the BD industries has already been reached 4.2 billion liters in 2020 [27]. Thus, crude GL disposal and its utilization have become a financial and environmental liability for the BD industries [28]. The market value of crude GL was 30–32 cents per liter in 2006 has come down to 18–20 cents per liter in 2018 (**Fig. 1.6**) [29]. Thus new applications for crude GL must be found to avoid the continuous fall in its price.

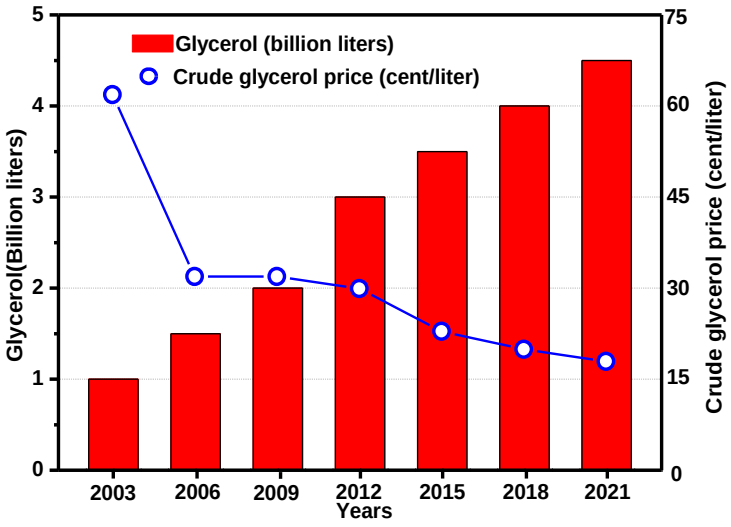

Fig. 1.6. Global crude glycerol production (from biodiesel industry) and price during 2003 to 2021.

1.3. Purification of crude glycerol

One of the significant challenges while utilizing the crude GL from the BD industry is the presence of a variety of impurities in it [2,6,30-32]. The GL coming out of BD manufacturing plants usually contains methanol (MeOH), water, and acid or base as impurities. Consequently, it remains unfit for the edible or pharma industries and thus having low commercial value. A comparison of the properties of crude GL from BD industry and its pure counterpart is provided in **Table 1.1**.

Table 1.1. Comparison of properties of crude (from BD) and pure glycerol.

Properties	Crude glycerol	Pure glycerol
Colour	Dark brown	Colorless
pH	9.6	6.7
Density at 20 °C (kg/m^3)	1.29	1.25
Flash point (°C)	180	177
Fire point (°C)	211	204
Carbon residue (%)	18	11.25
Ash content (%)	11.26	NA
Solubility with water	Miscible	Miscible

NA=not applicable

A representative purification procedure for GL purification typically involves neutralization, vacuum distillation, ion exchange, and activated carbon adsorptions processes (**Fig. 1.7**). However, the methods employed for the crude GL treatment are purification are costly and bound to enhance GL cost [33].

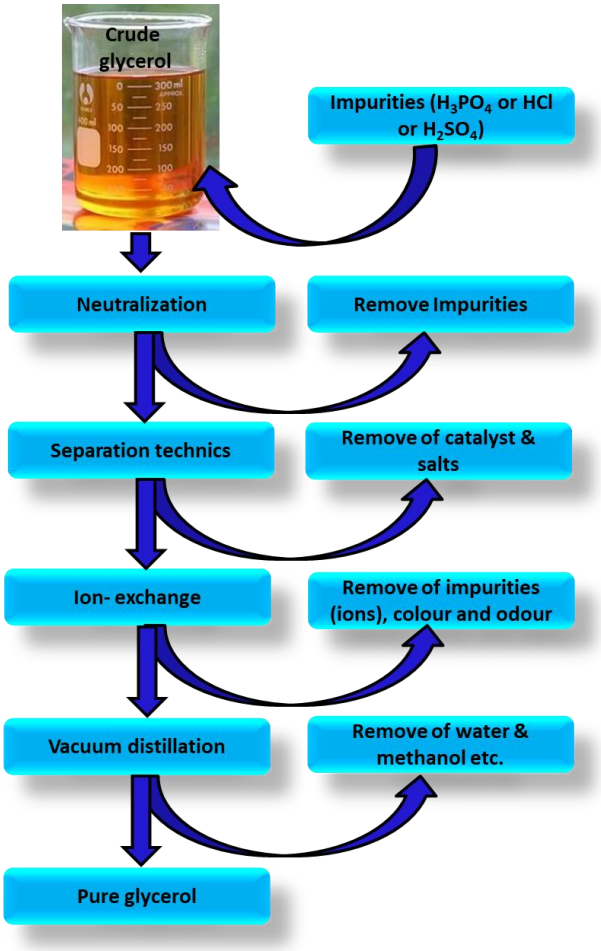

Fig. 1.7. Crude glycerol purification steps.

1.4. Application of crude glycerol

The crude GL coming from the BD and soap industries could be utilized directly or converted into other value-added products through chemical modifications. Crude GL can be refined into the pure form and utilized in food, pharmaceutical, and cosmetics industries [34]. On the other hand, crude GL can be directly used in composting, animal-feeding, and a nutrient in microbial fermentation and enzymatic processes [35,36].

1.4.1. Valorization of Glycerol

Due to the enormous overproduction of the GL in the last five years, its price is constantly decreasing; hence, researchers have paid attention to find out the suitable application of the crude GL to avoid the purification steps. [37]. Some of the frequently employed methods for GL valorization include acetylation, transesterification, etherification, dehydration and hydrogenolysis, etc. [38-43], as shown in **Fig. 1.8**. Out of these methods, GL acetylation (esterification) and transesterification are important methods for the production of acetins and glycerol carbonate, respectively [44,45].

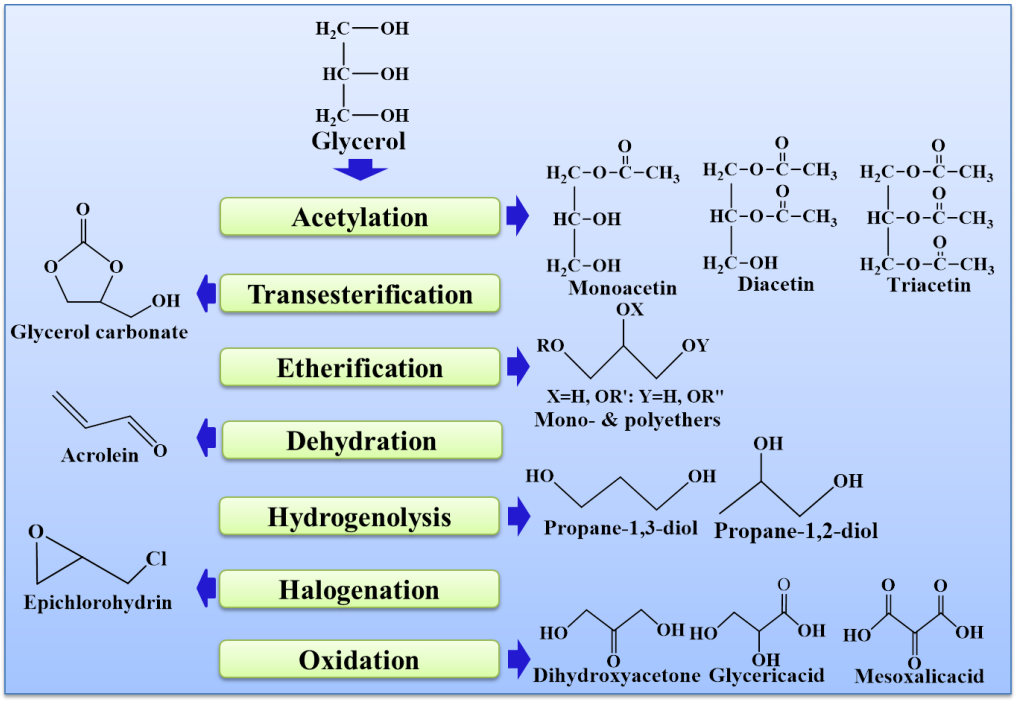

Fig. 1.8. Crude glycerol derivatives obtained in various chemical reactions

1.4.2. Acetins

Acetins, including mono-, di- and triacetin, are an essential category of glycerol derivatives, frequently prepared *via* GL acetylation employing acetic acid (AcA) or acetic anhydride (AcAn) as acetylating agents [46,47]. The acetylation of –OH functional group takes place in a stepwise fashion and leads to the formation of two isomers each of the monoacetin (MA) and diacetin (DA) molecules as shown in **Fig. 1.9**. Monoacetin is a clear, colorless, odorless, viscous liquid with high boiling (290 °C) point, also called glycerol monoacetate ($C_5H_{10}O_4$). It can be utilized in cosmetics, medicines, leather and food industries [48].

Diacetin is also a colorless, odorless, and viscous liquid with a high boiling (280 °C) point an also called as glycerol diacetate ($C_7H_{12}O_5$). It is used in the cosmetics, pharmaceutical, food, and fuel industries [49]. MA and DA also find applications as monomers for the production of biodegradable polyesters [50].

The triacetin (TA), generally known as glycerol triacetate ($C_9H_{14}O_6$), is a colorless, odorless, viscous liquid with a boiling point of 260 °C. Triacetin has a wide spectrum of versatile applications, for example, in fuel industry as an additive to improve the anti-knocking property of gasoline, and to improve the viscosity and cold flow property of biofuel [51-54], in food industry, in beverage industry as a flavor garnish, in pharmaceuticals as antifungal agents and plasticizer, in cosmetics to maintain the moisture of creams or lotions, in cigarette filters as a plasticizer and in the production of photographic films and various perfumes [28,42,55-64].

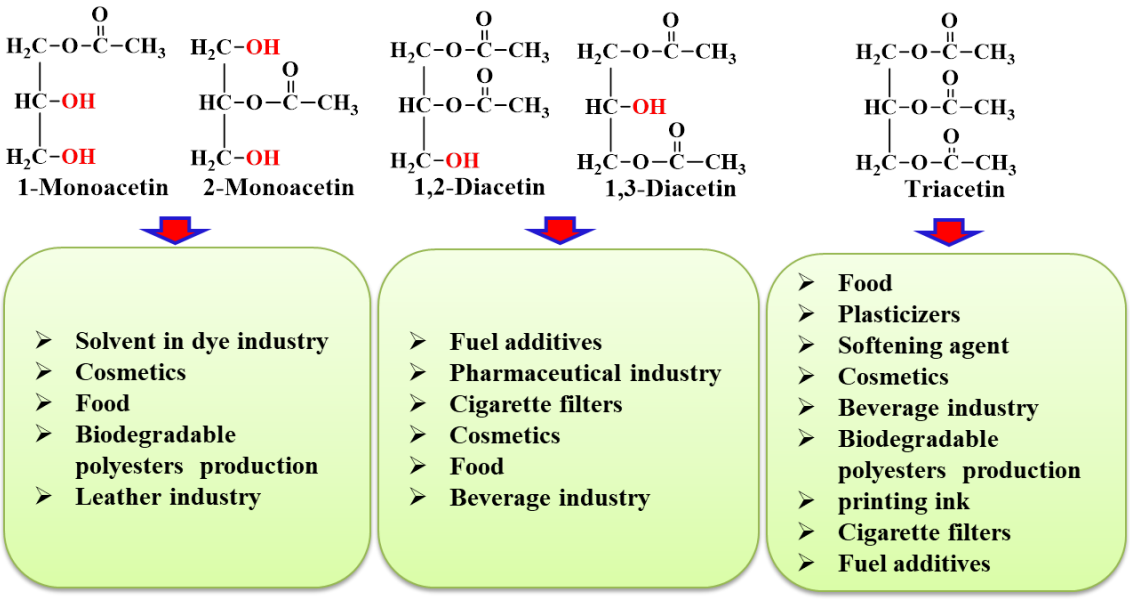

Fig. 1.9. Applications of the monoacetin, diacetin and triacetin.

The global TA estimated demand in 2021 is around 50000 tons/annum which is increasing 4-5 % annually [65,66]. China is one of the significant TA producers with an annual manufacturing capacity of 55000 tons, including 38500 tons for domestic consumption and 16500 tons for export [67]. The increasing consumption of TA influences growth and price in the TA market across the world.

One of the significant challenge in the TA synthesis is their selectivity, which should be close to 100 %, for most of the commercial applications [68]. Further, MA and DA as an exclusive product during the GL acetylation has not been reported so far [46].

1.4.2.1. Interesterification

During the conventional BD production, triglyceride is transesterified with MeOH to produce the BD as a main product and GL as a by-product, as shown in **Fig 1.4.** Low purity GL coming from the BD industries could not be directly used either as a fuel, because of its high viscosity and high atomization temperature or for other commercial applications due to the presence of impurities in it [69]. Thus crude GL required purification and further derivatization before it could be employed for other industrial applications. In order to address the issues of GL over-production and its subsequent derivatization, interesterification, instead of transesterification, could be performed. During this reaction, triglyceride is treated with methyl acetate to produce a mixture of BD and TA as shown in **Fig 1.10**. [70,71]. The TA produced during the reaction is completely soluble in the BD, and hence, this mixture could be directly employed as a fuel in diesel engines [69]. The main drawbacks of the reaction are low product yield and requirement of super critical conditions, which demand the reaction temperature up to 350 °C, and methyl acetate to triglyceride molar ratio of 42:1 [72]. Dhawan *et al.* reported triglyceride interesterification with methyl acetate in presence of hydrotalcite (Mg:Al mole ratio- 3:1) as a heterogeneous catalyst for achieving high triglyceride conversion (95.5 %) into BD (94.7 %) and TA (5.3 %) at 200 °C in 4 h reaction duration [73]. Recently, Brondani *et al*. employed γ-alumina as a heterogeneous catalyst during interesterification of triglyceride (macaw oil) with methyl acetate to obtain 80 % fatty acid methyl ester selectivity at 300 °C reaction temperature with 2 wt % of catalyst amount, 3 h reaction duration and methyl acetate/oil molar ratio being 10:1 [74].

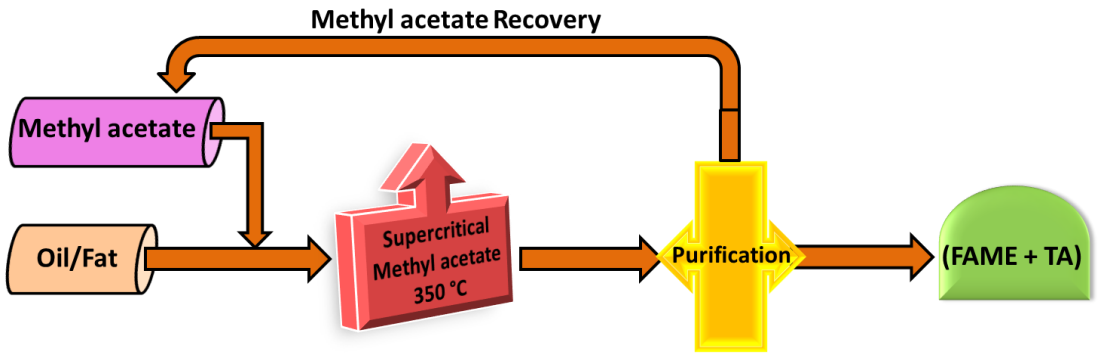

Fig. 1.10. Flow diagram for the interesterification process.

1.4.2.2. Acetins production with different acetylating agents

There are two frequently employed methods for the GL acetylation involving either acetic acid (AcA) or acetic anhydride (AcAn) as acetylating agents as shown in **Scheme 1.1**. The former as an acetylating agent required a relatively high temperature (up to 120 °C) and formed water as a side product. In comparison, the later reagent (AcAn) required a relatively low reaction temperature (room temperature to 100 °C) while forming the corrosive AcA as a by-product. Further, AcAn above 49 ^{o}C, forms an explosive mixture with air, and hence, not considered suitable for the large-scale manufacturing of acetins [75].

The use of AcA for GL acetylation is preferred as it is readily available at a lower price (~ 0.4 USD/kg) in comparison to AcAn (~ 0.98 USD/kg) [76,77]. On the other hand, AcAn availability is challenging in many countries due to its application in the production of heroin and in the creation of improvised explosive devices [78].

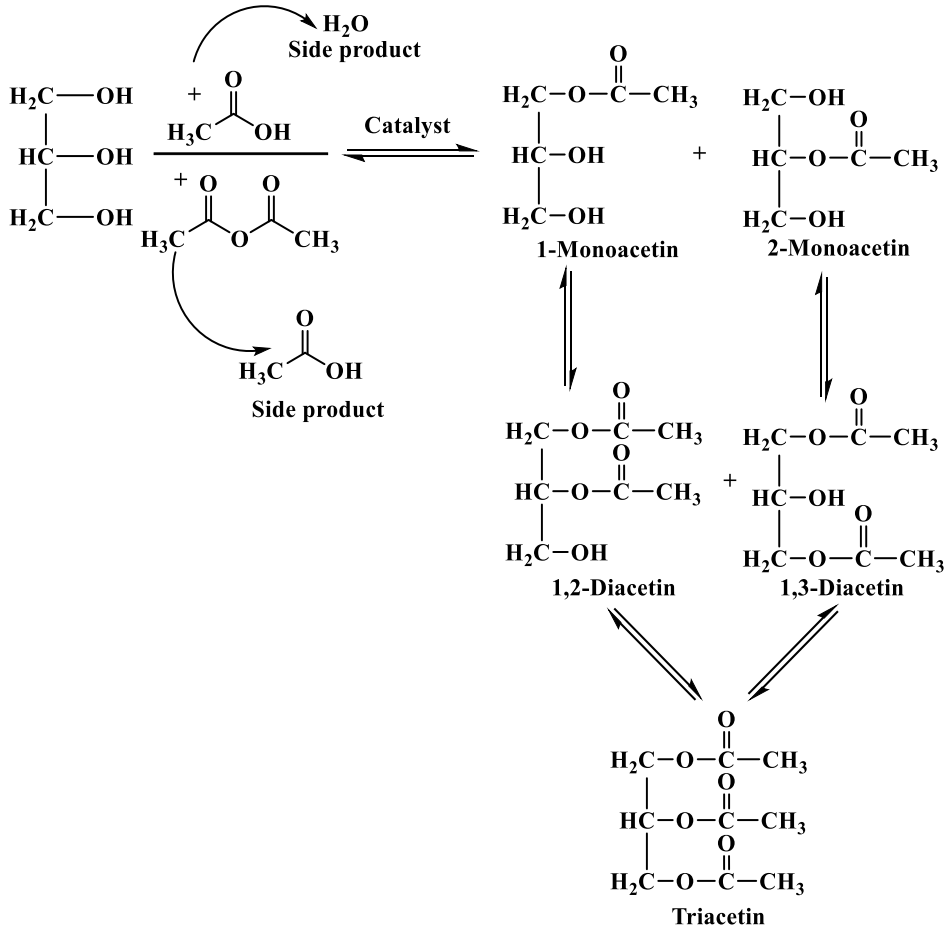

Scheme 1.1. Acetylation of glycerol with acetic acid or acetic anhydride.

1.4.2.3. Two-step process for triacetin production

From an industrial perspective, the conventional method for TA production, with 100 % selectivity, involves two-step processes, as shown in **Fig. 1.11** [75]. This process involves (i), GL acetylation with AcA without any catalyst at 105 °C for 4 h to form MA and water and (ii) reaction of MA, formed in step (i), with AcAn to form TA with 100 % selectivity and acetic acid as a by-product [79,80]. Acetic acid formed during step (ii) will be recycled again in step (i). Literature reports indicate that GL acetylation with AcAn is an exothermic process, and hence, TA formation requires lesser energy [81].

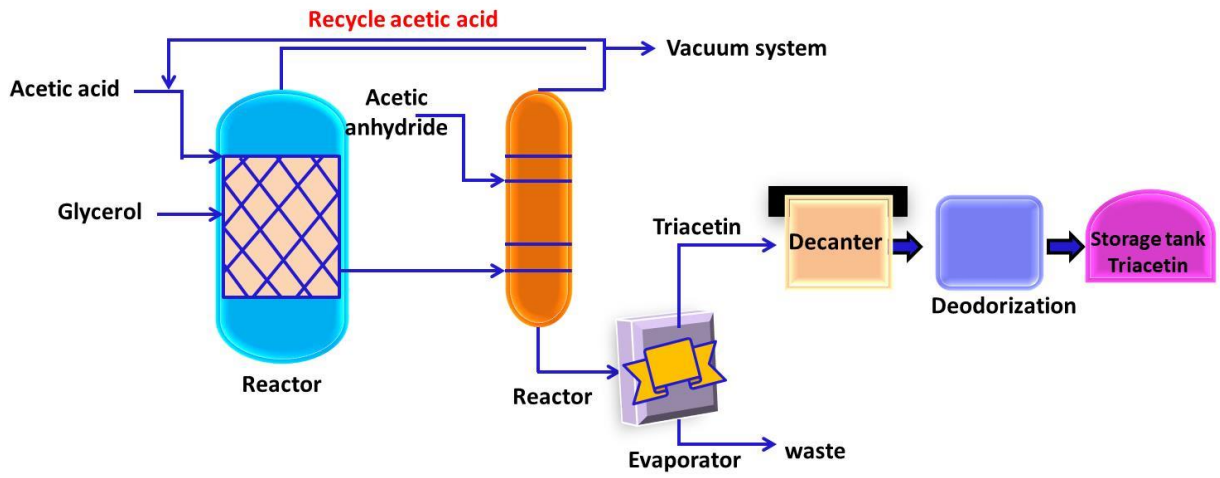

Fig. 1.11. Flow diagram of two-step process for the triacetin production.

1.5. Catalyst for glycerol acetylation

A comparison between heterogeneous and homogeneous acidic catalysts, employed for the AcA or AcAn mediated GL acetylation is summarized in **Fig. 1.12**. At present, acetins industry is dominated by homogeneous Brønsted acid catalyzed (H_2SO_4, H_3PO_4, HCl, p-toluene sulphonic acid, etc.,) acetylation (Fischer esterification) due to its cost effectiveness, higher product selectivity and higher GL conversion rate [82-84].

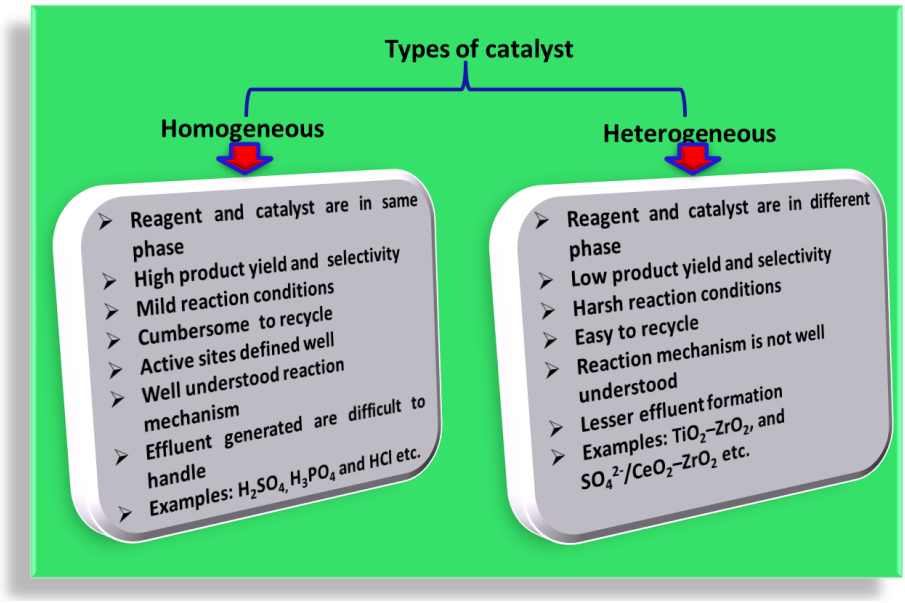

Fig. 1.12. Comparison of the homogeneous and heterogeneous catalysts employed for glycerol acetylation.

However, homogeneous Brønsted acidic catalysts are sensitive to water, which formed as a by-product during the GL acetylation, making the catalyst less effective towards the acetylation [85]. Such catalysts are harmful to the environment as they are highly corrosive and must be neutralized, separated, and washed away after the completion of the reaction. Large amounts of water are required during the process, and vast quantities of industrial effluents are generated, which must be disposed of safely [86]. Even the Brønsted presence homogeneous acidic catalysts mediated GL acetylation with AcA, demands high temperature (up to 135 ^{o}C) and a long reaction duration (up to 5 h) to achieve the partial conversion levels [87]. In order to address the issues related to the homogeneous acids, Brønsted or Lewis acidic group have been immobilized over the matrix to prepare a variety of the solid acid catalyst for the GL acetylation [88].

1.6. Catalyst preparation and characterization

Brønsted acidic functional groups (*e.g.*, SO_4^{2-}, PO_4^{3-}, heteropoly acids, etc.) could be immobilized over suitable matrix (*e.g.*, silica, alumina, mixed metal oxides, etc.) following a variety of catalyst perpetration techniques (*e.g.*, co-precipitations, sol-gel methods, etc.) [85,88,89]. Reddy *et al.* prepared the sulphated catalysts by impregnating sulphate group over the mixed metal oxides (CeO_2–ZrO_2 and CeO_2–Al_2O_3) based matrix [88]. The matrix for the sulphate group impregnation was prepared by the co-precipitation method in which the solutions of metal precursors (*e.g.,* metal-nitrates, chlorides, etc.) were mixed together under mild stirring and to this, solution of precipitating agents (*e.g.,* NH_3, citric acid, NaOH, or Na_2CO_3, etc.) were added to obtained the precipitate of mixed metal hydroxides. These hydroxides precipitates were initially dried at 100 °C and finally calcined upto 700 °C to obtain mixed metal oxides. The sulphate group over the matrix could be impregnated by wet impregnated method. In this method, un-calcined matrix is treated with diluted H_2SO_4 followed by calcination upto 600 °C as above this temperature sulphate group would decompose from the catalyst. The main limitation of the co-precipitation method is the inconsistency in the catalyst particle size and poor surface area [89,90]. In order to have better control over the catalyst surface area, pore volume, and particle size distribution, nowadays, wet impregnation and sol–gel methods are widely employed for the heterogeneous catalyst preparation [88-90]. These methods are inexpensive, less time-consuming, and provide better control over catalyst morphology to yield homogenous material [91].

In order to quantify the acidic sites present over the catalyst surface, temperature-programmed desorption of ammonia (NH_3-TPD) is frequently employed in the literature. In the same technique, a desorption peak obtained in the range of 100-400 °C signifies the presence of weak to moderate moderated acid sites [92]. In contrast, a desorption peak above 400 °C refers to the strong acidic sites over the matrix [68]. The amount of ammonia desorbed could be correlated to the number of acidic sites present. For instance, upon sulphate group incorporation over the CeO_2–ZrO_2 and CeO_2–Al_2O_3 matrix, two NH_3 desorption peaks were observed at 700 and 800 °C, to suggest the formation of strong acidic sites over these catalysts [88]. In the same study BET surface area of the matrix was found to be lower in comparison to the sulphated catalyst [93]. However, most of the reported work indicates the reduction in catalyst surface area due to the partial blockage of the matrix pores by the sulphate groups [94].

The FTIR technique found to be useful to confirm the incorporation of various Brønsted acidic groups over the catalyst support. The position of characteristics FTIR bands corresponding to these groups are provided in **Table 1.2.** For instance, the SO_4^{2-} group incorporation over the matrix, could be identified by the presence of bands in the range of at 900-1014 and 1162-1400 cm^{-1} due to S-O and S=O functional group, respectively [95-97]. The silica or zirconia matrix peaks could be observed at 802 and 1035 $cm^{-1,}$ respectively, due to Si-O and Zr-O, bonding, respectively [98-101]. Testa *et al*. reported the simultaneous incorporation of phosphate as well as sulphate groups over the zirconia matrix to yield $Zr_4(PO_4)_2(SO_4)_5$ catalyst for the GL acetylation with AcA to produce acetins [101]. From FTIR analysis, bands in the range of 900-1114 cm^{-1} [95,102] and 1400-1250 cm^{-1} [103] were correlated to the S-O and S=O bonding, respectively, of sulphate groups, while the presence of PO_4^{3-} group was supported by the presence of a band at 1050 cm^{-1} band due to P-O bonding [101-107]. In order to prepare the magnetic catalysts, active sites (Brønsted or Lewis acids) were incorporated over a magnetic core (Fe_3O_4). The presence of a band in the range of 583-591 cm^{-1} due to Fe-O linkage indicates the presence of Fe_3O_4 within the catalyst [108,109].

Table 1.2. Identification of catalyst functional groups with the help of FTIR technique.

Bands	Wavenumber (cm^{-1})	References
S-O	900-1114	[95-97]
S=O	1400-1250	[95-97,110]
P-O	474-1089	[101,104,106,107]
Si-O	798-1100	[98,100]
Fe-O	583–591	[108,109]
Zr-O	1353-1565	[99,111]

The Oxidation states of the element present in the catalyst could be identified by XPS analysis of the catalyst. A specific oxidation state of the element present could be correlated with the catalyst activity. In XPS, the presence of the sulphate group over the catalyst could be characterized by the presence of a typical doublet at 168.4 and 170.1 eV due to the S^{6+} $2p_{3/2}$ and S^{6+} $2p_{1/2}$ states, respectively [98,112]. Ghoreishi *et al*. reports the impregnation of PO_4^{3-} over the silica which was verified by the presence of binding energy peaks at 136.1 and 134.1 eV corresponding to P $2p_{1/2}$ and P $2p_{3/2}$ states, respectively, of P in +5 oxidation state [58]. Testa *et al*. prepared a Brønsted acid catalyst in which sulphate as well phosphate groups were simultaneously anchored over the zirconia matrix ($Zr_4(PO_4)_2(SO_4)_5$) [101]. The impregnation of the SO_4^{2-} and PO_4^{3-} over the zirconia surface was evaluated the presence of peaks at 170.5 and 135.2 eV, due to the S^{6+} $2p_{1/2}$ and P^{5+} $2p_{1/2}$ states, respectively [98,101]. In case of heterogeneous catalysts, the Brønsted acids usually remain anchored over the silica, or zirconia matrix. The binding energies of 103.6 eV and 102 eV indicate the $2p_{1/2}$ and $2p_{3/2}$ levels, respectively, of Si^{4+} state [98,113,114]. Furthermore, Zr^{4+} in ZrO_2 shows binding energy peaks at 185.1 and 182.7, corresponding to the Zr^{4+} $3d_{3/2}$ and Zr^{4+} $3d_{5/2}$ states, respectively [101,115]. The binding energies of few more reported catalysts having sulphate and phosphate groups are summarized in **Table 1.3**. To facilitate the magnetic separation of the catalyst, recently, our group has reported $Fe_3O_4@SiO_2@SO_4^{2-}$ as heterogeneous catalyst or the GL acetylation. The characterization of the same catalyst by XPS shows the peaks at 711.7 and 720.2 eV due to the +3 oxidation state of Fe $2p_{3/2}$, while those observed at 713.9 and 726.6 eV were correlated to the +2 oxidation state of Fe $2p_{1/2}$ [68]. Liu *et al*. reported that in case of sulphated Fe_2ZrO_2, binding energy peaks observed in the range of 710.0 - 711.5 eV and 724.3 - 725.5 eV could be ascribed

to the Fe^{3+} $2p_{3/2}$ and Fe^{2+} $2p_{1/2}$ electronic states, respectively [116-119]. The variation in the peak position was correlated to the varying sulphate concentration over the magnetic core.

Table. 1.3. XPS identification of electronic states of elements present in various catalysts.

Catalyst	Elements with oxidation and electronic state	Binding energy (eV)	Reference
$Fe_3O_4@SiO_2@SO_4^{2-}$, FeS_5Zr	Fe^{3+} $2p_{3/2}$	710.0-725.5	[68,116]
	Fe^{2+} $2p_{1/2}$	713.9- 726.6	
20-SO_4^{2-}/SiO_2, $Fe_3O_4@SiO_2@SO_4^{2-}$, $Zr_4(PO_4)_2(SO_4)_5$, CoMo-sZr, FeS_5Zr, SO_4^{2-}/ZrO_2	S^{6+} $2p_{3/2}$	168.4- 170.0	[58,68,101,110,116,120]
	S^{6+} $2p_{1/2}$	170.1- 170.5	
20-SO_4^{2-}/SiO_2, 20-PO_4^{3-}/SiO_2, $SO_4^{2-}/SiZrO_4$, $Fe_3O_4@SiO_2@SO_4^{2-}$	Si^{4+} $2p_{3/2}$	100.7- 103.6	[58,68,98]
	Si^{4+} $2p_{1/2}$	102.0- 104.1	
$SO_4^{2-}/SiZrO_4$, SO_4^{2-}/ZrO_2, CoMo-sZr	Zr^{4+} $3d_{3/2}$	184.0- 185.3	[98,120,121]
	Zr^{4+} $3d_{5/2}$	182.0- 182.9	
20-PO_4^{3-}/SiO_2, $Zr_4(PO_4)_2(SO_4)_5$	P^{5+} $2p_{3/2}$	136.2	[58,101]
	P^{5+} $2p_{1/2}$	134.6- 135.2	

1.7. Lewis acids as heterogeneous catalysts for glycerol acetylation

A wide range of heterogeneous acidic (Lewis as well as Brønsted) catalysts have been explored for the acetylation of GL to produce higher selectivity of acetins (MA or DA or TA) as well as GL conversion levels. The product selectivity in the literature was a function of matrix employed, acidic strength, surface area, and pore size of the catalyst [122,123]. Further, the reaction parameters have to be optimized with respect to the regent molar ratio, reaction temperature, catalyst amount, and reaction duration [124]. Lewis acids have been less explored in literature than the Brønsted acids, primarily due to their less activity. Pure or mixed metal oxides (ZrO_2, CeO_2-ZrO_2, TiO_2–ZrO_2, WOx/TiO_2–ZrO_2 and $MoOx/TiO_2$–ZrO_2 etc.) constitute the category of such Lewis acid catalysts [125-127]. In these catalysts, metal centers act as Lewis acids or electron acceptors (**Fig 1.13**) to initiate the catalytic cycles [128]. The mixed metal oxide based heterogeneous Lewis acidic catalysts are considered important due to their stability caused by metal oxide linkage, non-stoichiometric metal ratios, and redox properties [126,127].

Additionally, they can tolerate high temperature and pressure during the reaction without undergoing any significant deactivation [127]. Acetins selectivity and GL conversion depend upon the catalyst acidic strength and the nature of acidic sites (Lewis or Brønsted), which is a function of the catalyst surface area and oxidation state of the metal ions present in the catalyst [122,129]. Such catalysts could be prepared by the co-precipitation, wet impregnation, or sol-gel method employing the metal salts as precursors [85,88,89]. The Lewis acidic sites of heterogeneous catalysts could be identified by the presence of bands positioned at 1621, 1576 and 1455 cm^{-1} in the FTIR spectra of pyridine adsorbed catalysts [130-133]. These bands indicate the covalent interactions between Lewis acidic sites and pyridine molecule, as shown in **Fig. 1.13b**. The surface acidity of the catalysts could be quantified by the NH_3-TPD and Hemmett indicator test [134-136].

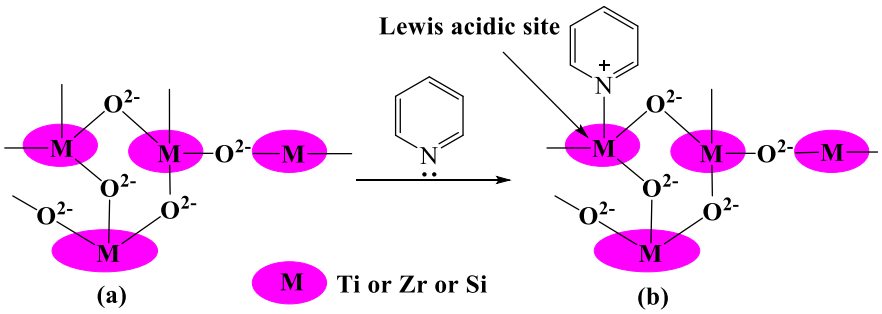

Fig. 1.13. The interaction of pyridine with Lewis acidic site.

Rane *et al*. reported that ammonia desorption peaks in the case of SO_4^{2-}/γ-Al_2O_3 catalyst, applied during GL acetylation with AcA, was observed in the range of 250–300 °C and 500–750 °C. The desorption peak at low temperature was suggested to weak acidic sites while at high temperature for strong acidic sites [129]. Similarly, Reddy *et al*. reported the same observation for the sulphated binary metal oxides (SO_4^{2-}/CeO_2-Al_2O_3 and SO_4^{2-}/CeO_2-ZrO_2) to indicate the NH_3 desorption peaks at 100, 300 and 400 °C. Usually, the NH_3 desorption peaks in the temperature range of 100-300 °C indicated the weak acidic sites, at 300-400 °C moderated acidic sites and above 400 °C strong acidic sites [88].

In order to improve the acidic strength and catalyst activity, Lewis acids sites of the metals could be functionalized with Brønsted acidic sites [121]. Balaraju *et al.* incorporated tungstophosphoric acid over niobic acid to prepare the solid acidic catalyst for the production of acetin by the GL

acetylation with AcA. The acidic strength of the catalyst was found to increase from 8.25 to 11.49 mol/g with the increase in tungstophosphoric acid amount from 5 to 25 % [137]. The catalyst with maximum acidity, in spite of having the smallest surface area, was found to demonstrate the maximum GL conversion levels. This observation clearly underlines catalyst acidity is more prominent than catalyst surface area during the GL acetylation reaction [138].

Nevertheless, heterogeneous Lewis acidic catalysts are less frequent in literature than their Brønsted counterpart, primarily as they were found to yield lesser product selectivity and conversion levels. For example, CeO_2-ZrO_2 based catalyst was found to yield ~57 % GL conversion, reaching as high as ~ 99 % upon employing the SO_4^{2-}/CeO_2-ZrO_2 as heterogeneous catalyst for the same reaction [126]. However, most of the mixed metal oxide based catalysts remain unaffected by the presence of water, which forms as a by-product during the GL acetylation [139]. The plausible mechanism of the Lewis acid catalyzed GL acetylation has been proposed, involving the following steps:

(i) Interaction of the Lewis acid with acetic acid or acetic anhydride carbonyl group followed by rearrangement , to form carbocation (I) as shown in **Scheme 1.2** [75].

(ii) The carbocation thus formed was attacked by the lone pair of oxygen (nucleophile) of GL hydroxy group to form the intermediate (II).

(iii) During the next step, a water molecule is given away by the intermediate (II), to form another intermediate (III) where carbonyl oxygen remains attached with the Lewis acidic site [140].

(iv) In the last step, product with the ester bond, monoacetin, gets detached from the catalyst surface. A similar, mechanism is expected to be followed to form DA or TA where two or three ester bonds, respectively, will form.

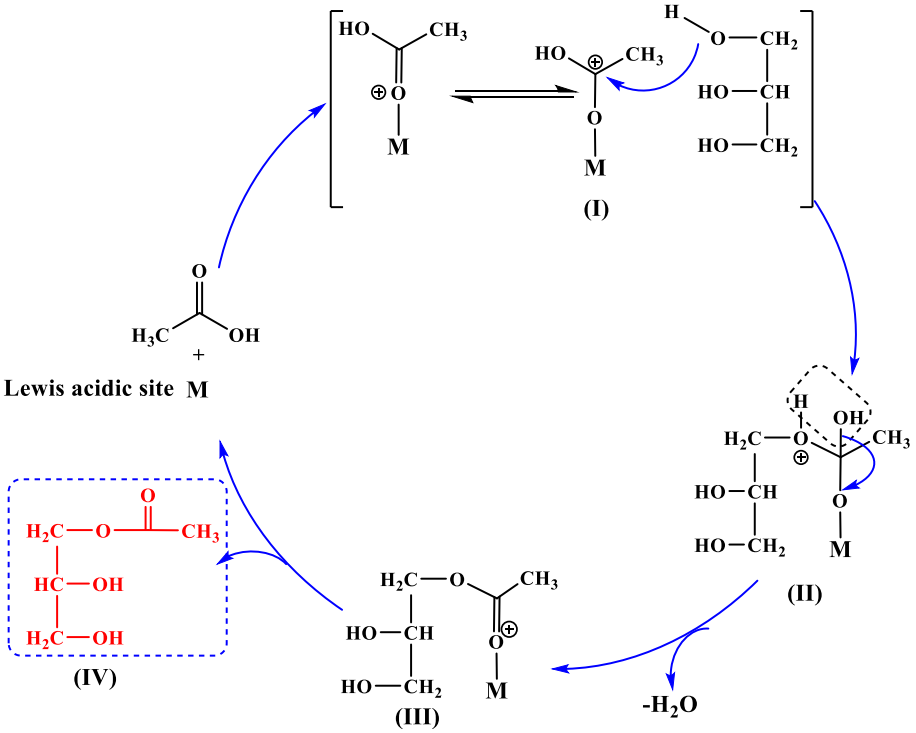

Scheme 1.2. Reaction mechanism of glycerol acetylation involving Lewis acidic site.

A variety of metal oxides has been explored as catalysts or support material for the sulphate or sulphonic acid group incorporation [88,126]. A few literatures reported Lewis acid based heterogeneous acidic catalysts for the production of acetins had been summarized in Table 1.4. Metal oxides such as ZrO_2, TiO_2–ZrO_2 and CeO_2-ZrO_2 possess Lewis acid sites which are found to impart the catalytic activity for the GL acetylation to form acetins [125,126]. Rane *et al*. used γ-Al_2O_3 as a matric to support the Cu or Ni or Cu-Ni or SO_4^{2-} to prepare the catalyst for the GL acetylation [128]. The sulphated alumina was found to demonstrate better activity among the prepared catalyst with 97 % GL conversion levels with MA, DA and TA selectivity of 27 %, 50 %, and 23 %, respectively. The catalyst was reused during 3 catalytic cycles without any significant loss in activity. The reaction was found to follow the pseudo-second order rate law [129], contrary to the other reports which have suggested the pseudo-first order kinetic model for the same reaction [60,141-143].

Table 1.4. Activity comparison of literature reported Lewis acidic catalysts employed for glycerol acetylation.

Catalyst	wt% (w.r.t. GL)	AcA/GL (mol/mol)	Temp (^oC)	Time (h)	MA %	DA %	TA %	GL conversion %	Catalyst reusability (# of cycles)	Reference
CeO_2-ZrO_2	5.0	10:1	100	3.0	85.39	14.13	0.48	57.96	NR	[126]
γ-Al_2O_3	2.5	9:1	110	5.0	86.7	12.9	0.5	82.0	NR	[129]
Cu/γ-Al_2O_3	2.5	9:1	110	5.0	70.7	27.0	2.3	84.0	NR	[129]
Ni/γ-Al_2O_3	2.5	9:1	110	5.0	68.9	28.4	2.6	97.0	NR	[129]
ZrO_2	5.0	6:1	120	3.0	86.32	36.67	5.39	86.32	NR	[127]
TiO_2–ZrO_2	5.0	6:1	120	3.0	54.72	39.40	5.88	91.53	NR	[127]
WO/TiO_2–ZrO_2	5.0	6:1	120	3.0	53.98	40.01	6.78	99.02	NR	[127]
MoO/TiO_2–ZrO_2	5.0	6:1	120	3.0	52.03	40.45	7.52	100	5	[127]

w.r.t. = with respect to, GL = glycerol, AcA = acetic acid, temp = reaction temperature, h = hours, MA = monoacetin, DA = diacetin, TA = triacetin, and NR = not reported

1.8. Brønsted acids as heterogeneous catalysts for glycerol acetylation

Homogeneous Brønsted acids *viz*., H_2SO_4, HCl, H_3PO_4, heteropoly acids, etc. have been employed to acetylate alcohols, including GL, in the literature [141,144,145]. In order to promote the separation and reusability of such catalysts they have been immobilized over a variety of matrix including SiO_2, ZrO_2, Nb_2O_5, SBA-15, MCM-41 and zeolites [85,121,126,145,146]. These catalysts have both, Brønsted as well as Lewis acidic sites, which could be identified by the FTIR analysis of the catalyst adsorbed with pyridine molecule [147]. Lewis acidic sites interact with pyridine through the coordinate bond as shown in **Fig 1.14a**, and this interaction could be identified by the appearance of bands at 1621, 1576 and 1455 cm^{-1} in the FTIR spectra [130,131-133]. On the other hand, H^+ of Brønsted acids leads to the formation of pyridinium ion (**Fig 1.14b**), on interaction with pyridine molecule, which could be identified by the presence of bands positioned at 1397, 1545 and 1635 cm^{-1} [133,148].

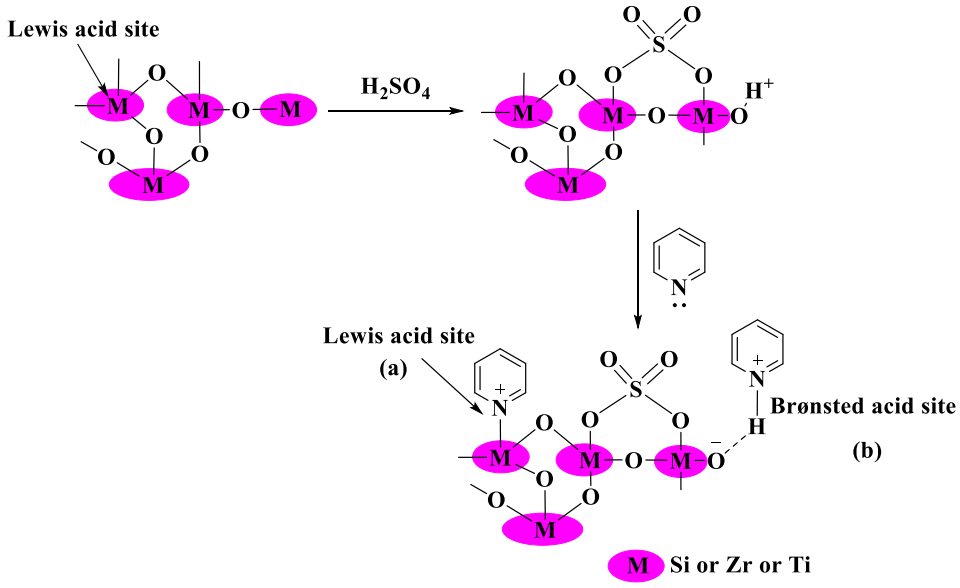

Fig. 1.14. Incorporation of Brønsted acid sites over the matrix and interaction of pyridine with Brønsted and Lewis acidic sites.

The plausible mechanism of the Brønsted acid catalyzed GL acetylation has been reported to involve the following steps:

i. The first step involves the protonation of the carbonyl oxygen of AcA by the proton, furnished by the Brønsted acid, to form the carbocation (I) as shown in **Scheme 1.3** [68].

ii. In second step the carbon of the carbocation (I) reacts with –O–H of GL to form another carbocation (II) as an intermediate [98].

iii. Now, intermediate (II) undergoes the rearrangement through proton transfer to form another cationic intermediate (III)

iv. Intermediate (III), give away a water molecule to form yet another intermediate (IV) where proton remains associated with O of the carbonyl group [98].

v. In the final step, the intermediate (IV) dissociated into a proton (Brønsted acid) and ester bond of MA. A similar mechanism is expected to be followed by the MA to form DA or TA where two or three ester bonds, respectively, will form [145,149].

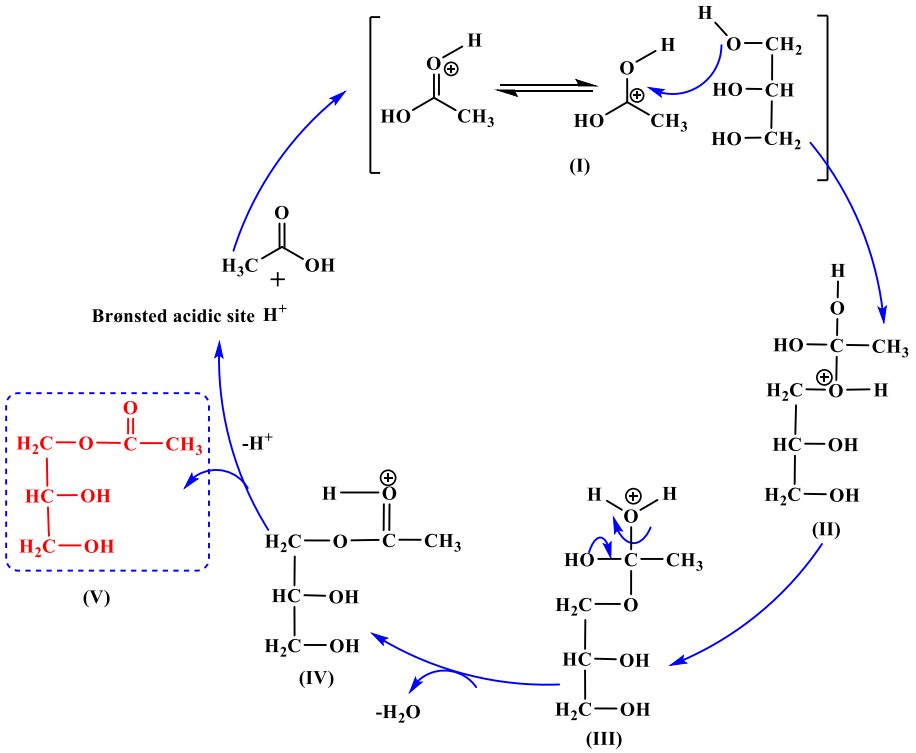

Scheme 1.3. Reaction mechanism of glycerol acetylation with acetic acid catalysed by Brønsted acidic site.

Thus, an ideal heterogeneous catalyst to carry out the GL acetylation must have high acidity, better reusability, and stability. In order to prepare the efficient heterogeneous acidic catalyst for the GL acetylation a variety of Brønsted acidic sites have been incorporated over a variety of matrix *viz.*, metal/mixed metal oxides, mesoporous silica, ion exchange, zeolites, carbon, clay and magnetic core [121,122,145,150-152].

1.8.1. Metal oxide based Brønsted acids

In literature reports, Brønsted acids are frequently employed for the acetylation of GL and other molecules. The acidic sites have been anchored over a variety of matrix surfaces. Among them, metal oxides (pure and mixed metals) have been extensively used to develop heterogeneous catalysts. Such catalysts have been reported to provide several advantages *viz.*, ease of preparation, high and tunable surface area, and high acidity and stability [88,150]. In literature, single metal (Zr, Al, Sn, etc.) oxides have been supported with sulphate or phosphate groups to prepare the solid catalysts for the GL acetylation with AcA to produce acetins [120,129,153].

Recently, $Zr(SO_4)_2$ and $Zr_3(PO_4)_4$ catalysts have been utilized during GL acetylation to obtain up to 81 % GL conversion levels under optimized reaction conditions as shown in Table 1.5. The catalyst with phosphate group was found to show better activity compared to the one with sulphate group. Rane *et al*. reported the preparation of sulphate impregnated γ-Al_2O_3 oxide as heterogeneous acidic catalysts employing the varying concentrations (0.2 - 4.8 M) of sulphate group [129]. The catalyst prepared with 2 M concentration of sulphate group (2 M SO_4^{2-}/γ-Al_2O_3) demonstrated higher TA selectivity (23.1 %) while maintaing the overall GL conversion level of 97 %. The TA selectivity varies with the sulphate concentration over the catalyst and follows the trends *viz.*, 2 M SO_4^{2-}/γ-Al_2O_3 > 4.8 M SO_4^{2-}/γ-Al_2O_3 > 0.2 M SO_4^{2-}/γ-Al_2O_3, while maintaining the total GL conversion of 97 % for all the catalysts [129]. In another report, SnO_2 was used as a matrix to incorporate sulphate or MoO_3 groups to prepare the solid catalysts. The SO_4^{2-}/SnO_2 catalyst was found to demonstrate better activity and reusability compared to the MoO_3 based catalyst [153]. However, the GL conversion decreased from ~77 to 52 % on repeated use of SO_4^{2-}/SnO_2 catalyst during four consecutive cycles. Although the overall GL conversion level was close to 100 %, the TA selectivity was not promising in case of heterogeneous catalysts prepared by incorporating the Brønsted acid over the single metal oxides. In an exciting approach, Testa *et al.* anchored both sulphate and phosphate over the zirconia surface to obtain the $Zr_4(PO_4)_2(SO_4)_5$ catalyst for the GL acetylation with AcA. TA selectivity was found to be 39 % while maintaining 100 % GL conversion at 105 °C within one h of reaction duration [101]. This catalyst was reused 5 times under optimized reaction conditions; however, a decline in catalyst activity and TA/DA selectivity was observed even during the 2nd cycle. In most cases, the catalyst deactivation was associated either with the active site blockage [129] or with the leaching of active components, such as sulphate group, from the catalyst surface [154].

In order to improve the TA selectivity and catalyst stability, to achieve the better reusability, mixed metal oxides based heterogeneous acidic catalysts have been employed for the GL acetylation during the past few years as shown in **Table 1.5**.

Mixed metal oxides based catalysts, consisting of two or more metals, have been found to demonstrate enhanced activity and stability compared to the single metal oxide based catalysts. Recently, Kulkarni *et al*. prepared sulphated mixed metal oxides (SO_4^{2-}/CeO_2–ZrO_2) which was

employed in 5 wt% amount (with respect to GL) for the GL acetylation utilizing the AcA/GL molar ratio of 10:1, at 100 °C reaction temperature. During the reaction, 99 % GL conversion levels were obtained with 22 %, 57 %, and 21 % MA, DA, and TA selectivity, respectively, within one h of reaction duration [126]. On similar lines, our group has anchored the sulphate group over the mixed metal oxides ($SiZrO_4$) matrix to prepare $SO_4^{2-}/SiZrO_4$ (SSZ) heterogeneous catalyst. The catalyst demonstrated the excellent TA selectivity (93 %) as well GL conversion (100 %) on employing 9:1 AcA/GL molar ratio and 3 wt% catalyst at 80 °C reaction temperature. The same catalyst was reused during 6 consecutive reaction cycles while retaining 54 % TA selectivity in the last cycle [98].

Table 1.5. Activity comparison of literature reported metal oxide based Brønsted acidic catalysts employed for glycerol acetylation.

Catalyst	wt% (w.r.t. GL)	AcA/GL (mol/mol)	Temp (^oC)	Time (h)	MA %	DA %	TA %	GL conversion %	Catalyst reusability (# of cycles)	Reference
$SO_4^{2-}/CeO_2–ZrO_2$	5.0	10:1	100	3.0	22.0	57.0	21.0	99.0	3	[126]
$SO_4^{2-}/SiZrO_4$	3.0	9:1	80	0.7	-	7.0	93.0	100	6	[98]
$Zr_4(PO_4)_2(SO_4)_5$	5.0	3:1	105	1.0	15.0	48.0	39.0	100	5	[101]
$Zr(SO_4)_2$	5.0	3:1	105	1.0	-	-	-	40.0	NR	[101]
$Zr_3(PO_4)_4$	5.0	3:1	105	1.0	-	-	-	81.0	NR	[101]
SO_4^{2-}/W-Zr	0.023	-	120	4.0	33.0	41.0	4.0	100	NR	[155]
HAlSi	22.16	6:1	110	3.0	76.4	7.9	12.0	96.4	NR	[156]
HZnAlSi	22.16	6:1	110	3.0	16.5	-	83.4	99.9	NR	[156]
Zr-S/PW	12.0	12:1	105	20.0	8.0	59.0	33.0	100	NR	[157]
0.2 M SO_4^{2-}/γ-Al_2O_3	2.5	9:1	110	5.0	30.5	53.6	15.9	97.0	NR	[129]
2 M SO_4^{2-}/γ-Al_2O_3	2.5	9:1	110	5.0	27.0	49.9	23.1	97.0	2	[129]
4.5 M SO_4^{2-}/γ-Al_2O_3	2.5	9:1	110	5.0	33.0	48.8	18.2	97.0	NR	[129]
Cu-Ni(3:1)/γ-Al_2O_3	2.5	9:1	110	5.0	75.4	23.2	1.4	89.0	NR	[129]
SO_4^{2-}/CeO_2-TiO_2-ZrO_2	6.0	9:1	120	2.0	22.1	59.5	18.4	100	NR	[150]
SO_3H /GO	1.0	10:1	120	6.0	10.0	50.0	39.0	100	4	[158]
$^A Sb_2O_5$	1.0	6:1	120	3.5	33.2	54.2	12.6	96.3	6	[50]
SO_4^{2-}/SnO_2	5.0	6:1	100	2.0	68.0	19.0	7.0	83.0	6	[153]
MoO_3/SnO_2	5.0	6:1	100	2.0	80.0	12.0	1.0	64.0	NR	[153]
25%TPA/Nb_2O_5	2.0	5:1	120	4.0	21.0	59.0	20.0	90.0	3	[137]

S = sulphate, A = saturated with H_2O_2, GO = Graphene oxide, and TPA = tungstophosphoric acid

1.8.2. Mesoporous silica based acidic catalyst

Silica (SiO_2) is a highly stable material with weak acidic sites over the surface in the form –O–H functional groups [159]. It could be easily modified by various organic and inorganic functional groups and be prepared as mesoporous material to increase its surface area [157]. In recent past, it has attracted much attention as a heterogeneous catalysts support because of the reasons mentioned above coupled with its low production cost. It can be synthesized by a wide variety of low-cost precursors with high surface area and large pore volume and in suitable morphology (*e.g.* spheres, fibers and tubules etc.) [160-162]. The strong Brønsted acidic sites over silica could be introduced by coupling it with sulphate functional group, as shown in **Fig. 1.15** [163].

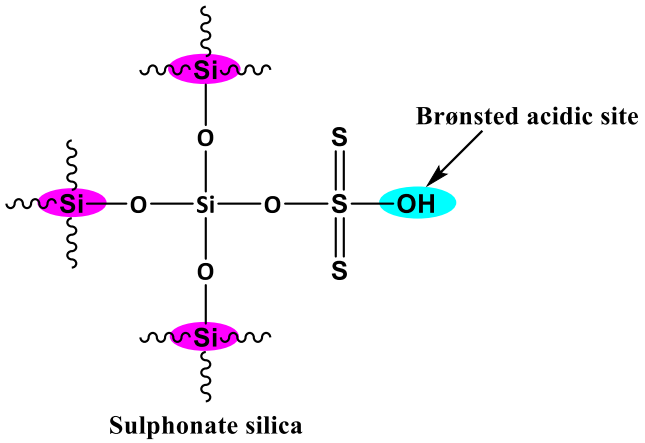

Fig. 1.15. A typical structure of formation of sulphonated silica catalyst.

To prepare the silica matrix, tetraethoxysilane (TEOS), a frequently used silica precursor, was mixed with ethanol under stirring and hydrolyzed under acidic or alkaline pH [164]. The use of an appropriate surfactant is necessary to obtain the silica particles of desired pore size [165,166]. The active site over the matrix surface could be attached either in a two- or single-step process [161]. In order to control the pore size, a sol-gel method was frequently employed for the matrix preparation. For example, Testa *et al*. prepared mesoporous silica by sol-gel method, which was later functionalized with sulphonic acid group [85]. The catalyst was employed for the GL acetylation with AcA to produce TA (49 % selectivity) with complete GL conversion at 105 °C within 1 h of reaction duration. The catalyst activity was reduced as GL conversion decreased from 100 to 20 % after 5 cycles. 3-Mercaptopropyltrimethoxy silane could be employed to form the silica support (SBA-15 and SBA-16) and later, 3-mercaptopropyl group was oxidized to a –

SO_3H group with the help of H_2O_2 to obtain heterogeneous acidic catalysts labeled as SO_3H-SBA-15 and SO_3H-SBA-16. The catalyst, SO_3H-SBA-15, exhibited higher activity towards GL acetylation with AcA to yield complete GL conversion with 21.5 % TA selectivity at 130 °C reaction temperature [146]. Patel and Singh also prepared 12-tungstophosphoric acid anchored silica based (MCM-41) heterogeneous acidic catalyst following the reported procedure [60]. In the first step, MCM-41 was synthesized employing cetyl trimethylammonium bromide (CTAB) as surfactant under alkaline pH of NaOH. To this, TEOS was added drop wise, to obtain a gel that was filtered, washed, dried at room temperature and then finally calcined at 550 °C to decompose the surfactant to obtain MCM-41. In the second step, the 10-40 % of 12-tungstophosphoric acid (TPA) was anchored over the MCM-41 by the impregnation method. In a typical method, MCM-41 was mixed with an aqueous solution of 12-tungstophosphoric acid of the desired concentration and the mixture was dried at 100 °C for 10 h to obtain TPA/MCM-41 catalyst, which was employed to catalyse the GL acetylation with AcA to yield 15 % of TA selectivity with 87 % GL conversion at 100 °C in 6 h of reaction duration. On recycling the catalyst, no significant drop in activity was observed during 4 catalytic cycles [60]. Our group recently synthesized sulphated zirconia-silica-based heterogeneous acidic catalysts employed for the GL acetylation with AcA to yield excellent TA selectivity (93 %) and complete GL conversion under mild reaction conditions. The same catalyst was reused during 6 catalytic cycles with a gradual decrease in TA selectivity which remain up to 54 % during the last run [98].

Recently, Mufrodi *el al*. reported the GL acetylation in the presence of a silica-alumina heterogeneous acidic catalyst, to obtain the moderate TA selectivity (47.69 %) with 87.43 % GL conversion at 110 °C [167]. The acidic sites (Lewis) in the catalyst could also be generated by incorporating transition metals over the matrix. Liu *et al*. compared the activity of bare MCM-41 with that of -SO_3H, Ru and Cu functionalized one [124,151]. As expected, the catalyst activity has been found to improve upon the incorporation of active species. In a similar approach, Ramalingam *et al*. prepared ruthenium and copper incorporated MCM-41 heterogeneous acidic catalyst by the sol-gel method and employed them for the GL acetylation with AcA [124]. The MCM-41-10Ru10Cu was found to demonstrate better activity than MCM-41-10Cu in terms of GL conversion (99.1 %), maintaining 45.2 % and 50.4 % of DA and TA selectivity, respectively, at 120 °C in 5 h of reaction duration. Reusability is one of the crucial features of heterogeneous

catalysts. However, as evident from **Table 1.6**, most of the silica based catalysts employed during the acetin synthesis were demonstrated poor reusability.

Table 1.6. Activity comparison of literature reported mesoporous silica based catalysts employed for glycerol acetylation.

Catalyst	wt% (w.r.t. GL)	AcA/GL (mol/mol)	Temp (^oC)	Time (h)	MA %	DA %	TA %	GL conversion %	Catalyst reusability (# of cycles)	Reference
MCM-41-10Cu	8.0	10:1	120	5.0	68.3	21.1	10.6	83.8	NR	[124]
MCM-41-10Ru10Cu	8.0	10:1	120	5.0	2.4	45.2	50.4	99.1	NR	[124]
Silica alumina	NR	3:1	110	1.0	18.47	32.84	47.69	87.43	NR	[167]
$SO_4^{2-}/SiZrO_4$	3.0	9:1	80	0.67	-	7.0	93.0	100	6	[98]
MCM-41	1.5	9:1	125	24.0	76.4	19.8	3.8	70.5	NR	[151]
SO_3H-SBA-15	2.5	6:1	130	4.0	21.3	57.2	21.5	100	3	[146]
SO_3H-SBA-16	2.5	6:1	130	4.0	35.5	46.4	18.1	NR	NR	[146]
Pr-SO_3H-SBA-15	5.0	6:1	100	2.5	13.0	32.0	55.0	96.0	2	[168]
TPA_3/MCM-41	1.5	6:1	100	6.0	-	60.0	15.0	87.0	4	[60]
SSBA	5.0	3:1	105	1.0	15.0	74.0	11.0	100	5	[85]
SAS	5.0	3:1	105	1.0	10.0	73.0	17.0	100	3	[85]
MP(1)/SBA-15	1.0	9:1	75	4.0	12.0	54.0	34.0	85.0	3	[46]
MP(1)/NbSBA-15	1.0	9:1	75	4.0	11.0	51.0	38.0	92.0	3	[46]

P = pressure, SSBA = propyl-SO_3H functionalized SBA-15, SAS = Propyl-SO_3H functionalized silica, and MP = 3-mercaptopropyl

1.8.3. Ion exchange resins as acidic catalyst

The idea of using the insoluble ion exchange materials in place of liquid mineral acids or bases is more than hundred years old [169]. Ion exchange resins consist of polymeric support (*e.g.*, polystyrene) and a labile ionic group (*e.g.*, sulphonic acid or tertiary ammonium hydroxide) attached with the benzene ring as indicated in the **Fig. 1.16**. They could be broadly divided into two categories:- (i) cation exchangers (*e.g.*, $-SO_3^-H^+$), having the capability to exchange their H^+ with other cations and extensively used in water softening and as acidic catalysts, and (ii) anionic exchangers (*e.g.*, $NR_4^+OH^-$) having the capability to exchange their OH^- with other anions and could be used in removing the anionic impurities from water and also as basic catalysts [38, 145,170,171]. Thus, they are suitable to replace the respective homogeneous catalysts due to acidic or basic functional groups. Moreover, due to their insoluble nature, such catalysts could

easily be isolated from the reaction media and could also be reused multiple times [172,173] and thus advantageous over their homogeneous counterpart [174].

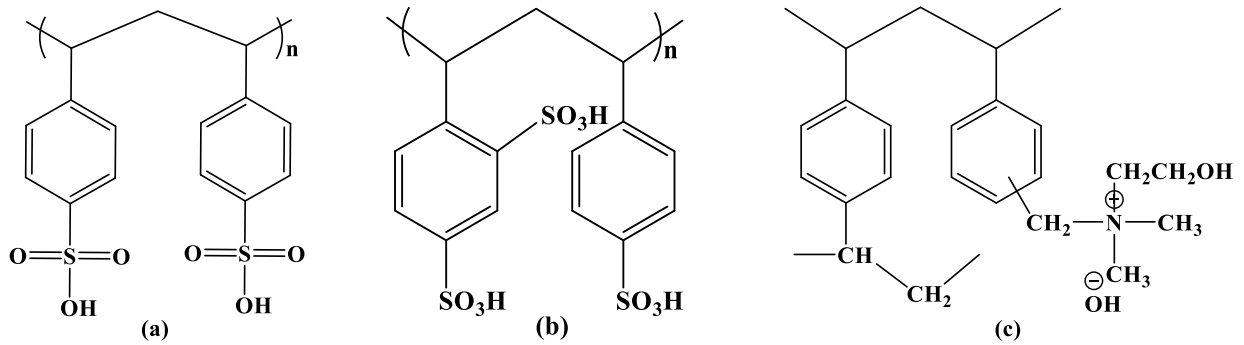

Fig. 1.16. Structure of commercially available cation exchange resin *e.g.*, (a) Amberlyst and (b) Dowex50, and anion exchange resin *e.g.*, (c) Lewatit catalyst.

In the last few years, commercially available ion exchange resins (*e.g.*, Amberlyst-15, Amberlyst-36, Amberlyst-70 and Dowex 50Wx2 etc.) have gained the attention as heterogeneous acidic catalysts for the production of acetins *via* GL acetylation with AcA [38,175]. Zhou *et al*. employed Amberlyst-15 for the GL acetylation with AcA to produce 44.47 % TA selectivity with 98.47 % GL conversion at 110 °C in 4.5 h of reaction duration [176]. However, they have used a relatively higher catalyst amount (26 wt % of GL) without mentioning its reusability. Later, the same catalyst (Amberlyst-15) have been reported for GL acetylation with AcA (AcA/GL molar ratio = 7:1) at 100 °C to achieve 100 % GL conversion, maintaining 14 % TA selectivity in 25 h reaction duration [139]. Under the same reaction conditions, Amberlyst-36 was found to yield 100 % GL conversion, including 13 % of TA selectivity. Jiang *et al.* employed Amberlyst-45 as a heterogeneous acidic catalyst to obtain 75.3 % GL conversion into the acetins at 70 °C in 7 h of reaction duration [177]. To further improve the GL conversion and catalyst reusability, Rodriguez and Gaigneaux employed the strong acidic ion exchange resins, Dowex 50Wx2, Dowex 50Wx4 and Dowex 50Wx8, for the GL acetylation. Dowex 50Wx2 and Dowex 50Wx4 catalysts showed higher GL conversion levels (> 94 %) in comparison to Dowex 50Wx8, at 105 °C reaction temperature [38]. Additionally, Dowex 50Wx2 ion exchange resin has been reused 5 consecutive times without any significant loss in activity under optimized reaction conditions, as shown in **Table 1.7**.

The literature review shows that most of the ion exchange resins are employed, as a catalyst for GL acetylation, in their native form without any further modifications. However, lower GL conversion levels accompanied by lower TA selectivity and poor catalyst reusability are major drawbacks of ion exchange resins while utilizing them as solid catalysts for the GL acetylation.

Table 1.7. Activity comparison of literature reported ion exchange resin based catalysts employed for glycerol acetylation.

Catalyst	wt% (w.r.t. GL)	AcA/GL (mol/mol)	Temp (^{o}C)	Time (h)	MA %	DA %	TA %	GL conversion %	Catalyst reusability (# of cycles)	Reference
Amberlyst-45	7.0	3:1	70	7.0	68.9	29.8	1.3	75.3	NR	[177]
Amberlyst-36^{P}	-	7:1	120	-	30.0	50.0	17.0	100	NR	[178]
DM-650C	4.0	9:1	120	4.0	11.0	52.0	34.0	100	5	[179]
Lewatit catalyst	3.0	7:1	100	1.5	-	-	-	66.91	NR	[180]
Amberlyst-36^{P}	7.0	7:1	100	25.0	43.0	44.0	13.0	100	3	[139]
Amberlyst-15^{P}	7.0	7:1	100	25.0	42.0	44.0	14.0	100	NR	[139]
Amberlyst-70	5.0	6:1	105	10.0	-	9.4	85.4	100	3	[175]
Amberlyst-15	26.0	9:1	110	4.5	8.65	46.56	44.79	98.47	NR	[176]
Dowex 50Wx2	6.25	8:1	105	1.6	71.9	3.3	-	95.2	5	[38]
Dowex 50Wx4	6.25	8:1	105	1.6	63.7	2.8	-	94.8	NR	[38]
Dowex 50Wx8	6.25	8:1	105	1.6	64.9	3.1	-	64.9	NR	[38]
Amberlyst-15	26.0	9:1	110	5.0	7.59	46.29	43.23	97.13	NR	[145]
Amberlyst-15	-	3:1	110	0.5	31.0	54.0	13.0	97.0	NR	[181]

DM = dowex monosphere, T = toluene, and P = pressure

1.8.4. Carbon based acidic catalyst

A new category of carbon based heterogeneous acidic catalysts has recently gained attention for the GL acetylation to produce acetins [182]. They are eco-friendly, demonstrate high catalyst activity, have better stability, and could be reused during GL acetylation several times without significant loss in catalytic activity [183]. This category of catalysts could be synthesized from biomass such as wood sources or vehicle residues (tyre rubber) or even from sugar molecules [184,185]. Reported sulphonated carbon based heterogeneous acidic catalysts are derived from low-cost biomass, and their acidic strength has been improved by varying the sulphonation condition [182,186]. An example of -SO_3H functionalized sugar derived carbon based catalyst is shown in **Fig. 1.17** [185].

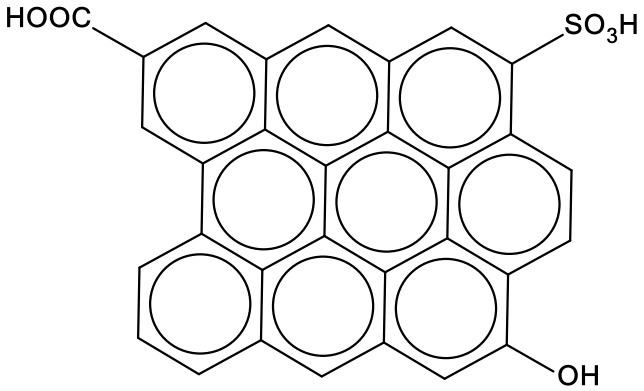

Fig. 1.17. Sulphonated carbon heterogeneous acidic catalyst.

Recently, Nda-Umar *et al.* prepared sulphonated biomass carbon based acidic catalysts in four steps: pre-treatment, template carbonization, template removal, and functionalization [187]. In the first step, the Palm Kernel Shells (PKS) were washed, dried and crushed. To this dilute HCl and Na_2SiO_3 mixture was added under stirring. After this, the mixture was allowed to polymerize at 50 °C followed by the calcination at 800 °C under CO_2 environment for 4 h to carbonize the template. During the third step, the carbonized template was removed by treating the calcined sample with dilute NaOH at 80 °C for 1 h, which was later washed with deionized water and finally dried at 120 °C. In the final step, the PKS derived carbon material was crushed and treated with 100 mL of 1 M organo-sulfonic acid under reflux at 90 °C for 5 h to obtain the ethanesulfonic acid (ESA) catalyst. The catalyst was employed for the production of acetins to obtain 37.73 % of TA selectivity at 120 °C reaction temperature in 3 h reaction duration with 8:1 AcA/GL molar ratio. The same catalyst was reused 5 times, without significant loss in activity (99 % GL conversion) in the last cycle; however, the TA selectivity was reduced to 12 %. The decline in activity has been correlated with the leaching of the acidic sites from the catalyst surface during the catalyst regeneration process.

In literature, SO_3H-functionalized carbon based acidic ($CS\text{-}H_2SO_4$) catalyst was also reported by Malaika *et al*. [182]. They have prepared the sugar-derived carbon spheres by mixing glucose (13.5 g) and phosphomolybdic acid hydrate (1.2 g) into distilled water, which was autoclaved at 160 °C for 8 h with constant stirring under argon atmosphere. The brown polymeric spheres, thus formed, were washed with distilled water and ethanol, dried overnight at 110 °C and finally

pyrolysed at 850 °C for 1 h under argon atmosphere. In the second step, the surface of carbon spheres was functionalized by treating them with H_2SO_4 at 140 °C for 20 h. The obtained mixture was cool down, transferred into distilled water, filtered and washed with hot distilled water and finally dried overnight at 110 °C. To verify the activity of carbon-based catalyst, GL acetylation with AcA was carried out to obtain the 97 % conversion with 21 % TA selectivity. TA selectivity was found to drop from 21 to 9 % during the fourth catalytic cycle.

Karnjanakom *et al*. also prepared SO_3H-GL-carbon based acidic catalyst for TA production from direct reaction of GL with AcA [122]. In this method, the catalyst was prepared from GL *via* in-situ hydrothermal carbonization and sulphonation. In brief, a desired amount of GL and concentrated H_2SO_4 were mixed and transferred into an autoclave and heated for 24 h at 150 °C. After heating, the SO_3H-GL-carbon catalyst was filtered out, washed with deionized water and ethanol multiple times to remove the excess sulphate ions, and dried for 12 h at 110 °C in vacuum oven. Employing the same catalyst (5 wt% with respect to GL) 82 % TA selectivity was achieved with 100 % of GL conversion at 100 °C within 3.5 h of reaction duration. The reusability study demonstrates that it could be reused during 10 consecutive cycles without any significant loss in GL conversion and TA selectivity.

As evident from the recent literature review, summarized in **Table. 1.8**, the carbon based acidic catalysts demonstrated the better reusability as well GL conversion levels, while yielding low TA selectivity.

Table 1.8. Activity comparison of literature reported carbon based catalysts employed for glycerol acetylation.

Catalyst	wt% (w.r.t. GL)	AcA/GL (mol/mol)	Temp (^oC)	Time (h)	MA %	DA %	TA %	GL conversion %	Catalyst reusability (# of cycles)	Reference
ESA	6.9	8:1	120	3.0	6.9	54.9	37.73	99.0	5	[187]
S-Glycerol	-	6:1	110	2.0	21.0	56.0	23.0	97.0	6	[188]
UiO-66/AC	6.0	6:1	90	3.0	26.74	55.3	17.9	NR	3	[189]
CSBA-15-BDS	7.0	6:1	110	6.0	53.0	33.0	13.0	100	4	[190]
PC400S	10.0	6:1	120	5.0	6.71	52.47	40.77	99.76	NR	[123]
PC800S	10.0	6:1	120	5.0	26.89	59.48	13.37	98.97	NR	[123]
MS-Carbon	4.5	10.4:1	126	3.0	4.9	27.8	66.5	97.0	5	[183]
^{A}HTC500-H_2SO_4	7.0	6:1	210	2.0	67.4	30.0	1.6	90.0	NR	[191]
^{A}HTC-H_2SO_4	7.0	6:1	210	1.0	68.7	30.0	1.3	80.0	NR	[191]
^{A}HTC-H_2SO_4	7.0	6:1	210	24.0	21.0	56.5	22.5	80.0	4	[191]
CS-H_2SO_4	-	6:1	80	24.0	25.0	58.0	21.0	97.0	4	[182]
SO_3H-GL-carbon	5.0	8:1	100	3.5	-	18.0	82.0	100	10	[122]
GBCC	2.0	3:1	110	3.0	7.0	48.0	53.0	100	7	[192]
[*Pr*SO_3HN][SO3CF3]/C-2	1.0	6:1	120	8.0	-	-	78.0	-	3	[193]
Sulfonated carbon	5.0	5:1	120	2.0	32.8	54.5	12.5	98.4	NR	[186]
SO_3H-carbon	5.0	4:1	115	1.0	22.0	67.0	11.0	100	5	[80]
C–SO_3H	5.0	9:1	180	4.0	-	-	50.0	100	NR	[194]
AC-SA5	8.0	8:1	120	3.0	38.0	28.0	34.0	91.0	4	[84]

PC = Palm kernel shells carbonized, MS = mesoporous sulphonated carbon, A = argon atmosphere, CS = SO_3H-functionalized carbon, GBCC = glycerol based carbon catalyst, C = carbon and AC = activated carbon

1.8.5. Zeolite based acidic catalyst

Zeolite is micro-porous crystalline solid material, and categorized as alumino-silicate minerals. It is used as acidic catalyst or matrix for the incorporation of active sites (Ce, Zr and PMo) over their surface, in order to increase their specific surface area, acidic strength and stability [195-197]. Modefied or native zeolites such as Ce-ZSM-5, ZSM-5, HZSM-5 and Zr-zeolite etc., can be applied as heterogeneous acidic catalysts in GL acetylation with AcA [168,195,196]. The acetylation reaction over zeolite based acidic catalysts depends on their crystal structure, Si/Al ratio, surface area, Brønsted or Lewis acidic sites, and extent of proton exchange [198]. Out of these, zeolite surface acidic strength is a prominent factor in deciding the catalyst activity towards GL acetylation reaction. The acidic strength could be tuned either by altering the Si/Al

ratio or by introducing the desired functionalization over the zeolite surface [199]. The acidity in aluminosilicate zeolites is introduced due to the substitution of Si (+4) by the Al (+3) and compensation of unit positive charge by a proton (H^+) as shown in **Fig. 1.18** [200]. Thus zeolite possesses Brønsted (H^+) as well as Lewis (M^{n+}) acidic sites and hydrophobic if high Si/Al ratio is maintained [199,200].

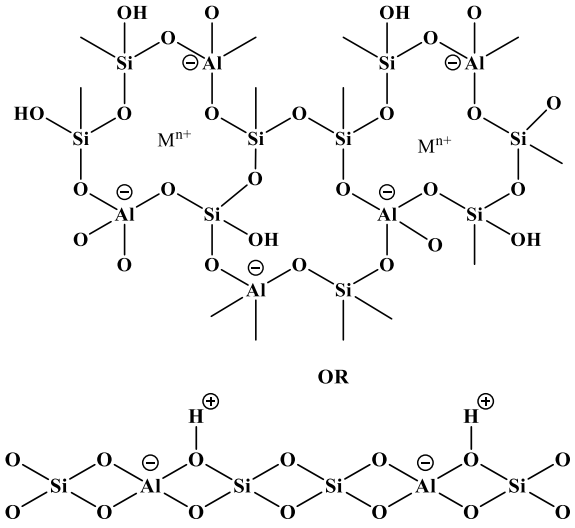

Fig. 1.18. Structure of zeolite with Brønsted acidic site.

Ferreira *et al*. neutralize the commercial HUSY zeolite (Si/Al = 30) before the incorporation of the dodecamolybdophosphoric acid over its surface. The HUSY zeolite protons were exchanged with sodium ions, by treating it with 2 M NaCl at 80 °C, washing with distilled water and drying at 120 °C to obtain NaUSY. Later, dodecamolybdophosphoric acid was incorporated over the NaUSY by treating it with molybdenum (VI) oxide and phosphoric acid [197]. The prepared catalyst (PMo-NaUSY) was used for the GL acetylation with AcA to obtain overall GL conversion of 68 % into the acetins at 120 °C in the presence of 1.9 wt % of catalyst concerning GL. The catalytic reusability was also evaluated during 4 catalytic cycles without any significant loss in the activity. Liu *at al.* also synthesized zeolite based HZSM-5/MCM-41 catalyst by treating ZSM-5 zeolite powder with aqueous NaOH and Na_2SiO_3 in presence of CTAB as a surfactant. After that, the mixture was autoclaved at 120 °C for 48 h, exposed to H_2SO_4, crystallized, and washed with deionized water and ethanol multiple times. The solid material, thus obtained, was dried at 100 °C and finally calcined at 550 °C for 5 h, and designated as ZSM-5/MCM-41. The prepared ZSM-5/MCM-41 catalyst has been employed in 1.5 wt%

amount (concerning GL), utilizing the AcA to GL molar ratio of 9:1, at 125 °C reaction temperature to obtain 100 % GL conversion and 81.9 % of TA selectivity in 24 h of reaction duration. The same catalyst was reused 4 times without any significant loss in activity and TA selectivity [151].

In a similar study, Marwan *et al*. employed chemically activated natural zeolite (CAN-zeolite) as a heterogeneous catalyst for GL acetylation with AcA, to obtain 8.3 % TA selectivity with complete GL conversion at 90 °C reaction temperature [201]. Recently, over research group, synthesized cerium modified ZSM-5 zeolite (Ce-ZSM-5), which was employed as a heterogeneous catalyst for the GL acetylation with AcA to obtain 98.5 % GL conversion level [195]. The same catalyst was recycled during 4 reaction cycles without any significant loss of GL conversion (from 98.5 to 88.25 %) in the last cycle.

Most of the zeolite based heterogeneous acidic catalyst employed during GL acetylation was able to yield high GL conversion (up to 100 %) using a high reaction temperature (up to 120 °C) as well as a long reaction duration (up to 24 h). However, low TA selectivity and poor reusability in such catalysts remain an issue as indicated in **Table 1.9**.

Table 1.9. Activity comparison of literature reported zeolites based catalysts employed for glycerol acetylation.

Catalyst	wt% (w.r.t. GL)	AcA/GL (mol/mol)	Temp (^{o}C)	Time (h)	MA %	DA %	TA %	GL conversion %	Catalyst reusability (# of cycles)	Reference
Ce-ZSM-5	8.0	9:1	120	5	53.5	45.0	-	98.5	4	[195]
CAN-Zeolite^{M}	3.0	9:1	90	1.0	80.1	15.4	4.5	95.0	NR	[201]
CAN-Zeolite^{M}	3.0	9:1	90	1.5	43.0	48.6	8.3	100	NR	[201]
ZM	1.5	9:1	125	24	55.9	23.4	20.7	92.6	NR	[151]
HZSM-5/MCM-41	1.5	9:1	125	24	0.20	17.9	81.9	100	4	[151]
H-ZSM-5	5.0	6:1	100	4.5	40.0	40.0	-	93.5	NR	[168]
H-Beta	5.0	6:1	100	4.5	21.0	61.0	18.0	91.3	NR	[168]
Zr-Zeolite	NR	NR	110	0.5	7.0	68.0	26.0	94.56	NR	[196]
HZSM-5	2.65	9:1	110	4.5	-	25.7	7.7	85.6	NR	[176]
HUSY	2.65	9:1	110	4.5	-	20.6	5.6	78.4	NR	[176]
NaUSY	1.9	-	-	3.0	64.0	25.0	1.0	14.0	NR	[197]
PMo3_NaUSY	1.9	-	-	3.0	37.0	59.0	2.0	68.0	4	[197]

ESA = ethanesulfonic acid, CAN =chemically activated natural zeolite, M = microwave, AN-Zeolite, and ZM = ZSM-5/MCM-41

1.8.6. Magnetic nanoparticles based acidic catalyst

The primary issue with literature reported heterogeneous acidic catalysts is their separation from the reaction mixture, which either is based on the gravitational settlement of the heterogeneous catalyst particles or centrifugation of the reaction mixture to remove the catalyst [98, 202]. The separation of the heterogeneous catalyst from the reaction mixture could be simplified by incorporating the magnetic core (*e.g.* Fe_3O_4) within the catalyst particles, as shown in **Fig. 1.19**. Now being magnetically active, such catalysts could be easily separated from the reaction mixture under the influence of an external magnetic field [68]. In literature, magnetic catalysts have been employed to catalyze various reactions (transesterification, esterification, etherification, dehydration etc.); however, their use in GL acetylation is rare [203-207]. In such catalysts sulphate group or tungstic acid remain the active site for the GL acetylation.

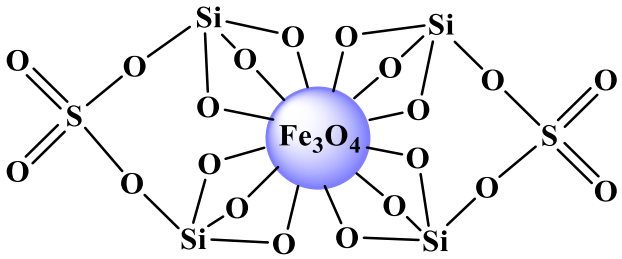

Fig. 1.19. Sulphated silica coated magnetic (SO_4^{2-}@SiO_2@Fe_3O_4) catalyst.

Tong *et al.* prepared heterogeneous magnetic acidic catalyst for the production of TA [208]. The catalyst was prepared in three steps process involving the mixing of ferrous sulphate and ferric sulphate in deionized water followed by heating at 45 °C with the eddition of ammonia solution to obtain the magnetic particles in the first step. In the second step, the stannic chloride pentahydrate was added to magnetic nanoparticles which were treated with tetrabutyl titanate at alkaline pH. The mixture was filtered, washed, dried at 100 °C, and isolated particles, in the last step, were soaked with $(NH_4)_2SO_4$ solution for 24 h, to obtain Fe–Sn–Ti/SO_4^{2-} catalyst. The same catalyst has been employed for the GL acetylation with AcA to achieve high conversion (100 %) levels with high TA selectivity (99 %) at 80 °C in 30 min. Our group also prepared the magnetic catalyst by attaching the sulphate group over the silica coated magnetic (SiO_2@Fe_3O_4) nanoparticles to prepare SO_4^{2-}@SiO_2@Fe_3O_4 heterogeneous magnetic acidic catalyst. The catalyst demonstrated the excellent TA selectivity (100 %) as well GL conversion (100 %) on employing 6:1 AcA/GL molar ratio and 5 wt% catalyst at 80 °C reaction temperature within 45

min of reaction duration [68]. The same catalyst was isolated under the influence of external magnetic field from the reaction mixture and reused during 6 consecutive reaction cycles while retaining ~59 % of TA selectivity during 4th cycle. In another approach, tungsto-polyacid was impregnated over silica coated magnetite to form a $Fe_4SiW_{12}O_{40}$ material, employed to facilitate the GL acetylation with AcA to attain the TA and DA selectivity of 7 % and 69 %, respectively [209]. The catalyst reusability has not been reported. As could be seen from **Table 1.10**, very few magnetic catalysts, so far, have been reported for the GL acetylation, although they have the potential to yield high GL conversion as well as TA selectivity and could also be separated easily from the reaction mixture.

Table 1.10. Activity comparison of literature reported magnetic catalysts employed for glycerol acetylation.

Catalyst	wt% (w.r.t. GL)	AcA/GL (mol/mol)	Temp (^oC)	Time (h)	MA %	DA %	TA %	GL conversion %	Catalyst reusability (# of cycles)	Reference
$SO_4^{2-}@SiO_2@Fe_3O_4$	5.0	6:1	80	0.6	-	-	100	100	6	[68]
$Fe\text{-}Sn\text{-}Ti/SO_4^{2-}$	5.0	-	80	0.5	-	-	99.0	100	4	[208]
$Fe_4SiW_{12}O_{40}$	6.0	3:1	60	8.0	24.0	69.0	7.0	100	NR	[209]

1.9. Conclusions

1. Glycerol is a colorless, odorless, and non-toxic compound and has application in food, paint, and pharmaceutical industries. At an industrial scale, glycerol is commonly produced by saponification and transesterification reactions.
2. The glycerol coming out of biodiesel manufacturing plants usually contains methanol, water, and acid or base as impurities. Consequently, it remains unfit for the edible or pharma industries and thus having low commercial value.
3. Acetins, including mono-, di- and triacetin, are an essential category of glycerol derivatives, frequently prepared *via* glycerol acetylation employing acetic acid or acetic anhydride as acetylating agents.
4. Mono-, di-, and triacetin can be utilized by many industries, such as cosmetics, pharmaceutical, leather, and food. TA and DA are used in the fuel industry, besides, TA

is employed as an additive to improve the anti-knocking property of gasoline, and to improve the viscosity and cold flow property of biofuel.

5. The acetins are frequently produced *via* a homogeneous Brønsted acid catalysed process. However, such catalysts are corrosive, non-reusable, difficult to separate from the reaction mixture, and sensitive to water, which is formed as a by-product during the glycerol acetylation.
6. To address the issues related to the homogeneous acids, Brønsted or Lewis acidic group have been immobilized over various matrices (e.g. mixed metal oxides, mesoporous silica, ion exchange resins, carbon, zeolites, and magnetic nanoparticles) to prepare the heterogeneous acidic catalysts for the glycerol acetylation.
7. In spite of having the advantage of reusability, reported heterogeneous catalysts often suffer the drawbacks of poor stability and limited reusability. Therefore more efforts must be made to have the catalyst with better stability.

1.10. Lacunae

Glycerol has been esterified to yield TA, DA, and MA in the presence of homogeneous and heterogeneous catalysts, and the following lacunae have been identified based on the literature survey.

i. In most of the reports, homogeneous catalysts have been employed, showing higher catalytic activity and selectivity towards the desired products but causes the reactor corrosion and demand extensive product purification step. Moreover, for product purification water could not be used due to the miscibility of acetins and GL in water.

ii. Compared to homogeneous catalysts, reported heterogeneous acidic catalysts provided insufficient GL conversion levels coupled with poor triacetin selectivity. In addition, the limited reusability of the reported heterogeneous catalysts, owing to their lesser stability, is another concern that limits their application at a commercial scale.

iii. The separation of the heterogeneous catalyst was mainly conducted either by centrifugation or simple filtration, which is a time-consuming process. Magnetic catalyst and their separation under the influence of external magnetic field from the reaction mixture have not been explored to a significant extent.

1.11. Objectives

1. Development of the mixed metal oxides based solid catalysts for the acetins synthesis from glycerol.
2. Characterization of the surface basic or acidic sites by temperature programmable desorption study and structural properties (by powder XRD) of the catalysts.
3. To test the efficacy of the prepared catalyst for the esterification of glycerol and optimizing the corresponding reaction parameters and study the kinetics of the reaction.

References

[1] Mario, P.; Michele, R. The future of glycerol 2nd Edition. *RSC Green Chem*. **2010**, 8, 1757-7040. https://doi.org/10.1039/9781849731089

[2] Chozhavendhan, S.; Devi, G. K.; Bharathiraja, B.; Kumar, R. P.; Elavazhagan, S. 9-Assessment of crude glycerol utilization for sustainable development of biorefineries, *Refining Biomass Residues for Sustainable Energy and Bioproducts* **2020**, 195-212. DOI: 10.1016/B978-0-12-818996-2.00009-0

[3] Songcheng, X.; Min, Gu, Kun, W.; and Guoying, L. Unraveling the interaction mechanism between collagen and alcohols with different chain lengths and hydroxyl positions. *Colloids Surf B: Bioint*. **2021**, 199, 111559. doi: 10.1016/j.colsurfb.2021.111559

[4] Nur, I. W. A.; Aizi, N. M.; Ramli, Nor, H. A.; Manas, Nurrulhidayah, S.; Rohaida, C. M.; Hesham, E. E. Glycerol In Food, Cosmetics And Pharmaceutical Industries: Basics And New Applications. *Int. J. Sci. Technol. Res*. **2019**, 8(12), 2277-8616. Corpus ID: 21654924

[5] Tan, H. W.; Abdul Aziz, A. R.; Aroua, M. K. Glycerol production and its applications as a raw material: A review. *Renew. Sustain. Energy Rev*., **2013**, 27, 118–127. https://doi.org/10.1016/j.rser.2013.06.035

[6] Quispe, C. A. G.; Coronado, C. J. R.; Carvalho, J. R. Glycerol: Production, consumption, prices, characterization and new trends in combustion. *Renew. Sustain. Energy Rev*. **2013**, 27, 475–493. http://dx.doi.org/10.1016/j.rser.2013.06.017

[7] Giuseppe, B.; Adolfo, I.; Aimaro, S.; Angelo, B. Glycerol Production and Transformation: A Critical Review with Particular Emphasis on Glycerol Reforming Reaction for Producing Hydrogen in Conventional and Membrane Reactors. *Membranes* **2017**, **7**, 17. doi: 10.3390/membranes7020017

[8] Lucio, L. Mechanism of Fat Splitting. *Ind. Eng. Chem. Res*., **1949**, 41, 4, 786–790. https://doi.org/10.1021/ie50472a025

[9] H. N. Bhatti, M. A. Hanif, and M. Qasim, Ata-ur-Rehman; Biodiesel production from waste tallow, Fuel, 2008, **87**, 2961–6. https://doi.org/10.1021/ie50472a025

[10] Jing, H. ; Yun, Z.; Muhammad, Y.; Huiying, Q.; Ruining, H.; Zhangfa, T. Fabrication of hollow cage-like CaO catalyst for the enhanced biodiesel production via transesterification of soybean oil and methanol. *Fuel* **2021**, 290, 119799. https://doi.org/10.1016/j.fuel.2020.119799

[11] Dean, A. O. C.; Allen, L. H. A.; Karl, T. Z. C.; Kevin, W. A. H. United States Patent (19). US005677160A. 11 Patent Number: 45. 5,677, **1997**, 160, 61-181390 8/1996 Japan. WO82,03873 11/1982 WIPO.

[12] Kong, P. S.; Aroua, M. K.; Daud, W. M. A. W. Conversion of crude and pure glycerol into derivatives: A feasibility evaluation. *Renew. Sustain. Energy Rev*. **2016**, 63, 533–555. https://doi.org/10.1016/j.rser.2016.05.054

[13] Dorota, S.; Katarzyna, L.; Włodzimierz, G. Impurities of crude glycerol and their effect on metabolite production. *Ann. Microbiol*. **2014**, 64, 891–898. doi: 10.1007/s13213-013-0767-x

[14] Bernardini, C. M. Process technology for Oleo Chemical Industry. https://www.cmbernardini.com/

[15] Glycerol Market Size, Share & Trends Analysis Report by Source (Biodiesel, Fatty Acids, Fatty Alcohols, Soap), by Region, And Segment Forecasts, **2020-2027**.

[16] Freedman, B. Methyl ester-manufacture and utilization. U.S. Department of Agriculture, Peoria, Illinois.

[17] Kale, S. B.; Lali, A. M.; Patel, B. M.; Jha, P.; Vanza, M. J.; Yelne, P. M.; Vinod, G.; Ashwani, K. K; Vineet, M. International Application Published Under the Patent Cooperation Treaty (Pct). *International Publication*. WO 2017/119007 Al.

[18] Israel, A U.; Obot, I. B.; Asuquo, J. E. Recovery of Glycerol from Spent Soap Lye by-Product of Soap Manufacture. *E-Journal Chem*. **2008**, 5(4), 940-945. DOI: 10.1155/2008/302609

[19] George, A.; Ypatia, Z.; Stamoulis, S.; Stamatis, K. Transesterification of Vegetable Oils with Ethanol and Characterization of the Key Fuel Properties of Ethyl Esters. *Energies*, **2009**, 2, 362-376. DOI: 10.3390/en20200362

[20] Chao, C.; Lei, C.; Lei, Z.; Wenqian, F.; Yanping, H.; Xiu, G.; Yan, J.; Liang, L.; Xianzai, Y.; Guoqiang, W. Transesterification of rice bran oil to biodiesel using mesoporous NaBeta zeolite-supported molybdenum catalyst: Experimental and kinetic studies. *Chem. Eng. J*., **2019**, 382, 122839. https://doi.org/10.1016/j.cej.2019.122839

[21] Polyesters, O.V.; Tessa, H.; Christopher, P.; Manjusri, M.; Amar, M. Improved utilization of crude glycerol from biodiesel industries: Synthesis and characterization of sustainable bio-based polyesters. *Ind. Crops Prod*., **2015**, 78, 141–147. DOI: 10.1016/j.indcrop.2015.10.019

[22] Benjamin, L. W.; Shuo, L.; Melanie, T.; David, S.; Mahdi, M. A. Solvent-Free Methods for Making Acetals Derived from Glycerol and Furfural and Their Use as a Biodiesel Fuel Component. *ACS Catal*., **2012**, 2(12), 2524–2530.https://doi.org/10.1021/cs300562e

[23] Sönnichsen, N. https://www.statista.com/statistics/271472/biodiesel-production-in-selected-countries/, **2021**

[24] Simone, P. S.; Joaquim, E. A. S.; Luiz, A. H. N. Feed stocks for biodiesel production: Brazilian and global perspectives. *Taylor and Francis*, **2018**, 9, 455-478. https://doi.org/10.1080/17597269.2017.1278931

[25] OECD-FAO Agricultural Outlook, **2020-2029**. http://www.fao.org/publications/oecd-fao-agricultural

[26] João, R. M. A.; Léia, C. L. F.; Betania, F. Q. Biodiesel biorefinery: opportunities and challenges for microbial production of fuels and chemicals from glycerol waste. *Biotechnol. Biofuel.* **2012**, 5, 48, http://www. biotechnologyforbiofuels.com/content/5/1/48

[27] Okoye, P. U.; Abdullah, A. Z.; Hameed, B. H. A review on recent developments and progress in the kinetics and deactivation of catalytic acetylation of glycerol-A by-product of biodiesel. *Renew. Sustain. Energy Rev*. **2017**, 74, 387-401. https://doi.org/10.1016/j.rser.2017.02.017

[28] Ardi, M. S.; Aroua, M. K.; Hashim, N. A. Progress, prospect and challenges in glycerol purification process: a review. *Renew. Sustain. Energy Rev*. **2015**, 42, 1164–73. https://doi.org/10.1016/j.rser.2014.10.091

[29] https://www.sciencedirect.com/topics/engineering/crude-glycerolI.

[30] Usman, N.; Irmawati, B. R.; Ernee, N. M.; Norsahida, A.; Uchenna, F. A.; Yun, H. T. Influence of Heterogeneous Catalysts and Reaction Parameters on the Acetylation of Glycerol to Acetin: A Review. *Appl. Sci*. **2020**, 10, 7155. DOI: 10.3390/app10207155

[31] He, Q. S.; Mcnutt, J.; Yang, J. Utilization of the residual glycerol from biodiesel production for renewable energy generation. *Renew. Sustain. Energy Rev*. **2017**, 71, 63–76. DOI: 10.1016/j.rser.2016.12.110

[32] Manosak, R.; Limpattayanate, S.; Quispe, M. H. Sequential-refining of crude glycerol derived from waste used-oil methyl ester plantvia a combined process of chemical and adsorption. *Fuel Proc. Technol.* **2009**, 92, 92–99. doi:10.1016/j.fuproc.2010.09.

[33] Pagliaro, M.; Ciriminna, R.; Kimura, H.; Rossi, M.; Pina, C. Recent advances in the conversion of bioglycerol into value-added products. *Europ. J. Lipid Sci. Technol*. **2009**, 111, 788–799. https://doi.org/10.1002/ejlt.200800210

[34] Tan, H. W.; Aziz, A. R. A.; Aroua, M. K. Glycerol production and its applications as a raw material: A review. *Renew. Sustain. Energy Rev*. **2013**, 27, 118–127. https://doi.org/10.1016/j.rser.2013.06.035

[35] Fangxia, Y.; Milford, A. H.; Runcang, S. Value-added uses for crude glycerol–a byproduct of biodiesel production. *Biotechnol. Biofuels* **2012**, 5, 13. http://www.biotechnologyforbiofuels.com/content/5/1/13

[36] Niravkumar, M. K.; Mahdieh, S.; Bijaya, K. U.; Sudip, K. R. Valorization of Biodiesel Byproduct Crude Glycerol for the Production of Bioenergy and Biochemicals. *Catalysts* **2020**, 10, 609. DOI: 10.3390/catal10060609

[37] Uprety, B. K.; Chaiwong, W.; Ewelike, C.; Rakshit, S. K. Biodiesel production using heterogeneous catalysts including wood ash and the importance of enhancing byproduct glycerol purity. *Energy Con. Management* **2016**, 115, 191–199. DOI: 10.1016/j.enconman.2016.02.032

[38] Dosuna-Rodríguez, I.; Gaigneaux, E. M. Glycerol acetylation catalysed by ion exchange resins. *Catal. Today* **2012**, 195, 14–21. https://doi.org/10.1016/j.apcata.2014.10.059

[39] Avneet, K.; Amjad, A.; Lithium Zirconate as a Selective and Cost-Effective Mixed Metal Oxide Catalyst for Glycerol Carbonate Production. *Ind. Eng. Chem. Res*. **2020**, 59, 2667−2679. DOI: 10.1021/acs.iecr.9b05747

[40] Kim, E. Y. Etherification of glycerol with isobutene on Amberlyst 35 ion exchange resin catalyst in presence of a cationic emulsifier. *Revista de Chimie.* **2009**, 60, 1338–1342.

[41] Huang, R.; W. Wang, Catalytic Synthesis of Glycerol tert-Butyl Ethers as Fuel Additives from the Biodiesel By-Product Glycerol. *J. Chem*. **2015**, 6. http://dx.doi.org/10.1155/2015/763854

[42] Farinha, J.; Caiado, M.; Castanheiro, J. E. Valorisation of glycerol into biofuel additives over heterogeneous catalysts. *Formatex Research Center* **2013**, 13, 422-429. DOI: 978-84-939843-7-3.

[43] Yanli, W.; Jinxia, Z.; Xinwen, G. Catalytic Hydrogenolysis of Glycerol to Propanediols: A Review, *RSC Adv*., 2015, **5**, 74611-74628. https://doi.org/10.1039/C5RA11957J

[44] Arun, P.; Pudi, S. M.; Biswas, P. Acetylation of Glycerol over Sulfated Alumina: Reaction Parameter Study and Optimization Using Response Surface Methodology, Energy Fuels, 2016, **30**, 584−593. DOI: 10.1021/ACS.ENERGYFUELS.5B01901

[45] Song, X.; Wu, Y.; Cai, F.; Pan, D.; Xiao, G. M. High-efficiency and low-cost Li/ZnO catalysts for synthesis of glycerol carbonate from glycerol transesterification: The role of Li and ZnO interaction. Appl. Catal. A: Gen., 2017, **532**, 77–85. https://doi.org/10.1016/j.apcata.2016.12.019

[46] Trejda, M.; Stawicka, K.; Dubinska, A.; Ziolek, M. Development of niobium containing acidic catalysts for glycerol esterification, Catal. Today, 2012, **187**, 129– 134.DOI: 10.1016/J.CATTOD.2011.10.033

[47] Konwar, L. J.; Mäki-Arvela, P.; Begum, P.; Ashim, N. K.; Thakur, J.; Mikkol, J.; Dek, R. C.; Dek, D. Shape selectivity and acidity effects in glycerol acetylation with acetic anhydride: Selective synthesis of triacetin over Y-zeolite and sulfonated mesoporous carbons, J. Catal., 2015, **329**, 237–247. https://doi.org/10.1016/j.jcat.2015.05.021

[48] Wypych, A. Databook of Plasticizers (Second Edition), **2017**, https://www.sciencedirect.com/topics/engineering/monoacetin

[49] Bakht, Z.; Seongjoon, J.; Chonglong, W.; Tenzin, T.; Seong-Hee, J.; Hogyun, S.; Jung-Hoon, S.; Kyung-Jin, K.; Seon-Won, K. Metabolic engineering of Escherichia coli for production of non-natural acetins from glycerol†. *Green Chem*. **2020**, 22, 7788-7802. DOI: 10.1039/D0GC02395G

[50] Hu, W.; Zhang, Y.; Huang, Y.; Wang, J.; Gao, J.; Xu, J. Selective esterification of glycerol with acetic acid to diacetin using antimony pentoxide as reusable catalyst. *J. Energy Chem*. **2015**, 24, 632–636. DOI: 10.1016/j.jechem.2015.08.001

[51] Rastegari, H.; Ghaziaskar, H. S.; Yalpani, M. Valorization of biodiesel derived glycerol to acetins by continuous esterification in acetic acid: focusing on high selectivity to diacetin and triacetin with no byproducts. *Ind. Eng. Chem. Res*. **2015**, 54, 3279–3284. https://doi.org/10.1021/acs.iecr.5b00234

[52] Meireles, B. A.; Pereira, V. L. P. Synthesis of bio-additives: transesterification of ethyl acetate with glycerol using homogeneous or heterogeneous acid catalysts. *J. Braz. Chem. Soc*. **2013**, 24, 17–25. DOI: 10.1590/S0103-50532013000100004

[53] Rachel, C. E.; Michael, S.; Lindsay, S. Cold Flow Properties of Fatty Acid Methyl Ester Blends with and without Triacetin. *Energy Fuels* **2016**, 30, 7400−7409. https://doi.org/10.1021/acs.energyfuels.6b01334

[54] Bonet, J.; Costa, J.; Sire, R.; Reneaume, J.; Pleşu, A.E.; Pleşu, V.; Bozga, G. Revalorization of glycerol: Comestible oil from biodiesel synthesis. 2009, 87(3), 171-178, https://doi.org/10.1016/j.fbp.2009.06.003

[55] Nuno, G.; Ricardo, S.; Bruno, G.; Rui, S.; Artur, F. Triacetin as a Secondary PVC Plasticizer. *J. Polymers Environ*. **2019**, 27, 1294–1301. DOI: 10.1007/s10924-019-01432-z

[56] Nebel, B.; Mittelbach, M.; Uray, G. Determination of the composition of acetylglycerol mixtures by 1H NMR followed by GC investigation. *Anal. Chem*. **2008**, 80, 8712. https://doi.org/10.1021/ac800706s

[57] Zhou, C. H.; Beltramini, J. N.; Fan, Y. X.; Lu, G. Q. Chemoselective catalytic conversion of glycerol as a biorenewable source to valuable commodity chemicals. *Chem. Soci. Rev.* 2008, 37, 527. https://doi.org/10.1039/B707343G

[58] Khadijeh, B. G.; Nilofar, A.; Mohd, A. Y.; Mohd, Mesoporous phosphated and sulphated silica as solid acid catalysts for glycerol acetylation. *Chem. Papers.* **2014**, 68(9), 1194–1204. DOI: 10.2478/s11696-014-0550-x

[59] Bagheri, S.; Julkapli, N. M.; Yehye, W. A. Catalytic conversion of biodiesel derived raw glycerol to value added products. *Renew. Sustain. Energy Rev*. **2015**, 41, 113–127. DOI: 10.1016/j.rser.2014.08.031

[60] Patel, A.; Singh, A. S. Green and sustainable approach for esterification of glycerol using 12-tungstophosphoric acid anchored to different supports: kinetics and effect of support. *Fuel*, **2014**, 118, 358–64. https://doi.org/10.1016/j.fuel.2013.11.005

[61] Rao, P. V.; Rao, B. V. A. Effect of adding Triacetin additive with Coconut oil methyl ester (COME) in performance and emission characteristics of DI diesel engine. *Int. J. Therm. Technol*. **2011**, 1(1), 2277–4114.

[62] Mufrodi, Z.; Rochmadi, R.; Sutijan, S.; Budiman, A. Synthesis acetylation of glycerol using batch reactor and continuous reactive distillation column. *Eng. J*. **2014**, 18, 29–40. DOI: https://doi.org/10.4186/ej.2014.18.2.29

[63] Ferreira, P.; Fonseca, I. M.; Ramos, M.; Vital, J.; Castanheiro J. E. Esterification of glycerol with acetic acid over dodecamolybdophosphoric acid encaged in USY zeolite. *Catal. Commun*. **2009**, 10, 481–4. DOI: 10.1016/j.catcom.2008.10.015

[64] Ferreira, P.; Fonseca, I. M.; Ramos, M.; Vital, J.; Castanheiro J. E. Acetylation of glycerol over heteropolyacids supported on activated carbon. *Catal. Commun*. **2011**, 12, 573–576. https://doi.org/10.1016/j.catcom.2010.11.022

[65] https://www.sciencedirect.com/topics/neuroscience/triacetin.

[66] https://www.marketwatch.com/press-release/triacetin-market-**2021**-global-industry analysis-by-top-countries-data-types-and-application-top-key-players-regions-and forecast-by-**2026-2021**-04-05.

[67] https://www.globenewswire.com/news-release/**2020**/07/29/2069278/0/en/Global Triacetin-Industry.html.

[68] Abida, K.; Chudasama, B.; Ali, A.; Development and functionalization of magnetic nanoparticles as stable and reusable catalysts for triacetin synthesis†. *New J. Chem*. **2020**, 44, 9365-9376. https://doi.org/10.1039/D0NJ00488J

[69] Wong, W.; Lim, S.; Pang, Y.; Shuit, S.; Chenc, W.; Lee, K. Synthesis of renewable heterogeneous acid catalyst from oil palm empty fruit bunch for glycerol-free biodiesel production. *Sci. Total Environ*. **2020**, 727, 138534. https://doi.org/10.1016/j.scitotenv.2020.138534

[70] Silva, L. N.; Gonçalves, V. L. C.; Mota, C. J.A. Catalytic acetylation of glycerol with acetic anhydride. *Catal. Commun*. **2010**, 11, 1036–1039. https://doi.org/10.1016/j.catcom.2010.05.007

[71] Shao, G. N.; Sheikh, R.; Hilonga, A.; Lee, J. E.; Park, Y.; Kim, H. T. Biodiesel production by sulfated mesoporous titania–silica catalysts synthesized by the sol–gel process from less expensive precursors. *Chem. Eng. J*. **2013**, 215(216), 600–607. https://doi.org/10.1016/j.cej.2012.11.059

[72] Sendzikiene, E.; Makareviciene, V. Biodiesel fuel synthesis by interesterification of triglycerides with carboxylate esters of low molecular weight. *Rev. Chem. Eng*. **2021**, 37(2), 259-276. DOI: 10.1515/revce-2018-0083

[73] Dhawan, M. S.; Barton, S. C.; Yadav, G. D. Interesterification of triglycerides with methyl acetate for the co-production biodiesel and triacetin using hydrotalcite as a heterogenous base catalyst, *Catal. Today*, **2020**, DOI: 10.1016/j.cattod.2020.07.056.

[74] Brondani, L. N.; Ribeiro, J. S.; Castilhos, F. A new kinetic model for simultaneous interesterification and esterification reactions from methyl acetate and highly acidic oil. *Renew. Energy*, **2020**, 156, 579-590. https://doi.org/10.1016/j.renene.2020.04.063

[75] Kong, P. S.; Aroua, M. K.; Wan, D. W. A.; Lee, H. V.; Cognet, P.; Pérès, Y. Catalytic role of solid acid catalysts in glycerol acetylation for the production of bio-additives: a review. *RSC Adv*. **2016**, 6, 68885–68905. https://doi.org/10.1039/C6RA10686B

[76] https://www.indiamart.com/proddetail/acetic-acid-6238559212.html.

[77] https://www.pharmacompass.com/price/acetic-anhydride.

[78] https://www.unodc.org/documents/india/ccch5.pdf.

[79] Liao, X.; Zhu, Y.; Wang, S.; Li, Y. Producing triacetylglycerol with glycerol by two steps: Esterification and acetylation. *Fuel Proc. Technol*. **2009**, 90, 988–993. DOI: 10.1016/j.fuproc.2009.03.015

[80] Chandrakala, U.; Prasad, R. B. N.; Devi, B. L. A. Glycerol Valorization as Biofuel Additives by Employing a Carbon-Based Solid Acid Catalyst Derived from Glycerol. *Ind. Eng. Chem. Res*. **2014**, 53, 42, 16164–16169. https://doi.org/10.1021/ie503079m

[81] Liao, X.; Zhu, Y.; Wang, S. G.; Chen, H.; Li, Y. Theoretical elucidation of acetylating glycerol with acetic acid and acetic anhydride. *Appl. Catal. B: Environ*. **2010**, 94, 64-70. DOI: 10.1016/j.apcatb.2009.10.021

[82] Laís, P. D.; Débora, M. K.; André, M. F. W.; Claudiney, S. C.; Microwave-irradiated acetylation of glycerol catalyzed by acid activated clays. *Reaction Kinetics, Mech. Catal*. **2019**, 127, 991–1004. https://doi.org/10.1007/s11144-019-01594-w

[83] Cayo, E. G.; Letícia, O. L.; Abiney, L. C.; Márcio, J. S.; Bioadditive synthesis from $H_3PW_{12}O_{40}$-catalyzed glycerol esterification with HOAc under mild reaction conditions. *Fuel Proc. Technol*. **2012**, 102, 46–52. https://doi.org/10.1016/j.fuproc.2012.04.027

[84] Russbueldt, B.; Hoelderich, W. New rare earth oxide catalysts for the transesterification of triglycerides with methanol resulting in biodiesel and pure glycerol. *J. Catal*. **2010**, 271, 290. https://doi.org/10.1016/j.jcat.2010.02.005

[85] Testa, M. L.; Parola, V. L.; Liotta, L. F.; Venezia, A. M. Screening of different solid acid catalysts for glycerol acetylation. *J. Mol. Catal. A: Chem*. **2013**, 367, 69–76. DOI: 10.1016/j.molcata.2012.10.027

[86] Dosuna-Rodriguez, I.; Adriany, C.; Gaigneaux, E. M. Glycerol acetylation on sulphated zirconia in mild conditions. *Catal. Today*, **2011**, 167, 56–63. https://doi.org/10.1016/j.cattod.2010.11.057

[87] Khayoon, M. S.; Hameed, B. H. Acetylation of glycerol to biofuel additives over sulfated activated carbon catalyst. *Bioresour Technol*. **2011**, 102, 9229–9235. https://doi.org/10.1016/j.biortech.2011.07.035

[88] Reddy, P. S.; Sudarsanam, P.; Raju, G.; Reddy, B. M. Selective acetylation of glycerol over CeO_2–M and SO_4^{2-}/CeO_2–M (M = ZrO_2 and Al_2O_3) catalysts for synthesis of bioadditives. *J. Ind. Eng. Chem*. **2012**, 18, 648–654. https://doi.org/10.1016/j.jiec.2011.11.063

[89] Vijay kumar, S.; Marakatti, S. M.; Eric, M. G. Sulfated Zirconia an Efficient Catalyst for the Friedel- Crafts Monoalkylation of Resorcinol with Methyl tertiary butyl ether to 4-Tertiary butylresorcinol. *New J. Chem*. **2019**, 43, 7733-7742. https://doi.org/10.1039/C9NJ01311C

[90] Nasrallah, M. D. The comparative jurisprudence of catalysts preparation methods: I. precipitation and impregnation methods. *J. Ind. Environ. Chem*. 2018, 2(1), 19-21. http://www.alliedacademies.org/journal-industrial-environmental-chemistry/

[91] Laura, M. E.; Juliana, L. S.; Alexander, C.; Hugo, A. O.; Fabio, B. P. Catalyst preparation methods to reduce contaminants in A high-yield purification process of multiwalled carbon nanotubes. *Braz. J. Chem. Eng*. **2019**, 36(4), 1678-4383. dx.doi.org/10.1590/0104-6632.20190364s20190251

[92] Meng, C.; Cao, G.; Li, X.; Yan, Y.; Zhao, E.; Hou, L.; Shi, H. Structure of the SO_4^{2-}/TiO_2 solid acid catalyst and its catalytic activity in cellulose acetylation. *React. Kinet. Mech. Catal*. **2017**, 121(2), 719–734. DOI: 10.1007/s11144-017-1165-3

[93] David, J. Z.; Saeed, A.; Patricia, K.D. Characterization of catalytically active sulfated zirconia. *Catal. Today* **1999**, 53, 419–432. https://doi.org/10.1016/S0920-5861(99)00137-6

[94] Ward, A. J.; Pujari, A. A.; Costanzo, L.; Masters, A. F.; Maschmeyer, T. Ionic liquid-templated preparation of mesoporous silica embedded with nanocrystalline sulfated zirconia. *Nanoscale Res. Lett*. **2011**, 6, 192. doi: 10.1186/1556-276X-6-192.

[95] Wei, T.; Jiaming, W.; Lulu, L.; Annai, L.; Ge, S.; Kai, G.; Yidan, L.; Fudong, L.; Fei, G.; Lin, D. Gas phase sulfation of ceria-zirconia solid solutions for generating highly efficient and SO_2 resistant NH_3-SCR catalysts for NO removal. *J. Hazardous Mat*. **2020**, 388, 121729. https://doi.org/10.1016/j.jhazmat.2019.121729

[96] Yang, S.; Guo, Y.; Chang, H.; Ma, L.; Peng, Y.; Qu, Z.; Yan, N.; Wang, C.; Li, J. Novel effect of SO_2 on the SCR reaction over CeO_2: Mechanism and significance. *Appl. Catal. B: Environ*. **2013**, 136, 19-28. https://doi.org/10.1016/j.apcatb.2013.01.028

[97] Zhang, L.; Zou, W.; Ma, K.; Cao, Y.; Xiong, Y.; Wu, S.; Tang, C.; Gao, F.; Dong, L. Sulfated temperature effects on the catalytic activity of CeO_2 in NH_3-selective catalytic reduction conditions. *J Phy. Chem. C* **2015**, 119, 1155-1163. https://doi.org/10.1021/jp511282c

[98] Abida, K.; Ali, A. Sulphuric acid-functionalized siliceous zirconia as an efficient and reusable catalyst for the synthesis of glycerol triacetate. *Chem. Papers* **2020**, 74, 3627–3639. https://doi.org/10.1007/s11696-020-01189-z

[99] Xiaomin, D.; Dinesh, M.; Charles, U. P.; Shuo, Y. Remediating fluoride from water using hydrous zirconium oxide. *Chem. Eng. J*. **2012**, 198(199), 236–245. https://doi.org/10.1016/j.cej.2012.05.084

[100] Kamlesh, P.; Manjeet, J.; Ashwini, K. A. In situ synthesis of Ag–SiO_2 Janus particles with epoxy functionalityfor textile applications. *Particuology* **2015**, 19, 107-112. https://doi.org/10.1016/j.partic.2014.06.007

[101] Testa, M. L.; Parola, V. L.; Mesrar, F.; Ouanji, F.; Kacimi, M.; Ziyad, M.; Liotta, L. F. Use of Zirconium Phosphate-Sulphate as Acid Catalyst for Synthesis of Glycerol-Based Fuel Additives. *Catalysts* **2019**, 9, 148. https://doi.org/10.3390/catal9020148

[102] Jin, T.; Yamaguchi, T.; Tanabe, K. Mechanism of acidity generation on sulfurpromoted metal oxides. *J. Phys. Chem*. **1986**, 90, 4794-4796. https://doi.org/10.1021/j100411a017

[103] Waqif, M.; Bazin, P.; Saur, O.; Lavalley, J.C.; Blanchard, G.; Touret, O. Study of ceria sulfation. *Appl. Catal. B Environ*. **1997**, 11, 193-205. https://doi.org/10.1016/S0926-3373(96)00040-9

[104] Markovic, M.; Fowler, B.O.; Tung, J.; Preparation and comprehensive characterization of a calcium hydroxyapatite reference material. *Res. Natl. Inst. Stand. Technol*. **2004**, 109, 553-568. doi: 10.6028/jres.109.042

[105] Escalona, P. E.; Peñarroya, M. M.; Otero, A. C.; Zecchina, A. FTIR Studies on the Acidity of Sulfated Zirconia Prepared by Thermolysis of Zirconium Sulfate. *J. Catal*. **1996**, 162, 268–276. https://doi.org/10.1006/jcat.1996.0284

[106] Rack, S. J.; Hee, S. D. Preparation of new solid superacid catalyst, zirconium sulfate supported on alumina and activity for acid catalysis. *Catal. Today* **2003**, 87, 219–226. https://doi.org/10.1016/j.cattod.2003.09.010

[107] Takarroumta, N.; Kacimi, M.; Bozon-Verduraz, F.; Liotta, L. F.; Ziyad, M. Characterization and performance of the bifunctional platinum-loaded calcium-hydroxyapatite in the one-step synthesis of methyl isobutyl ketone. *J. Mol. Catal. A* **2013**, 377, 42–50. https://doi.org/10.1016/j.molcata.2013.04.017

[108] Liu, Z. L.; Wang, X.; Yao, K. L.; Du, G. H.; Lu, Q. H.; Ding, Z. H.; Tao, J. Synthesis of magnetite nanoparticles in W/O microemulsion. *J. Mater. Sci*. **2004**, 39, 2633–2636. https://doi.org/10.1023/B:JMSC.0000020046.68106.22

[109] Pourjavadi, A.; Hosseini, S. H.; Doulabi, M.; Fakoorpoor, S. M.; Seidi, F. Multi-Layer Functionalized Poly(Ionic Liquid) Coated Magnetic Nanoparticles: Highly Recoverable and Magnetically Separable Brønsted Acid Catalyst. *ACS Catal*. **2012**, 2, 1259–1266. https://doi.org/10.1021/cs300140j

[110] Periasamy, A.; Muruganand, S.; Palaniswamy, M. Vibrational studies of Na_2SO_4, K_2SO_4, $NaHSO_4$ and $KHSO_4$ crystals. Rasayan J. Cheme. 2009, 4, 981-989.

[111] Khan, S.; Kaur, G.; Singh, K. Effect of ZrO_2 on dielectric, optical and structural properties of yttrium calcium borosilicate glasses. *Ceram. Int*. **2017**, 43, 722–727. https://doi.org/10.1016/j.ceramint.2016.09.219

[112] Hino, H.; Kurashige, M.; Matsuhashi, H.; Arata, K. The surface structure of sulfated zirconia: studies of XPS and thermal analysis. *Thermochim Acta*. **2006**, 441, 35–41. https://doi.org/10.1016/j.tca.2005.11.042

[113] Chernavskii, P. A.; Khodakov, A. Y.; Pankina, G. V. In situ characterization of the genesis of cobalt metal particles in silica-supported Fischer–Tropsch catalysts using Foner magnetic method. *Appl. Catal. A Gen*. **2006**, 306, 108–119. https://doi.org/10.1016/j.apcata.2006.03.033

[114] Malhotra, R.; Ali, A.; 5-Na/ZnO doped mesoporous silica as reusable solid catalyst for biodiesel production via transesterification of virgin cottonseed oil. *Renew. Energy* **2019**, 133, 606–619. https://doi.org/10.1016/j.renene.2018.10.055

[115] Desmartin-Chomel, A.; Flores, J. L.; Bourane, A.; Clacens, J. M.; Figueras, F.; Delahay, G.; Giroir, F. A.; Lehaut-Burnouf, C. Calorimetric and FTIR study of the acid properties of sulfated titanias. *J Phys Chem B* **2006**, 110, 858–863. https://doi.org/10.1021/jp0530698

[116] Liu, C.; Wang, H.; Bia, Y.; Zhang, Z.; A study on the selective catalytic reduction of NOx by ammonia on sulphated iron-based catalysts. *RSC Adv*. **2020**, 10, 40948. https://doi.org/10.1039/D0RA06697D

[117] Yuanpeng, W.; Tao, Z.; Zhaohui, Z.; Xiaobin, D.; Yuxing, P. A facile approach to Fe_3O_4@Au nanoparticles with magnetic recyclable catalytic Properties. *Mater. Res. Bull*. **2010**, 45, 513–517. https://doi.org/10.1016/j.materresbull.2009.11.012

[118] Pacheco, R. F.; Arruebo, M.; Marquina, C.; Ibarra, R.; Arbiol, J.; Santamaria, J. Highly magnetic silica-coated iron nanoparticles prepared by the arc-discharge method. *Nanotechnol.* **2006**, 17, 1188–1192. DOI: 10.1088/0957-4484/17/5/004

[119] Allen, G. C.; Curtis, M. T.; Hooper, A. J.; Tucker, P. M. X-Ray photoelectron spectroscopy of iron–oxygen systems. *J. Chem. Soc. Dalton Trans*. **1974**, 1525–1530. https://doi.org/10.1039/DT9740001525

[120] Wang, L.; Liu, Q.; Zhou, M.; Xiao, G. Synthesis of glycerin triacetate over molding zirconia-loaded sulfuric acid catalyst. *J. Natural Gas Chem*. **2012**, 21, 25-28. https://doi.org/10.1016/S1003-9953(11)60328-9

[121] Song, W.; Lai, W.; Lian, Y.; Jiang, X.; Yang, W. Sulfated ZrO_2 supported CoMo sulfide catalyst by surface exsolution for enhanced hydrodeoxygenation of lignin derived ethers to aromatics. *Fuel*, **2020**, 263, 116705. DOI: 10.1016/j.fuel.2019.116705

[122] Karnjanakom, S.; Maneechakr, P.; Samart, C.; Guan, G. Ultrasound-assisted acetylation of glycerol for triacetin production over green catalyst: A liquid biofuel candidate. *Energy Con. Manag*. **2018**, 173, 262–270. DOI: 10.1016/j.enconman.2018.07.086

[123] Nda-Umar, U. I.; Ramli, I.; Muhamad, E. N.; Taufiq-Yap, Y. H.; Azri, N. Synthesis and characterization of sulfonated carbon catalysts derived from biomass waste and its evaluation in glycerol acetylation. *Biomass Con. Biorefinery* **2020**, https://doi.org/10.1007/s13399-020-00784-0.

[124] Ramalingam, R. J.; Appaturi, J. N.; Pulingam, T.; Al-Lohedan, H. A.; Al-dhayan, D. M. In-situ incorporation of ruthenium/copper nanoparticles in mesoporous silica derived from rice husk ash for catalytic acetylation of glycerol. *Renew. Energy* **2020**, 160, 564-574. DOI: 10.1016/j.renene.2020.06.095

[125] Ifrah, S.; Li, W.; Buissette, V.; Denaire, S.; Coelho, J.; Miguel, M. R. Cerium-and zirconium-based mixed oxides, U.S. Patent Application, 2019, **16(96)**, 279. WO/2017/185224

[126] Kulkarni, R. M.; Britto, P. J.; Narula, A.; Saqline, S.; Anand, D.; Bhagyalakshmi, C.; N. Herle, R. Kinetic studies on the synthesis of fuel additives from glycerol using CeO_2–ZrO_2 metal oxide catalyst. *Biofuel Res. J.* **2020**, 25, 1100-1108. DOI: 10.18331/BRJ2020.7.1.2

[127] P. S. Reddy, P. Sudarsanam, G. Raju, and B. M. Reddy, Synthesis of bio-additives: Acetylation of glycerol over zirconia-based solid acid catalysts, Catal. Commun., 2010, **11**, 1224–1228. DOI: 10.1016/j.catcom.2010.07.006

[128] Gawande, M. B.; Pandey, R. K.; Jayaram, R. V. Role of mixed metal oxides in catalysis science-versatile applications in organic synthesis. *Catal. Sci. Technol*. **2012**, 2, 1113–1125. DOI: 10.1039/C2CY00490A

[129] Rane, S. A.; Pudi, S. M.; Biswas, P. Esterification of Glycerol with Acetic Acid over Highly Active and Stable Alumina-based Catalysts: A Reaction Kinetics Study. *Chem. Biochem. Eng. Q*. **2016**, 30 (1), 33–45. doi: 10.15255/CABEQ.2014.2093

[130] Kung, M. C.; Kung, H. H. IR Studies of NH_3, Pyridine, CO, and NO Adsorbed on Transition Metal Oxides. *Catal. Rev. Sci. Eng*. **1985**, 27(3), 425-460. https://doi.org/10.1080/01614948508064741

[131] Ferwerda, R.; Van der Maas, J.; Duijneveldt, F. B. Pyridine adsorption onto metal oxides: an initio study of model systems. *J. Mol. Catal. A Chem.* **1996**, 104(3), 319-328. https://doi.org/10.1016/1381-1169(95)00179-4

[132] Zaccheria, F.; Santoro, F.; Iftitah, E. D.; Ravasio, N. Brønsted and Lewis Solid Acid Catalysts in the Valorization of Citronellal. *Catalysts*, **2018**, 8, 410. https://doi.org/10.3390/catal8100410

[133] Zaki, M. I.; Hasan, M. A.; Al-Sagheer, F. A.; Pasupulety, L. In situ FTIR spectra of pyridine adsorbed on SiO_2–Al_2O_3, TiO_2, ZrO_2 and CeO_2: general considerations for the identification of acid sites on surfaces of finely divided metal oxides. *Colloids and Surf. A: Physicochem. Eng. Asp.* **2001**, 190(3), 261-274. https://doi.org/10.1016/S0927-7757(01)00690-2

[134] Chen, X.; Ju, Y.; Mou, C. Direct Synthesis of Mesoporous Sulfated Silica-Zirconia Catalysts with High Catalytic Activity for Biodiesel via Esterification. *J. Phy. Chem. C*, **2007**, 111, 18731-18737. https://doi.org/10.1021/jp0749221

[135] Hashlmoto, K.; Masuda, T.; Motoyama, H.; YakushlJI, H.; Ono, M. Method for Measuring Acid Strength Distribution on Solid Acid Catalysts by Use of Chemisorption Isotherms of Hammett Indicators. Ind. Eng. Chem. Prod. Res. Devel. **1986**, 25, 243-250. https://doi.org/10.1021/i300022a020

[136] Chen, W.; Yi, X.; Huang, L.; Liu, W.; Li, G.; Acharya, D.; Sun, X.; Zheng, A. Can Hammett indicators Accurately Measure the Acidity of Zeolite Catalysts with Confined Space? Insights into the Mechanism of Coloration. *Catal. Sci. Technol*. **2019**, 9, 5045-5057. https://doi.org/10.1039/C9CY01392J

[137] Balaraju, M.; Nikhitha, P.; Jagadeeswaraiah, K.; Srilatha, K.; Sai Prasad, P. S.; Lingaiah, N. Acetylation of glycerol to synthesize bioadditives over niobic acid supported tungstophosphoric acid catalysts. *Fuel Proc. Technol*. **2010**, 91, 249–253. https://doi.org/10.1016/j.fuproc.2009.10.005

[138] Srilatha, K.; Lingaiah, N.; Prabhavathi Devi, B. L. A.; Prasad, R. B. N.; Venkateswar, S.; Sai Prasad, P. S. Esterification of free fatty acids for biodiesel production over heteropoly tungstates supported on niobia catalysts. *Appl. Catal. A*, **2009**, 365, 28–33. https://doi.org/10.1016/j.apcata.2009.05.025

[139] Melero, A.J.; Grieken, R.; Morales, G.; Paniagua, M. Acidic Mesoporous Silica for the Acetylation of Glycerol: Synthesis of Bioadditives to Petrol Fuel, *Energy & Fuels*, **2007**, 21, 1782-1791. https://doi.org/10.1021/ef060647q

[140] Yan, S.; Salley, S. O.; Simon Ng, K. Y. Simultaneous transesterification and esterification of unrefined or waste oils over ZnO-La_2O_3 catalysts. *Appl. Catal. A: Gen*. **2009**, 353, 203–212. https://doi.org/10.1016/j.apcata.2008.10.053

[141] Pankajakshan, A.; Pudi, S. M.; Biswas, P. Acetylation of glycerol over highly stable and active sulfated alumina catalyst: reaction mechanism, kinetic modeling and estimation of kinetic parameters. *Int. J. Chem. Kinet*. **2018**, 50(2), 98-111. https://doi.org/10.1002/kin.21144

[142] Khayoon, M. S.; Triwahyono, S.; Hameed, B. H.; Jalil, A. A. Improved production of fuel oxygenates via glycerol acetylation with acetic acid. *Chem. Eng. J*. **2014**, 243, 473–484. DOI: 10.1016/j.cej.2014.01.027

[143] Mufrodi, Z.; Sutijan, Rochmadi, Budiman, A. Chemical Kinetics for Synthesis of Triacetin from Biodiesel Byproduct. *Int. J. Chem*. **2012**, 4, 101–107. DOI:10.5539/ijc.v4n2p101

[144] Appaturi, J. N.; Jothi Ramalingam, R. J.; Selvaraj, M.; Chia, S.; Huat Tan, S.; Khoerunnisa, F.; Ling, T. C.; Ng, E. Selective synthesis of triacetyl glyceride biofuel additive via acetylation of glycerol over NiO-supported TiO_2 catalyst enhanced by non-microwave instant heating. *Appl. Surf. Sci*. **2021**, 545, 149017. DOI: 10.1016/j.apsusc.2021.149017

[145] Zhou, L.; Nguyen, T.; Adesina, A. A. The acetylation of glycerol over amberlyst-15: Kinetic and product distribution. *Fuel Proc. Technol*. **2012**, 104, 310–318. https://doi.org/10.1016/j.fuproc.2012.06.001

[146] Popova, M.; Lazarova, H.; Szegedi, A.; Mihályi, M. R.; Rangus, M.; Likozar, B.; Dasireddy, V. D. B. C. Renewable glycerol esterification over sulfonic-modified mesoporous silicas. *J. Serb. Chem. Soc*. **2018**, 83 (1), 39–50. DOI: 10.2298/JSC170306071P

[147] Stawicka, K.; Trejda, M.; Ziolek, M. The production of biofuels additives on sulphonated MCF materialsmodified with Nb and Ta—Towards efficient solid catalysts of esterification. *Appl. Catal. A: Gen*. **2013**, 467, 325– 334. https://doi.org/10.1016/j.apcata.2013.07.036

[148] Jin, T.; Yamaguchi, T.; Tanabe, K. Mechanism of acidity generation on sulfur-promoted metal oxides. *J. Phys. Chem*. **1986**, 90(20), 4794–4796. https://doi.org/10.1021/j100411a017

[149] Troncea, S. B.; Wuttke, S.; Kemnitz, E.; Coman, S. M.; Parvulescu, V. I. Hydroxylated magnesium fluorides as environmentally friendly catalysts for glycerol acetylation. *Appl. Catal. B: Environ*. **2011**, 107, 260-267. https://doi.org/10.1016/j.apcatb.2011.07.021

[150] Xun, L.; Dan, Y.; Xingchen, A.; Wenting, F. Preparation of mesoporous SO_4^{2-}/CeO_2–TiO_2–ZrO_2 solid acid catalyst and its application in acetylation of glycerol. *J. Biobased Mat. Bioenergy* **2015**, 9, 50–54. DOI: 10.1016/j.jiec.2011.11.063

[151] Liu, J.; Wang, Z.; Sun, Y.; Jian, R.; Jian, P.; Wang, D.; Selective synthesis of triacetin from glycerol catalyzed by HZSM-5/MCM-41 micro/mesoporous molecular sieve. *Chin. J. Chem. Eng*. **2019**, 27, 1073–1078. DOI: 10.1016/j.cjche.2018.09.013

[152] Yanti, N. R.; Heryani, H.; Putra, M. D.; Nugroho, A. triacetin production from glycerol using heterogeneous catalysts prepared from peat clay. *Int. J. Technol*. **2019**, 10(5), 970-978. https://doi.org/10.14716/ijtech.v10i5.2685

[153] Mallesham, B.; Sudarsanam, P.; Reddy, B. M. Production of Biofuel Additives from Esterification and Acetalization of Bioglycerol over SnO_2-Based Solid Acids. *Ind. Eng. Chem. Res*. **2014**, 53, 18775−18785. https://doi.org/10.1021/ie501133c

[154] Yang, T.; Chang, T.; Yeh, C.; Acidities of sulfate species formed on a super acid of sulfated alumina. *J. Mol. Catal. A: Chem*. **1997**, 115**,** 339. https://doi.org/10.1016/S1381-1169(96)00283-X

[155] Lei, Q.; Li, D.; Li, J.; Liu, C.; Xu, C.; Dong, W. Glycerol Esterification to Glyceryl Diacetate over SO_4^{2-}/W-Zr Complex Solid Super Acid Catalysts. *Chem. Select*, **2019**, 4, 2780 –2786. https://doi.org/10.1002/slct.201803820

[156] Diwakar, J.; Viswanadham, N.; Kumar, S.; Kumar, A.; Saxena, S. K. One-pot synthesis of ordered nanoporous amorphous H-Zn-aluminosilicate for catalysis of bulky molecules†. *Sustain. Energy Fuels* **2018**, 2, 1693. DOI: 10.1039/C8SE00150B

[157] Chamacka, M.; Mahjoub, A. R.; Akbari, A. Zirconium-modified Mesoporous Silica as an Efficient Catalyst for the Production of Fuel Additives from Glycerol. *Catal. Commun*. **2018**, 110, 1-4. https://doi.org/10.1016/j.catcom.2018.02.021

[158] Gao, X.; Zhu, S.; Li, Y. Graphene oxide as a facile solid acid catalyst for the production of bioadditives from glycerol esterification. *Catal. Commun*. **2015,** 62, 48–51. DOI: 10.1016/j.catcom.2015.01.007

[159] Chen, H.; Huh, S.; Wiench, J. W.; Pruski, M.; Lin, V. S. Y. Dialkylaminopyridine-Functionalized Mesoporous Silica Nanosphere as an Efficient and Highly Stable Heterogeneous Nucleophilic Catalyst. *J. Am. Chem. Soc*. **2005**, 127, 13305-13311. https://doi.org/10.1021/ja0524898

[160] Kresge, C. T.; Leonowicz, M. E.; Roth, W. J.; Vartuli, J. C.; Beck, J. S. Ordered mesoporous molecular sieves synthesized by a liquid-crystal template mechanism. *Nature* **1992**, 359, 710–712. DOIhttps://doi.org/10.1038/359710a0

[161] Shagufta, Ahmad, I.; Dhar, R. Sulfonic Acid-Functionalized Solid Acid Catalyst in Esterification and Transesterification Reactions, Catal. Surv. Asia., 2017, **21**, 53–69.

[162] Yanagisawa, T.; Shimizu, T.; Kuroda, K.; Kato, C. The preparation of alkyltriinethylaininonium–kaneinite complexes and their conversion to microporous materials. *Bull. Chem. Soc. Jpn*. **1990**, 63, 988–992. https://doi.org/10.1246/bcsj.63.988

[163] Hasan, Z.; Yoon, J. W.; Jhung, S. W. Esterification and acetylation reactions over in situ synthesized mesoporous sulfonated silica. *Chem. Eng. J*. **2015**, 278, 105–112. DOI: 10.1016/j.cej.2014.12.025

[164] Wu, S.; Mou, C.; Lin, H. Synthesis of mesoporous silica nanoparticles†, *Chem. Soc. Rev*. **2013**, 42, 3862. https://doi.org/10.1080/1061186X.2020.1812614

[165] Mann, S.; Burkett, S. L.; Davis, S. A.; Fowler, C. E.; Mendelson, N. H.; Sims, S. D.; Walsh, D.; Whilton, N. T. Sol-Gel Synthesis of Organized Matter. *Chem. Mater*. **1997**, 9, 2300–2310. https://doi.org/10.1021/cm970274u

[166] Ying, J. Y.; Mehnert, C. P.; Wong, M. S. Synthesis and Applications of Supramolecular-Templated Mesoporous Materials. *Chem., Int. Ed*. **1999**, 38, 56–77. https://doi.org/10.1002/(SICI)1521-3773(19990115)38:1/2<56::AID-ANIE56>3.0.CO;2-E

[167] Mufrodi, Z.; Astuti, E.; Syamsiro, M.; Santosa, B.; Sutiman, Purwono, S. Triacetin Synthesis as Bio-Additive from Glycerol Using Homogeneous and Heterogeneous Catalysts. *Key Eng. Mater*. **2020**, 84990-84995. DOI: 10.4028/www.scientific.net/KEM.849.90

[168] Costa, B. O.; Dalla, H. P.; Decolatti, M. S.; Legnoverde, C. A.; Querini, Influence of acidic properties of different solid acid catalysts for glycerol acetylation. *Catalysis Today* **2016**, 0920–5861. https://doi.org/10.1016/j.cattod.2016.09.015

[169] Kumar, S.; Jain, S. History, Introduction, and Kinetics of Ion Exchange Materials. *J. Chem*. **2013**, https://doi.org/10.1155/2013/957647.

[170] Pepper, K. Sulphonated Cross-Linked Polystyrene: A Monofunctional Cation-Exchange Resin. *J. Appl. Chem*. **1951**, 124-132. https://doi.org/10.1002/jctb.5010010307

[171] Hartono, R.; Mulia, B.; Sahlan, M.; Utami, T. S.; Wijanarko, A.; Hermansyah, H. The modification of ion exchange heterogeneous catalysts for biodiesel synthesis. *Renew. Energy Technol. Innovation Sustain. Develop*. **2017**, 1826, 020020. https://doi.org/10.1063/1.4979236

[172] Chakrabarti, A.; Sharma, M. M. Cationic ion exchange resins as catalyst. *React. Polym*. **1993**, 20, 1-45. https://doi.org/10.1016/0923-1137(93)90064-M

[173] Wheaton, R. M.; Harrington, D. F. Preparation of Cation Exchange Resins of High Physical Stability. *Ind. Eng. Chem*. **1952**, 44(8), 1796-1800. https://doi.org/10.1021/ie50512a029

[174] Abrams, I. High Porosity Polystyrene Cation Exchange Resins. *Chem. Proc*. **1956**, 48(9), 1469-1472. https://doi.org/10.1021/ie51400a030

[175] Kale, S.; Umbarkarb, S. B.; Dongare, M. K.; Eckelta, R.; Armbrustera, U.; Martin, A. Selective formation of triacetin by glycerol acetylation using acidicion-exchange resins as catalyst and toluene as an entrainer. *Appl. Catal. A: Ge.* **2015**, 490, 10–16. https://doi.org/10.1016/j.apcata.2014.10.059

[176] Zhou, L.; Al-Zaini, E.; Adesina, A. A. Catalytic characteristics and parameters optimization of the glycerol acetylation over solid acid catalysts. *Fuel*, **2013**, 103, 617–625. https://doi.org/10.1016/j.fuel.2012.05.042

[177] Jianga, Y.; Lia, X.; Zhaoa, H.; Hou, Z. Esterification of glycerol with acetic acid over SO3H-functionalized phenolic resin. *Fuel*, **2019**, 255, 115842. DOI: 10.1016/j.fuel.2019.115842

[178] Aghbashlo, M.; Tabatabaei, M.; Jazinid, H.; Ghaziaskar, H.S. Exergoeconomic and exergoenvironmental co-optimization of continuous fuel additives (acetins) synthesis from glycerol esterification with acetic acid using Amberlyst 36 catalyst. *Energy Con. Manag*. **2018**, 165, 183–194. https://doi.org/10.1016/j.enconman.2018.03.054

[179] Reinoso, D. M.; Tonetto, G. M. Bioadditives synthesis from selective glycerol esterification over acidic ion exchange resin as catalyst. *J. Environ. Chem. Eng*. **2018**, 6, 3399–3407. https://doi.org/10.1515/ijcre-2020-0171

[180] Setyaningsih, L.; Siddiq, F.; Pramezy, A. Esterification of glycerol with acetic acid over Lewatit catalyst. *Matec Web of Conf*. **2018**, 154, 01028. https://doi.org/10.1051/matecconf/201815401028

[181] Valter, L. C.; Goncalves, Bianca, P.; Pinto, Joao, C.; Silva, Claudio, J. A.; Mota, Acetylation of glycerol catalyzed by different solid acids. *Catal. Today*, **2008**, 133(135), 673–677. https://doi.org/10.1016/j.cattod.2007.12.037

[182] Malaika, A.; Kozłowski, M. Glycerol conversion towards valuable fuel blending compounds with the assistance of SO_3H-functionalized carbon xerogels and spheres. *Fuel Proc. Technol.* **2019**, 184, 19–26. https://doi.org/10.1016/j.fuproc.2018.11.006

[183] Nda-Umar, U. I.; Ramli, I.; Muhamad, E. N.; Azri, N.; Taufiq-Yap Y. H. Optimization and Characterization of Mesoporous Sulfonated Carbon Catalyst and Its Application in Modeling and Optimization of Acetin Production. *Molecules*, **2020**, 25, 5221. doi: 10.3390/molecules25225221

[184] Russo, P. A.; Antunes, M. M.; Neves, P.; Wiper, P. V.; Fazio, E.; Neri, F.; Barreca, F.; Mafra, L.; Pillinger, M.; Pinna, N.; Valente, A. A. Mesoporous carbon-silica acid catalyst for producing useful bio-products within the sugar platform of biorefineries. *Green Chem*. **2014**, 16, 4292–4305. https://doi.org/10.1039/C4GC01037J

[185] Mahajan, A.; Gupta, P. Carbon-based solid acids: a review. *Environ. Chem. Letters* **2020**, 18, 299–314. DOIhttps://doi.org/10.1007/s10311-019-00940-7

[186] Tao, M.; Guan, H.; Wang, X.; Liu, Y.; Louh, R. Fabrication of sulfonated carbon catalyst from biomass waste and its use for glycerol esterification. *Fuel Proc. Technol*. **2015**, 138, 355–360. https://doi.org/10.1016/j.fuproc.2015.06.021

[187] Nda-Umar, U. I.; Irmawati, R.; Muhamad, E. N.; Azria, N.; Shafizah, N.; Ishaka, N. S.; Yahaya, M.; Taufiq-Yap, U. H. Organosulfonic acid-functionalized biomass-derived carbon as a catalyst for glycerol acetylation and optimization studies via response surface methodology. *J. Taiwan Inst. Chem. Eng*. **2021**, 118, 355-370. https://doi.org/10.1016/j.jtice.2020.12.021

[188] Malaika, A.; Ptaszynska, K.; Kozłowski, M. Conversion of renewable feedstock to bio-carbons dedicated for the production of green fuel additives from glycerol. *Fuel*, **2021,** 288, 119609. DOI: 10.1016/j.fuel.2020.119609

[189] Dizoğlu, G.; Sert, E. Fuel additive synthesis by acetylation of glycerol using activated carbon/UiO-66 composite materials. *Fuel*, **2020**, 281, 118584. DOI: 10.1016/j.fuel.2020.118584

[190] Goscianska, J.; Malaika, A. A facile post-synthetic modification of ordered mesoporous carbon to get efficient catalysts for the formation of acetins. *Catal. Today* **2020**, 375(1), 84-93. DOI: 10.1016/j.cattod.2019.02.049

[191] Malaika, A.; Heinrich, M.; Goscianska, J.; Kozłowski, M. Synergistic effect of functional groups in carbonaceous spheres on the formation of fuel enhancers from glycerol. *Fuel*, **2020**, 280, 118523. DOI: 10.1016/j.fuel.2020.118523

[192] Okoye, P. U.; Abdullah, A. Z.; Hameed, B. H. Synthesis of oxygenated fuel additives via glycerol esterification with acetic acid over bio-derived carbon catalyst. *Fuel* **2017**, 209, 538–544. DOI: 10.1016/j.fuel.2017.08.024

[193] Sun, Y.; Hu, J.; An, S.; Zhang, Q.; Guo, Y.; Song, D.; Shang, Q. Selective esterification of glycerol with acetic acid or lauric acid over rod-like carbon-based sulfonic acid functionalized ionic liquids. *Fuel*, **2017**, 207, 136–145. DOI: 10.1016/j.fuel.2017.118584

[194] Sánchez, J. A.; Hernández, D. L.; Moreno, J. A.; Mondragón, F.; Fernández, J. J. Alternative carbon based acid catalyst for selective esterification of glycerol to Acetylglycerols, *Appl. Catal. A: Gen*. **2011**, 405, 55–60. https://doi.org/10.1016/j.apcata.2011.07.027

[195] Gautam, P.; Barman, S.; Ali, A. Catalytic performance of cerium-modified ZSM-5 zeolite as a catalyst for the esterification of glycerol with acetic acid. *Int. J. Chem. React. Eng*. **2020**, 18(9), 20200081. DOI: 10.1515/ijcre-2020-0081

[196] Rochim, B.; Cahyono, Mufrodi, Z.; Hidayat, A.; Budiman, A. A. Acetylation Of Glycerol For Triacetin Production Using Zr-Natural Zeolite Catalyst. *J. Eng. Appl. Sci*. **2016**, 11(8), 1819-6608.

[197] Ferreira, P.; Fonseca, I. M.; Ramos, A. M.; Vital, J.; Castanheiro, J. E. Esterification of glycerol with acetic acid over dodecamolybdophosphoric acid encaged in USY zeolite. *Catal. Commun*. **2009**, 10, 481–484. DOI: 10.1016/j.catcom.2008.10.015

[198] Gründling, C.; Lercher, J. A.; Goodman, D. W. Preparation of mixed Al_2O_3/SiO_2 thin films supported on Mo(100). *Surf. Sci*. **1994**, 318, 97-103. https://doi.org/10.1016/0039-6028(94)90345-X

[199] Zhang, J.; Uknalis, J.; Chen, L.; Moreau, R. A.; Ngo, H. Development of Magnesium Oxide–Zeolite Catalysts for Isomerization of Fatty Acids. *Catal. Letters* **2019**, 149, 303–312. DOIhttps://doi.org/10.1007/s10562-018-2601-3

[200] Baile, P.; Fernández, E.; Vidal, L.; Canals, A. Zeolites and zeolite-based materials in extraction and microextraction techniques. *Analyst* **2019**, 144, 366. https://doi.org/10.1039/C8AN01194J

[201] Marwan, M.; Indarti, E.; Darmadi, D.; Rinaldi, W.; Hamzah, D.; Rinaldi, T. Production of Triacetin by Microwave Assisted Esterification of Glycerol Using Activated Natural Zeolite. *Bull. Chem. Reaction Eng. Catal*. **2019**, 14 (3), 672-677. DOI: 10.9767/bcrec.14.3.4250.672-677

[202] Kulkarni, R. M.; Arvind, N. Acetalization of glycerol and benzaldehyde to synthesize biofuel additives using $SO_4^{2-}/CeO_2–ZrO_2$ catalyst. *Heliyon* **2021**, 7, 06018. https://doi.org/10.1016/j.heliyon.2021.e06018

[203] Dai, Y.; Wang, Y.; Chen, C. Synthesis and characterization of magnetic $LiFe_5O_8$-$LiFeO_2$ as a solid basic catalyst for biodiesel production. *Catal. Commun*. **2018**, 106, 20–24. https://doi.org/10.1016/j.catcom.2017.12.002

[204] Wang, J.; Liang, Y.; Wang, S.; Okoye, P. U.; Chen, H.; Zhou, Y.; Xu, J.; Meng, Z.; Wang, L.; Li, S. Using Diaper Waste to Prepare Magnetic Catalyst for the Synthesis of Glycerol Carbonate. *Int. J. Poly. Sci.* **2020**, 4, 1-9. https://doi.org/10.1155/2020/9403714

[205] Wang, Y.; Yang, X.; Xu, J.; Wang, H.; Wang, Z.; Zhang, Z.; Wang, S.; Liang, J. Biodiesel production from esterification of oleic acid by a sulfonated magnetic solid acid catalyst. *Renew. Energy* **2019**, 139, 688-695. DOI: 10.1016/j.renene.2019.02.111

[206] Cheng, M.; Xie, W.; Zong, B.; Sun, B.; Qiao, M. When Magnetic Catalyst Meets Magnetic Reactor: Etherification of FCC Light Gasoline as an Example. *Sci. Reports* **2013**, 9, 1973. DOI: https://doi.org/10.1038/srep01973

[207] Elsayed, I.; Mashaly, M.; Eltaweel, F.; Jackson, M. A.; Hassan, E. B. Dehydration of glucose to 5-hydroxymethylfurfural by a core-shell Fe_3O_4@SiO_2-SO_3H magnetic nanoparticle catalyst. *Fuel* **2018**, 221, 407–416. https://doi.org/10.1016/j.fuel.2018.02.135

[208] Sun, J.; Tong, X.; Yu, L.; Wan, J. An efficient and sustainable production of triacetin from the acetylation of glycerol using magnetic solid acid catalysts under mild conditions. *Catal. Today* **2016**, 264, 115-122. DOI: 10.1016/j.cattod.2015.07.011

[209] Silva, M. J. D.; Liberto, N. A.; Leles, L. D.; Pereira, U. A. $Fe_4(SiW_{12}O_{40})$ catalyzed glycerol acetylation: Synthesis of bioadditives by using highly active Lewis acid catalyst. *J. Mol. Catal. A: Chem*. **2016,** 422, 69–83. https://doi.org/10.1016/j.molcata.2016.03.003

Materials and Methods

Overview of the Chapter

The chapter includes the list of chemicals and details of experimental and analytical techniques which are employed in the present thesis.

2.1. Chemicals

Zirconium (IV) oxychloride octahydrate, Tetraethoxysilane (98 %), and deuterated water (D_2O), were procured from Sigma-Aldrich (USA). Ferrous sulfate (99 %), ferric chloride (97 %), titanium tetrachloride (99.5 %), cerous nitrate hexahydrate (99.9 %), Niobium (V) oxide (99 %), ammonia solution (25 % v/v), sulphuric acid, triacetin (99 %), acetic acid (99 %), acetic anhydride (99 %) and glycerol (99 %) were obtained from Loba Chemie Ltd. (India). HPLC grade iso-propanol (IPA) and hexane were purchased from Spectrochem Ltd. (India).

2.2. Pyridine adsorption study

To study the nature of the catalytic acidic (Brønsted or Lewis acid) sites, the samples were saturated with pyridine at room temperature and then dried at 50 °C for 2 h and further heated for 10 min at 300 °C in a muffle furnace. Finally, the diffuse reflectance FTIR (DRIFT) spectra of the pyridine treated catalysts were recorded in KBr matrix in the mid IR range (400-4000 cm^{-1}).

2.3. Turn over frequency

The turnover frequency (TOF) of the catalysts is calculated from equation 2.1 [1,2].

$$TOF = \frac{\text{mmol}_{\text{actual}}}{f_m \times m_{cat} \times t} \qquad 2.1$$

where, $\text{mmol}_{\text{actual}}$ is the mmoles of the product formed, m_{cat} is the mass of the catalyst (in g), t is the reaction duration (in h), and f_m is active sites of the catalyst (in mmol g^{-1}), as calculated by NH_3-TPD.

2.4. Reaction kinetics and thermodynamics

GL acetylation can be assumed as an irreversible reaction [3,4] and the backward reactions in each step can be ignored for developing the kinetics as given in steps **R_1**, **R_2** and **R_3** [5].

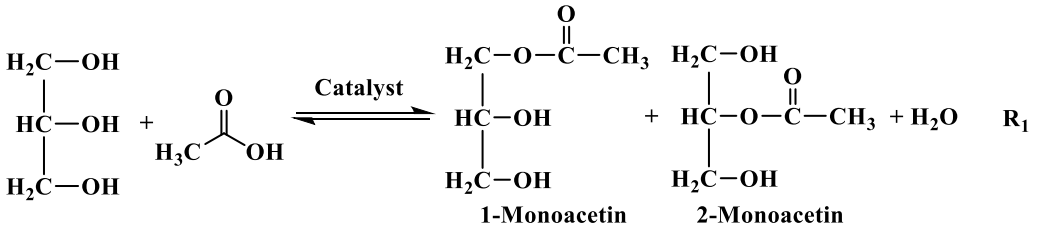

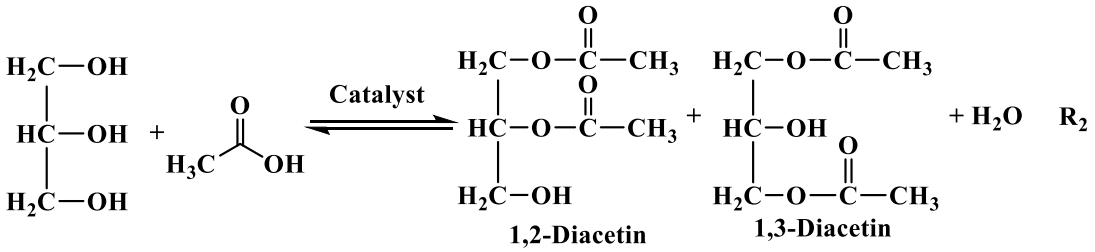

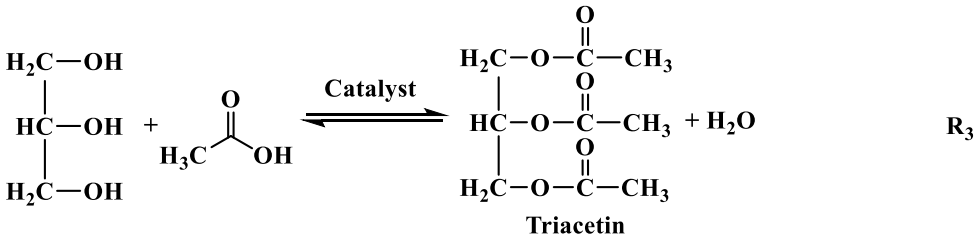

In order to find out the rate constant (k) and order of the reaction, the conversion of GL ($X_{glycerol}$) at different reaction times (t) was obtained, and appropriate values were fitted in zero-order (I), first-order (II), and second-order kinetic (II) models. The equation which gives the best fitting has been used to calculate the corresponding rate constants.

$$\frac{t}{100} = X_{glycerol} \qquad \text{(I)}$$

$$k = -\ln\{(1-X_{glycerol})/t\} \qquad \text{(II)}$$

$$100t = \frac{X_{glycerol}}{1-X_{glycerol}} \qquad \text{(III)}$$

where k is the rate constant, $X_{glycerol}$ is the GL conversion at time t

To calculate the activation energy (E_a), reactions were carried by varying the temperatures between 30 and 90 ºC. The Arrhenius equation (IV) was employed to calculate the activation energy (E_a) following the reported procedure [6-8].

$$\ln k = -E_a/RT + \ln A \qquad \text{(IV)}$$

where E_a is the activation energy (kJ mol^{-1}), A is the pre-exponential factor (min^{-1}), R is the gas constant (8.31×10^{-3} kJ K^{-1} mol^{-1}) and T is the reaction temperature (K).

The thermodynamic parameters, *viz.*, enthalpy ($\Delta H^{\ddagger}$), entropy ($\Delta S^{\ddagger}$), and the Gibb's free energy of activation ($\Delta G^{\ddagger}$), were calculated from Eyring-Polanyi equation (V) [9].

$$k = \frac{k_B T}{h} e - \frac{\Delta G^{\ddagger}}{RT} \qquad \text{(V)}$$

Taking the natural log of equation (V) and substituting the value of $\Delta G^{\ddagger} = \Delta H^{\ddagger} - T\Delta S^{\ddagger}$, equation (VI) will be obtained.

$$\ln \frac{k}{T} = \frac{-\Delta H^{\ddagger}}{R} \cdot \frac{1}{T} + ln \frac{k_B}{h} + \frac{\Delta S^{\ddagger}}{R} \qquad \text{(VI)}$$

where k_B is the Boltzmann constant (1.38×10^{-23} J K^{-1}) and h is the Planck constant (6.63×10^{-34} Js). The plot of 1/T versus ln(k/T) were drawn in which slope and intercept would be equals to $-\Delta H^{\ddagger}/R$ and ln (k_B/h) + $\Delta S^{\ddagger}/R$, respectively. The superscript ‡ notation refers to the value of the interest in the activated complex.

2.5. Instruments

2.5.1. Powder X-ray diffraction (XRD)

Powder X-ray diffraction data were collected using a PANalytical's X'Pert Pro using Cu-Ka radiation (operated at 45 kV) in the 2θ range of 10 to 80°. The phases present in the samples were identified by comparing the results with the JCPDS (Joint Committee of the Powder Diffraction Standards) database files.

2.5.2. Fourier transformation infra-red spectroscopy (FTIR)

Fourier transform-infrared spectra (FTIR) of solid samples were recorded in a Potassium bromide (KBr) matrix and liquid samples over attenuated total reflectance (ATR) accessory in mid IR range (400-4000 cm^{-1}) on an Agilent Cary-660 spectrophotometer.

2.5.3. Brunauer-Emmett-Teller (BET)

The specific surface area was measured by the Brunauer-Emmett-Teller (BET) method and the pore size by the BJH method using a Microtrac-BEL mini-II instrument. Prior to the analysis, the samples were heated at 100 °C for 3 h under vacuum to remove any adsorbed molecules from the catalyst surface.

2.5.4. NH_3-Temperature programmed desorption (NH_3-TPD)

The total surface acidity of the catalysts were calculated by conducting a temperature programmed desorption study of NH_3 (NH_3-TPD) using a Microtrac-BEL Corp. BELCAT II instrument which utilizes a thermal conductivity detector (TCD) for quantifying the evolved gases. In a typical experiment, 0.05 g of catalyst sample was loaded in a U shaped glass sample tube, and heated at 300 °C under the He gas flow for 1 h to remove the moisture and physically adsorbed gases. For ammonia adsorption, the sample was then exposed to a mixture of NH_3/He gases (5/95; v/v) at the 100 °C for 30 min. Afterward, to desorb the NH_3, the sample was heated in the temperature range of 100 to 700 °C under the He gas flow and evolved gases were quantified with the help of thermal conductivity detector.

2.5.5. Scanning electron microscopy-Energy Dispersive X-ray analysis (SEM-EDX)

Scanning electron microscopy coupled with energy dispersive X-ray spectrometry (SEM-EDX) was performed on a JEOL JSM 6510LV instrument. For analysis of the catalyst samples, initially solid samples were ultrasonicated in ethanol for 3 h. A drop of the prepared suspension was mounted on a sample holder with the help of carbon tape. The sample was then sputter-coated with gold and visualized with the instrument to assess the particle morphology.

2.5.6. Transmission electron microscopy (TEM)

Transmission Electron Microscope (TEM) images were recorded on Hitachi 7500 instruments. The powdered sample was ultrasonicated with ethanol for 2 h and a drop of the prepared suspension was placed on a copper grid. Prior to analysis, the suspension was dried to remove the solvent.

2.5.7. X-ray photoelectron spectroscopy (XPS)

X-ray photoelectron spectroscopy (XPS) was performed by using an ESCA+, (omicron nanotechnology, Oxford Instrument Germany) equipped with a monochromator Aluminium Source (Al K radiation $h\nu$ = 1486.7 eV) operated at 15 kV and 20 mA. To overcome the charging problem, a charge neutralizer of 2 keV was applied, and the binding energy was calibrated with the help of C 1s peak (284.2 eV) by employing it as internal standard [10].

2.5.8. Vibrating sample magnetometer (VSM)

Magnetic properties of the catalyst were investigated by Lakeshore 7404 vibrating sample magnetometer (VSM). In this technique, powdered sample with known mass was placed in a sample vial and vibrated at constant frequency within the pole gap of an electromagnet. Vibrating sample within the pole-gap produced induced emf which is detected by the pick-up coils and measured with lock-in amplifier. This induced emf is directly proportional to the magnetic moment and hence the magnetization of the sample. Thus, VSM can measure the magnetic properties like magnetic saturation magnetization (M_s), coercivity (H_C), remanence (M_R), etc. by measuring the hysteresis M-H loops. In this study, M-H loops were measured at room temperature (300 K) in the field range of -10 kOe to + 10 kOe. Before measurement, magnetometer was calibrated with Nickel standard.

2.5.9. Fourier transform-nuclear magnetic resonance (FT-NMR)

Fourier transform-nuclear magnetic resonance (FT-NMR) spectra of organic molecules were recorded on a JEOL ECS-400 (400 MHz) spectrophotometer in D_2O solvent using tertramethyl silane (TMS) as an internal reference, and chemical shifts (δ) were expressed in parts per million (ppm).

2.5.10. High performance liquid chromatography (HPLC)

The organic products have been quantified by high-performance liquid chromatography (HPLC) over an Agilent Infinity 1200 instrument. During the analysis iso-propanol (IPA)/hexane (60/40; v/v) was employed as the mobile phase with a flow rate of 0.6 mL min^{-1}, the RX-SIL column (4.6 × 250 mm, 5 µ) as the stationary phase and the peaks were identified by using a refractive index (RI) detector. All samples were analysed by maintaining a column temperature of 35 °C and injecting a fixed sample volume of 20 µL.

References

[1] Setyaningsih, L.; Mutiara, T.; Chafidz, A.; Zulkania, A.; Andrianto, M. A.; Farikha, N. L. Kinetic modelling of esterification of glycerol with acetic acid catalyzed by lewatite. *Mater. Sci. Eng*. **2019**, 543, 012008. DOI:10.1088/1757-899X/543/1/012008

[2] Ladero, M.; Gracia, M. D.; Tamayo, J. J.; Ahumada, I. L. D.; Trujilo, F.; Garcia-Ochoa, F. Kinetic Modelling of The Esterification of Rosin and Glycerol: Application to Industrial Operation. *Chem. Eng. J*. **2011**, 169, 319. https://doi.org/10.1016/j.cej.2011.03.012

[3] Okoye, P. U.; Abdullah, A. Z.; Hameed, B. H. A review on recent developments and progress in the kinetics and deactivation of catalytic acetylation of glycerol-A byproduct of biodiesel. *Renew. Sustain. Energy Rev*. **2017**, 74, 387–401. https://doi.org/10.1016/j.rser.2017.02.017

[4] Kumar, D.; Abida, K.; Ali, A. Aminolysis of triglycerides using nanocrystalline nickel doped CaO as an efficient solid catalyst†. *RSC Adv*. **2016**, 6, 66822-66832. https://doi.org/10.1039/C6RA12114D

[5] Talebian-Kiakalaieh, A.; Amin, N. A. S. Kinetic Study on Catalytic Conversion of Glycerol to Renewable Acrolein. *Chem. Eng. Trans*. **2017**, 56, 655-660. DOI:10.33303/CET1756110

[6] Balbino, J. M.; Menezes, E.W.; Benvenutti, E.V.; Cataluna, R.; Ebeling, G.; Dupont, J. Silica-supported guanidine catalyst for continuous flow biodiesel production. *Green Chem*. **2011**, 13, 3111–3116. DOI: 10.1039/c1gc15727b

[7] Ong, L. K.; Kurniawan, A.; Suwandi, A. C.; Lin, C. X.; Zhao, X. S.; Ismadji, S. Transesterification of leather tanning waste to biodiesel at supercritical condition: Kinetics and thermodynamics studies. *J. Supercrit. Fluid*. **2013**, 75, 11-20. https://doi.org/10.1016/j.supflu.2012.12.018

[8] Burungale, V. V.; Devan, R. S.; Pawar, S. A.; Harale, N. S.; Patil, V. L.; Rao, V. K.; Ma, Y.; Eun Ae, J.; Kim, J. H.; Patil, P. S. Chemically synthesized PbS nanoparticulate thin films for a rapid NO_2 gas sensor. *Mat. Sci. Poland*, **2016**, 34(1), 204-211. DOI: 10.1515/msp-2016-0001

[9] Tao, G.; Hua, Z.; Gao, Z.; Chen, Y.; Wang, L.; He, Q.; Chena, H.; Shi, J. Synthesis and catalytic activity of mesostructured $KF/Ca_xAl_2O_{(x+3)}$ for the transesterification reaction to produce biodiesel. *RSC Adv*. **2012**, 2, 12337–12345. https://doi.org/10.1039/C2RA22218C

[10] Kaur, A.; Ali, A. Lithium Zirconate as a Selective and Cost-Effective Mixed Metal Oxide Catalyst for Glycerol Carbonate Production. *Ind. Eng. Chem. Res*. **2020**, 59, 2667−2679. DOI: 10.1021/acs.iecr.9b05747

Sulphuric acid-functionalized siliceous zirconia as an efficient and reusable catalyst for the synthesis of triacetin

Overview of the Chapter

In the present study, a sulphated siliceous zirconia catalyst (SSZ-550) has been prepared and characterized by XRD and FTIR analysis to indicate the incorporation of the sulphate group over the matrix. X-ray photoelectron spectroscopy also revealed that the sulphate group was incorporated over the matrix to impart the Brønsted acidity to the catalyst which is vital for the acetylation activity. The catalyst was successfully employed for glycerol acetylation with acetic acid to obtain 93 % selectivity towards triacetin within 40 min of reaction duration at 80 °C reaction temperature. The catalyst was recovered from the reaction mixture and reused during six consecutive reaction runs while retaining 54 % triacetin selectivity in the last cycle. A plausible mechanism suggests the heterogeneous catalyst-assisted protonation of carbonyl group of acetic acid to initiate the stepwise acetylation of the hydroxyl groups of glycerol.

3.1. Introduction

Glycerol, a by-product from BD and soap industries, can be used as an eco-friendly and renewable substrate for the production of GL derivatives, such as, MA, DA, and TA which have their applications in the pharmaceuticals, polymer, cosmetic and food industries [1-4]. All these molecules could be produced by employing mineral acids, *e.g.*, H_2SO_4, HF, H_3PO_4, etc., as homogeneous catalysts [5]. However, most mineral acids are harmful to the environment and require a complicated reactor design to make them acid resistant [6]. After the completion of the reaction, acid neutralization with alkali and removal of the salt formed generate a vast quantity of industrial effluents, which are difficult to dispose of. Moreover, GL acetylation with AcA in the presence of homogeneous acidic catalyst demands high reaction temperature (up to 135 °C) with a long reaction duration (up to 3 h) to yield the partial TA selectivity along with MA and DA as a by-product [5]. Moreover, such catalysts are not only toxic and corrosive but also non-reusable and difficult to separate from the reaction medium.

To overcome the limitations of the homogeneous acidic catalysts, in literature, a variety of heterogeneous acidic catalysts were employed for the production of TA employing GL acetylation with AcA as discussed in Chapter 1. TA selectivity was also found to be a function of reaction duration, reagent ratio, and reaction temperature along with the catalytic sites. Hence, an optimal combination of all these parameters is essential to achieve the maximum selectivity of TA.

In this chapter, acidic, stable, and recyclable heterogeneous catalyst, sulphated siliceous zirconia was synthesized and employed to catalyze the GL acetylation to obtain TA molecolue. Further, the reaction conditions have been optimized to achieve the maximum TA selectivity during the GL acetylation reaction. The catalyst stability and reusability has been evaluated with recovered catalyst, and reason for the decline in catalyst activity has also been investigated.

3.2. Experimental section

3.2.1. Preparation of siliceous zirconia

The $Si(OH)_4Zr(OH)_4$ matrix has been prepared by sol–gel method using $ZrOCl_2{\cdot}8H_2O$ as a precursor of zirconia. In a usual preparation method, $ZrOCl_2{\cdot}8H_2O$ (5 g) was dissolved in 20 mL deionized water under constant stirring at room temperature (35 °C). Aqueous ammonia

solution was added drop wise until 10 pH was obtained, and the resulting mixture was stirred for 15 min. To this, TEOS was added (corresponding to theoretical 1:1 molar ratio of Si/Zr) slowly, under constant stirring for 1 h at room temperature. The precipitate formed was filtered and washed with deionized water multiple times to remove the chloride ions and then dried at 100 °C for 12 h to obtain the matrix $Si(OH)_4Zr(OH)_4$ which is referred as SZ.

3.2.2. Anchoring of sulphate ion over the matrix

Prepared SZ matrix (1 g) was powdered and suspended in 20 mL deionized water. To this, 1 molar H_2SO_4 solution (3 mL) was added. The resulted mixture was stirred for 24 h at room temperature, then dried for 12 h at 100 °C and finally calcined at 550 °C for 4 h in a muffle furnace. The catalyst (referred as SSZ-550) preparation is shown in **Scheme 3.1**.

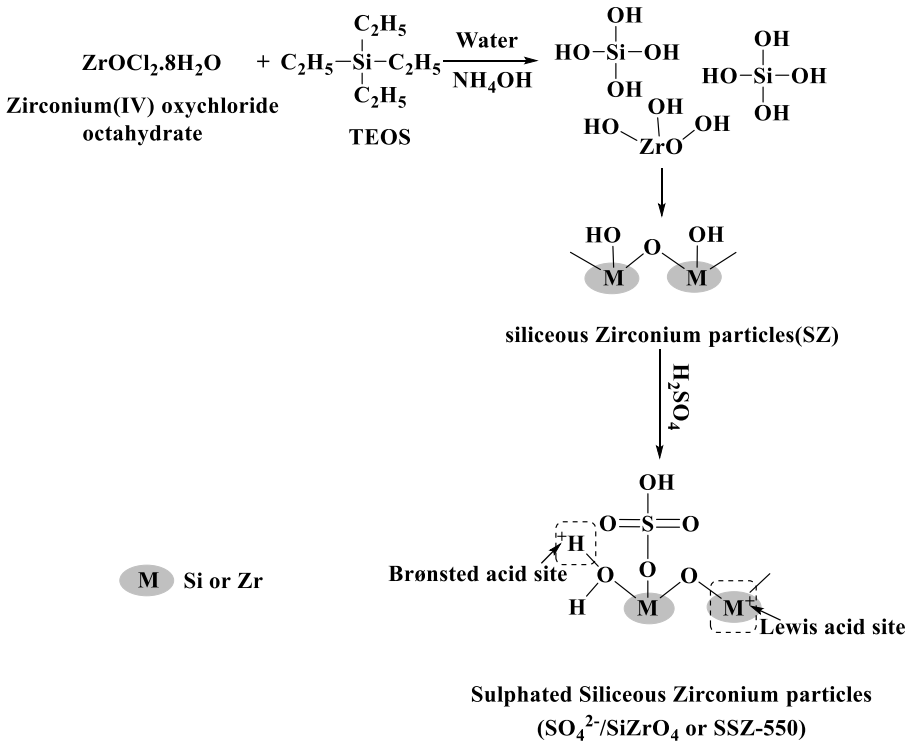

Scheme 3.1. Schematic representation for the formation of sulphated siliceous zirconia (SSZ-550) catalyst.

3.2.3. Acetylation of glycerol with acetic acid

A series of the GL acetylation reaction was performed to establish the optimum conditions to achieve the maximum TA selectivity. One parameter at a time was varied out of the reaction temperature (30–100 °C), AcA/GL molar ratio (3–12), reaction duration (1–50 min), and catalyst amount (1–5 wt% of GL). To evaluate the catalyst reusability, it was recovered from

the reaction mixture by centrifugation, washed with methanol, and calcined at 550 °C. The catalyst thus regenerated was employed in six successive cycles under the same experimental and regeneration conditions.

3.3. Results and discussion

3.3.1. Catalyst Characterization

3.3.1.1. XRD analysis

The X-ray diffraction (XRD) patterns for SZ demonstrate a broad hump (2θ = 22), as shown in **Fig. 3.1a**, to support the amorphous nature of the prepared matrix. On incorporating the sulphate group over the matrix, SSZ-550 has been formed which was found to exist in the crystalline phase as evident by the appearance of the sharp peaks in the XRD patterns (**Fig. 3.1b**). The crystalline nature of the material was due to the formation of $ZrSiO_2$ as minor phase (JCPDF = 01-081-0590) and $Zr(SO_4)_2$ as major phase (JCPDF = 00-024-1492), as shown in **Fig. 3.1b**. The crystallite size of the $Zr(SO_4)_2$ phase, calculated by the Scherrer equation, was found to be 13.2 nm.

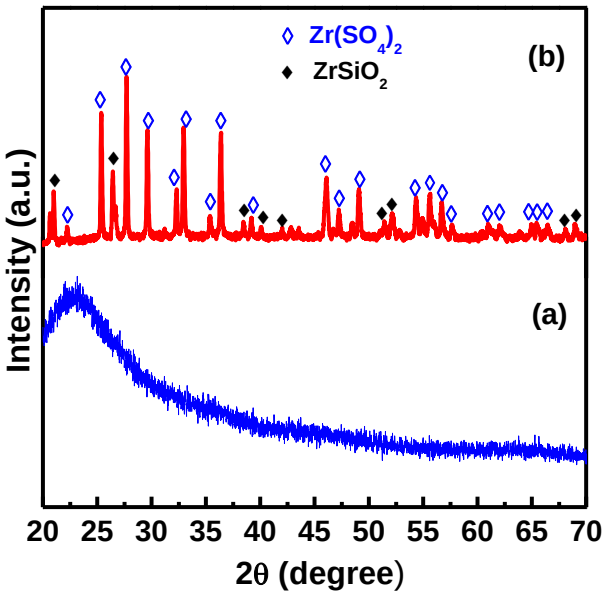

Fig. 3.1. X-ray diffraction patterns of (a) SZ and (b) SSZ-550.

3.3.1.2. FTIR analysis

The FTIR spectra of the prepared SZ and SSZ-550 are compared in **Fig. 3.2** to indicate the sulphate group anchoring over the siliceous zirconia surface. Both the samples show a strong band at ~ 802 cm^{-1} due to Si–O–Si bond vibrations. In literature, the presence of a band at 808 cm^{-1} has been reported to indicate the presence of Si–O–Si bonding [7]. In the case of

SSZ-550, new bands in the range of ~ 1028–1266 cm^{-1} were observed (**Fig. 3.2b**), due to the stretching vibrations corresponding to S–O and S=O bonds to support the incorporation of the sulphate group over the siliceous zirconia matrix. A similar observation was reported by Sun and Garcia where the bands in the range of 1045–1223 cm^{-1} have been reported to indicate sulphate ion anchoring over the siliceous zirconia matrix [8-9].

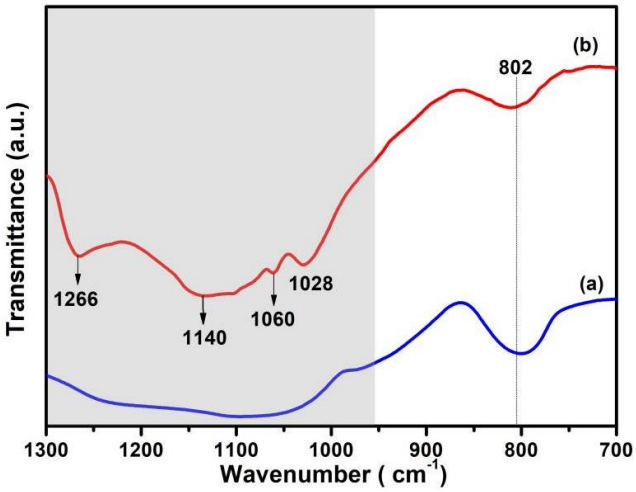

Fig. 3.2. FTIR spectra of (a) SZ and (b) SSZ-550.

3.3.1.3. BET analysis

The BET surface area of SZ and SSZ-550 was measured by N_2 adsorption-desorption isotherms as represented in **Fig. 3.3**. All the samples were found to exhibit type-IV curves of IUPAC classification, which indicates the mesoporous nature of the samples. In case of siliceous zirconia, matrix surface area and pore volume were found to be 197 m^2g^{-1} and 0.3 cm^3g^{-1}, respectively, as shown in **Fig. 3.3a**.

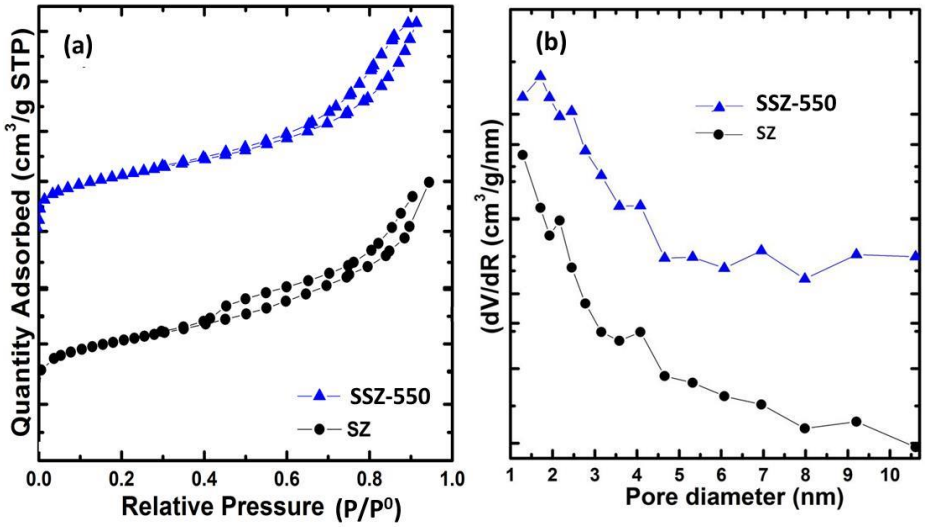

Fig. 3.3. (a) N_2 adsorption-desorption isotherms and (b) Pore size distribution.

However, upon sulphate group impregnation over the matrix, the surface area as well as pore volume was found to decrease to 70 m^2g^{-1} and 0.1 cm^3g^{-1}, respectively (**Table 3.1**). The drop in the surface area could be ascribed to the pore blockage of the matrix upon sulphate group attachment. Ward *et al*. also observed the reduction of surface area (from 709 to 342 m^2g^{-1}) as well as pore volume (from 0.8 to 0.4 cm^2g^{-1}) when sulphated zirconia was impregnated over the mesoporous silica surface [10].

Table 3.1. Comparison of the BET specific surface area, pore volume, and total acidity of SZ and SSZ-550.

Catalyst	BET surface area (m^2g^{-1})	Pore volume (cm^3/g^{-1})	Total acidity (mmol g^{-1})
SZ	197	0.3	0.43
SSZ-550	67	0.1	4.96

3.3.1.4. NH_3-Temperature Programmed Desorption study

The acidic sites present over the catalyst surface were quantified by the temperature-programmed desorption of ammonia (NH_3-TPD). The TPD profiles of the desorbed NH_3 from SZ and SSZ-550 catalysts are shown in **Fig. 3.4.** A broad peak in the range of 233–243 °C, for both the samples, was observed owing to the ammonia desorption from weak acidic sites. However, sulphate incorporation over the siliceous zirconia demonstrates an additional desorption peak at 473 °C (4.96 mmol g^{-1}) to indicate the formation of strong acidic sites (**Table 3.1**). Chen *et al*. observed that sulphated silica–zirconia nanoparticles demonstrated desorption peaks in the range of 210–290 °C and 460–600 °C to indicated the presence of weak and strong acidic sites, respectively, over the catalyst surface [11,12].

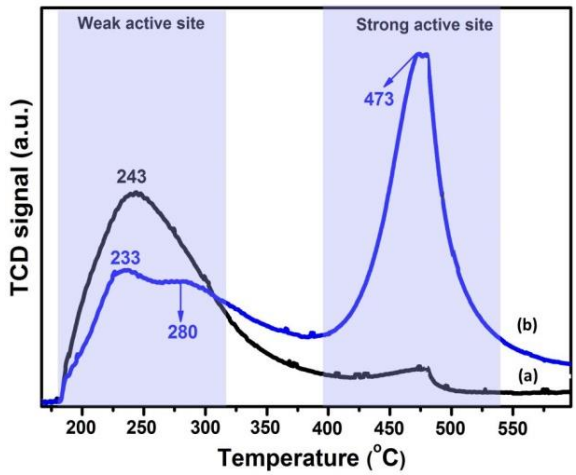

Fig. 3.4. NH_3-TPD profiles for (a) SZ and (b) SSZ-550.

3.3.1.5. Pyridine adsorption DRIFT study

To study the nature of the acidic sites present over the catalyst surface, pyridine-saturated matrix and catalyst were subjected to FTIR spectroscopy. Through this method, Brønsted and Lewis acid sites present over the catalyst could be identified and differentiated [13]. As shown in **Fig. 3.5**, the siliceous zirconia matrix shows a single band at 1636 cm^{-1} owing to the presence of Brønsted (B) acidic sites on its surface in the form of –OH group. Upon SO_4^{2-} incorporation over the SZ matrix, new bands at 1445, 1490, 1545 and 1613 cm^{-1} were observed in addition to the band observed for the native matrix. Thus, incorporation of sulphate group over the matrix leads to the formation of Brønsted as well as Lewis acidic sites. The Brønsted sites interact with pyridine, which leads to the formation of pyridinium ions, and same could be identified due to band at 1545 cm^{-1} in the FTIR spectrum. The presence of a band at 1490 cm^{-1} is indicative of pyridine coordinated to Lewis acid sites. In literature, similar band was also reported at 1540 cm^{-1}, to support the formation of pyridinium ions, owing to the interaction of pyridine with Brønsted acids and the presence of the bands at 1450 and 1487 cm^{-1} are indicative of pyridine coordinated to Lewis acidic sites [14-16]. Desmartin-Chomel *et al*. concluded that sulphate group is mainly responsible for generating strong acidic sites that impart the acetylation activity to the catalyst [17].

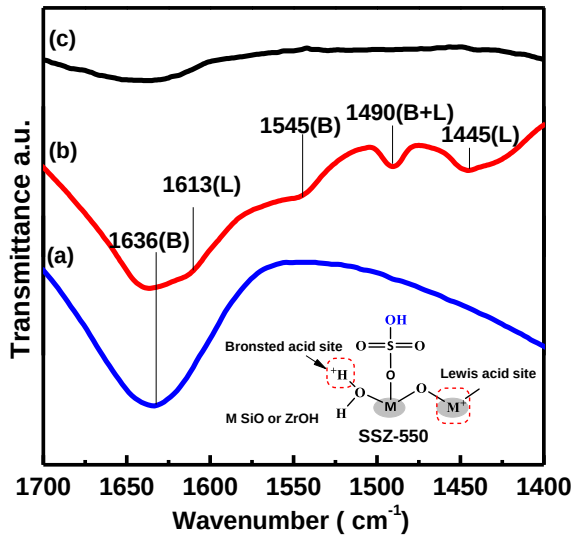

Fig. 3.5. FTIR spectra of pyridine adsorbed on (a) SZ, (b) SSZ-550 and (c) without pyridine adsorption of SSZ-550.

3.3.1.6. SEM, EDX and elements mapping analysis

The morphology and elemental distributions of the catalyst particles were examined by SEM–EDX technique, and corresponding elemental mapping is shown in **Fig. 3.6**. The SEM images of the siliceous zirconia (**Fig. 3.6a**) and sulphated siliceous zirconia (**Fig. 3.6b**) show

the formation of agglomerated nanoparticles in irregular geometries. Elemental mapping clearly demonstrates that all the elements (O, Si, Zr and S) are uniformly distributed over the catalyst surface.

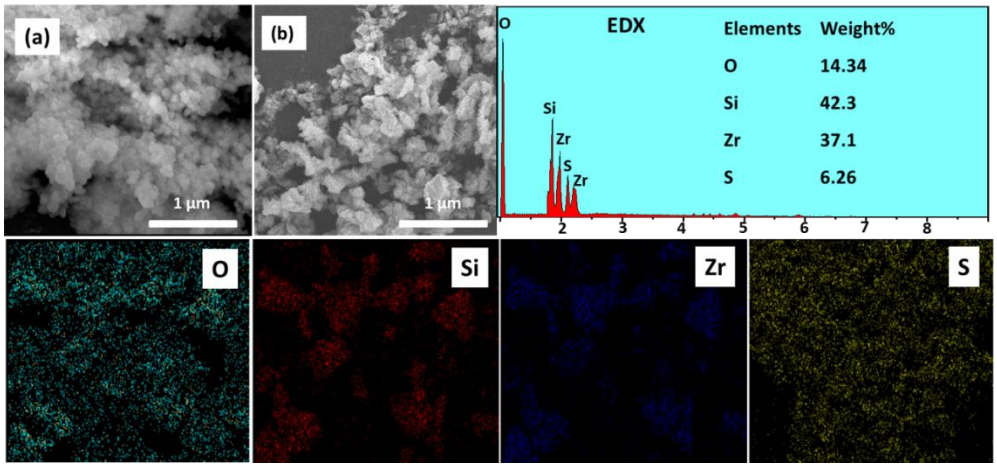

Fig. 3.6. SEM images of (a) SZ, (b) SSZ-550, EDX and elemental mapping of SSZ-550.

3.3.1.7. TEM analysis

TEM image of SSZ-550 was studied in order to get information about the particle size and geometry, as shown in **Fig. 3.7**. The TEM analysis of SSZ-550 revealed the formation of spherical agglomerated particles (~16 nm size), which is close to the crystallite size (13.2 nm) calculated from XRD data. The smaller particle size could be correlated with the higher catalyst surface exposure to the reactants, facilitating the higher catalyst activity.

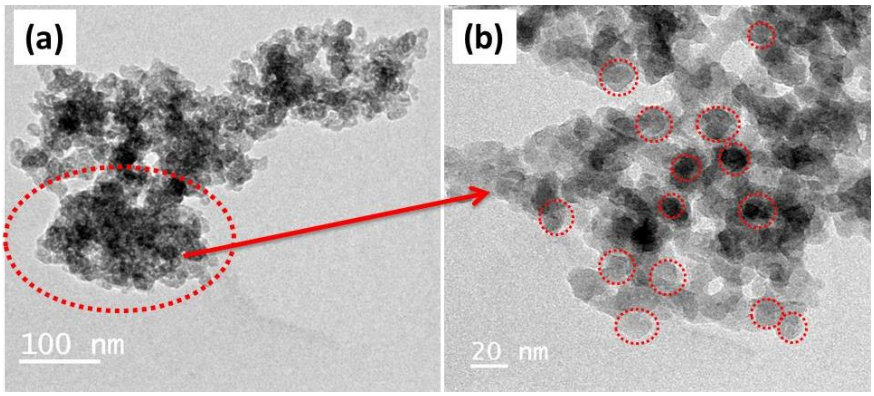

Fig. 3.7. TEM images of (a) and (b) SSZ-550.

3.3.1.8. XPS analysis

The XPS spectra of silicon, sulfur, zirconia, and oxygen, present in SSZ-550 catalyst, are shown in **Fig. 3.8** for determining the electronic state of the elements. The full scan XPS spectrum of the SSZ-550 confirmed the presence of Si, S, Zr, and O elements over the

catalyst surface as shown in **Fig. 3.8a**.The peak observed at 103.6 eV and 102 eV could be attributed to $2p_{1/2}$ and $2p_{3/2}$ level of Si^{4+} as shown in **Fig. 3.8b**. Observed values are very close to the literature reported values of 103.1 eV and 102 eV for Si^{4+} $2p$ state present in SiO_2 material [18,19]. The presence of sulphate functional group over the siliceous zirconia matrix could be attributed to the presence of two peaks at 168.4 and 170.1 eV corresponding to the S^{6+} $2p_{3/2}$ and S^{6+} $2p_{1/2}$ states, respectively (**Fig. 3.8c**). These binding energy values also support the linkages of the sulphate group with zirconia/silica matrix as the corresponding values for the sulphate group linked to ZrO_2 matrix were reported at 168.9 and 169.2 eV [20]. The XRD analysis of the same material also indicates the formation of $Zr(SO_4)_2$; however, owing to the amorphous nature of the silica, no peak due to silica sulphate has been observed. Anchoring of the sulphate group over the matrix was also supported by the FTIR analysis of the catalyst as discussed in the earlier section. Furthermore, the XPS spectrum shows (**Fig. 3.8d**) peaks at 185.1 and 182.7 eV corresponding to the Zr^{4+} $3d_{3/2}$ and Zr^{4+} $3d_{5/2}$ states, respectively. This study could be correlated with the literature, where the presence of Zr^{4+} has been attributed to the appearance of peaks at 182.9 and 185.3 eV for Zr^{4+} $3d_{5/2}$ and Zr^{4+} $3d_{3/2}$ states, respectively, in ZrO_2 phase [21]. The peaks (**Fig. 3.8e**) at 528.7, 533.1, and 531.4 eV may be due to the presence of O^{2-} 1*s* state of lattice oxygen and could also be ascribed to the various linkages of oxygen present in the catalyst, *viz.* Si–O–Si, S–O–Zr, and Zr–O–Si, respectively. Similar observations were reported, where the presence of O^{2-} 1*s* in the sulphated siliceous zirconia nanoparticles was supported by peaks at 532.4 and 532.5 eV corresponding to Si–O–Si or Zr–O–Si and S–O–Zr linkage, respectively [22].

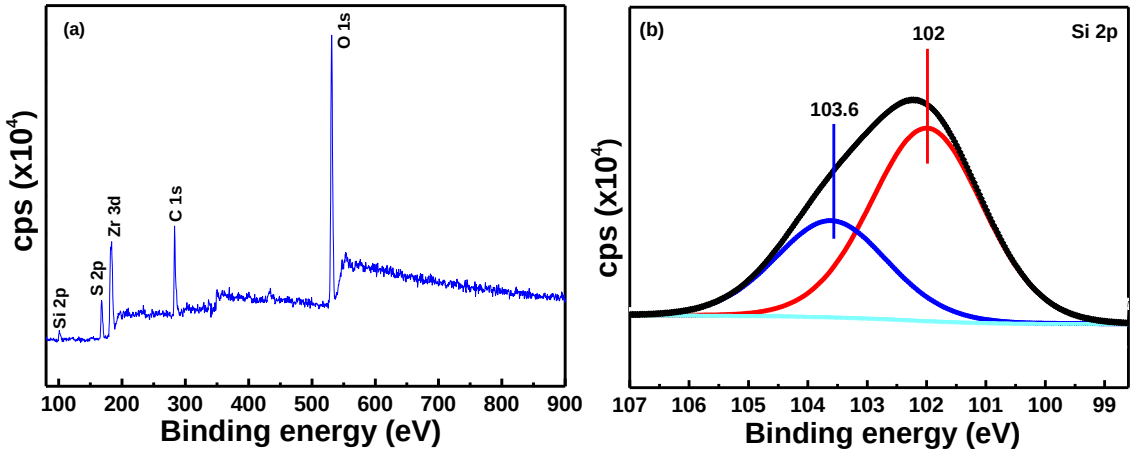

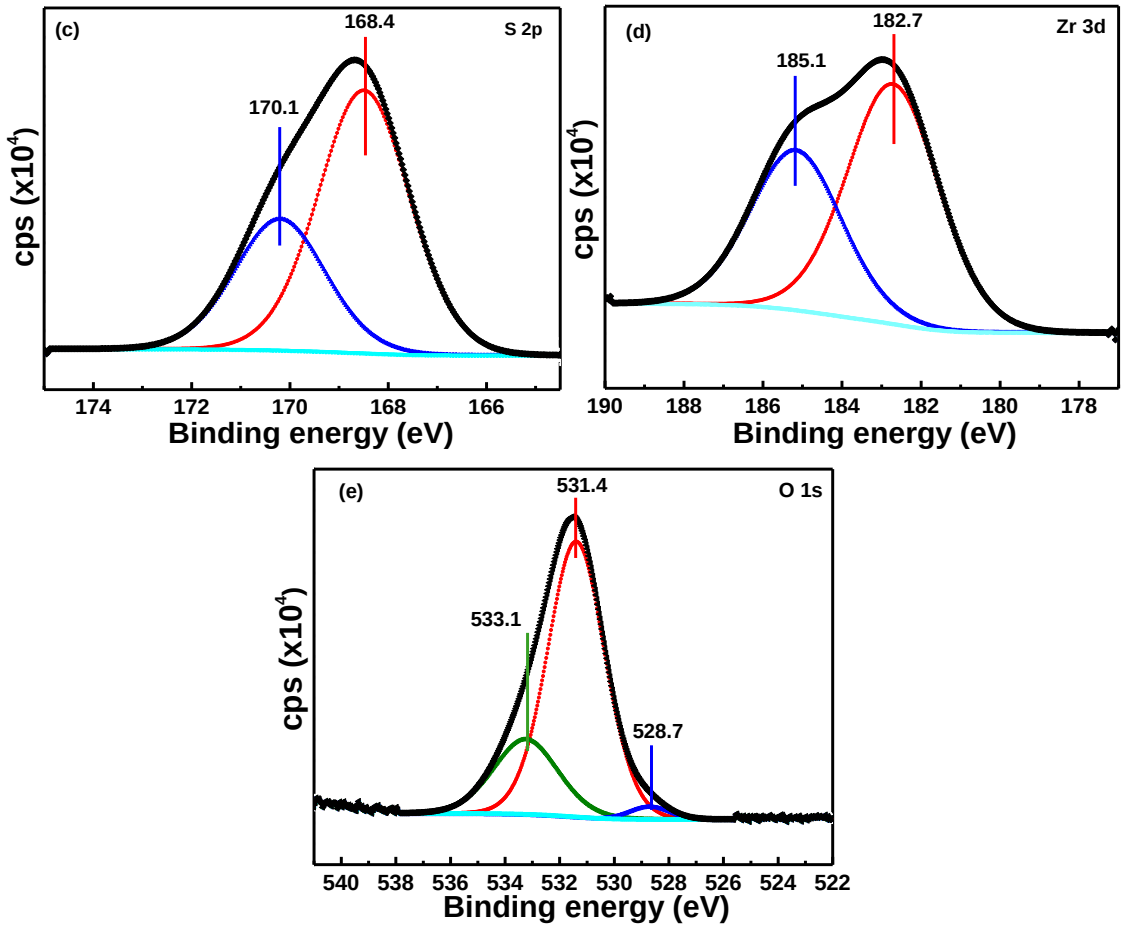

Fig. 3.8. XPS spectra of SSZ-550 catalyst (a) full scan, (b) Si 2p, (c) S 2p, (d) Zr 3p, and (e) O 1s.

3.3.2. Product analysis

3.3.2.1. FTIR analysis

Formation of the TA could be supported with the help of the FTIR spectroscopic technique. In the FTIR spectra of GL, two bands at 1042 and 3300 cm^{-1} were observed due to the C–O and O–H group stretching frequencies, respectively, as shown in **Fig. 3.9a**. Upon GL acetylation, a new band at 1737 cm^{-1} (**Fig. 3.9b**), due to –C=O group, was observed to support the formation of the ester bond. The absence of any band in –OH region further supports the acetylation of GL hydroxyl groups.

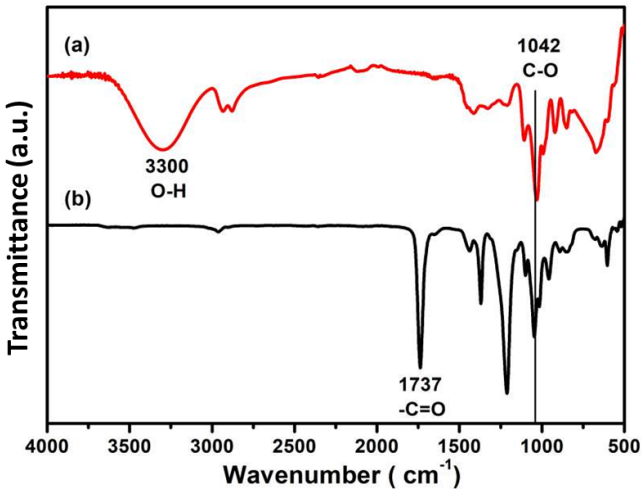

Fig. 3.9. FTIR spectra of (a) glycerol, and (b) triacetin produced during glycerol acetylation.

3.3.2.2. HPLC analysis

The primary product, TA, formed during the reaction was confirmed by comparing its retention time (6.30 min) with that of the standard TA sample, as shown in the HPLC chromatogram in **Fig. 3.10**. The HPLC chromatogram (**Fig. 3.10c**) of reaction products show no peak corresponding to the GL (8.90 min) to confirm its 100 % conversion into the product molecules. The quantitative analysis of the product mixture further supports the TA selectivity of 93 % while the remaining 7 % being the DA.

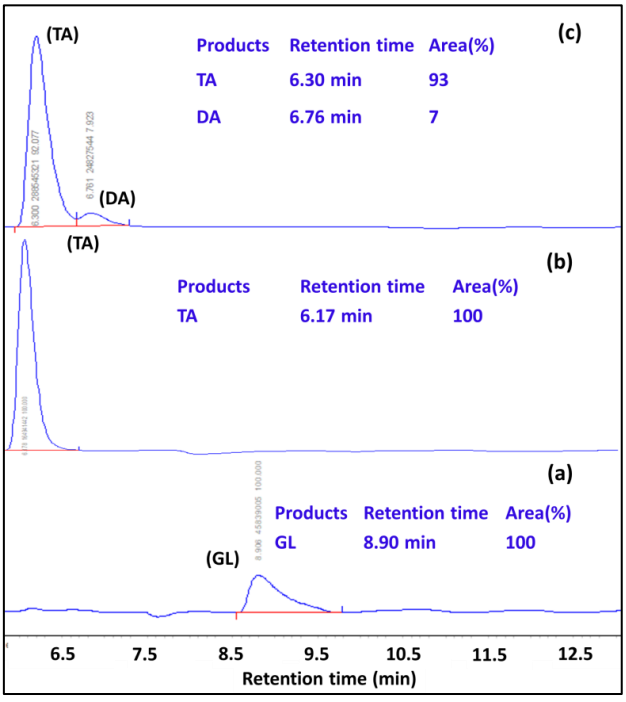

Fig. 3.10. HPLC chromatogram of (a) pure glycerol (b) pure triacetin and (c) triacetin produced during glycerol acetylation.

3.3.3. Catalyst screening

Prior to the catalyst screening, in blank runs, acetylation of GL with AcA was performed in absence of catalyst, or in the presence of bare siliceous zirconia matrix. It is evident from **Fig. 3.11** that in absence of catalyst merely 11.5 % GL conversion with negligible TA selectivity was obtained, while the bare siliceous zirconia was able to yield 69 % GL conversion with 1.6 % TA selectivity. Thus, sulphate group anchoring over the matrix is required to generate the acidic site which is primarily responsible for catalysing the GL acetylation. Reddy *et al*. also suggested that sulphate impregnated CeO_2–ZrO_2 and CeO_2–Al_2O_3 catalysts demonstrate better TA selectivity (90 %) at 120 °C reaction temperature while carrying out the reaction with 6:1 AcA/GL molar ratio and in the presence of 5 wt% of catalyst amount [23,24]. To demonstrate the effect of reaction parameters on the catalyst activity, in the present study, the reagent ratio, catalyst amount, reaction temperature and reaction time have been sequentially varied as discussed in the subsequent section.

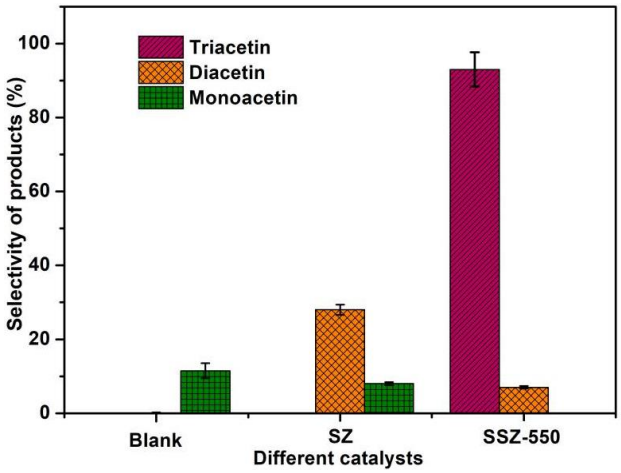

Fig. 3.11. Effect of the various catalysts over the acetylation of glycerol. [*Reaction conditions:* AcA/GL = 9:1 molar ratio, reaction time = 40 min, catalyst amount = 3 wt% (with respect to GL) and reaction temperature = 80 ºC]

3.3.3.1. Effect of AcA/GL molar ratio on product selectivity

Conversion of GL and TA selectivity over SSZ-550 catalyst at 80 °C on 3 wt% of catalyst (concerning GL) with varying AcA/GL molar ratio (from 3 to 12) is shown in **Fig. 3.12a**. Theoretically, every molecule of GL required three molecules of AcA to achieve the 100 % TA selectivity. However, to push the equilibrium in the forward direction, the reaction is usually performed in the presence of an excess amount of AcA. During the present study, the use of lower AcA/GL molar ratio (up to 3) was found to yield a mixture of products which consists of MA (41 %), DA (34 %), TA (12 %) and unreacted GL. On increasing the molar

ratio up to 9, TA yield increased up to 93 % within 40 min of reaction duration. Such a high TA selectivity has not been frequently reported during heterogeneous catalyst assisted acetylation of GL. In the literature, at 3:1 AcA/GL molar ratio, $SO_4^{2-}/CeO_2–ZrO_2$ catalyst was found to demonstrate the poor TA selectivity of 5 % along with MA yield of 25 %. Even on increasing the molar ratio up to 6, the TA selectivity was found to increase marginally (from 5 to 16 %) that too at higher reaction temperature of 120 °C and after a prolonged duration of 3 h [24].

3.3.3.2. Effect of catalyst amount on product selectivity

In order to optimize the catalyst amount, acetylation of GL was performed employing 9:1 AcA/GL molar ratio, 1–5 wt% catalyst (concerning GL) at 80 °C for 40 min of reaction duration. It can be seen that at a lower catalyst amount (up to 2 wt%), 90 % GL conversion was observed but yielding the lower TA selectivity (46 %) along with the formation of some MA (14%) and DA (30 %) by-products. Maximum TA selectivity of 93 % was obtained, at the cost of MA and DA, when 3 wt% of catalyst was employed, and a further increase in catalyst amount (up to 5 wt%) was neither found to improve the selectivity nor able to reduce the reaction duration (**Fig. 3.12b**). The same phenomenon is also reported for the acetylation of GL with AcA (7:1 AcA/GL molar ratio) at 100 °C reaction temperature in the presence of an acidic catalyst, where an increase in catalyst amount from 2 to 3 wt% was also found to improve the TA selectivity from 56.28 to 66.91 % [25]. Additionally, the TOF calculation also supports that the presence of 3 wt% of catalyst exhibited a maximum turnover frequency (262 h^{-1}) as compared to 1 wt% (131 h^{-1}) of catalyst. Hence, 3 wt% catalyst was employed for optimizing the other reaction parameters to achieve the maximum TA selectivity.

3.3.3.3. Effect of reaction temperature on product selectivity

Acetylation of GL in the literature has been reported to follow the endothermic pathway and hence, an external source of heat is essential to push the reaction in the forward direction [4]. In order to study the effect of temperature on GL conversion as well as product selectivity, a series of reactions was performed in the presence of SSZ-550 catalyst by varying the temperature in the range of 30 to 100 °C, as shown in **Fig. 3.12c**. A significant increase in TA selectivity from 0 to 93 % was observed when the reaction temperature was raised from 30 to 80 °C. A further increase in the reaction temperature (up to 100 °C) has not resulted in any significant rise in TA selectivity. Hence, SSZ-550 catalyzed reaction should be performed at 80 °C to achieve the optimum catalyst activity.

3.3.3.4. Effect of reaction time on product selectivity

To establish the reaction duration to achieve the maximum TA selectivity, a series of GL acetylation was performed at 80 °C in the presence of 3 wt% catalyst at a constant AcA/GL molar ratio of 9:1. It is evident from the plot (**Fig. 3.12d**) that during first 20 min of reaction period DA (25 %) is the leading product and remains predominant till 30 min of reaction duration. However, after 40 min, TA became the exclusive product (93 %) to support that GL acetylation proceeds in a step wise fashion. Reddy *et al*. have also studied the extent of GL acetylation at various time intervals over $SO_4^{2-}/CeO_2–ZrO_2$ catalyst at 120 °C and observed 63 % and 11 % selectivity of DA and TA, respectively, within 0.5 h of reaction duration [23,24]. Same study reported a maximum TA selectivity of 90 %, nevertheless, after a prolonged reaction duration of 4 h. Thus, our research, as well as literature report, supported the stepwise acetylation of GL and an increase in TA selectivity on increasing the reaction duration.

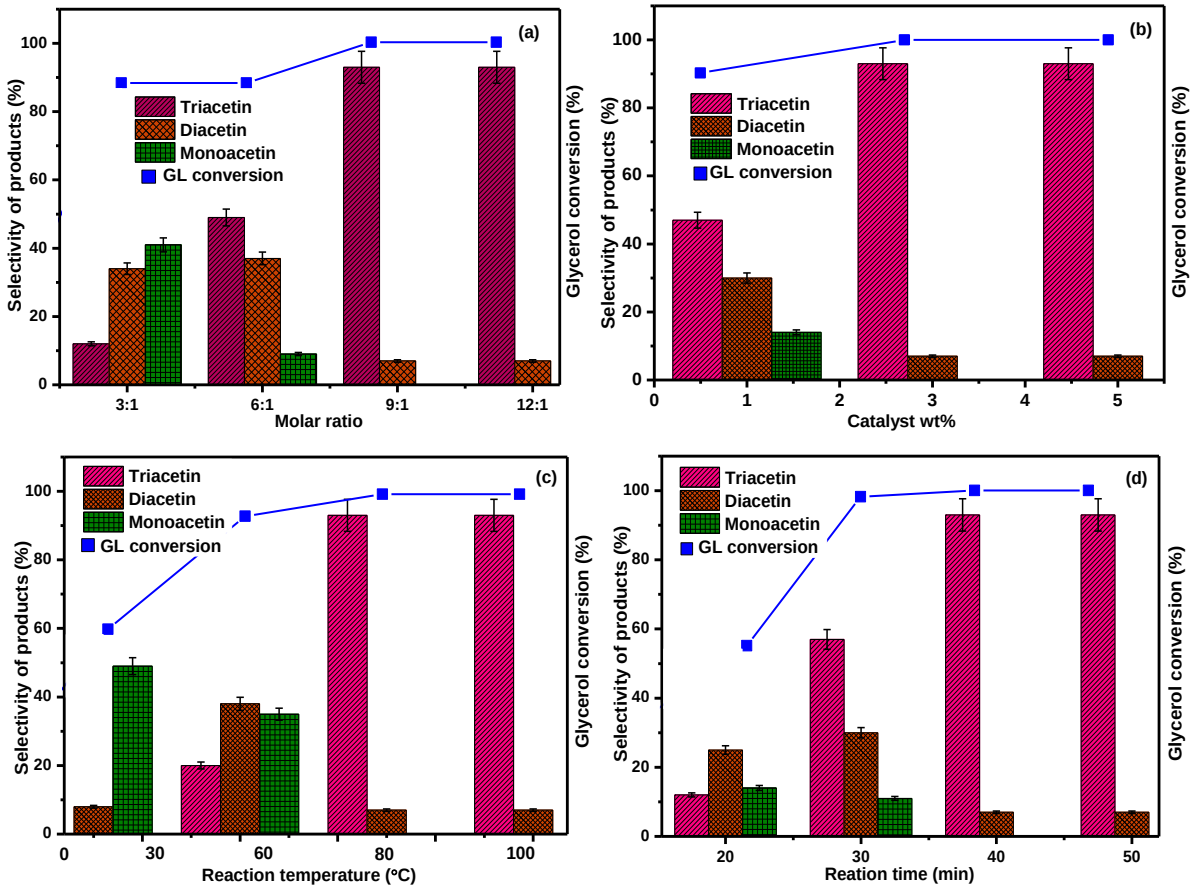

Fig. 3.12. Influence of various reaction parameters on SSZ-550 assisted glycerol acetylation (a) molar ratio of AcA/GL, (b) catalyst amount with respect to GL, (c) reaction temperature and (d) reaction time.

3.3.4. The reusability and stability

The reusability of SSZ-550 catalyst was evaluated under the optimized reaction conditions, *viz.*, AcA/GL molar ratio of 9:1, 3 wt% of catalyst (concerning GL), 80 °C reaction temperature, and 40 min of reaction duration. As shown in **Fig. 3.13**, the SSZ-550 catalyst was employed during six catalytic runs under identical reaction conditions. After every run the catalyst was recovered from the mixture through filtration, washed with methanol to remove the reactants/products from the catalyst surface, dried at 100 °C for 12 h and finally calcined at 550 °C for 4 h. The results revealed that recovered catalyst, during the first 3 catalytic cycles, was able to yield up to 80 % TA selectivity, which declined gradually to 50 % in the 6^{th} cycle.

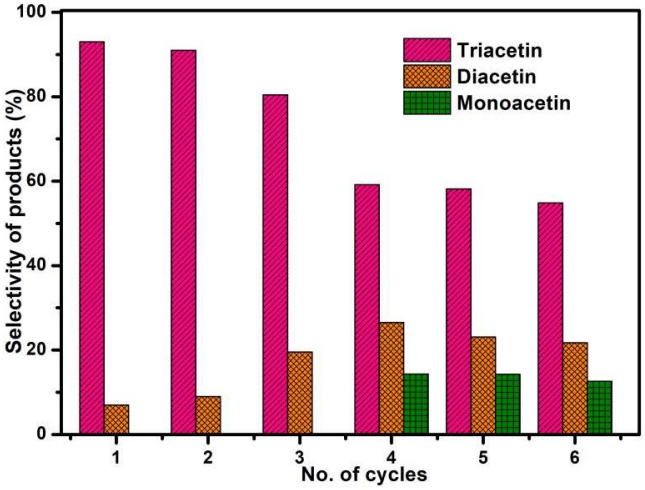

Fig. 3.13. Study of the SSZ-550 reusability during the glycerol acetylation with acetic acid. [*Reaction conditions:* AcA/GL = 9:1 molar ratio, reaction time = 40 min, catalyst amount = 3 wt% (with respect to GL) and reaction temperature = 80 ºC]

To establish the reason(s) behind the loss in catalytic activity, NH_3-TPD profile of fresh and reused catalysts is compared in **Fig. 3.14a**. The fresh catalyst exhibited the strong acid sites, as revealed from the desorption peak at 473 °C, with a total acidity of 4.96 mmol g^{-1} in comparison with 1.36 mmol g^{-1} for the spent catalyst at the same desorption temperature. Thus, a decrease in catalyst acidity could be attributed to loss of acidic sites which might be due to the loss of sulphate species from the catalyst surface.

In order to evaluate the loss of sulphate ions from the catalyst surface, the FTIR spectra of fresh and spent catalyst are compared in **Fig. 3.14b**. The partial loss of SO_4^{2-} moiety from the spent catalyst is evident due to the decrease of IR bands intensity positioned at 1028, 1140, and 1266 cm^{-1}. The absence of any vibrational band associated with the TA or GL in the

FTIR of reused catalyst further maintained that organic molecules have not collected over the catalyst facade to hinder the active sites.

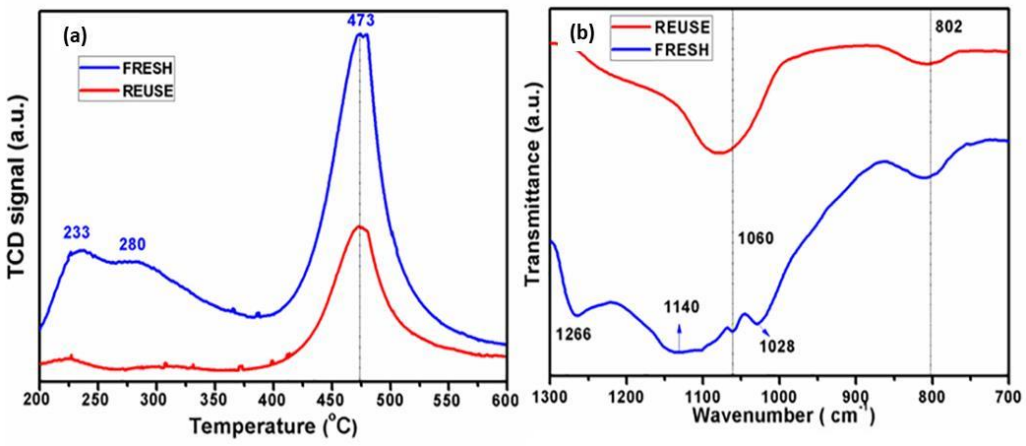

Fig. 3.14. Comparison of (a) NH_3-TPD and (b) FTIR plot of fresh and reused catalyst.

As evident from the FTIR study, the sulphate group has been detached from the catalyst surface during the repeated use. The leached active sites from the matrix may catalyze the reaction similar to the homogeneous catalyst. To quantify the homogeneous contribution in the catalyst activity, a hot filtration test was performed. During the trial, acetylation of GL was performed under optimized reaction parameters for 20 min and after that catalyst was separated from the reaction mixture with the help of simple filtration. Now, the reaction mixture, without catalyst, was allowed to react for an additional 20 min. As evident from **Fig. 3.15**, no significant change in the GL conversion level was observed when the reaction was allowed to continue in the absence of catalyst. Thus, it is safe to assume that dissolved catalyst contents, if any, were not able to catalyze the reaction to a significant extent, and heterogeneous catalyst is primarily responsible for almost the entire catalytic activity.

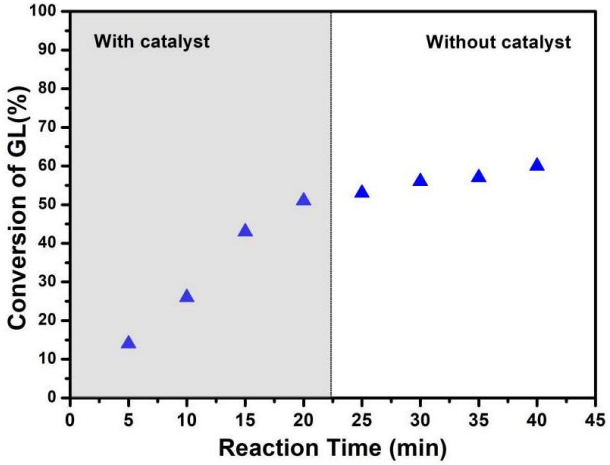

Fig. 3.15. Study of homogeneous contribution during the acetylation of glycerol with acetic acid.

3.4. Proposed mechanism for the acetylation of glycerol with acetic acid

As indicated by the blank experiments ("Catalyst screening" section), in the absence of catalyst, merely 11.5 % GL conversion with negligible TA selectivity was obtained. On the other hand, bare siliceous zirconia yielded merely 1.6 % TA selectivity with a higher GL conversion level of 69 %. These experiments clearly indicate the catalytic role of strong Brønsted acidic sites during the synthesis of TA. However, relatively higher GL conversion levels were obtained with bare catalyst, due to the presence of surface Brønsted acidic sites ($O^{-}H^{+}$) as shown in structure I in **Scheme 3.2**. Nevertheless, these sites are not strong enough to yield higher TA selectivity. Sulphate group anchoring over the siliceous zirconia matrix imparted the strong Brønsted acidity, and consequently, the SSZ-550 catalyst was able to produce 93 % TA selectivity with overall 100 % GL conversion within 40 min of reaction duration. Sulphuric acid, as a homogeneous catalyst, has also been reported to catalyze the acetylation of mono as well tri-alcohol (GL) and found to follow the (pseudo) first-order kinetic model [25,26]. Consequently, in the present study, sulphate groups have been proposed as the reaction centres for initiating the TA synthesis.

As discussed earlier ("Effect of reaction time on product selectivity" section), the MA selectivity was found to be maximum at the beginning of the reaction, which gradually got converted into the DA and TA to support the stepwise acetylation of the GL. During the present study ("Effect of AcA/GL molar ratio on product selectivity" section), when the AcA concentration was varied, the rate of TA formation was also found to change. However, the same was not found to be affected when GL concentration was varied.

Thus, a plausible mechanism assumes the sulphate group assisted protonation of the AcA carbonyl group during the first step of the reaction to form the carbocation (II) as an intermediate as shown in **Scheme 3.2** [26-28]. Now the carbocation (II) may react with the –O–H of GL to form another intermediate (III). A water molecule has been given away by the intermediate (III) to generate a new carbocation (IV). Carbocation (IV) ultimately regenerates the catalyst and leads to the formation of the MA (V). Now, one of the remaining two –OH groups of MA would further react with AcA, following the similar mechanism as described above, to form DA. The remaining –OH group of DA may further react with AcA to form the TA molecule following the similar mechanism as described for MA synthesis.

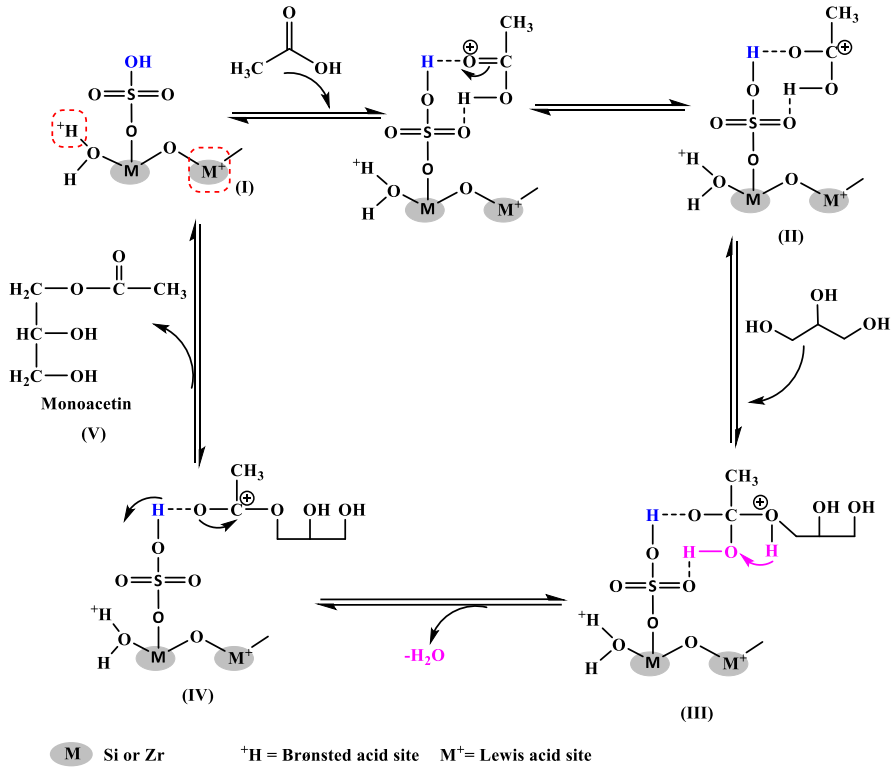

Scheme 3.2. Proposed mechanism for the glycerol acetylation with acetic acid in presence of SSZ-550 catalyst.

3.5. Conclusions

Glycerol acetylation with acetic acid was performed in the presence of the SSZ-550 heterogeneous acid catalyst to yield the 93 % triacetin selectivity during a quick succession of 40 min. The presence of Brønsted acidic sites, in the form of sulphate group, was found to be accountable for the higher catalytic activity. The catalyst was recovered from the reaction mixture and reused during 6 catalytic runs albeit, with partial loss in activity owing to the fractional loss of sulphate group from the catalyst surface. Presently, efforts are in progress in our lab to improve the catalyst stability and reusability.

References

[1] Edward, M.; Peter, O.; Hilary, R. The use of impregnated perlite as a heterogeneous catalyst for biodiesel production from marula oil. *Chem. Papers* **2014**, 68 (10), 1341–1349. DOIhttps://doi.org/10.2478/s11696-014-0583-1

[2] Malaika, A.; Kozłowski, M. Glycerol conversion towards valuable fuel blending compounds with the assistance of SO_3H-functionalized carbon xerogels and spheres. *Fuel Process. Technol*. **2018**, 184, 19–26. https://doi.org/10.1016/j.fuproc.2018.11.006

[3] Goscianska, J.; Malaika, A. A facile post-synthetic modification of ordered mesoporous carbon to get efficient catalysts for the formation of acetins. *Catal. Today* **2019**, 00, 1–10. https://doi.org/10.1016/j.cattod.2019.02.049

[4] Patel, A.; Singh, S. A green and sustainable approach for esterification of glycerol using 12-tungstophosphoric acid anchored to different supports: Kinetics and effect of support. *Fuel* **2014**, 118, 358–364. https://doi.org/10.1016/j.fuel.2013.11.005

[5] Khayoon, M. S.; Hameed, B. H. Acetylation of glycerol to biofuel additives over sulfated activated carbon catalyst. *Bioresour. Technol*. **2011**, 102, 9229–9235. https://doi.org/10.1016/j.biortech.2011.07.035

[6] Kong, P. S.; Aroua, M. K.; Wan, Daud, W. M. A.; Lee, H. V.; Cognet, P.; Pérès, Y. Catalytic role of solid acid catalysts in glycerol acetylation for the production of bio-additives: a review. *RSC Adv*. **2016**, 6, 68885–68905. https://doi.org/10.1039/C6RA10686B

[7] Hu, X.; Hao, X.; Wu, Y.; Zhang, J.; Zhang, X.; Wang, P. C.; Zou, G.; Liang, X. J. Multifunctional hybrid silica nanoparticles for controlled doxorubicin loading and release with thermal and pH dual response. *J. Mater. Chem. B* **2013**, 1, 1109–1118. https://doi.org/10.1039/C2TB00223J

[8] Garcia, C. M.; Teixeira, S.; Marciniuk, L. L.; Schuchardt, U. Transesterification of soybean oil catalyzed by sulfated zirconia. *Bioresour. Technol*. **2008**, 99, 6608–6613. https://doi.org/10.1016/j.biortech.2007.09.092

[9] Sun, Y.; Ma, S.; Du, Y.; Yuan, L.; Wang, S.; Yang, J. Solvent-Free Preparation of Nanosized Sulfated Zirconia with Brønsted Acidic Sites from a Simple Calcination. *J. Phys. Chem. B* **2005**, 109, 2567–2572. https://doi.org/10.1021/jp046335a

[10] Ward, A. J.; Pujari, A. A.; Costanzo, Masters, A. F.; Maschmeyer, T. Ionic liquid-templated preparation of mesoporous silica embedded with nanocrystalline sulfated zirconia. *Nanoscale Res. Lett*. **2011**, 192. DOIhttps://doi.org/10.1186/1556276X-6-192

[11] Chen, X. ; Ju, Y.; Mou, C. Direct Synthesis of Mesoporous Sulfated Silica-Zirconia Catalysts with High Catalytic Activity for Biodiesel via Esterification. *J. Phys. Chem. C* **2007**, 111(50), 18731–18737. https://doi.org/10.1021/jp0749221

[12] Ganpat, V.; Gbadebo, Y. Mesoporous nanocrystalline sulfated zirconia synthesis and itsapplication for FFA esterification in oils. *Appl. Catal. A Gen*. **2013**, 463, 196–206. https://doi.org/10.1016/j.apcata.2013.05.005

[13] Parry, E. P. An Infrared Study of Pyridine Adsorbed on Acidic Solids. Characterization of Surface Acidity. *J. Catal*. **1963**, 2, 371–379. https://doi.org/10.1016/0021-9517(63)90102-7

[14] Kansedo, J.; Lee, K. T. Transesterification of palm oil and crude sea mango (Cerberaodollam) oil: The active role of simplified sulfated zirconiacatalyst. *Biomass Bioenerg*. **2012**, 40, 96–104. https://doi.org/10.1016/j.biombioe.2012.02.006

[15] Yang, Y.; Kou, Y. Determination of the Lewis acidity of ionic liquids by means of an IR spectroscopic probe. *Chem. Commun.* **2014**, 226-227. DOI: 10.1039/b311615h

[16] Massam, J.; Brown, D. R.The roles of Bronsted and Lewis surface acid sites in acid-treated montmorillonite supported ZnC_{12} alkylation catalysts. *Catal. Lett*. **1995**, 35, 335–343. DOI https://doi.org/10.1007/BF00807190

[17] Desmartin-Chomel, A.; Flores, J. L.; Bourane, A.; Clacens, J. M.; Figueras, F.; Delahay, G.; Giroir, F. A. Lehaut-Burnouf, C.; Calorimetric and FTIR Study of the Acid Properties of Sulfated Titanias. *J. Phys. Chem.* B **2006**, 110, 858–863. https://doi.org/10.1021/jp0530698

[18] Chernavskii, P. A.; Khodakov, A. Y.; Pankina, G. V. In situ characterization of the genesis of cobalt metal particles in silica-supported Fischer-Tropsch catalysts using Foner magnetic method. *Appl. Catal. A Gen*. **2006**, 306, 108–119. https://doi.org/10.1016/j.apcata.2006.03.033

[19] Malhotra, R.; Ali, A. 5-Na/ZnO doped mesoporous silica as reusable solid catalyst for biodiesel production *via* transesterification of virgin cottonseed oil. *Renew. Energy* **2019**, 133, 606-619. https://doi.org/10.1016/j.renene.2018.10.055

[20] Hino, H.; Kurashige, M.; Matsuhashi, H.; Arata, K. The surface structure of sulfated zirconia: Studies of XPS and thermal analysis. *Thermochim. Acta*. **2006**, 441, 35–41. https://doi.org/10.1016/j.tca.2005.11.042

[21] Desmartin-Chomel, A.; Flores, J. L.; Bourane, A.; Clacens, J. M. Figueras, F.; Delahay, G.; Giroir, F. M.; Lehaut-Burnouf, C. Calorimetric and FTIR Study of the Acid Properties of Sulfated Titanias. *J. Phys. Chem. B* **2006**, 110, 858–863. https://doi.org/10.1021/jp0530698

[22] Rosenberg, D. J.; Coloma, F.; Anderson, J. A. Modification of the Acid Properties of Silica–Zirconia Aerogels by in Situ and ex Situ Sulfation. *J. Catal*. **2002**, 228, 218–228. https://doi.org/10.1006/jcat.2002.3656

[23] Reddy, P. S.; Sudarsanam, P.; Raju, G.; Reddy, B. M. Selective acetylation of glycerol over CeO_2–M and SO_4^{2-}/CeO_2–M (M = ZrO_2 and Al_2O_3) catalysts for synthesis of bioadditives. *J. Ind. Eng. Chem*. **2012**, 18, 648–654. https://doi.org/10.1016/j.jiec.2011.11.063

[24] Trejda, M.; Stawicka, K.; Dubinska, A.; Ziolek, M. Development of niobium containing acidic catalysts for glycerol esterification. *Catal. Today* **2012**, 187, 129–134. DOI:10.10.1016/J.CATTOD.2011.10.033

[25] Setyaningsih, L.; Siddiq, F.; Pramezy, A. Esterification of glycerol with acetic acid over Lewatit catalyst. *MATEC Web Conf.* **2018**, 154, 01028. https://doi.org/10.1051/matecconf/201815401028

[26] Zhou, L.; Nguyen, T.; Adesina, A. The acetylation of glycerol over amberlyst-15: Kinetic and product distribution. *Fuel Process. Technol*. **2012**, 104, 310–318. https://doi.org/10.1016/j.fuproc.2012.06.001

[27] Kale, S.; Umbarkar, S. B.; Dongare, M. K.; Eckelt, R.; Armbruster, U.; Martin, Selective formation of triacetin by glycerol acetylation using acidicion-exchange resins as catalyst and toluene as an entrainer. *Appl. Catal. A Gen*. **2015**, 490, 10–16. https://doi.org/10.1016/j.apcata.2014.10.059

[28] Venkatesha, N. J.; Bhat, Y. S.; Prakash, B. S. J. Volume accessibility of acid sites in modified montmorillonite and triacetin selectivity in acetylation of glycerol. *RSC Adv*. **2016**, 10, 45819–45828. https://doi.org/10.1039/C6RA05720A

Development and functionalization of magnetic nanoparticles as stable and reusable catalyst for triacetin synthesis

Overview of the Chapter

The application of magnetic nanoparticles as an adsorbent and catalyst support in solving the environmental issues has recently received significant attention due to their unique physical and chemical properties, such as high surface area, ease of anchoring the functional groups, lower processing cost, high stability and ease of separation under an external magnetic field. A magnetic catalyst was prepared in the present study by embedding magnetite (Fe_3O_4) within the silica shell on which sulphate ions were anchored ($Fe_3O_4@SiO_2@SO_4^{2-}$). The catalyst was successfully employed for glycerol acetylation with acetic acid to obtain 100 % selectivity towards triacetin within 45 min of reaction duration at 80 °C. The catalyst was successfully isolated from the reaction medium magnetically and reused for 6 consecutive reaction cycles while retaining 90 % glycerol conversion levels and 50 % triacetin selectivity in the last reaction cycles.

4.1. Introduction

In the previous Chapter, GL was esterified with AcA in the presence of sulphated siliceous zirconia (SSZ) catalyst to produce TA. The heterogeneous catalyst from the reaction mixture was removed by filtration or centrifugation which is a time consuming and cumbersome process. The separation of the catalyst could be simplified by impregnating the catalytically active species over the Fe_3O_4 MNPs to facilitate the magnetic separation of the catalyst from the reaction mixture [1]. Thus incorporation of Brønsted as well as Lewis acid sites over the magnetic support may make the heterogeneous catalyst capable of carrying out the acetylation reaction and separable from the reaction mixture under the influence of an external magnetic field [2-4].

To the best of our knowledge, the synthesis of TA, as an exclusive product employing a magnetic catalyst has not been reported. Therefore, in the present study, the $Fe_3O_4@SiO_2@SO_4^{2-}$ magnetic heterogeneous acidic catalyst has been prepared to obtain TA as an exclusive product and to facilitate the magnetic separation of the catalyst from the reaction mixture. The recovered catalyst was also reused for 6 successive reaction cycles.

4.2. Experimental Section

4.2.1. Preparation of Fe_3O_4

The Fe_3O_4 MNPs were synthesized by the chemical co-precipitation method by following the reported method [5]. The solutions of $FeSO_4.7H_2O$ (0.017 M) and $FeCl_3.6H_2O$ (0.035 M), to maintain Fe^{+2}/Fe^{+3} ratio of 1:2, were mixed together under mild stirring at 35 °C in a glass beaker. After 10 min, 1.5 M NaOH solution was slowly added into the reaction mixture, until a pH 10 was achieved, with constant stirring for 2 h at 80 °C. The black precipitate formed was separated by external magnetic force (**Fig. 4.1a**), repeatedly washed with deionized water until the pH 7 of the filtrate was achieved. Finally, dark colored Fe_3O_4 nanoparticles thus obtained was dried at 70 °C for 12 h. The chemical equation involved in the synthesis of Fe_3O_4 MNPs are shown below [6]:

$$Fe^{+3} + 3OH^- \rightarrow Fe(OH)_3 \ldots\ldots\ldots\ldots\ldots\ldots\ldots\ldots (1)$$

$$Fe(OH)_3 \rightarrow FeOOH + H_2O \ldots\ldots\ldots\ldots\ldots\ldots\ldots\ldots (2)$$

$$Fe^{2+} + 2OH^- \rightarrow Fe(OH)_2 \ldots\ldots\ldots\ldots\ldots\ldots\ldots\ldots (3)$$

$$Fe(OH)_2 + 2FeOOH \rightarrow Fe_3O_4 + 2H_2O \ldots\ldots (4)$$

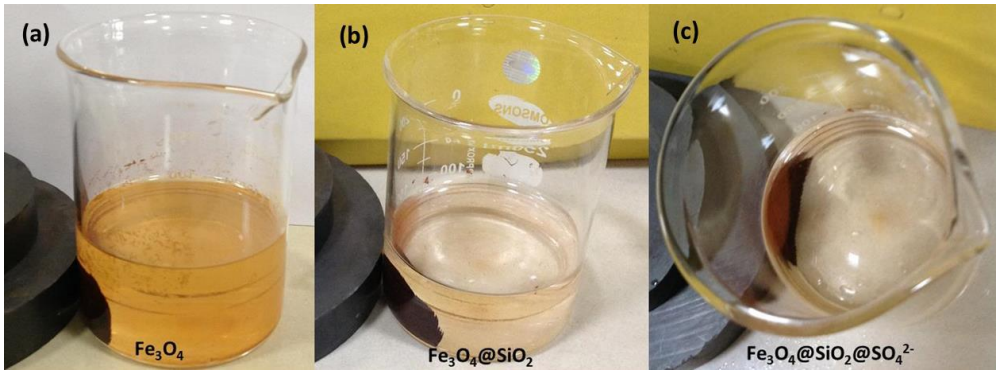

Fig. 4.1. Magnetic separation with the external magnet during the preparation of the magnetic catalyst.

4.2.2. Preparation of $Fe_3O_4@SiO_2$

Silica coated Fe_3O_4 MNPs were prepared by the sol-gel method as shown in **Scheme 4.1** (step-I) [7]. In this method, Fe_3O_4 (0.5 g) MNPs were dispersed in the ethanol/deionized water (4: 1, v/v) mixture in a beaker, and then NH_4OH solution was gradually added to maintain the pH 9 of the reaction mixture and to this TEOS (0.53 mL) was added under vigorous. After 12 h of stirring, the silica coated MNPs ($Fe_3O_4@SiO_2$) was separated with the help of a magnet (**Fig. 4.1b**) and washed with deionized water until pH 7 of the filtrate was achieved. The recovered $Fe_3O_4@SiO_2$ was dried at 70 °C for 12 h.

4.2.3. Preparation of $Fe_3O_4@SiO_2@SO_4^{2-}$

The sulphate group over $Fe_3O_4@SiO_2$ particles, was anchored by the wet impregnation method as shown in **Scheme 4.1** (step-II). The dried $Fe_3O_4@SiO_2$ (0.25 g) was immersed in 20 mL, 3 M H_2SO_4 solution for 12 h with constant stirring at 35 °C. Finally, the solid material was separated by using a permanent magnet (**Fig. 4.1c**), dried, and calcined at desired temperatures (550 to 650 °C) for 4 h to obtain magnetic heterogeneous acidic catalyst $Fe_3O_4@SiO_2@SO_4^{2-}$.

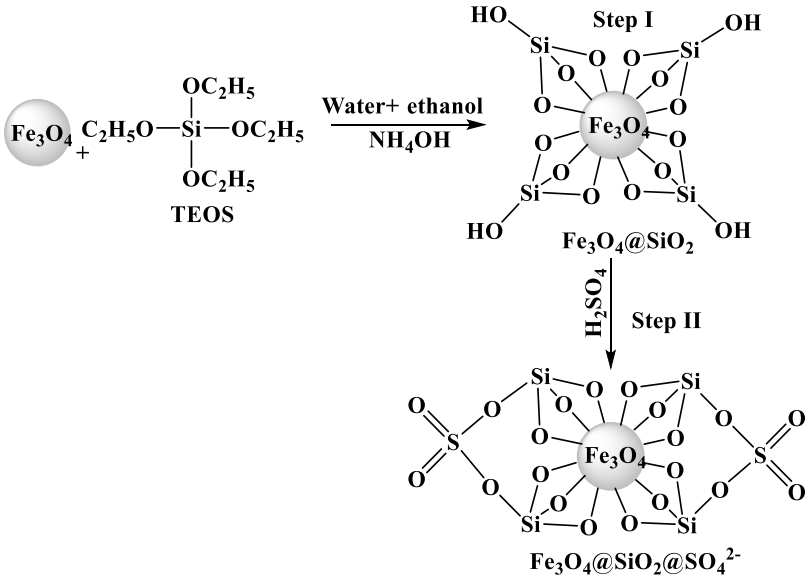

Scheme 4.1. Preparation steps for fabricating sulphate group over Fe_3O_4@SiO_2.

4.2.4. Acetylation of glycerol with acetic acid

The acetylation of GL with AcA was performed in a 50 mL two neck round bottom flask furnished with a water cooled condenser, hot plate, and magnetic stirrer. 5 g of GL and desired amounts of AcA and catalyst were charged into the round bottom flask which was constantly stirred at 80 °C for 45 min. After the reaction, the magnetic acidic catalyst was separated from the reaction mixture with the help of an external magnet (**Fig. 4.2**) and then the by-product (H_2O) was evaporated with the help of a rotary evaporator. The product thus obtained was characterized by ^{1}H-NMR and FTIR techniques and quantified by the HPLC technique.

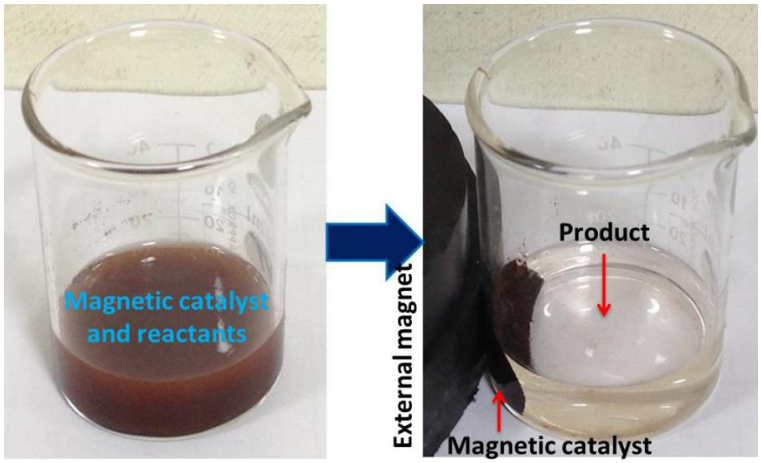

Fig. 4.2. Separation of magnetic catalyst from the reaction mixture with the help of external magnet.

4.3. Results and discussion

4.3.1. Catalyst Characterization

4.3.1.1. XRD analysis

The phase evolution of the prepared magnetic catalysts was studied by powder XRD technique and corresponding diffractograms are shown in **Fig. 4.3**. In case of Fe_3O_4, the diffraction peaks positioned at 30.40°, 35.58°, 43.37° 53.97°, 56.80°, and 62.92° (**Fig. 4.3a**) corresponding to the (220), (311), (400), (422), (511), and (440) planes, supports the inverse spinel cubic structure of Fe_3O_4. The diffraction patterns also match with the JCPDS card no 00-003-0862 recorded for Fe_3O_4 MNPs [8]. Peak broadening of X-ray diffraction peaks is because of the formation of nano-sized particles (16.79 nm). The silica coating of the Fe_3O_4 MNPs followed by calcination at 550 °C leads to the formation of $Fe_3O_4@SiO_2$ core-shell nanoparticles. In the X-ray diffraction pattern (**Fig. 4.3b**) of these nanoparticles, a broad hump centred around 23° is observed. This is a typical characteristic of amorphous silica, which further confirms the formation of the amorphous silica shell over the magnetic nanoparticles [3]. Silica coating over the magnetic nanoparticles was also confirmed by the FTIR study as discussed in the subsequent section. Sulphate impregnation over the $Fe_3O_4@SiO_2$ nanoparticles leads to the formation of $Fe_3O_4@SiO_2@SO_4^{2-}$, which is supported by the formation of a new rhombohedral phase of $Fe_2(SO_4)_3$ as confirmed by the diffraction peaks positioned at 25.70, 33.23, and 53.97 (**Fig. 4.3c**) corresponding to the (113), (116), and (404) planes, respectively (JCPDS card no. 00-042-0229).

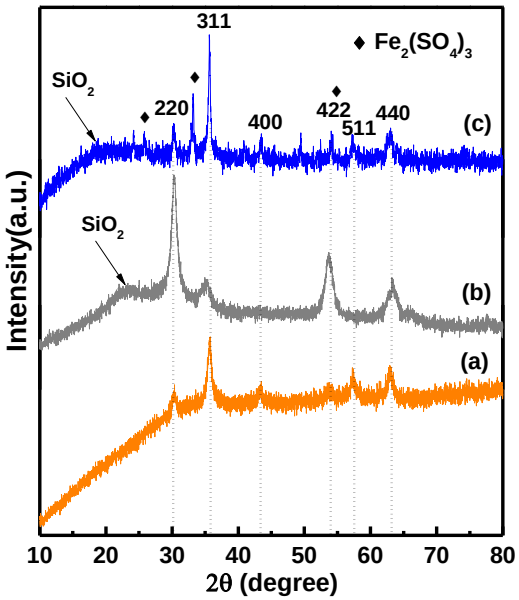

Fig. 4.3. X-ray diffraction patterns of (a) Fe_3O_4, (b) $Fe_3O_4@SiO_2$ and (c) $Fe_3O_4@SiO_2@SO_4^{2-}$.

4.3.1.2. FTIR analysis

A comparison among the FTIR spectra of Fe_3O_4, $Fe_3O_4@SiO_2$, and $Fe_3O_4@SiO_2@SO_4^{2-}$ is provided in **Fig. 4.4**. In the FTIR spectra (**Fig. 4.4a**), the band at ~571 cm^{-1} is due to the characteristic vibrations of the Fe–O bond. In the literature, the presence of the Fe–O bond, in Fe_3O_4, has been supported by the presence of a band in the range of 583–591 cm^{-1} [9,10]. Silica coating over the magnetic nanoparticles is confirmed by the appearance of a new band at ~1060 cm^{-1} owing to the Si–O–Si bending vibrations in $Fe_3O_4@SiO_2$ as well as $Fe_3O_4@SiO_2@SO_4^{2-}$ nanoparticles (**Fig. 4.4b**). Pourjavadi *et al*. have supported the presence of the Si–O–Si bond due to the presence of a band at ~1035 cm^{-1} in case of silica coated Fe_3O_4 particles [9,11]. The functionalization of the $Fe_3O_4@SiO_2$ nanoparticles with the sulphate group ($Fe_3O_4@SiO_2@SO_4^{2-}$) is evidenced by the appearance of band at 1233 cm^{-1} related to the asymmetric stretching vibrations of the S=O functional groups (**Fig. 4.4c**). A similar observation was reported by Kumar *et al*. where the presence of the sulphate group was supported by the presence of bands at 1139 and 1237 cm^{-1} in the IR spectrum of sulphated TiO_2 particles [12]. The band observed at 1409 cm^{-1} also suggested the existence of SO_4^{2-} species over the $Fe_3O_4@SiO_2$ MNPs. A similar observation also reported by Ghoreishi *et al.* where the attachment of SO_4^{2-} group over silica was supported by the presence of IR band at 1400 cm^{-1} [13].

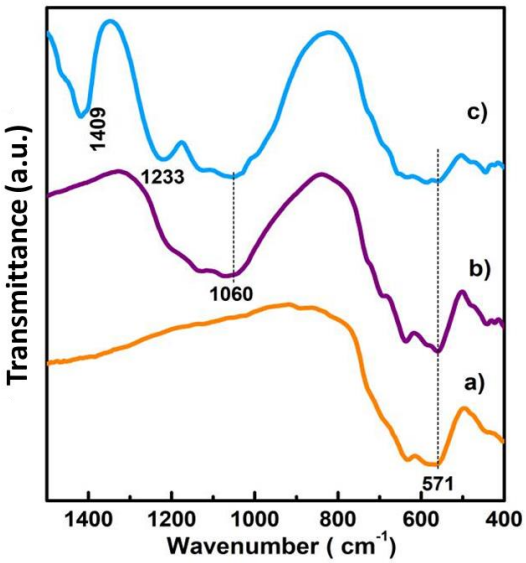

Fig. 4.4. FTIR spectra of (a) Fe_3O_4, (b) $Fe_3O_4@SiO_2$, and (c) $Fe_3O_4@SiO_2@SO_4^{2-}$.

4.3.1.3. Pyridine adsorption DRIFT study

To study the nature of the acidic sites, the samples saturated with pyridine vapours were subjected to diffuse reflectance infrared Fourier transform (DRIFT) spectroscopy and the corresponding spectra are shown in **Fig. 4.5**. In the DRIFT spectra of bare Fe_3O_4 MNPs (**Fig. 4.5a**), a peak at 1627 cm^{-1} was observed to indicate the formation of covalent bonds due to the donation of electron pairs from pyridine (Lewis base) to Fe_3O_4 (Lewis acid). Upon silica coating over the Fe_3O_4 MNPs, weak bands at 1546 and 1490 cm^{-1} were observed (**Fig. 4.5b**) to indicate the presence of Brønsted acidic sites due to the presence of –OH groups at the silica surface. Sulphate impregnation over silica coated MNPs at 550 °C also demonstrates both Lewis as well as Brønsted acidic sites due to the presence of H^+ ions in the sulphate group, which may react with pyridine and leads to the formation of pyridinium ions.

The interaction between Lewis acid sites and pyridine molecule was supported by the band at 1614 cm^{-1} in the DRIFT spectra as shown in **Fig. 4.5c**. It has been reported in the literature that the observed at 1640 cm^{-1} and at 1540 and 1445 cm^{-1} could be marked to the pyridine coordination with Lewis acidic and/or Brønsted acidic sites [14,15]. The bands corresponding to the Brønsted acidity were no longer found in the DRIFT spectra of the catalyst calcined at 650 °C (**Fig. 4.5d**) to support the destruction of the Brønsted acidic sites from the catalyst due to sulphate group decomposition. According to the literature report, the SO_4^{2-} group was found to be responsible for generating the strong acidic sites over the ZrO_2–SiO_2/SO_4^{2-} catalyst surface which are capable in catalyzing the GL acetylation [14].

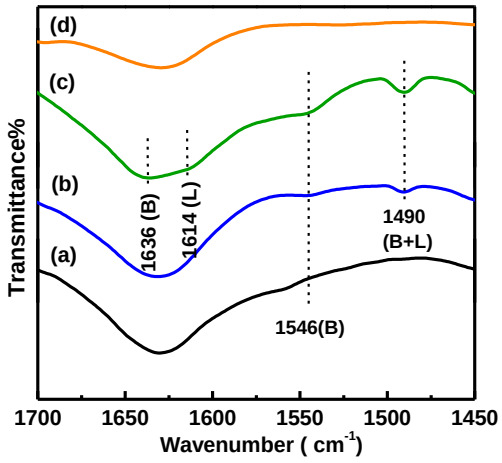

Fig. 4.5. FTIR spectra of pyridine absorbed on (a) Fe_3O_4, (b) Fe_3O_4@SiO_2 (c) Fe_3O_4@SiO_2@SO_4^{2-}-550 °C and Fe_3O_4@SiO_2@SO_4^{2-}-650 °C.

4.3.1.4. NH_3 -Temperature Programmed Desorption study

The NH_3 desorption technique was used to quantify the acidic sites as well as the strength of these sites. The NH_3 temperature programmed desorption (TPD) curves of magnetic nanoparticles (Fe_3O_4), silica coated magnetic nanoparticles ($Fe_3O_4@SiO_2$) and sulphate impregnated silica coated MNPs ($Fe_3O_4@SiO_2@SO_4^{2-}$) are shown in **Fig. 4.6a–c**, for the sake of comparison. It was observed that for all three samples, a broad desorption peak at 180 °C was observed reflecting the presence of weak acidic sites over the catalyst surface. A less intense desorption peak was found at 451 °C, over the silica coated MNPs to support the presence of fewer acidic sites (1.27 mmol g^{-1}) over the catalyst surface in the absence of the sulphate group. However, the incorporation of the sulphate group over the $Fe_3O_4@SiO_2$ nanoparticles was found to increase the acidic sites (8.63 mmol g^{-1}) of the catalyst as supported by the desorbed peak intensity. In the literature, the desorption peak in the temperature range of 100 to 290 °C has been reported in the case of sulphated silica zirconia and sulphated zirconia owing to the presence of weak acidic sites. Another peak in the range of 460- 600 °C has been reported to indicate the presence of strong acidic sites over the catalyst surface [16,17].

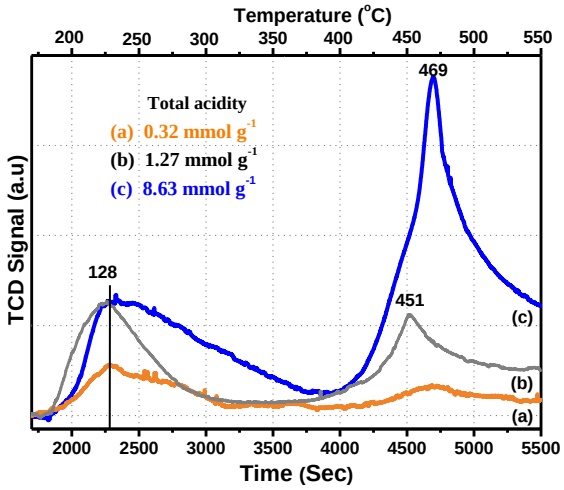

Fig. 4.6. NH_3-TPD profiles for (a) Fe_3O_4, (b) $Fe_3O_4@SiO_2$ and (c) $Fe_3O_4@SiO_2@SO_4^{2-}$.

4.3.1.5. BET analysis

The nitrogen adsorption-desorption isotherms of Fe_3O_4 and $Fe_3O_4@SiO_2@SO_4^{2-}$ are shown in **Fig. 4.7a**, which reveal the surface porosity and pore size behaviour of these nanoparticles. Fe_3O_4 and $Fe_3O_4@SiO_2@SO_4^{2-}$ were found to show type-IV adsorption-desorption isotherms having the H1 type hysteresis loops. The Fe_3O_4 MNPs show the hysteresis loops at p/p0 = 0.8–

1.0, and a relatively higher pore size of 11 nm as measured by the N_2 adsorption-desorption isotherm (**Fig. 4.7a**). Upon silica and sulphate impregnation, the hysteresis loop shifts to relatively low pressure of p/p0 = 0.7–0.9 with a pore size of 10 nm, as shown in **Fig. 4.7a**. The quantity of adsorbed nitrogen also decreases upon silica and sulphate impregnation over the Fe_3O_4 MNPs due to the reduction in surface area from 129 $m^2\ g^{-1}$ to 69 $m^2\ g^{-1}$. The decrease in the surface area could also be ascribed to the partial blockage of the porous silica upon sulphate group anchoring. The total pore volume (from 0.5 to 0.3 cm^3/g^{-1}) as well as the pore diameter (from 11 to 10 nm) of the MNPs were observed to decrease due to the particle pore blockage upon sulphate group incorporation. Ward *et al*. reported that the sulphate and zirconia impregnation over the silica nanoparticles were also found to reduce the pore volume and the pore diameter due to the pore blockage of the particles [18].

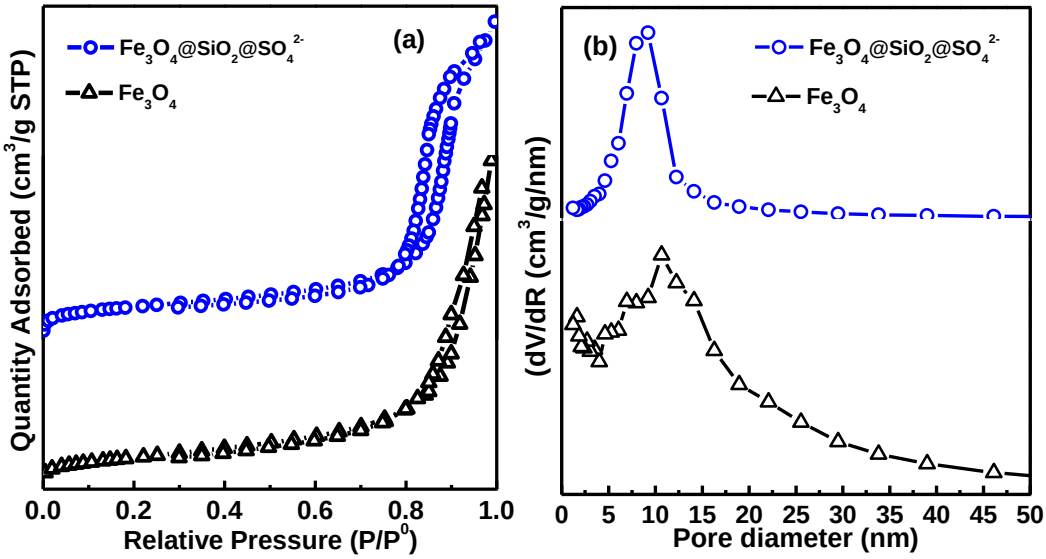

Fig. 4.7. (a) N_2 adsorption-desorption isotherms and (b) Pore size distribution.

4.3.1.6. Magnetization efficiency of the catalyst

The magnetic property of the catalyst was studied by using a vibrating sample magnetometer (VSM). Hysteresis loops (M–H) of Fe_3O_4, $Fe_3O_4@SiO_2$ and $Fe_3O_4@SiO_2@SO_4^{2-}$ were measured at room temperature (**Fig. 4.8**). A soft ferromagnetic behaviour of Fe_3O_4, $Fe_3O_4@SiO_2$ and $Fe_3O_4@SiO_2@SO_4^{2-}$ nanoparticles can be observed in these M–H loops. Magnetic parameters such as coercivity (H_C), retentivity (M_R) and saturation magnetization (M_S) were determined from these hysteresis loops. For Fe_3O_4, H_C, M_R and M_S were found 32 G, 1 emu g^{-1} and 45 emu

g^{-1}, respectively. Low values of H_C and M_R indicate the formation of very small size nanoparticles close to their super-paramagnetic limit. The M_S of $Fe_3O_4@SiO_2$ and $Fe_3O_4@SiO_2@SO_4^{2-}$ nanoparticles was 41 emu g^{-1} and 30 emu g^{-1}, respectively. This decrease in the M_S of catalysts ($Fe_3O_4@SiO_2$ and $Fe_3O_4@SiO_2@SO_4^{2-}$) can be attributed to the dilution of the magnetically active phases (ferromagnetic contribution) due to silica and sulphate loading. As shown in **Fig. 4.8**, H_C and M_R values also decrease significantly with the silica and sulphate loading over the Fe_3O_4 nanoparticles [19,20]. This might be because of the decrease in the amount of clustering between MNPs. Owing to the strong magnetization of $Fe_3O_4@SiO_2$ (41 emu g^{-1}) and $Fe_3O_4@SiO_2@SO_4^{2-}$ (30 emu g^{-1}) nanoparticles, it is possible to separate these catalysts from the reaction mixture with the help of an external magnet. The recovered catalysts could then be successfully reused multiple times for successive acetylation cycles of GL with AcA.

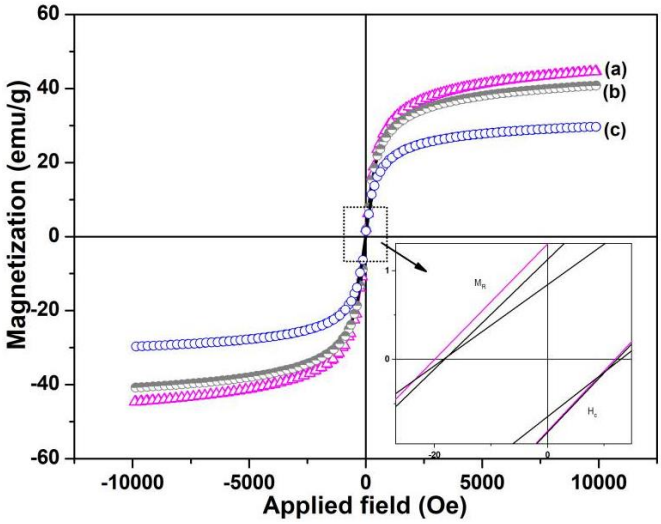

Fig. 4.8. Magnetization curves of (a) Fe_3O_4, (b) $Fe_3O_4@SiO_2$ and (c) $Fe_3O_4@SiO_2@SO_4^{2-}$.

4.3.1.7. SEM-EDX and elements mapping analysis

The morphology and elemental distributions of the magnetic catalysts were examined using the SEM-EDX technique and the representative micrograph and elemental mapping are shown in **Fig. 4.9**. The SEM images of the Fe_3O_4 (**Fig. 4.9a**) and $Fe_3O_4@SiO_2@SO_4^{2-}$ (**Fig. 4.10a**) show the formation of agglomerated nanoparticles in irregular geometries. The partial overlapping of dispersion areas corresponding to these elements indicates that Fe, Si, S and O are uniformly

distributed over the catalyst surface. The qualitative estimation of all these elements was performed by EDX analysis.

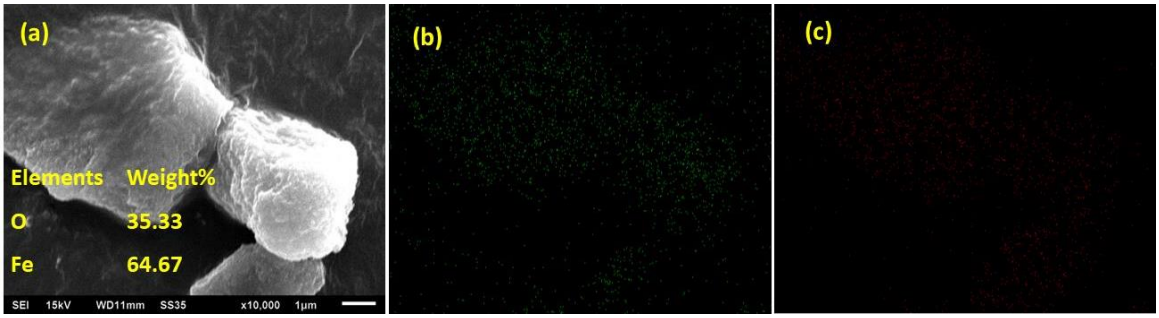

Fig. 4.9. (a) SEM image of Fe_3O_4 and colour mapping of the elements present (b) O and (c) Fe.

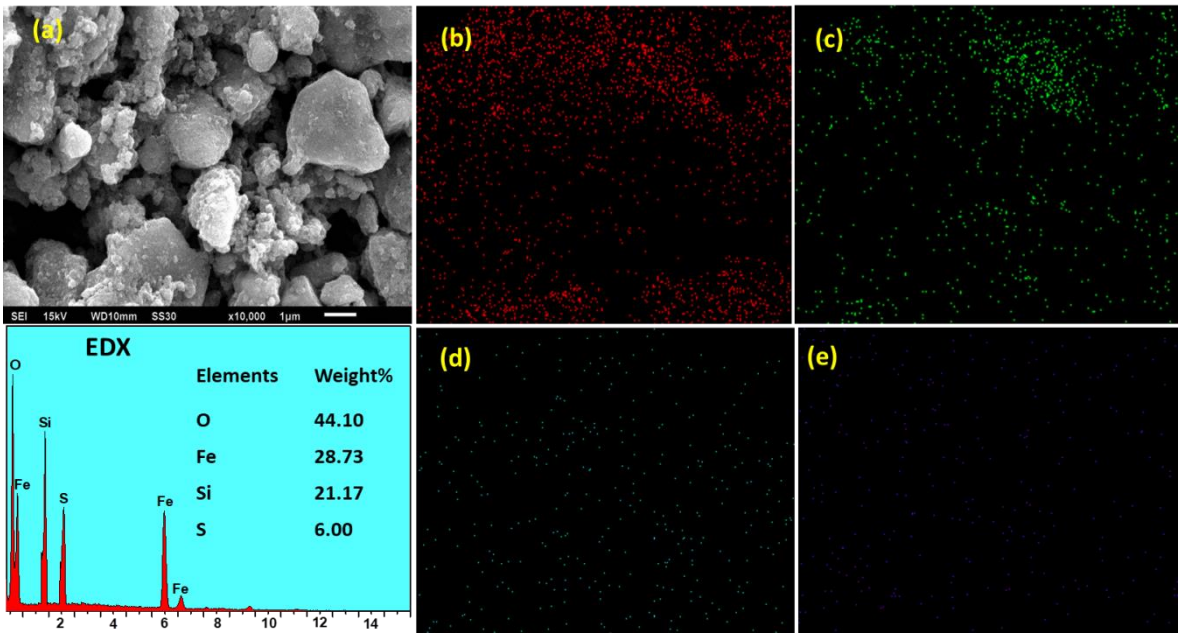

Fig. 4.10. (a) SEM image of $Fe_3O_4@SiO_2@SO_4^{2-}$, EDX spectra and colour mapping of the elements present (b) O, (c) Fe, (d) Si and (e) S.

4.3.1.8. HR-TEM analysis

TEM analysis was performed to obtain more information on the morphology and distribution of SiO_2 over the Fe_3O_4 particles, as shown in **Fig. 4.11a–c**. The TEM analysis further revealed that the agglomerated magnetic catalyst consists of spherical shaped particles of ~18 nm size, which is in the range of the crystallite size (16.8 nm) calculated from XRD data by Scherrer's formula. From the magnified TEM image (**Fig. 4.11d and e**) of $Fe_3O_4@SiO_2@SO_4^{2-}$, it can be clearly

seen that SiO_2 is homogeneously dispersed over the Fe_3O_4 MNPs surface, forming a layer of ~2.6 nm thickness. Fig. 4.11d also shows lattice spacings of 0.25 and 0.29 nm, which could be ascribed to the (311) and (220) lattice planes, respectively, confirming the inverse spinel structure of Fe_3O_4 phase. Additionally, the selected area electron diffraction (SAED) pattern study (**Fig. 4.11f**) shows the concentric rings, which consist of an almost continuous series of the spots. This type of pattern could be ascribed to the polycrystalline nature of the prepared catalysts, and the same is also consistent with the powder XRD data of the catalyst.

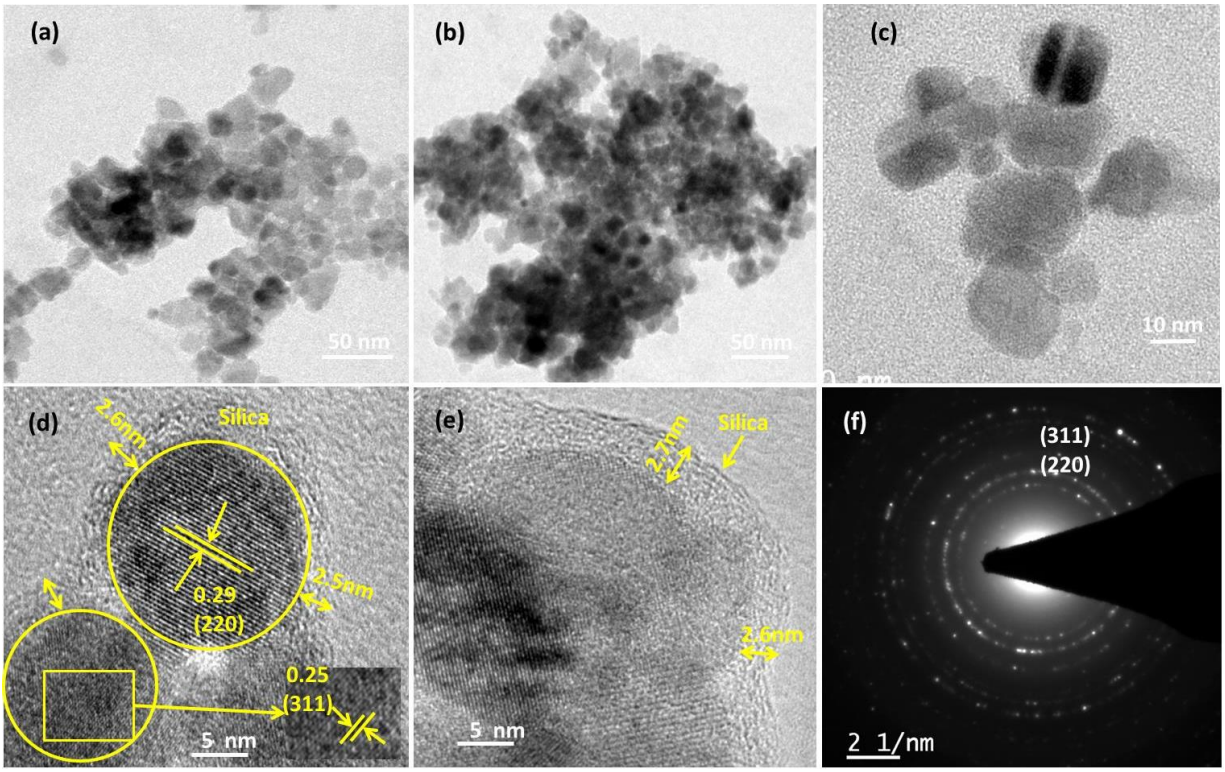

Fig. 4.11. TEM imaging of $Fe_3O_4@SiO_2@SO_4^{2-}$ catalyst (a-c), lattice spacing (d-e) and SAED pattern (f).

4.3.1.9. XPS analysis

The X-ray photoelectron spectroscopy (XPS) technique was used for determining the electronic state of the elements present in the catalyst ($Fe_3O_4@SiO_2@SO_4^{2-}$) as shown in **Fig. 4.12**. The full scan XPS spectrum of the $Fe_3O_4@SiO_2@SO_4^{2-}$confirmed the presence of O, Fe, Si, and S elements over the catalyst surface as shown in **Fig. 4.12a**. The two peaks (**Fig. 4.12b**) at 532.1 and 533.6 eV indicate the existence of the O^{2-} 1s state in Si–O–Si or S–O–Si or Fe–O–Si

linkages. The study reveals that the surface of the matrix is covered by the silica and sulphate group which is also supported by the FTIR analysis of the sample. Similar observations were reported in the literature, where the presence of O^{2-} 1s in Si–O–Si, S–O–Si, and Fe–O–Si linkages was supported by the presence of peaks at 533 and 532.5 eV for the silica coated magnetic nanoparticles [14,21]. Furthermore, the spectrum shows (**Fig. 4.12c**) peaks at 711.7 and 720.2 eV corresponding to the Fe^{3+} $2p_{3/2}$ state and at 713.9 and 726.6 eV concerning the Fe^{2+} $2p_{1/2}$ state. This study could be correlated with the literature, where Fe^{3+} $2p_{3/2}$ and Fe^{2+} $2p_{1/2}$ states were supported by the binding energy peaks at 711.2 and 719.8 eV and 723.8 and 711.4 eV due to the formation of Fe_3O_4 and $Fe_2(SO_4)_3$ states, respectively [22-24]. The binding energies of Si^{4+} 2p state were observed at 100.7 and 103.6 eV, which can be ascribed to the Si–O–Si linkages as shown in **Fig. 4.12d**. The literature is also consistent with the observation where peaks at 100 and 103.1 eV supported Si^{4+} 2p state of SiO_2 material [25, 26]. The presence of the sulphate functional group over the silica particles could be supported by the presence of peaks at 168.4 and 170.1 eV corresponding to the S^{6+} $2p_{3/2}$ and S^{6+} $2p_{1/2}$ states, respectively (**Fig. 4.12e**). These binding energies are also attributed to the S–O linkage for SO_4^{2-} species. The literature reports also revealed that binding energies of 168.3 and 171.0 eV could be ascribed to the S^{6+} $2p_{3/2}$ and S^{6+} $2p_{1/2}$ states present in the sulphate group over the surface of silica coated magnetic nanoparticles [14,27].

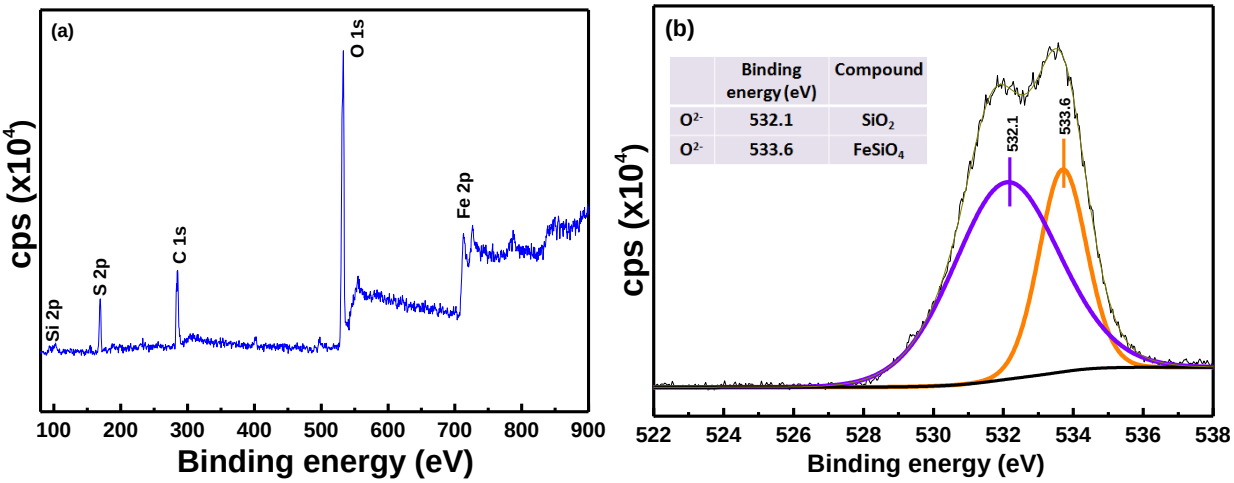

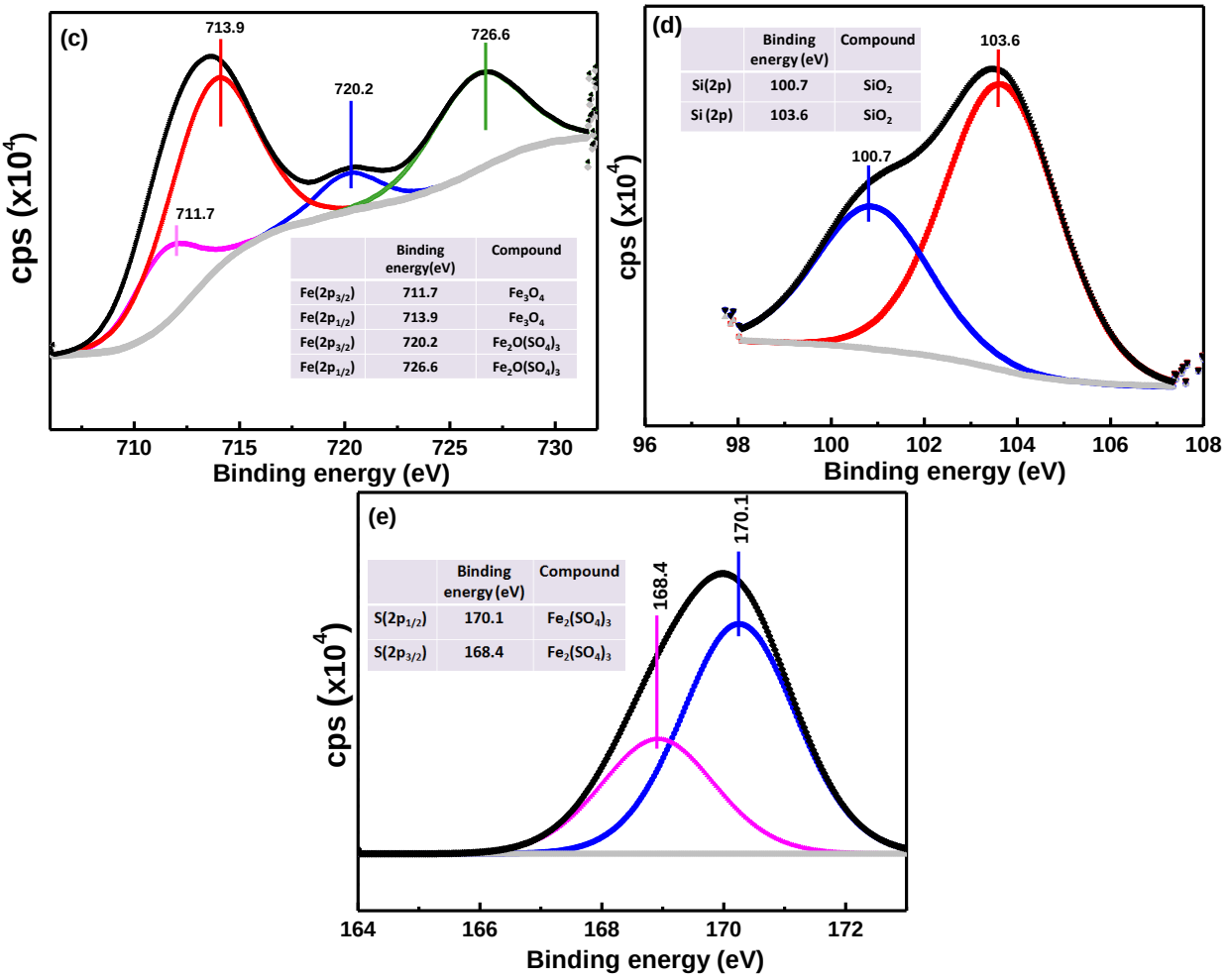

Fig. 4.12. XPS spectra of $Fe_3O_4@SiO_2@SO_4^{2-}$ catalyst (a) full scan (b) O 1s, (c) Fe 2p, (d) Si 2p and (e) S 2p.

4.3.2. Product analysis

4.3.2.1. FTIR analysis

The formation of the TA has confirmed with the help of FTIR spectroscopic technique. The FTIR spectra (**Fig. 4.13a**) of GL depict two bands at 1042 and 3297 cm^{-1} due to the C—O and O—H stretching vibrational frequencies, respectively. Upon GL acetylation, a new band at 1726 cm^{-1} (**Fig. 4.13b**), due to —C=O group, was observed to support the formation of ester bond in TA.

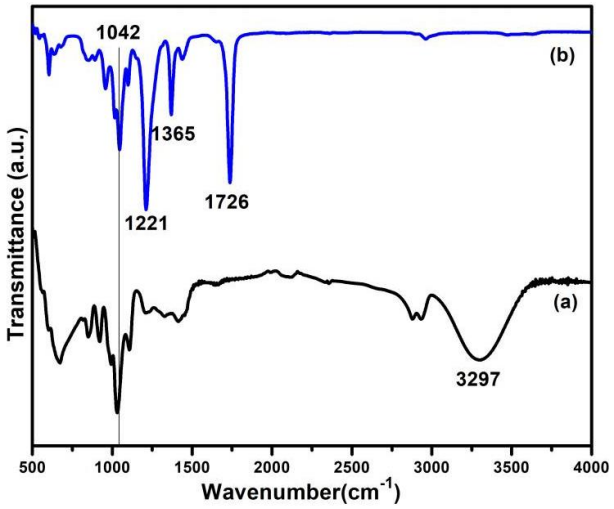

Fig. 4.13. FTIR spectra of (a) glycerol, and (b) triacetin produced during glycerol acetylation.

4.3.2.2. NMR analysis

In ^{1}H-NMR spectra of GL, peaks observed at 3.32-3.50 (g_1) and 3.59 ppm (g_2) are due to the CH_2 and CH protons, respectively, as shown in **Fig. 4.14a**. Upon acetylation, the formation of TA is confirmed by the appearance of two singlets corresponding to methyl (-CH_3) protons, at 1.92 (k_1) and 1.94 ppm (k_2). The position of the glyceridic protons also shifts at 4.07-4.22 ppm due to t_1 protons and at 5.13 ppm due to t_2 protons as shown in **Fig. 4.14b**. No additional peaks corresponding to the MA or DA molecules were observed in the ^{1}H-NMR spectrum to support that TA has formed as an exclusive product under optimized conditions during the reaction.

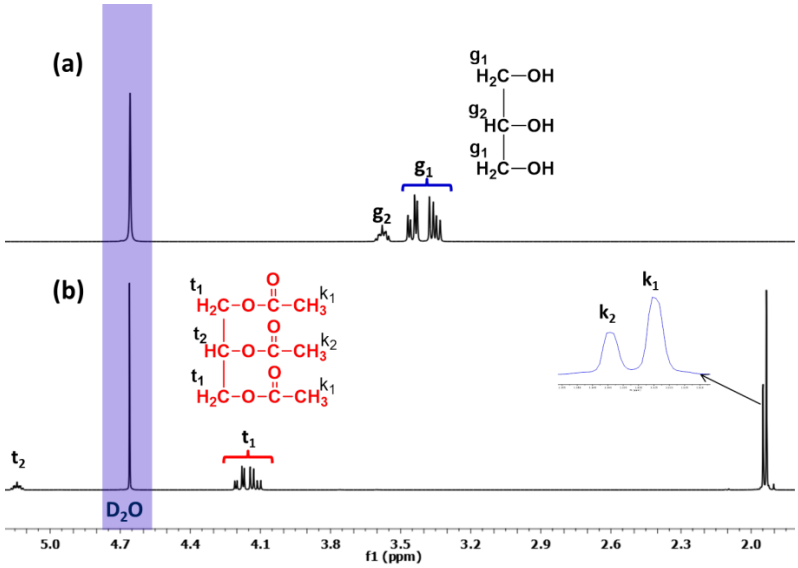

Fig. 4.14. ^{1}H NMR spectra of (a) glycerol, and (b) triacetin produced during glycerol acetylation.

4.3.3. Catalyst Screening

In the present study, silica-coated Fe_3O_4 nanoparticles were employed to anchor the catalytically active sulphate ions. In the absence of the catalyst or in the presence of bare magnetic/silica coated magnetic nanoparticles, negligible conversion of GL into acetins was observed to support the necessity of the sulphate group to achieve the catalytic ($Fe_3O_4@SiO_2@SO_4^{2-}$) activity (**Fig. 4.15**). These observations were in line with the literature reports, where Ma *et al*. suggested that sulphate impregnation over titanium coated magnetic nanoparticles was found to have more Brønsted acidic sites, which in turn were found to enhance the acetylation activity of the catalyst [15].

In the present study, to establish the optimum reaction conditions for the catalyst activity for TA synthesis, the influence of the reaction parameters such as catalyst amount, AcA/GL molar ratio, reaction temperature and reaction time was studied.

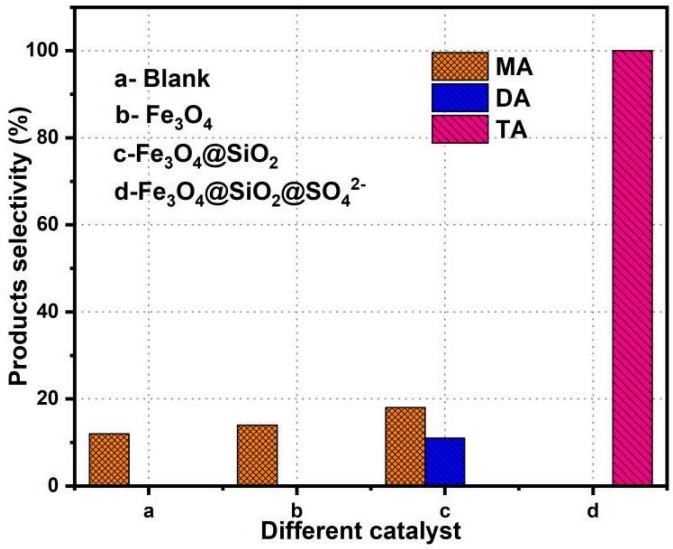

Fig. 4.15. Effect of the various catalysts over the acetylation of glycerol. [*Reaction conditions:* AcA/GL molar ratio = 6:1, catalyst amount = 5 wt% (with respect to GL), 80°C = reaction temperature, and reaction time = 45 min]

4.3.3.1. Effect of catalyst amount on product selectivity

To optimize the catalyst amount, acetylation of GL was studied over the $Fe_3O_4@SiO_2@SO_4^{2-}$ catalyst using AcA as the acetylating agent. Upon acetylation of GL with AcA (6:1; mol/mol) in the presence of 1–7 wt% catalyst (with respect to GL) at 80 °C, the TA selectivity increases with

the catalyst amount. A maximum TA selectivity of 100 % was obtained with 5 wt% of catalyst amount. A further increase in the catalyst amount was neither found to improve the yield nor able to reduce the reaction duration (**Fig. 4.16a**). These data correlate with the literature reported acetylation of GL with AcA (1:8 molar ratio) at 120 °C reaction temperature in the presence of sulphated carbon as a catalyst. The conversion of GL was found to be a function of the catalyst concentration and availability of active sites over the catalyst surface; however, the maximum GL conversion level was 91 % with a TA selectivity of 34 % only [28]. Additionally, the TOF calculation also supports that the presence of 5 wt% of catalyst exhibited a maximum turnover frequency (258 h^{-1}) as compared to 1 wt% (226 h^{-1}) and 3 wt % (252 h^{-1}) of catalyst. Hence, 5 wt% catalyst was employed for optimizing the other reaction parameters to achieve the maximum TA selectivity.

4.3.3.2. Effect of AcA/GL molar ratio on product selectivity

The AcA/GL ratio was found to affect the TA yield as well as the cost of the process. A 3:1 stoichiometric molar ratio of AcA/GL is required to convert the GL completely into TA. However, GL acetylation being a reversible reaction, usually a higher molar ratio of the AcA is engaged to push the reaction into the forward direction. In the present study to establish the optimum AcA/GL molar ratio, the reaction was performed in the presence of 5 wt% catalyst ($Fe_3O_4@SiO_2@SO_4^{2-}$) at 80 °C for 45 min by varying the AcA/GL molar ratio from 1 to 9 as shown in **Fig. 4.16b**. The use of lower AcA concentration (up to 2:1 molar ratio or AcA/GL) primarily yielded a mixture of products that is dominated by the MA, DA and unreacted GL. On increasing the AcA/GL molar ratio up to 3 and higher, TA was found to be the predominating product and 100 % TA selectivity was achieved with a 6:1 AcA/GL molar ratio within 45 min of reaction duration. Elsewhere, TPA/Nb_2O_5 catalysts have been employed for the GL acetylation with AcA to obtain TA. The catalyst was found to yield a higher MA selectivity (49 %) when the AcA/GL molar ratio was 3. On increasing the AcA content up to a molar ratio of 5, the selectivity towards TA was found to increase (from 5 to 20 %) at 120 °C temperature in 4 h of reaction duration [26].

4.3.3.3. Effect of reaction temperature on product selectivity

The reaction temperature was also found to influence the product selectivity, as shown in **Fig. 4.16c.** To study the effect of temperature the GL acetylation experiments was performed by varying the reaction temperatures but maintaining a fixed AcA molar ratio of 6:1, 5 wt% catalyst and reaction duration of 45 min. As observed from **4.16c**, at room temperature (30 °C), the main product was found to be MA (52 %). TA formation was initiated at 60 °C, although MA and DA still dominate the product profile. A further increase in the reaction temperature (80 °C) yielded TA as an exclusive product, within 45 min of reaction time. Thus, the prepared catalyst was found to be efficient even at a relatively lower reaction temperature of 80 °C, while in the literature reports, the optimum temperature was reported in the range of 90 to 110 °C to obtain the varying TA yield of 7 to 65 % [12]. Very few reports have been found claiming more than 99 % TA selectivity [8]. It has been observed that at a high reaction temperature (110 °C) the acylium ion formation, from AcA, was facilitated, which ultimately acetylate the GL to form the acetins [29].

4.3.3.4. Effect of reaction time on product selectivity

The effect of reaction time on the TA selectivity is shown in **Fig. 4.16d** while performing the reaction at 80 °C, employing 6:1 AcA/GL molar ratio in the presence of 5 wt% catalyst. It is evident from the plot that during the first 15 min of reaction period MA (51 %) is the leading product along with minor amount of DA (12 %). As the reaction proceeds, MA and DA remain the predominant products even after 30 min of the reaction period. However, after 45 min, TA became the exclusive product (100 %) to support that GL acetylation took place in a stepwise fashion.

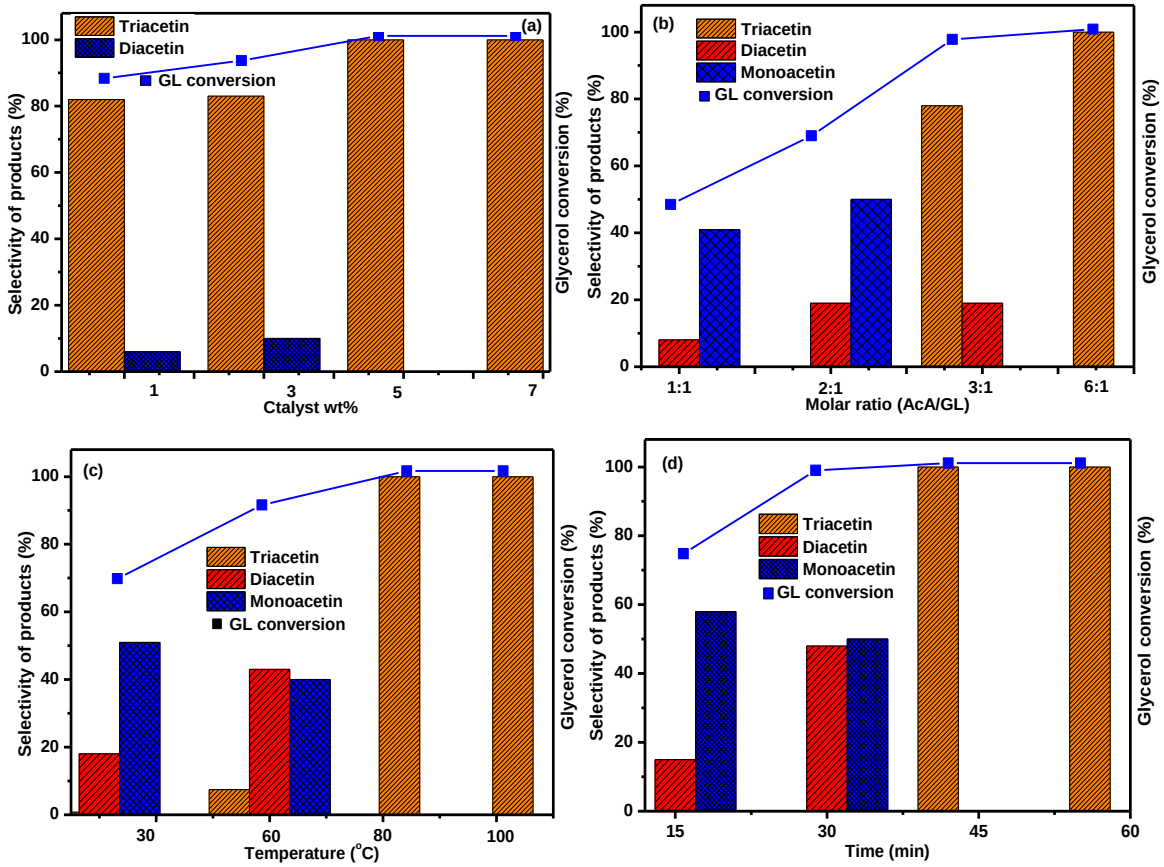

Fig. 4.16. Influence of various reaction parameters on $Fe_3O_4@SiO_2@SO_4^{2-}$ assisted glycerol acetylation (a) catalyst amount with respect to GL, (b) AcA/GL molar ratio, (c) reaction temperature and (d) reaction time.

4.3.4. The reusability and stability

To examine the recovery, reusability and stability of the magnetic catalyst under the optimized reaction conditions, it was first recuperated from the reaction mixture under the influence of an external magnetic field (**Fig. 4.2**). To regenerate the recovered catalyst, it was washed with ethanol to remove any adsorbed substrate molecules, dried at 70 °C and finally calcined at 550 °C for 4 h. Catalyst activation *via* re-calcination is necessary to regain its activity as just washed, and dried catalyst was able to yield only 40 % TA selectivity even during the first reusability experiment. The regenerated catalyst was subjected to 6 successive catalytic cycles under a similar set of recovery and regeneration procedures as shown in **Fig. 4.17**. The results indicated that this catalyst was stable during 3 consecutive cycles as up to 80 % TA selectivity during the 3rd run was maintained. However, during the 4th and subsequent cycles, less than 59 % of TA

selectivity was retained. This loss of activity might be due to either catalyst deactivation or leaching of the catalytically active sites in reaction media.

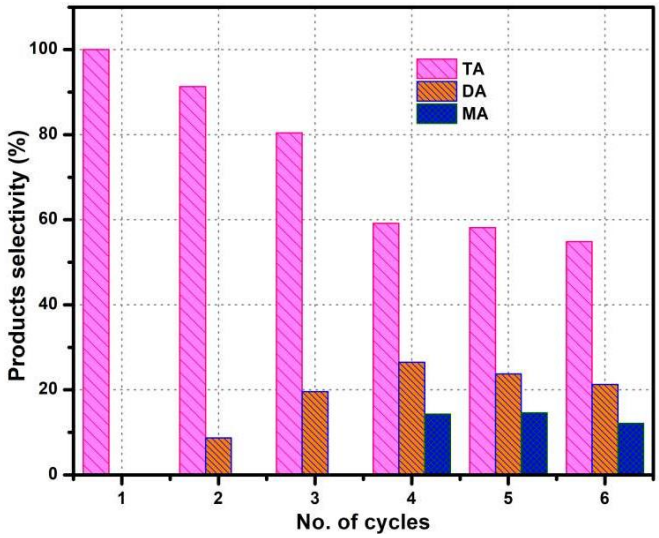

Fig. 4.17. Study of the $Fe_3O_4@SiO_2@SO_4^{2-}$ reusability during the glycerol acetylation with acetic acid. [*Reaction conditions:* AcA/GL molar ratio = 6:1, catalyst amount = 5 wt% (with respect to GL), 80°C = reaction temperature, and 45 min = reaction time]

The presence of acidic sites imparts the acetylation activity; thus, it is essential to investigate the sulphur content in the regenerated catalyst. The sulphur content in the reused catalyst was found to be lower (1.7 wt%) than that in the fresh catalyst (6 wt%). Similarly, the FTIR analysis also supports the partial loss of the sulphate group from the regenerated catalyst (**Fig. 4.18a**). Therefore, the leakage of the sulphate group from the catalyst could be the main reason behind the loss of catalyst activity.

The magnetic strength (MS) of the catalyst was also found to decrease upon repeated use as supported by the VSM profiles of the regenerated catalysts (**Fig. 4.18b**). The fresh $Fe_3O_4@SiO_2@SO_4^{2-}$ catalyst exhibited higher M_S (30 emu g^{-1}) and MR (0.7 emu g^{-1}) values in comparison to the used catalyst (M_S = 2.0 emu g^{-1} and MR = 0.09 emu g^{-1}). The observed increase in H_C (from 15 to 44 G) can be attributed to the aggregation of catalyst, during its regeneration, to cause the increase in particle size [19]. The reduction in M_S and M_R values may be ascribed to the presence of nonmagnetic particles over the surface of the regenerated catalyst [30,31].

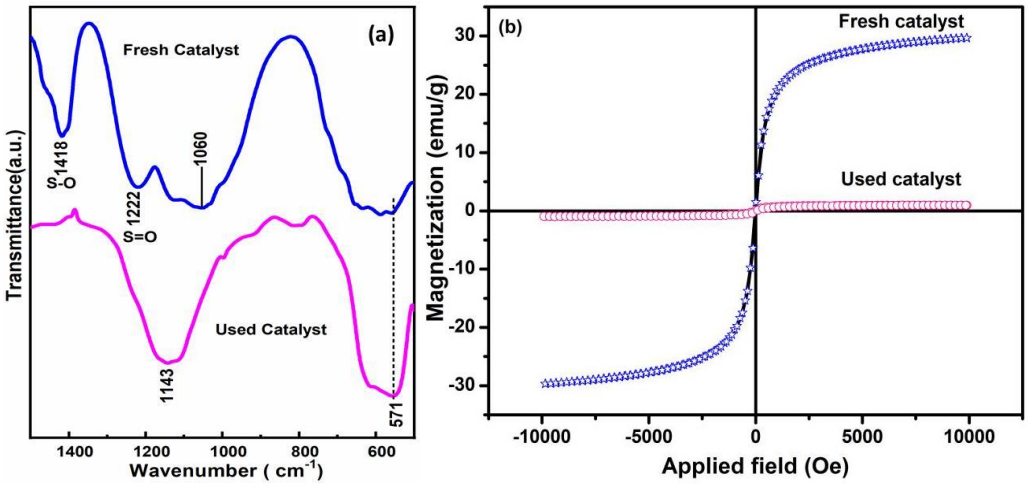

Fig. 4.18. Comparison of (a) FTIR and (b) VSM spectra of fresh and used magnetic catalyst.

As supported by the elemental and FTIR analysis, the loss of catalyst activity was linked to the loss of sulphate ions from the catalyst surface. In the reaction mixture, the dissolved sulphate ions may catalyze the reaction similar to a homogeneous catalyst. Thus it is imperative to establish the homogeneous contribution in catalyst activity and to demonstrate the same, a hot filtration test was performed. In this test, GL acetylation was performed under optimized reaction parameters for 20 min and after that the catalyst was separated from the reaction mixture with the help of simple filtration. Now, the reaction mixture without the catalyst was allowed to react for an additional 20 min. However, no significant change in the product profile of the reaction mixture, without the catalyst, was observed as shown in **Fig. 4.19**. Thus, it is safe to assume that dissolved catalyst contents could not catalyse the reaction. It is the solid catalyst which is responsible for almost entire catalytic activity.

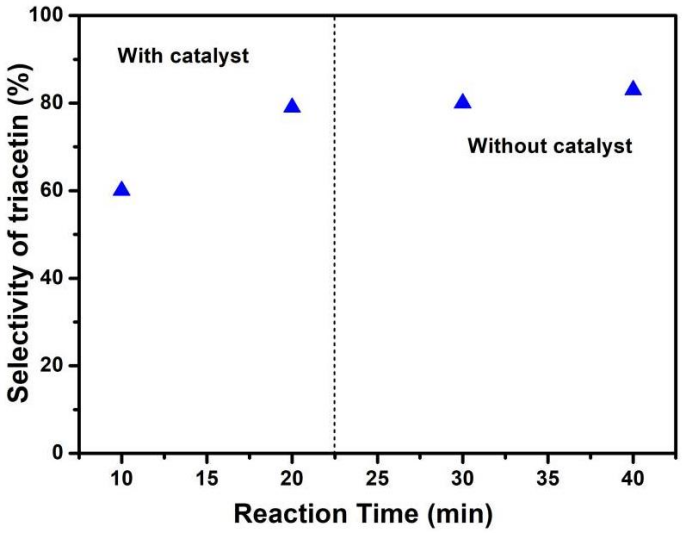

Fig. 4.19. Study of homogeneous contribution during the acetylation of glycerol with acetic acid [*Reaction conditions:* AcA/GL molar ratio = 6:1, catalyst amount = 5 wt% with respect to GL, and 80°C = reaction temperature]

4.4. Proposed mechanism for the acetylation of glycerol with acetic acid

Acetylation of the GL in the absence of catalyst resulted in partial conversion levels into acetin even after a long-lasting reaction duration of 3 h. However, in the presence of $Fe_3O_4@SiO_2@SO_4^{2-}$ magnetic catalyst, a reaction time of 45 min is required for the complete acetylation of GL. This observation clearly reveals the role of sulphate as catalytic species in the GL acetylation. Homogeneous sulphuric acid catalyzed acetylation of mono- as well tri-alcohol (GL) has been reported to follow the first-order kinetic model [32,33] In such reactions, the rate of the reaction was found to be a function of AcA concentration. During the present study as well, when the AcA concentration was varied, the rate of TA formation was also found to change. However, the same was not found to be effected when the GL concentration was varied. Thus, the plausible mechanism involves the protonation of the AcA in the first step [34] where the proton is furnished by the magnetic heterogeneous acid catalyst (I) as shown in **Scheme 3.2 (Chapter 3)**. Protonation of the AcA eventually leads to the formation of a carbocation (II), which reacted with the alcoholic –O– to form intermediate (III) formation. A water molecule has been given away by intermediate (III) to generate a new carbocation (IV) which ultimately decomposes into the catalyst and MA (V). The remaining two alcoholic groups of the MA would react with AcA following a similar mechanism as described above to form a TA molecule.

4.5. Conclusions

The magnetic heterogeneous acid catalyst, $Fe_3O_4@SiO_2@SO_4^{2-+}$, was prepared and successfully employed to acetylate the glycerol with acetic acid to achieve a triacetin selectivity of 100 % within 45 min at 80 °C. The magnetic catalyst with the sulphate group and calcined at 550 °C was found to demonstrate a better activity among the prepared catalysts. Under the optimized reaction conditions of catalyst amount (5 wt%, concerning glycerol), molar ratio of AcA/GL (6:1), and temperature (80 °C), 100 % triacetin selectivity was obtained. The catalyst was reused for 6 consecutive reaction cycles; however, >80 % triacetin selectivity was observed during the first 3 cycles.

References

1. Vishal, K.; Fahlman, B. D.; Sasidhar, S.; Patil, S. A.; Patil, S. A. Magnetic Nanoparticle-Supported N-Heterocyclic Carbene-Palladium(II): A Convenient, Efficient and Recyclable Catalyst for Suzuki–Miyaura Cross-Coupling Reactions. *Catal. Lett*, **2017**, 147, 900–918. https://doi.org/10.1007/s10562-017-1987-7
2. Tangestanifard, M.; Ghaziaskar, H. S. Arenesulfonic Acid-Functionalized Bentonite as Catalyst in Glycerol Esterification with Acetic Acid. *Catalysts* **2017**, 7, 211. https://doi.org/10.3390/catal7070211
3. Naeimi, H.; Mohamadabadi, S. Sulfonic acid-functionalized silica-coated magnetic nanoparticles as an efficient reusable catalyst for the synthesis of 1-substituted 1H-tetrazoles under solvent-free conditions. *Dalton. Trans*. **2014**, 43, 12967. https://doi.org/10.1039/C4DT01664E
4. Elsayed, I.; Mashaly, M.; Eltaweel, F.; Jacksonc, M. A.; Hassan, E. B. Dehydration of glucose to 5-hydroxymethylfurfural by a core-shell Fe_3O_4@SiO_2-SO_3H magnetic nanoparticle catalyst. *Fuel*, **2018**, 221, 407-416. https://doi.org/10.1016/j.fuel.2018.02.135
5. Pazoki, F.; Salamatmanesh, A.; Bagheri, S.; Heydari, A. Synthesis and Characterization of Copper(I)-Cysteine Complex Supported on Magnetic Layered Double Hydroxide as an Efficient and Recyclable Catalyst System for Click Chemistry Using Choline Azide as Reagent and Reaction Medium. *Catal. Lett*. **2020**, 150, 1186–1195. DOI: https://doi.org/10.1007/s10562-019-03011-2
6. Iwasaki, T.; Mizutani, N.; Watano, S.; Yanagida, T.; Kawai, T. Hydrothermal synthesis of magnetite nanoparticles via sequential formation of iron hydroxide precipitates. *J. Exp. Nanosci*. **2012**, 7(4), 355-365. DOI: 10.1080/17458080.2010.515250
7. Long, Y.; Zhao, Z.; Wu, L.; Luo, S.; Wen, H.; Wu, W.; Zhang, H.; Ma, J. Distinctive ligand effects of functionalized magnetic micro particles immobilizing palladium acetate as heterogeneous coordination catalysts for selective oxidation of styrene to acetophenone. *Mol. Catal*. **2017**, 433, 291–300. https://doi.org/10.1016/j.mcat.2017.02.028
8. Sun, J.; Tong, X.; Yu, L.; Wan, J. An efficient and sustainable production of triacetin from the acetylation of glycerol using magnetic solid acid catalysts under mild conditions. *Catal. Today* **2015**, 264, 115-122. DOI: 10.1016/j.cattod.2015.07.011
9. Liu, Z. L.; Wang, X.; Yao, K. L.; Du, G. H.; H. Q.; Lu, Ding, Z. H.; Tao, J. Synthesis of magnetite nanoparticles in W/O microemulsion. *J. Mater. Sci*. **2004**, 39, 2633–2636. https://doi.org/10.1023/B:JMSC.0000020046.68106.22
10. Pourjavadi, A.; Hosseini, S. H.; Doulabi, M.; Fakoorpoor, S. M.; Seidi, F. Multi-Layer Functionalized Poly(Ionic Liquid) Coated Magnetic Nanoparticles: Highly Recoverable and Magnetically Separable Brønsted Acid Catalyst. *ACS. Catal*. **2012**, 2, 1259−1266. https://doi.org/10.1021/cs300140j
11. Khan, S.; Kaur, G.; Singh, K. Effect of ZrO_2 on dielectric, optical and structural properties of yttrium calcium borosilicate glasses. *Ceram. Int*. **2017**, 43, 722–727. https://doi.org/10.1016/j.ceramint.2016.09.219
12. Kumar, K. S.; Rajendran, S.; Prabhu, M. R. A Study of influence on sulfonated TiO_2-Poly (Vinylidene fluoride-co-hexafluoropropylene) nano composite membranes for PEM Fuel cell application. *Appl. Surf. Sci*. **2017**, 418, 64–71. https://doi.org/10.1016/j.apsusc.2016.11.139

13. Ghoreishi, K. B.; Asim, N.; Yarmo, M. A.; Amsudin, M. W. Mesoporous phosphated and sulphated silica as solid acid catalysts for glycerol acetylation. *Chem. Papers* **2014**, 68(9), 1194–1204. https://doi.org/10.2478/s11696-014-0550-x
14. Parry, E. P. An Infrared Study of Pyridine Adsorbed on Acidic Solids. Characterization of Surface Acidity. *J. Catalysis.* **1963**, 2, 371-379. https://doi.org/10.1016/0021-9517(63)90102-7
15. Ma, L.; Li, J.; Ke, R.; Fu, L. Catalytic Performance, Characterization, and Mechanism Study of $Fe_2(SO_4)_3/TiO_2$ Catalyst for Selective Catalytic Reduction of NOx by Ammonia. *J. Phys. Chem. C*. **2011**, 115, 7603–7612. https://doi.org/10.1021/jp200488p
16. Deshmane, V. J.; Adewuyi, Y. J. Mesoporous nanocrystalline sulfated zirconia synthesis and itsapplication for FFA esterification in oils. *App. Catal. A: Gen*. **2013**, 463, 196–206. https://doi.org/10.1016/j.apcata.2013.05.005
17. Chen, X.; Ju, Y.; Mou, C. Direct Synthesis of Mesoporous Sulfated Silica-Zirconia Catalysts with High Catalytic Activity for Biodiesel via Esterification. *J. Phys. Chem. C*. **2007**, 111, 18731-18737. https://doi.org/10.1021/jp0749221
18. Ward, A. J.; Pujari, A. A.; Costanzo, L.; Masters, A. F.; Maschmeyer, T. Ionic liquid-templated preparation of mesoporous silica embedded with nanocrystalline sulfated zirconia. *Nan. Res. Let*. **2011**, 6, 192. https://doi.org/10.1186/1556-276X-6-192
19. Xiao, G.; Chien, C. L. Giant magnetic coercivity and percolation effects in granular $Fe(SiO_2)$ solids. *Appl. Phys. Lett*. **1987**, 51, 1280. DOI: 10.1063/1.98705
20. Ankita, G.; Bansalb, S.; Chudasamac, B.; Tikood, K. B.; Kumard, V.; Singhal, S. Augmenting the catalytic performance of spinel nanoferrites ($CoFe_2O_4$ and $NiFe_2O_4$) via incorporation of Al in to the lattice. *New J. Chem*. **2017**, 7(41), 8320. DOI: 10.1039/c7nj01486d
21. Paparazzo, E. XPS and auger spectroscopy studies on mixtures of the oxides SiO_2, Al_2O_3, Fe_2O_3 and Cr_2O_3. J. *Electron. Spectrosc, Relat. Phemon*. **1987**, 43, 97. https://doi.org/10.1016/0368-2048(87)80022-1
22. Yuanpeng, W.; Tao, Z.; Zhaohui, Z.; Xiaobin, D.; Yuxing, P. A facile approach to Fe_3O_4@Au nanoparticles with magnetic recyclable catalytic Properties. *Mater. Res. Bull*. **2010**, 45, 513–517. https://doi.org/10.1016/j.materresbull.2009.11.012
23. Pacheco, R. F.; Arruebo, M.; Marquina, C.; Ibarra, R.; Arbiol, J.; Santamaria, J. Highly magnetic silica-coated iron nanoparticles prepared by the arc-discharge method. *Nanotechnology* **2006**. 17, 1188–1192. 10.1088/0957-4484/17/5/004
24. Allen, G. C.; Curtis, M. T.; Hooper, A. J.; Tucker, P. M. X-Ray photoelectron spectroscopy of iron–oxygen systems. *J. Chem. Soc. Dalton. Trans*. **1974**, 1525-1530. https://doi.org/10.1039/DT9740001525
25. Chernavskii, P. A.; Khodakov, A. Y.; Pankina, G. V.; Girardon, J. S.; Quinet, E. In situ characterization of the genesis of cobalt metal particles in silica-supported Fischer-Tropsch catalysts using Foner magnetic method. *Appl. Catal. A: Gen*. **2006**, 306, 108–119. https://doi.org/10.1016/j.apcata.2006.03.033
26. Alexander, M. R.; Short, R. D.; Jones, F. R.; Stollenwerk, M. J.; Zabol, M. W. An X-ray photoelectron spectroscopic investigation into the chemical structure of deposits formed from hexamethyldisiloxane/oxygen plasmas. *J. Mat. Sci*., **1996,** 31(7), 1879-1885. https://doi.org/10.1007/BF00372203

27. Yen, C.; Lee, C.; Lin, Y.; Lin, H.; Hsiao, Y.; Liao, S.; Chuang, C.; Ma, C. M. Sol–gel derived sulfonated-silica/Nafion® composite membrane for direct methanol fuel cell. *J. Power Sources.* **2007**, 173, 36–44. https://doi.org/10.1016/j.jpowsour.2007.08.017
28. Balaraju, M.; Nikhitha, P.; Jagadeeswaraiah, K.; Srilatha, K.; Sai-Prasad, P. S.; Lingaiah, N. Acetylation of glycerol to synthesize bioadditives over niobic acid supported tungstophosphoric acid catalysts. *Fuel Proc, Technol*. **2010**, 91, 249–253. https://doi.org/10.1016/j.fuproc.2009.10.005
29. Khayoon, M. S.; Triwahyono, S.; Hameed, B. H.; Jalil, A. A. Improved production of fuel oxygenates via glycerol acetylation with acetic acid. *Chem. Eng. J.* **2014**, 243, 473–484. DOI: 10.1016/j.cej.2014.01.027
30. Kubo, O.; Ido, T.; Yokoyam, H.; Koike, Y. Particle size effects on magnetic properties of BaFe12−2xTixCoxO19 fine particles. *J. Appl. Phys*. **1985**, 57, 1. https://doi.org/10.1063/1.334585
31. Kneller, E. F.; Luborsky, F. E. Particle Size Dependence of Coercivity and Remanence of Single Domain particles. *J. Appl. Phys.* **1963**, 34, 656. https://doi.org/10.1063/1.1729324
32. Mufrodi, Z.; Sutijan, R.; Budiman, A. Chemical Kinetics for Synthesis of Triacetin from Biodiesel Byproduct. *Inter. J. Chem*. **2012**, 4(2). **DOI:**10.5539/ijc.v4n2p101
33. Beula, C.; Sai, P. S. T. Kinetics of Esterification of Palmitic acid with Ethanol-Optimization Using Statistical Design of Experiments. *Inter. J. Chem. Eng. Appl*. **2013**, 4(6), 388-392. DOI: 10.7763/IJCEA.2013.V4.331
34. Kong, P. S.; Aroua, M. K.; Daud, W. M. A. W.; Lee, H. V.; Cognetc, P.; Peresc, Y. Catalytic role of solid acid catalysts in glycerol acetylation for the production of bio-additives: a review. *RSC Adv*. **2016**, 6, 68885- 68905. https://doi.org/10.1039/C6RA10686B

Nb modified magnetic nanoparticles (Nb@Fe_3O_4) as reusable and stable catalyst for the acetylation of glycerol with acetic acid

Overview of the Chapter

An efficient and reusable heterogeneous catalyst for glycerol acetylation has been prepared by incorporating niobium over magnetic Fe_3O_4 nanoparticles. The XRD analysis suggests the existence of mixed phases of $FeNb_2O_6$ and $FeNbO_4$ in the catalyst in which niobium is present in +5 oxidation state as indicated by XPS analysis. The FTIR study suggests the existence of Lewis acidic sites over the catalyst surface, which was found to impart the acetylation activity to the catalyst. The prepared catalyst in 7 wt% (concerning glycerol) in the reaction mixture of acetic acid to glycerol ratio (9:1 mol/mol), at 90 °C reaction temperature, was found to yield 92 % triacetin within 80 min of reaction duration. The glycerol acetylation with acetic acid in the prepared catalyst was found to follow the pseudo first-order kinetic equation. The thermodynamic parameters *viz.*, enthalpy ($\Delta H^{\ddagger}$), entropy ($\Delta S^{\ddagger}$), and Gibbs free energy ($\Delta G^{\ddagger}$) of the reaction were also determined to suggest the endothermic and unspontaneous nature of the reaction. Upon completion of the reaction, the catalyst was recovered from the reaction mixture under the influence of an external magnetic field and reused during seven consecutive reaction cycles.

5.1. Introduction

In the earlier Chapters, sulphated magnetic and non-magnetic catalysts, having Lewis as well as Brønsted acidic sites have been employed for the GL acetylation to obtain TA. While reusing sulphated catalysts, the catalytically active species (sulphate group) was found to be partially soluble in the reaction mixture and hence, catalyst stability remains an issue, as discussed in Chapter 1, 3 and 4. On the other hand, Lewis acids as heterogeneous catalysts have been less explored for the GL acetylation.

Thus, to improve the catalyst stability, in the present study, niobium oxide (Lewis acid) has been incorporated over the magnetic support of Fe_3O_4 and the activity of the resulted catalyst has been explored for the TA synthesis. The catalyst was found stable during seven catalytic cycles of GL acetylation without significant loss in activity. The various reaction parameters such as catalyst amount, reaction duration, AcA/GL molar ratio, and reaction temperature were optimized to set the maximum TA selectivity and yield conditions.

5.2. Experimental Section

5.2.1. Preparation of Fe_3O_4

The Fe_3O_4 MNPs were synthesized by the chemical co-precipitation method following the same procedure as provided in Chapter 3.

5.2.2. Preparation of Nb@Fe_3O_4

The niobium oxide was impregnated over the Fe_3O_4 MNPs following the modified reported procedure [1,2]. In a typical method, 1 g of Fe_3O_4 MNPs was suspended in 100 mL deionized water. To this, desired amount (1-3 wt%) of Nb_2O_5 was added and resulted mixture was sonicated for 30 min at 35 °C. Then, the suspension was allowed to stir with the help of a mechanical stirrer at 35 °C for 6 h. The resulting mixture was dried at 100 °C for 4 h and finally calcined at the desired temperature (400−700 °C) for 3 h to obtain the Nb@Fe_3O_4 magnetic catalyst.

Prepared Nb@Fe_3O_4 magnetic catalysts were named x-@Fe_3O_4-T, where x, and T represent the impregnated niobium content (wt%), and calcination temperature (°C), respectively.

5.2.3. Acetylation of glycerol with acetic acid

The GL acetylation with AcA was performed in a 100 mL double necked-round bottomed flask equipped with a magnetic stirrer and temperature controller. The optimum reaction conditions for the acetylation of GL were established by varying the molar ratio of AcA/GL (1-12), reaction temperature (30-120 °C), reaction time (20-100 min), and catalyst amount (1-9 wt% concerning GL). The obtained products (TA, DA, and MA) were quantified by the HPLC technique.

To evaluate the catalyst reusability, it was recovered from the reaction mixture under the influence of external magnetic force (**Fig. 5.1**) and then washed with ethanol (C_2H_5OH) and finally calcined at 700 °C. The recovered catalyst was reused seven times under similar reaction and regeneration conditions.

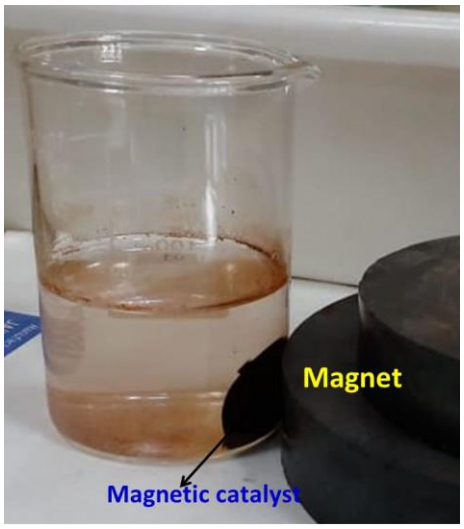

Fig. 5.1. Separation of the magnetic catalyst from reaction mixture with the help of external magnetic force.

5.3. Results and discussion

5.3.1. Catalyst Characterization

5.3.1.1. XRD analysis

To find out the structural changes upon niobium loading over Fe_3O_4, a varying amount of former (0-5 wt%) was loaded over native Fe_3O_4 at a fixed calcination temperature of 700 °C and corresponding structural changes were studied by powder XRD study as shown in **Fig. 5.2a**. For Fe_3O_4 particles, diffraction peaks at 2θ = 30.40°, 35.58°, 43.37°, 53.97°, 56.80° and 62.92°

support the formation of inverse spinel cubic structure of Fe_3O_4 (JCPDS card no. 00-003-0862). With lower niobium content (up to 1 wt%) over Fe_3O_4 MNPs tetragonal and monoclinic phases corresponding to $FeNb_2O_6$ (JCPDS card no. 00-077-1290) and $FeNbO_4$ (JCPDS card no. 01-071-1850), respectively, were found to form at 700 °C calcination temperature. Increasing the niobium content gradually (up to 5 wt%), the formation of $FeNbO_4$ (monoclinic) phase was also found to increase.

To study the effect of calcination temperature on the 3-Nb@Fe_3O_4 structure, it was calcined in the temperatures range of 400−700 °C and corresponding XRD patterns have been compared in **Fig.5.2b**. At 400−500 °C, characteristic reflections corresponding to the $FeNbO_4$ monoclinic phase, (JCPDS card no. 01-071-1850) has been observed. On increasing the calcination temperature up to 700 °C, a new tetragonal phase of $FeNb_2O_6$ (JCPDS card no. 00-077-1290) was observed. In addition, the XRD peak width gradually decreases on increasing the calcination temperature due to the sintering of the particles. Braga *et al*, reports the effect of calcination temperature on Nb_2O_5 loaded SiO_2-Al_2O_3 based catalyst and concluded that higher calcination temperature (up to 800 °C) made stronger interactions of niobium oxide with the matrix material [3].

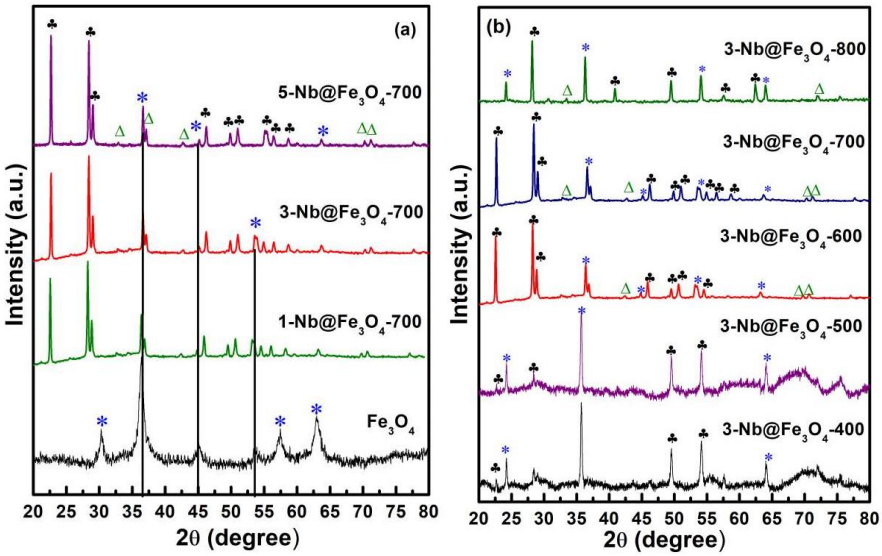

Fig. 5.2. Comparison of X-ray diffraction patterns of the Nb@Fe_3O_4 magnetic catalyst prepared by (a) varying niobium loadings and (b) varying calcination temperature. [* = Fe_3O_4 (JCPDS card no. 00-026-1136), Δ= $FeNb_2O_6$ (JCPDS card no. 01-077-1290), and ♣ = $FeNbO_4$ (JCPDS card no. 01-071-1850)].

5.3.1.2. Pyridine adsorption DRIFT study

During the acetylation of organic acid with alcohol, acidic catalyst sites have been reported to play the vital role [4]. In order to establish the nature of the acidic sites present over Nb@Fe_3O_4, FTIR spectra of pyridine adsorbed Fe_3O_4, 1-Nb@Fe_3O_4-700, and 3-Nb@Fe_3O_4-700 catalysts are compared in **Fig. 5.3a**. As could be seen from the FTIR spectra, a broad band at 1630 cm^{-1} indicates the formation of coordinate bond between pyridine and Lewis acid sites present in native Fe_3O_4 as well as niobium loaded (1-3 wt%) one. The niobium loading (1-3 wt%) over Fe_3O_4 was found to generate new Lewis acidic sites over the catalyst surface, which could be characterized by the appearance of a new bands at 1435 cm^{-1}. Datka *et al*. also report similar observations for the pyridine adsorbed 5-Nb_2O_5/Al_2O_3 and 5-Nb_2O_5/TiO_2 catalysts, where the presence of Lewis acidic sites were supported by the IR bands in the range of 1440-1460 and 1600-1635 cm^{-1} [5]. According to the literature, the Nb_2O_5 was found to be responsible for generating the strong acidic sites over the Nb_2O_5/Al_2O_3 and 5-Nb_2O_5/TiO_2 catalysts surface [5].

5.3.1.3. NH_3-Temperature Programmed Desorption study

The acidic strength of the catalysts (Fe_3O_4, 1-Nb@Fe_3O_4-700, and 3-Nb@Fe_3O_4-700), is determined by the temperature programmed NH_3 desorption technique (**Fig. 5.3b**). All samples demonstrated, desorption of ammonia from weak acidic sites at around 200 °C. Similarly, desorption peaks at 580 °C and 670 °C, reflects the presence of strong acidic sites over the catalyst surface with high catalyst acidity (4.1 mmol g^{-1}).

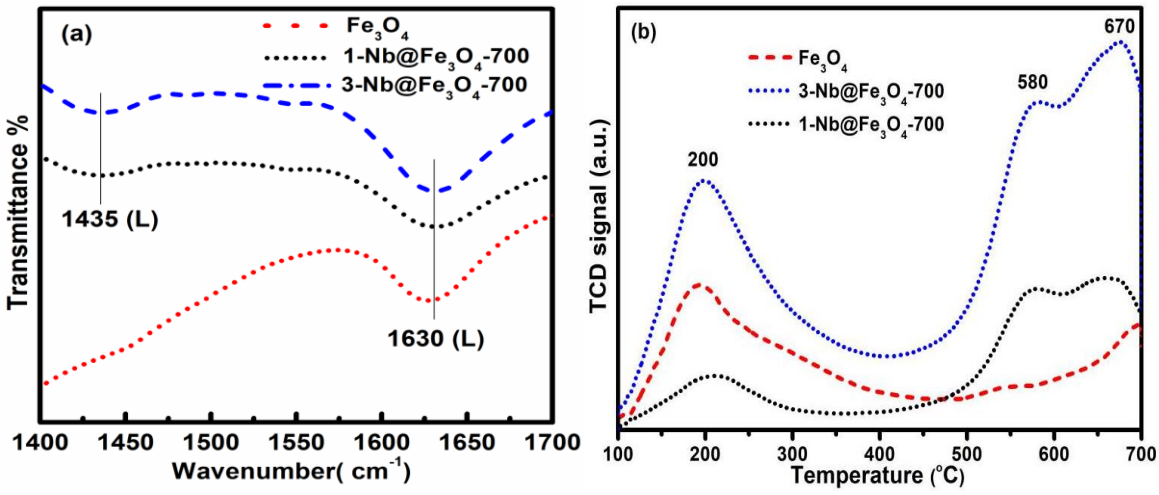

Fig. 5.3. (a) FTIR spectra of pyridine adsorption and (b) NH_3-TPD profiles for the catalysts.

In addition, the amount of desorbed gases was found to increase with the niobium loading (1 to 3 wt%) to support that formation of acidic sites is directly related to the niobium loading over the catalyst (**Table 5.1**). The amount of ammonia desorbed was found to be maximum (4.1 mmol g^{-1}) in case of 3-Nb@Fe_3O_4-700. Cheng *et al*. also reports the desorption peak in the temperature range of 100 to 450 °C, in the case of Nb_2O_5 loaded WO_3/ZrO_2 catalyst owing to the presence of weak/moderate acidic sites and another desorption peak in the range of 450- 600 ºC due to the presence of strong acidic sites over the catalyst surface [6]. Thus FTIR and TPD analysis of the catalyst indicates the incorporation of the acidic sites over the catalyst due to the niobium impregnation.

Table 5.1. Comparison of the BET specific surface area, pore volume, pore size, and total acidity of Fe_3O_4 and 3-Nb@Fe_3O_4-700.

Catalyst	BET surface area (m^2g^{-1})	Pore volume (cm^3/g^{-1})	Pore size (nm)	Total acidity (mmol g^{-1})
Fe_3O_4	129	0.5	11	0.32
3-Nb@Fe_3O_4-700	69	0.23	9	4.1

5.3.1.4. BET analysis

The nitrogen adsorption-desorption isotherms of the Fe_3O_4 and 1-Nb@Fe_3O_4-700, and 3-Nb@Fe_3O_4-700 magnetic catalysts are compared in the **Fig. 5.4a**, which reveal the surface porosity and pore size behaviour of these magnetic catalysts. The Fe_3O_4, as well as 1-Nb@Fe_3O_4-700, and 3-Nb@Fe_3O_4-700 were found to show type- IV adsorption-desorption isotherm having the H1 type hysteresis loops. The Fe_3O_4 MNPs show the hysteresis loops at p/p0 = 0.8-1.0, and the relatively larger pore size of 11 nm as measured by N_2 adsorption-desorption isotherm (**Fig. 5.4a**). Upon niobium impregnation (1-3 wt%), the quantity of adsorbed nitrogen gas decreases due to the reduction in of surface area from 129 m^2g^{-1} to 69 m^2g^{-1} and the hysteresis loop shifts to low pressure (p/p0 = 0.7-0.9), with a pore size of 9 nm as shown in **Table 5.1**. The loss of surface area can be ascribed due to the clustering of particles during niobium impregnation over the Fe_3O_4 MNPs.

Similarly, Opris *et al*. observed that cobalt incorporation (1-4 wt%) over the Nb_2O_5@Fe_3O_4 MNPs was found to reduce the surface area from 68 to 30 m^2g^{-1} [2], Gunathilake and Jaroniec also reported the reduction of surface area (from 968 to 261 m^2 g^{-1}) as well as pore size (from

0.10 to 0.06 cm^3g^{-1}) upon magnesium incorporation over silica surface, due to the filling of SiO_2 pores by magnesium or clustering of the nanoparticles [7].

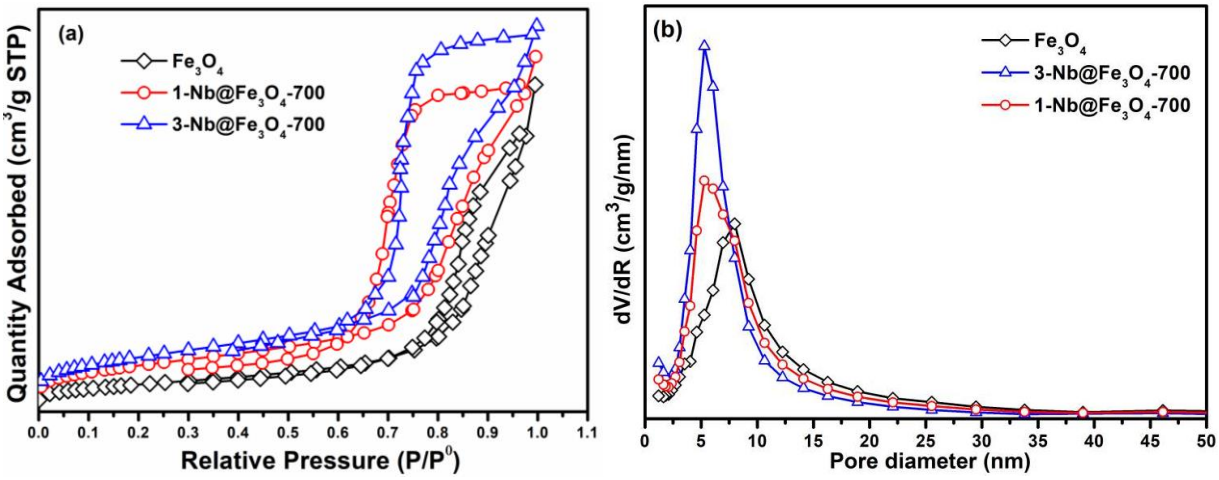

Fig. 5.4. (a) N_2 adsorption-desorption isotherms and (b) pore size distribution.

5.3.1.5. Magnetization efficiency of the catalyst

The magnetic property of the catalysts was studied with the help of a vibrating sample magnetometer (VSM). Hysteresis loops (M-H) of Fe_3O_4, 1-Nb@Fe_3O_4-700, and 3-Nb@Fe_3O_4-700 was measured at room temperature (**Fig. 5.5**). All of these magnetic material show the ferromagnetic behaviour with the saturation magnetization (M_S) at 35.38, 34.69 and 27.87 emu/g^{-1}, respectively. The Ms value for Fe_3O_4 was 35.38 emu/g^{-1} which was higher compared to the niobium loaded MNPs (Fe_3O_4 >1-Nb@Fe_3O_4-700 >3-Nb@Fe_3O_4-700). The reduction in M_S value is due to the effective increase in the non-magnetic mass (niobium oxide) over the magnetic Fe_3O_4 particles. The coercivity (H_C) and remanence (M_R) values do not show any significant difference between the samples either with or without niobium (1- 3 wt%) loading. Low values of H_c (upto 15.17 G) and M_R (upto 0.84 emu/g^{-1}) indicate the formation of small sized MNPs which may be close to their super paramagnetic limit. Thus, separation of all these catalysts from the reaction mixture is possible by applying external magnetic force. The results were according to the reports by Naeimi and Nazif for the Fe_3O_4 magnetic catalyst, where M_S value decreases (from 50.86 to 15 emu/g^{-1}) upon sulphonic acid incorporation over the silica coated Fe_3O_4 particles [8]. Goyal *et al*. also report that saturation magnetization of $CoFe_2O_4$ (19.4 emu/g^{-1}) decreases upon the non-magnetic aluminium coating over MNPs (3.7 emu/g^{-1}) [9].

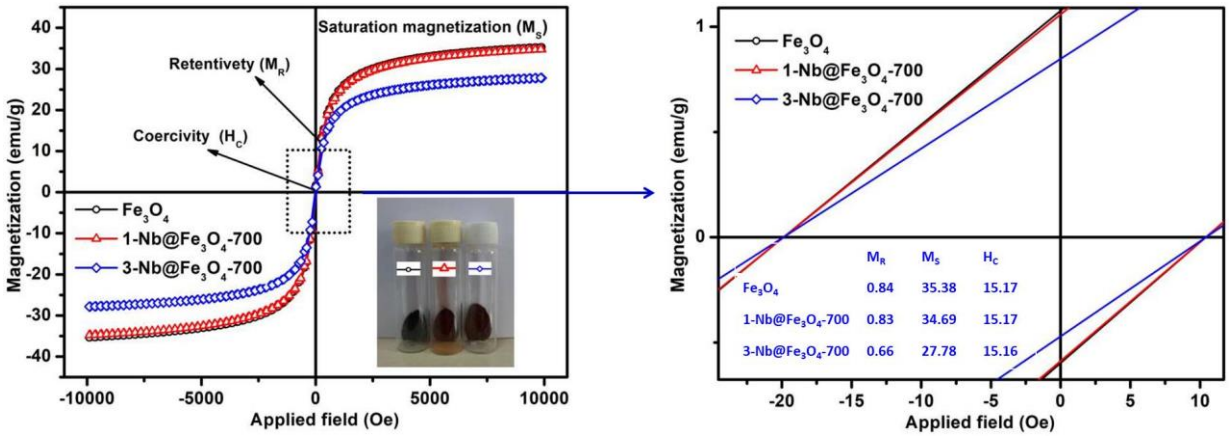

Fig. 5.5. Magnetization curves of Fe_3O_4, 1-Nb@Fe_3O_4-700 and 3-Nb@Fe_3O_4-700.

5.3.1.6. SEM-EDX analysis

The surface morphology of the magnetic catalysts (Fe_3O_4 and 3-Nb@Fe_3O_4-700) was determined by the SEM-EDX technique, as shown in **Fig. 5.6**. The SEM images of Fe_3O_4 MNPs show the formation of these particles in spherical shape (**Fig. 5.6a**), which, upon Nb loading, forms the agglomerates of 3-Nb@Fe_3O_4-700 particles (**Fig. 5.6b**). The EDX analysis was carried out to determine the elementals composition of the Fe_3O_4 MNPs as well as magnetic catalyst (3-Nb@Fe_3O_4-700). The EDX data revealed the presence of Fe and O in the Fe_3O_4 MNPs with a mass percentage of 66.76 wt% and 33.24 wt%, respectively. On the other hand, the EDX of the niobium loaded sample (3-Nb@Fe_3O_4-700) show the presence of 2.91 wt% Nb along with the presence of Fe and O.

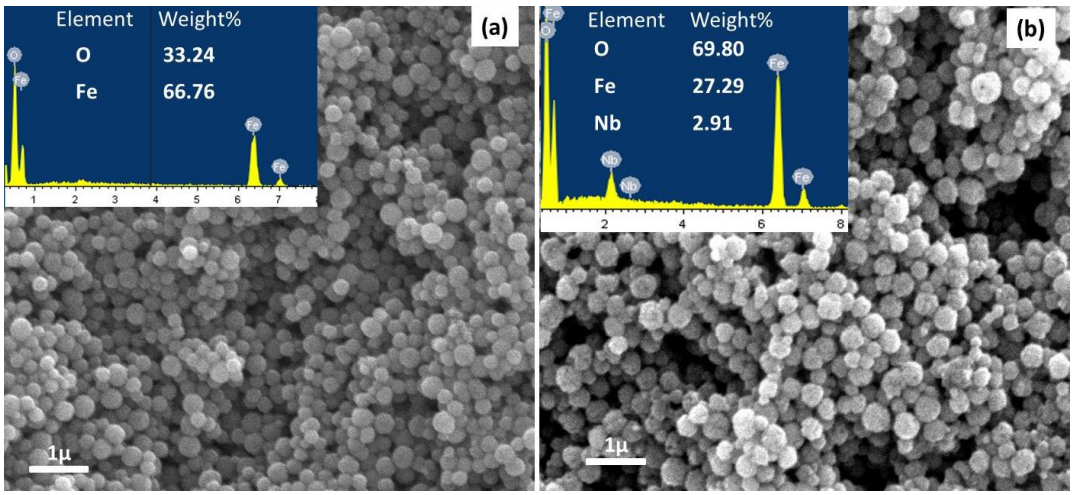

Fig. 5.6. SEM-EDX images of (a) Fe_3O_4, and (b) 3-Nb@Fe_3O_4-700.

5.3.1.7. TEM analysis

The TEM images of Fe_3O_4 and 3-Nb@Fe_3O_4-700 magnetic catalysts are given in **Fig. 5.7**. As shown in **Fig. 5.7a-b**, the Fe_3O_4 MNPs are clusters of spherical or oval-shaped particles with a smooth surface and an average particle size of ~127 nm. Moreover, the TEM image of 3-Nb@Fe_3O_4-700 shows the formation of an additional rough layer owing to the niobium impregnation over the Fe_3O_4 MNPs (**Fig. 5.7c-d**). The average size of these particles was found to be ~135 nm. The crystallite size, calculated by Scherrer's formula, of the Fe_3O_4 (~119 nm) and 3-Nb@Fe_3O_4-700 (~131) particles, also matches with the size of these particles calculated from TEM imaging.

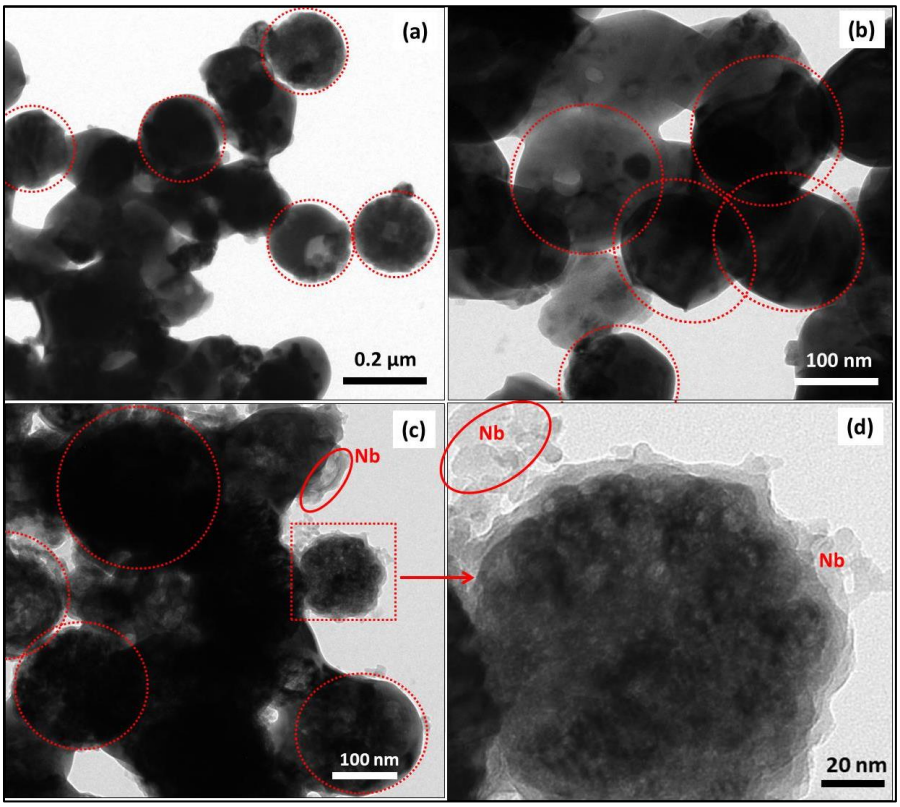

Fig. 5.7. TEM images of (a-b) Fe_3O_4, and (c-d) 3-Nb@Fe_3O_4-700.

5.3.1.8. XPS analysis

The X-ray photoelectron spectroscopy (XPS) analysis was used to recognize the electronic state of the elements present in the catalyst (3-Nb@Fe_3O_4-700) as shown in **Fig. 5.8**. The full scan XPS spectrum of the 3-Nb@Fe_3O_4-700 confirmed the presence of Nb, Fe, and O elements over the catalyst surface as shown in **Fig. 5.8a**.The niobium in the catalyst exists in +5 oxidation state,

as indicated by two close peaks at 207 and 209.6 eV (**Fig. 5.8b**). This kind of pattern also supports the presence of niobium in $3d_{5/2,}$ and $3d_{3/2}$ state present in Nb_2O_5 and $FeNb_2O_6$ or $FeNbO_4$ molecules, respectively. Opris *et al.* also reported the presence of Nb^{5+} in cobalt loaded $Nb_2O_5@Fe_3O_4$ owing to the presence of peak doublet centered at 207.4 eV [2].

The two peaks centered at 528.17 eV and 530.6 eV (**Fig. 5.8c**) indicate the presence of O^{2-} 1s state, which could be ascribed to the Nb–O and Fe–O–Nb linkages, respectively [2, 10]. Thus, XPS and TEM study support the Nb_2O_5 incorporation over the Fe_3O_4 MNPs surface. In literature, the binding energy below 534 eV, for O 1s state, is typically attributed to the metal oxide formation. Furthermore, the spectrum revealed (**Fig. 5.8d**) the peaks at 712.6, 719.3 and 726.2 eV corresponding to the Fe^{2+} $2p_{3/2}$ state and at 714.7, 721.8, and 729.1 eV corresponding to the Fe^{3+} $2p_{1/2}$ state. This study can be associated with Yang *et al*, where the presence of Fe^{2+} and Fe^{3+} states in Fe_3O_4 were supported by the peaks centered at 712.18 (Fe^{2+} $2p_{3/2}$) and 725.51 eV (Fe^{3+} $2p_{1/2}$), respectively [11].

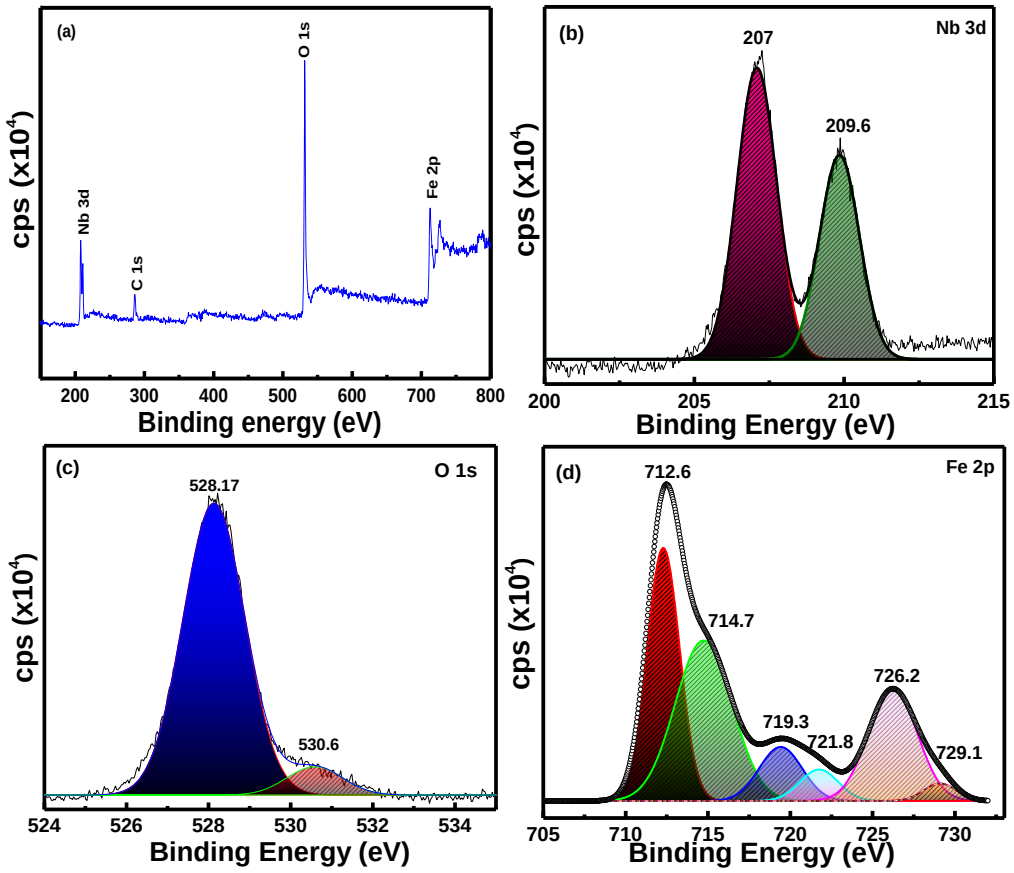

Fig. 5.8. XPS spectra of 3-$Nb@Fe_3O_4$-700 catalyst (a) full scan, (b) Nb 3p, (c) O 1s, and (d) Fe 2p.

5.3.2. Product analysis

5.3.2.1. FTIR analysis

The TA formation upon GL acetylation, was supported by the FTIR spectroscopic technique as shown in **Fig. 5.9**. In the FTIR spectra of GL, two bands positioned at 1030 and 3291 cm^{-1} were observed due to the C—O and O—H group vibrational frequencies, respectively (**Fig 5.9a**). Upon GL acetylation, a new band at 1722 cm^{-1} was observed due to the carbonyl of the ester group to support the ester bond formation in TA molecule (**Fig. 5.9b**).

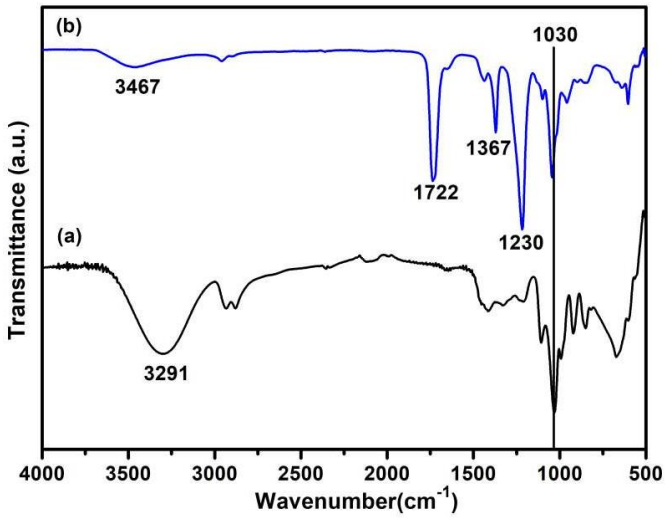

Fig. 5.9. FTIR spectra of (a) glycerol and (b) triacetin produced during glycerol acetylation.

5.3.2.2. NMR analysis

In ^{1}H-NMR spectra of GL, peaks observed at 3.32-3.50 (g_1) and 3.59 ppm (g_2) are due to the CH_2 and CH protons, respectively, as shown in **Fig. 5.10a**. Upon acetylation, the formation of TA is confirmed by the appearance of two singlets corresponding to methyl ($-CH_3$) protons, at 1.92 (k_1) and 1.94 ppm (k_2). The position of the glyceridic protons also shifts at 4.07- 4.22 ppm due to t_1 protons and at 5.13 ppm due to t_2 protons. Peaks centred at 3.99 ppm also indicate the presence of minor amount of DA in the products as shown in **Fig. 5.10b**.

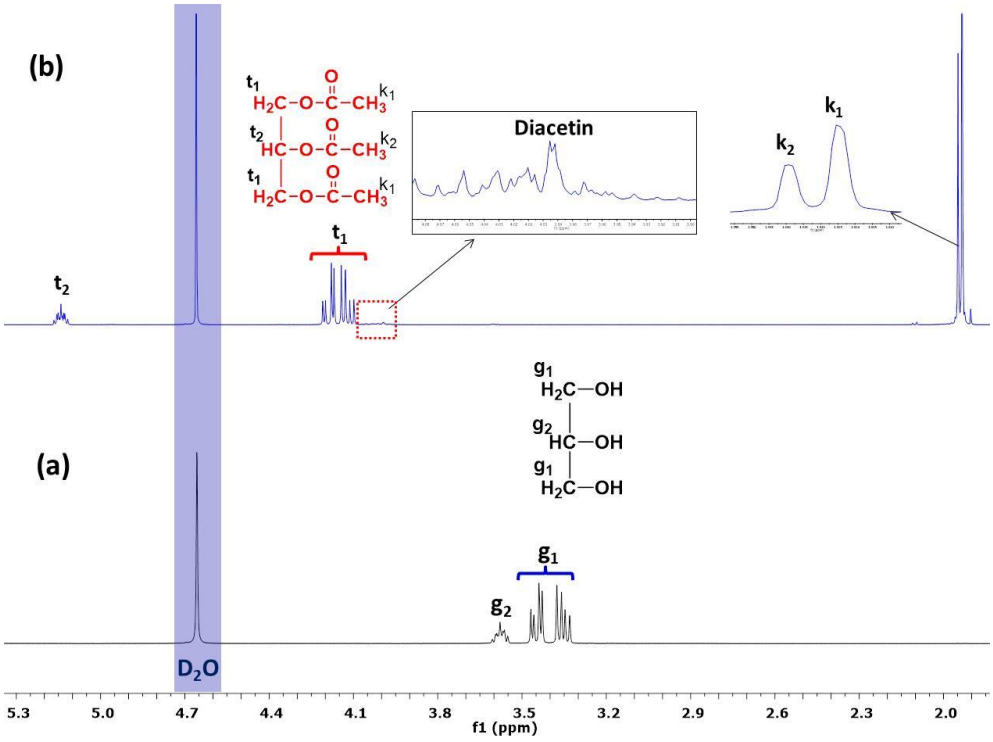

Fig. 5.10. ^{1}H NMR spectra of (a) glycerol and (b) triacetin produced during GL acetylation.

5.3.2.3. HPLC analysis

The products formed during 3-Nb@Fe_3O_4-700 catalyzed reaction were quantified by running the normal phase HPLC. In the HPLC plot, the peaks observed at 6.30, 6.76 and 8.17 min were assigned to TA, DA and GL, respectively (**Fig. 5.11**). The area under a specific peak was found to be proportional to the amount of the molecule it is associated with. During 3-Nb@Fe_3O_4-700 catalyzed GL acetylation, under optimized reaction parameters, a maximum of 92 % TA selectivity with 100 % GL conversion was obtained.

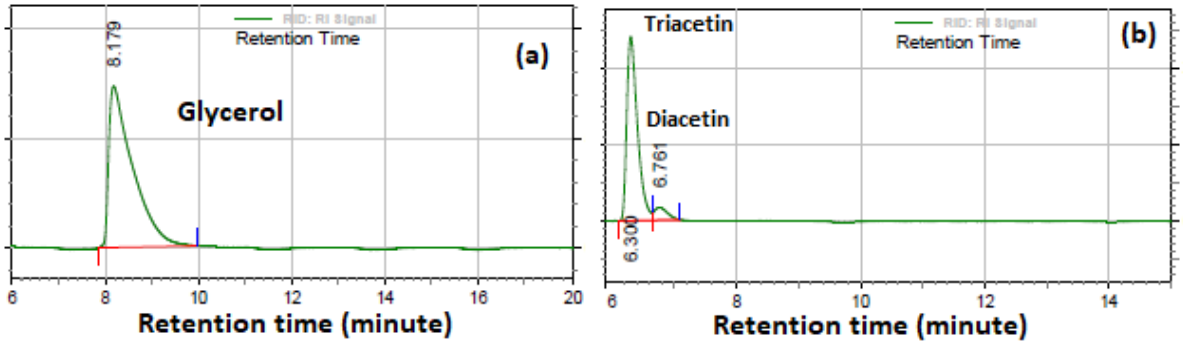

Fig. 5.11. HPLC chromatogram of (a) pure glycerol and (b) triacetin produced during glycerol acetylation.

5.3.3. Catalyst Screening

The acetylation of GL with AcA required the presence of acidic catalysts. When reaction was carried out either in absence of any catalyst or in the presence of bare Fe_3O_4 magnetic particles, almost negligible conversion levels were achieved to maintain that magnetic particles remain silent during the reaction. While the application of the niobium incorporated Fe_3O_4 particles (3-Nb@Fe_3O_4-700) was found to catalyze the GL acetylation as indicated in **Fig. 5.12**, to support that Thus, Lewis acidic sites, formed by the niobium oxide impregnation, are responsible for the catalyst activity. Moreover, catalyst with 3 wt% of niobium oxide showed a maximum TOF (137 h^{-1}) as compared to the one with 1 wt% (97 h^{-1}) of niobium oxide. Thus, in the present study, reaction parameters of 3-Nb@Fe_3O_4-700 catalyzed GL acetylation was examined to obtain the maximum TA selectivity.

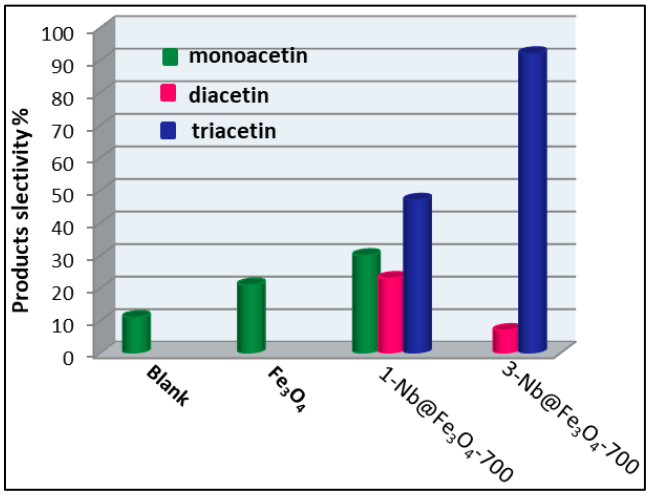

Fig. 5.12. Effect of the various catalysts over the acetylation of glycerol.

5.3.3.1. Effect of catalyst amount on product selectivity

In order to find out the optimum catalyst amount to achieve the maximum TA selectivity, a series of GL acetylation reactions was performed by employing AcA/GL molar ratio of 9:1 at 90 °C reaction temperature for 80 min of reaction duration but varying the catalyst amount (1 to 9 wt% concerning GL) as indicated in **Fig. 5.13a**. Upon acetylation, the TA selectivity rises (from 0-92 %) on increasing the catalyst amount (from 1 to 7 wt%). Maximum TA selectivity (92 %) was obtained with 7 wt% of catalyst amount. A further increase in catalyst amount (up to 9 wt%) was not found to improve the selectivity or not reduce the reaction duration.

This observation could be correlated with the literature reports where employing AcA/GL (4:1 molar ratio) at 110 °C in the presence of 3%Y/SBA-3 catalyst, the TA selectivity was found to increase gradually from 5 to 44 % with the increase in catalyst amount (from 0.05 to 2 wt% concerning GL) [12]. Thus, TA selectivity as well yield was found to be a function of the available active (acidic) sites, which would depend upon the presence of catalyst contents in the reaction mixture.

5.3.3.2. Effect of AcA/GL molar ratio on the product selectivity

The variation of AcA/GL molar ratio (1 to 12) to achieve the highest TA selectivity during the GL acetylation was evaluated by performing the reaction for 80 min in the presence of 7 wt% catalyst at 90 °C reaction temperature as shown in **Fig. 5.13b**. It can be observed that at lower AcA concentration (1 to 3 molar ratios), MA (40 %) was found to be the major product in the reaction mixture. On increasing the AcA/GL molar ratio, up to 9, TA selectivity increases and it was observed as the major product (92 %). A further increase in the concentration of AcA was not found to make any significant change in the TA selectivity, as shown in **Fig 13b**.

In earlier reports Khayoon *et al*. studied the sulfate functionalized activated carbon (S-AC) to study the GL acetylation with AcA [13]. During this study, the catalyst was found to yield higher MA selectivity (44 %) while employing AcA/GL molar ratio of 5 at 120 °C within 3 h of reaction duration. Furthermore, the TA selectivity increases linearly with the increase in AcA concentration and at 8 molar ratio of AcA/GL, maximum TA selectivity (34 %) was obtained.

5.3.3.3. Effect of reaction temperature on the product selectivity

In order to study the effect of temperature on product selectivity, a series of reaction was performed in the presence of 7 wt% of catalyst (concerning GL) at 90 °C with 9 molar ratio of AcA/GL by varying the temperature from 30 to 120 °C as shown in **Fig. 5.13c**. A significant increase in TA selectivity (from 0 to 92%) was observed when the reaction temperature was raised from 30 to 90 °C. However, a further increase in the reaction temperature (up to 120 °C) was not found to change TA selectivity and yield significantly.

A similar trend has been reported in the literature, where most of the GL acetylation reactions with AcA were performed in the temperature range of 80 to 120 °C to obtain the maximum TA

selectivity of 65 % [13-16]. However, very few reports have been found in the literature which claimed > 90 % TA selectivity [17].

5.3.3.4. Effect of reaction time on the product selectivity

In order to optimize the effect of reaction time over the GL acetylation, a series of reaction was performed in the presence of 7 wt% of catalyst employing AcA/GL molar ratio of 9:1, at 90 ^{o}C reaction temperature while varying the reaction time from 20 to 100 min (**Fig. 5.13d**). The TA selectivity was found to rise from 0 to 92 % with the reaction duration (from 20 to 80 min) at the expense of MA and DA selectivity. A further increase in reaction time (up to 100 min) was not found to change the TA selectivity to any significant extent. The observation is in line with the literature reports where the selectivity of MA and DA was found to be higher during the initial phase of the GL acetylation reaction [18]. The study also supported the stepwise acetylation of GL alcoholic groups during the reaction.

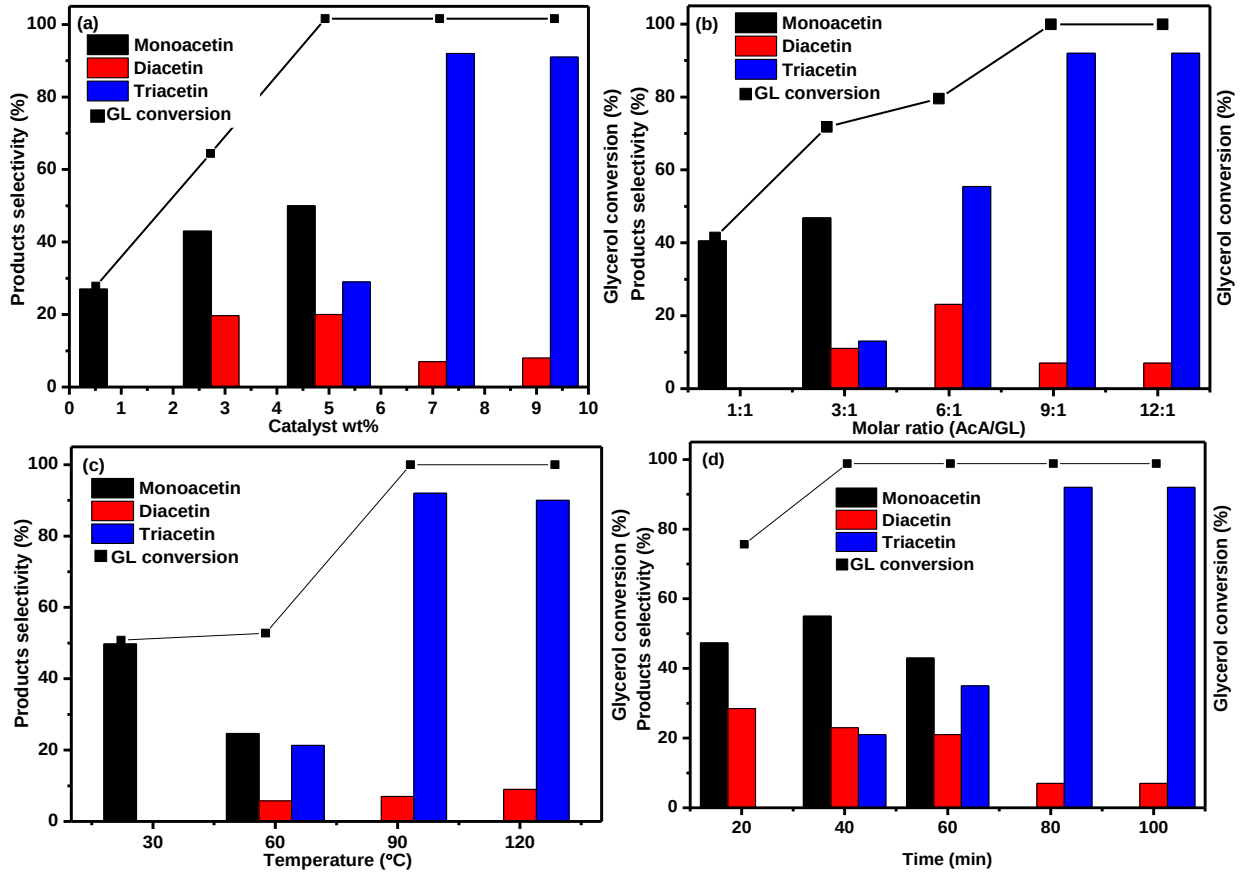

Fig. 5.13. Influence of various reaction parameters on 3-Nb@Fe_3O_4-700 assisted glycerol acetylation (a) catalyst amount, (b) AcA/GL molar ratio, (c) reaction temperature and (d) reaction time.

Thus on the basis of described study, the optimized reaction condition to achieve 92 % TA selectivity and 99 % GL conversion, during the 3-Nb@Fe_3O_4-700 catalyzed reaction was established as:- AcA/GL molar ratio of 9:1, 90 °C reaction temperature, catalyst amount of 7 wt% (concerning GL), and 80 min of reaction duration.

5.3.4. The reusability and stability

The incorporation of the magnetic core in heterogeneous catalysts allows their magnetic separation after the completion of the reaction. To evaluate the catalyst reusability, GL acetylation was performed under the optimized reaction conditions as established during the previous section. Upon completion of the reaction, the catalyst was removed from the reaction mixture under the influence of an external magnetic field as shown in **Fig. 5.1**. The recovered catalyst was washed with ethanol multiple times, dried at 100 °C for 4 h and calcined at 700 °C for 3 h. The regenerated catalyst was further reused during 6 consecutive reaction cycles under the same set of recovery and regeneration procedures (**Fig. 5.14**). It can be noticed from the results that the catalyst was able to yield more than 57 % TA yield while maintaining the overall GL conversion of more than 90 % during the fourth run. However, during the 5th run, the catalyst activity was found to decline to a significant extent as TA selectivity remained lesser than 40 %.

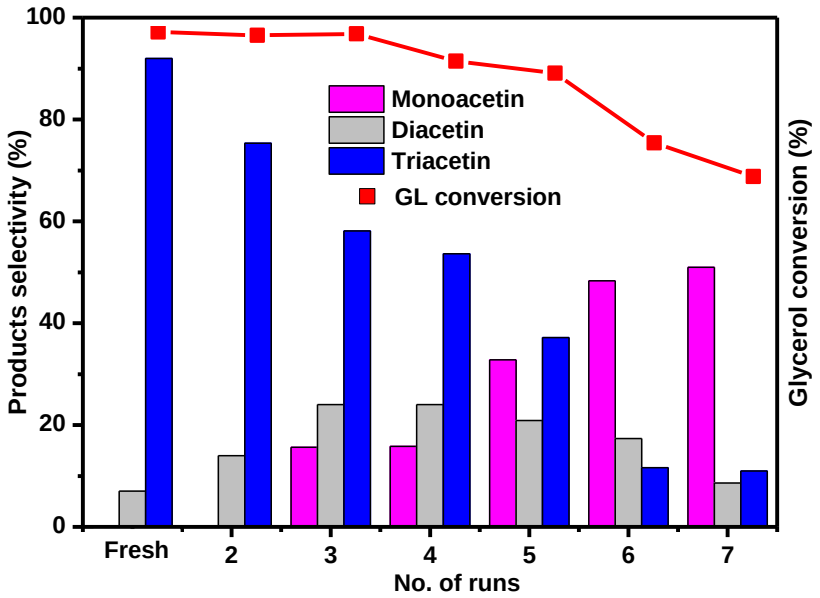

Fig. 5.14. Study of the 3-Nb@Fe_3O_4-700 reusability during the glycerol acetylation with acetic acid.

In order to study the factors responsible for the loss in catalyst activity, the catalyst stability was evaluated by comparing the niobium contents in fresh and reused catalysts based on EDX analysis. The niobium content in the fresh catalyst was higher (2.91 wt%) as compared to reused catalyst (1.09 wt%), as shown in **Fig. 15a**. Similarly, NH_3-TPD analysis also supports a decline in acidic sites (from 4.1 to 0.83 mmol g^{-1}) for the reused catalyst (**Fig. 5.15b**). Therefore, the detachment of niobium (active sites) from the catalyst surface might be the main reason behind the loss in catalytic activity.

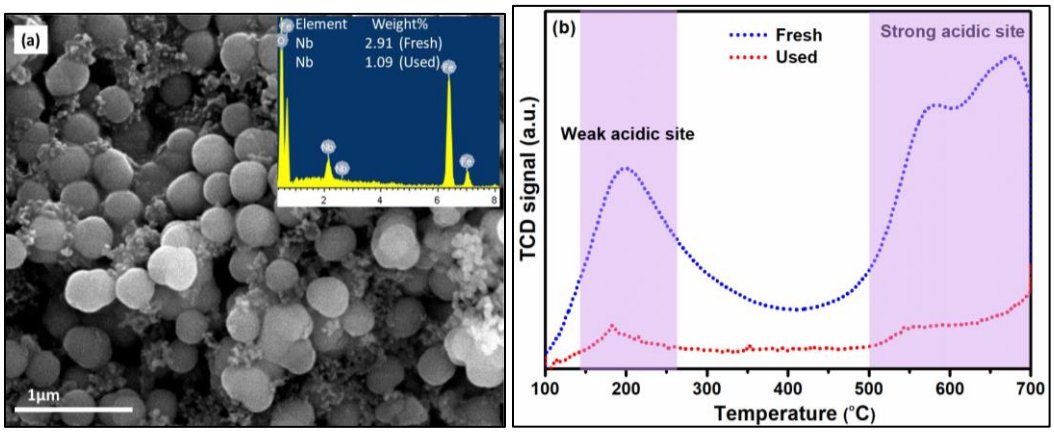

Fig. 5.15. Comparison of fresh and used catalyst (a) SEM-EDX and (b) NH_3–TPD analysis.

As supported by the SEM-EDX and NH_3-TPD analysis, the detachment of the active sites (niobium oxide) from the catalyst was found to be responsible for the loss in activity. The leached niobium oxide may also catalyze the reaction similar to a homogeneous catalyst. Thus it is imperative to establish the homogeneous contribution in catalyst activity which could be demonstrated with the help of a hot filtration test. In this test, GL acetylation was performed under the optimized reaction conditions but for 40 min. After that catalyst was magnetically separated from the reaction mixture, and reaction mixture, without catalyst, was allowed to react for additional 40 min. The GL conversion during the reaction was analyzed as indicated in **Fig. 5.16**. As evident from the figure, no significant increase in the conversion level was observed when reaction was performed in absence of catalyst to indicate that the leached metal oxide has not catalyzed the reaction to significant extent. Thus, it is safe to assume that the heterogeneous catalyst is responsible for almost the entire catalytic activity.

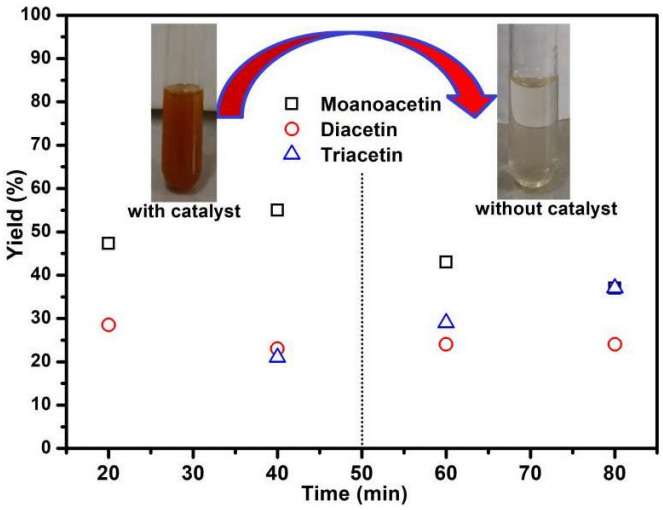

Fig. 5.16. Study of homogeneous contribution during the acetylation of glycerol with acetic acid

5.3.5. Kinetic study

The kinetics of the GL acetylation have been studied under optimized reaction conditions but varying the reaction temperature (30 to 90 °C) in the presence of 3-Nb@Fe_3O_4-700 catalyst. The aliquots from the reaction mixture have been withdrawn every 20 min, and GL conversion levels were quantified by HPLC technique.

The appropriate value of the data was fitted in zero-, first- and second-order kinetic models (Chapter 2), as shown in **Fig 5.17**. However, a better fitting with first order equation indicates that the reaction has followed the pseudo first-order kinetic model.

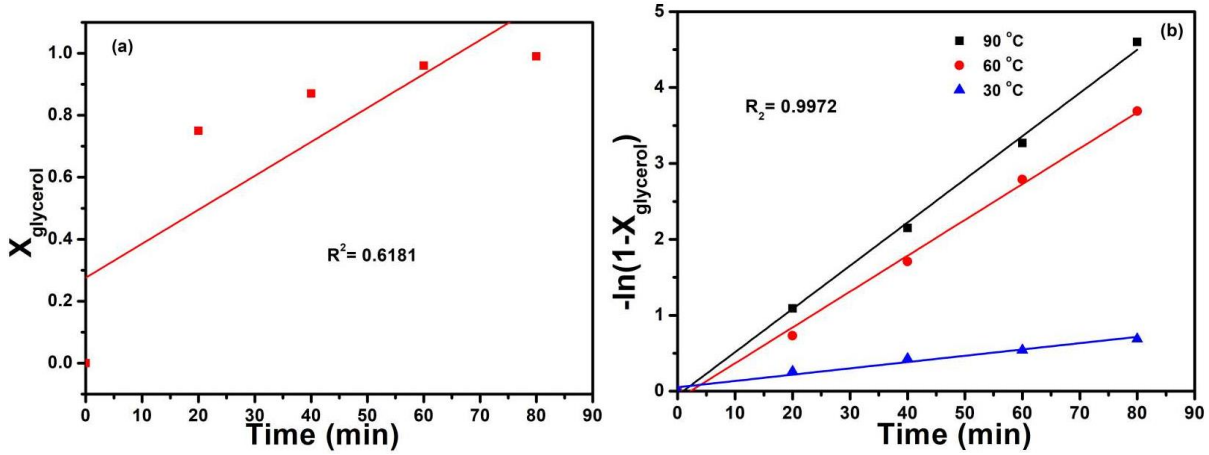

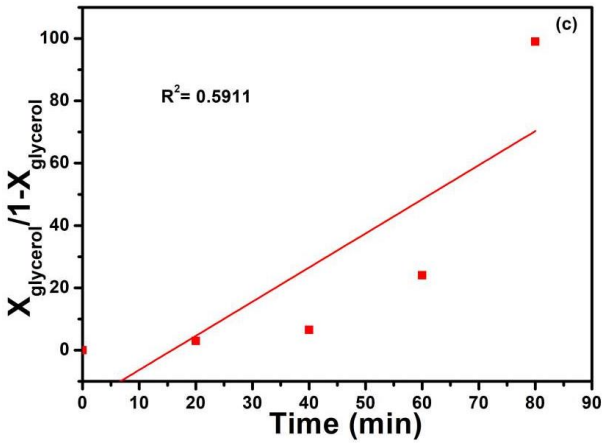

Fig. 5.17. Plots of fitting in (a) Zero-, (b) first-, and (c) second-order equation for the 3-Nb@Fe_3O_4-700 catalyzed GL acetylation.

The rate constant (k) from this plot (**Fig. 17b**) were found to be 0.057, 0.048, and 0.0083 min^{-1} at 90, 60, and 30 °C reaction temperature, respectively.

To determine the activation energy (E_a) for the same reaction, the appropriate values were fitted in Arrhenius equation (Chapter 2). From the Arrhenius plot (**Fig. 5.18a**) the E_a for the GL acetylation was found to be 28.21 kJ mol^{-1}. Veluturla *et al*. reported the activation energy, during the GL acetylation into acetins using cesium supported heteropoly acid (CsPWA) catalyst, in the range of 24.99 – 51.73 kJ mol^{-1} [19-20]. A value of E_a > 24 kJ mol^{-1} specifies that the reaction is chemically controlled and not by the mass transfer limitations [20-21].

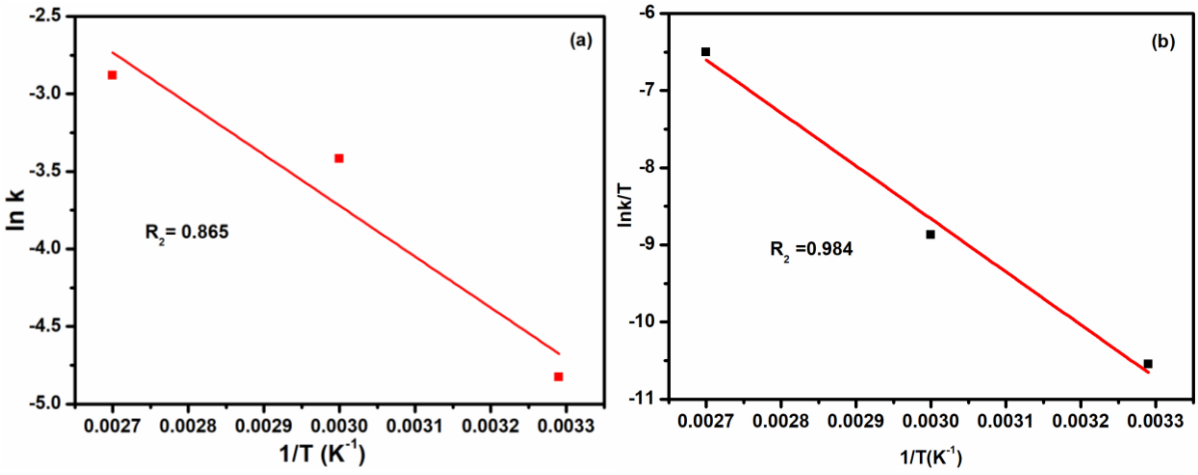

Fig. 5.18. (a) Arrhenius and (b) Eyring plot for the glycerol acetylation with acetic acid over the 3-Nb@Fe_3O_4-700 catalyst.

The thermodynamic parameters, such as enthalpy ($\Delta H^{\ddagger}$) and entropy ($\Delta S^{\ddagger}$) were not frequently studied for the GL acetylation reaction in the presence of heterogeneous catalyst. Therefore, in the present Chapter these parameters were evaluated following the Eyring-Polanyi equation (Chapter 2). The $\Delta H^{\ddagger}$ and $\Delta S^{\ddagger}$ values from the plot, (**Fig. 5.18b**) were found to be +57.11 kJ mol^{-1} and -296.8 J mol^{-1} K^{-1}, respectively. The positive value of $\Delta H^{\ddagger}$ indicates the endothermic nature of the reaction, and thus, an external heating source is needed to push the reaction in forward direction [22]. On the other hand, the value of $\Delta S^{\ddagger}$ was negative to suggest that the reactant species might have combined over the catalyst surface to make a more ordered transition state.

Gibb's free energy ($\Delta G^{\ddagger}$) of the reaction was +164.6 kJ mol^{-1} as calculated following the fundamental thermodynamics equation (Chapter 2). Thus, the positive value of $\Delta G^{\ddagger}$ for the GL acetylation with AcA indicates the unspontaneous nature of the reaction.

5.4. Conclusions

The acetylation of glycerol with acetic acid was performed over 3-Nb@Fe_3O_4-700 magnetic catalyst. The reaction parameters (reactant ratio, catalyst amount, reaction duration and reaction temperature) have been optimized to obtain superior glycerol conversion level (99 %) with higher TA selectivity of 92 %. The catalyst was recovered from the reaction mixture under the influence of external magnetic field and reused during seven catalytic cycles; however, the efficacy of the catalyst was found to reduce during the successive runs. In addition, the catalyst was partially soluble into the reaction mixture; however, the dissolved catalyst has not catalyzed the glycerol conversion into the acetins.

References

[1] Nadar, A.; Banerjee, A. M.; Pai, M. R.; Meena, S. S.; Pai, R. V.; Tewari, R.; Yusuf, S. M.; Tripathi, A. K.; Bharadwaj, S. R. Nanostructured Fe_2O_3 dispersed on SiO_2 as catalyst for high temperature sulfuric acid decomposition-Structural and morphological modifications on catalytic use and relevance of Fe_2O_3-SiO_2 interactions. *Appl. Catal. B Environ*. **2017**, 217, 154–168. https://doi.org/10.1016/j.apcatb.2017.05.045

[2] Opris, C.; Cojocaru, B.; Gheorghe, N.; Tudorache, M.; Coman, S. M.; Parvulescu, V. I.; Duraki, B.; Krumeich, F.; Bokhoven, J. A. Lignin fragmentation over magnetically recyclable composite Co@Nb_2O_5@Fe_3O_4 catalyst. *J. Catal*. **2016**, 339, 209–227. https://doi.org/10.1016/j.jcat.2016.04.002

[3] Braga, V. S.; Dias, J. A.; Dias, S. C. L.; Macedo, J. L. Catalyst Materials Based on Nb_2O_5 Supported on SiO_2-Al_2O_3: Preparation and Structural Characterization. *Chem. Mater*. **2005**, 17, 690-695. https://doi.org/10.1021/cm048673u

[4] Tabatabaei, M.; Aghbashlo, M.; Najafi, B.; Hosseinzadeh-Bandbafha, H.; Ardabili, S. F.; Akbarian, E.; Khalife, E.; Mohammadi, P.; Rastegari, H.; Ghaziaskar, H. S. Environmental impact assessment of the mechanical shaft work produced in a diesel engine running on diesel/biodiesel blends containing glycerolderived Triacetin. *J. Cleaner Prod*. **2019**, 223, 466-486. https://doi.org/10.1016/j.jclepro.2019.03.106

[5] Datka, J.; Turek, A. M.; Jehng, J. M.; Wachs, I. E. Acidic Properties of Supported Niobium Oxide Catalysts: An Infrared Spectroscopy Investigation. *J. Catal*. **1992**, 135, 186-199. https://doi.org/10.1016/0021-9517(92)90279-Q

[6] Sung, K.; Cheng, S. Effect of Nb doping in WO_3/ZrO_2 catalysts on gas phase dehydration of glycerol to form acrolein†, *RSC Adv*. **2017**, 7, 41880. DOI:10.1039/C7RA08154E

[7] Gunathilake, C.; Jaroniec, M. Mesoporous calcium oxide–silica and magnesium oxide–silica composites for CO_2 capture at ambient and elevated temperatures†. *J. Mater. Chem. A* **2016**, 4, 10914-10924. https://doi.org/10.1039/C6TA03916B

[8] Naeimi, H.; Nazif, Z. S. A highly efficient nano-Fe_3O_4 encapsulated-silica particles bearing sulfonic acid groups as a solid acid catalyst for synthesis of 1,8-dioxo-octahydroxanthene derivatives. *J. Nanopart. Res*. **2013**, 15, 2026. doi: 10.1007/s11051-013-2026-2

[9] Goyal, A.; Bansal, S.; Chudasama, B.; Tikoo, K. B.; Kumard, V.; Singhal, S. Augmenting the catalytic performance of spinel nanoferrites ($CoFe_2O_4$ and $NiFe_2O_4$) via incorporation of Al in to the lattice. *New J. Chem*. **2017**, 7(41), 8320. DOI: 10.1039/c7nj01486d

[10] Fang, J.; Bi, X.; Si, D.; Jiang, Z.; Huang, W. Spectroscopic studies of interfacial structures of CeO_2–TiO_2 mixed oxides. *Appl. Surf. Sci*. **2007**, 253, 8952–8961. https://doi.org/10.1016/j.apsusc.2007.05.013

[11] Yamashita, T.; Hayes, P. Analysis of XPS spectra of Fe^{2+} and Fe^{3+} ions in oxide materials. *Appl. Surf. Sci*. **2008**, 254, 2441–2449. https://doi.org/10.1016/j.apsusc.2007.09.063

[12] Khayoon, M. S.; Triwahyono, S.; Hameed, B. H.; Jalil, A. A. Improved production of fuel oxygenates via glycerol acetylation with acetic acid. *Chem. Eng. J*. **2014**, 243, 473–484. DOI: 10.1016/j.cej.2014.01.027

[13] Khayoon, M. S.; Hameed, B. H. Acetylation of glycerol to biofuel additives over sulfated activated carbon catalyst. *Bioresour. Technol*. **2011**, 102, 9229–9235. https://doi.org/10.1016/j.biortech.2011.07.035

[14] Malaika, A.; Kozłowsk, M. Glycerol conversion towards valuable fuel blending compounds with the assistance of SO_3H-functionalized carbon xerogels and spheres. *Fuel Proc. Technol*. **2019**, 184, 19–26. https://doi.org/10.1016/j.fuproc.2018.11.006

[15] Kulkarni, R. M.; Britto, P. J.; Narula, A.; Saqline, S.; Anand, D.; Bhagyalakshmi, C.; Herle, R. N. Kinetic studies on the synthesis of fuel additives from glycerol using CeO_2–ZrO_2 metal oxide catalyst. *Biofuel Res. J*. **2020**, 25, 1100-1108. DOI: 10.18331/BRJ2020.7.1.2

[16] Mufrodi, Z.; Amelia, S. Esterification of Glycerol with Acetic Acid in Bioadditive Triacetin with Fe_2O_3/Activated Carbon Catalyst. *Key Eng. Mater*. **2020**, 849, 125-129. https://doi.org/10.4028/www.scientific.net/KEM.849.125

[17] Abida, K.; Ali, A. Sulphuric acid-functionalized siliceous zirconia as an efficient and reusable catalyst for the synthesis of glycerol triacetate. *Chem. Papers* **2020**, 74, 3627–3639. https://doi.org/10.1007/s11696-020-01189-z

[18] Trejda, M.; Stawicka, K.; Dubinska, A.; Ziolek, M. Development of niobium containing acidic catalysts for glycerol esterification. *Catal. Today* **2012**, 187, 129–134. DOI:10.1016/J.CATTOD.2011.10.033

[19] Ladero, M.; Gracia, M. D.; Tamayo, J. J.; Ahumada, I. L. D.; Trujilo, F.; Garcia-Ochoa, F. Kinetic Modelling of The Esterification of Rosin and Glycerol: Application to Industrial Operation. *Chem. Eng. J*. **2011**, 169, 319. DOI: 10.1016/j.cej.2011.03.012

[20] Veluturla, S.; Narula, A.; Rao, D. S.; Shetty, S. P. Kinetic study of synthesis of bio-fuel additives from glycerol using a Hetropoly acid. *Resource-Efficient Technol*. **2017**, 3(3), 337-341. https://doi.org/10.1016/j.reffit.2017.02.005

[21] Zhoua, L.; Nguyenb, T. H.; Adesinab, A. A. The acetylation of glycerol over amberlyst-15: kinetic and product distribution. *Fuel Proces. Technol*. **2012**, 104, 310-318. https://doi.org/10.1016/j.fuproc.2012.06.001

[22] Kaur, A.; Ali, A. Lithium Zirconate as a Selective and Cost-Effective Mixed Metal Oxide Catalyst for Glycerol Carbonate Production. *Ind. Eng. Chem. Res*. **2020**, 59, 2667−2679. DOI: 10.1021/acs.iecr.9b05747

Development of acidic heterogeneous catalyst for diacetin synthesis from glycerol

Overview of the Chapter

This Chapter reports the preparation and application of $Ce/TiZrO_4@SO_4^{2-}$ as a heterogeneous acid catalyst for the acetylation of glycerol with acetic acid to prepare diacetin molecule as an exclusive product. The XRD and FTIR analysis of the catalyst support the impregnation of sulphate group over the $TiZrO_4$ matrix. The same was found to impart the acetylation activity to the catalyst due to the presence of Lewis as well as Brønsted acidic sites. Total acid sites of the catalyst were measured by the NH_3 temperature programmed desorption (TPD) study and found to be 8.15 mmol g^{-1}. The XPS study of the catalyst indicates the presence of Ce, Ti, and Zr metal ions in +4 oxidation state. The presence of Ce^{4+} was found to enhance the sulphate group impregnation over the matrix. The prepared catalyst, $Ce/TiZrO_4@SO_4^{2-}$, demonstrated almost 96 % diacetin selectivity in 60 min by employing acetic acid to glycerol molar ratio of 6:1 at 120 °C reaction temperature. The catalyst was recycled in five successive reaction cycles while retaining ~36 % activity during the last cycle.

6.1. Introduction

The GL valorization into value-added products can be regarded as valuable schemes in the fine chemical industry [1,2]. Among the various processes designed for GL conversion, acetylation of GL is considered as one of the most remarkable reactions [3]. All three main products of GL acetylation (MA, DA, and TA) have a host of applications in various industries. For example, DA and TA have been used as fuel additives to improve the fuel viscosity and could also be used in pharmaceutical, cosmetic and food industry [4,5]. Mixtures of MA, DA, and TA have also been used as solvents for printing ink and dye stuffs, as plasticizers and as softening agents [6]. Between two acetylating agents, AcA and AcAn, used for GL acetylation, AcA is considered as the most desired one because of its lower price in comparison to AcAn and ease of viability [7]. However, the use of AcA as an acetylating agent decreases the selectivity of reaction toward a specific product (MA or DA or TA) [8].

A variety of heterogeneous acid catalysts such as $SO_4^{2-}/CeO_2–ZrO_2$, $MoO_3/TiO_2–ZrO_2$, and PW-S were found to yield up to 70 % DA selectivity at 120 ^oC [8-10]. No reported work, so far, has claimed more than the 70 % DA selectivity in presence of heterogeneous catalysts. Even the commercially available DA (Sigma-Aldrich, CAS no 25395-31-7) was found to have a maximum of 50 % DA along with the MA, TA and GL as impurities.

To develop the reusable heterogeneous catalyst for the GL acetylation with AcA, sulphate group has been appended over Ce doped matrix ($Ce/TiZrO_4$) in the present study. Further, the reaction conditions have been optimized to achieve the maximum DA selectivity during the GL acetylation reaction. The catalyst stability and reusability have been analyzed, and the reason for the decline of the catalyst activity has also been investigated.

6.2. Experimental Section

6.2.1. Preparation of catalysts

The mixed oxide of zirconium and titanium ($Ti(OH)_4$-$Zr(OH)_4$) was prepared *via* co-precipitation method in a glass beaker equipped with a magnetic stirrer. In a representative synthesis, $TiCl_4$ (5.5 mL) and $ZrOCl_2.8H_2O$ (8.05 g) in 1:1 molar ratios were mixed in 100 ml deionized water and stirred vigorously for 5 min at 30 ^oC. The pH of this mixture was maintained at 10 by adding an appropriate amount of NH_3 solution (25 %, v/v), and the resulting mixture was further stirred for 4 h at the same temperature. The precipitate formed was filtered out, washed with deionized water until it became free from chloride ions and dried at 120 ^oC for 24 h, to obtain a colorless powder of $Ti(OH)_4$-$Zr(OH)_4$.

To anchor the SO_4^{2-} species group over the matrix, 1 g of $Ti(OH)_4$-$Zr(OH)_4$ was mixed in 20 mL deionized water along with x mL of 1 M H_2SO_4 and $Ce(NO)_3.6H_2O$ (0.067 g) and stirred for 24 h at room temperature. The resulting mixture was initially dried at 120 °C for 24 h and finally calcined at 600 ^oC for another 4 h to obtain $Ce/TiZrO_4@SO_4^{2-}$ catalyst.

6.2.2. Acetylation of glycerol with acetic acid

Glycerol acetylation was performed in a 50 mL two-neck round bottom flask equipped with an oil bath, a magnetic stirrer and a water cooled reflux condenser. To the flask, 10 g of GL, desired amount of AcA and catalyst were mixed and stirred at the desired temperature for a specific duration. After the completion of the reaction, the reaction mixture was initially centrifuged to remove the solid catalyst, and then rotary evaporated to separate the water and AcA from the products formed. HPLC of the isolated product was accomplished to quantify the DA formed.

6.3. Results and discussion

6.3.1. Catalyst Characterization

6.3.1.1. XRD analysis

To analyze the phase and crystal structure of the matrix and sulphated catalyst, they were subjected to powder XRD analysis. As could be seen from the **Fig. 6.1a**, a small peak at 2θ ~ 32° due to the formation of monoclinic $H_2Ti_3O_7$ (JCPDS card no. 00-049-0467) was observed in the XRD patterns of the matrix to maintain its poorly crystalline nature. However, impregnation of cerium (4 wt%) and sulphate over the same matrix, followed by calcination at 600 $^\circ$C, initiated the formation of new phases of orthorhombic $TiOSO_4$ (JCPDS card no. 00-049-0467), orthorhombic $Zr(SO_4)_2$ (JCPDS card no. 01-072-0608), orthorhombic $TiZrO_4$ (JCPDS card no. 00-034-0415), hexagonal TiO_2 (JCPDS card no. 00-033-138), rhombohedral Ce_7O_{12} (JCPDS card no. 01-089-8433), and tetragonal $Ce_{10}S_{14}O$ (JCPDS card no. 00-043-0339) as shown in **Fig. 6.1b**. The formation of zirconia and titanium sulphate evidently indicates the anchoring of the sulphate group on the matrix. Reddy *et al*. reported $SO_4^{2-}/CeO_2–ZrO_2$ catalyst also exhibited the formation of mixed phases of $CeOSO_4$ and $Zr(SO_4)_2$ [9]. The average crystallite size of the catalyst particles, based on XRD data, was found to be 15 nm.

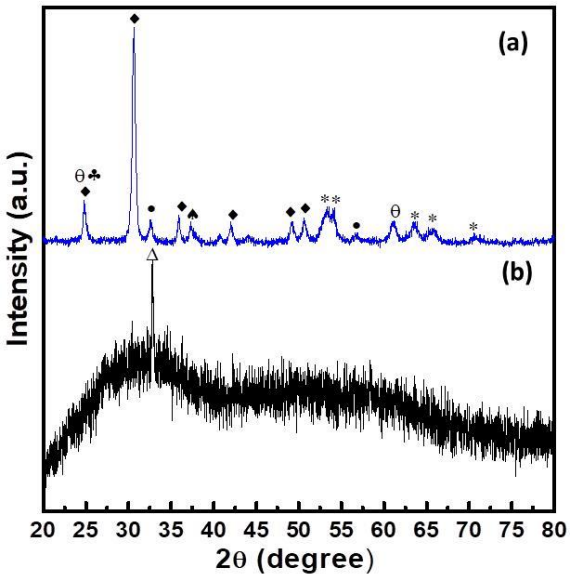

Fig. 6.1. X-ray diffraction patterns of (a) $Ti(OH)_4$-$Zr(OH)_4$, (b) $Ce/TiZrO_4@SO_4^{2-}$. [$H_2Ti_3O_7$ = Δ, $TiOSO_4$ = θ, $TiZrO_4$ = *, $Zr(SO_4)_2$ = ♦, TiO_2 = ♠, $Ce_{10}S_{14}O$ = ♣, CeO_2 = ●]

6.3.1.2. FE-SEM-EDX and HR-TEM analysis

The catalyst morphology was analyzed by FE-SEM imaging as demonstrated in **Fig. 6.2**. The FE-SEM image (**Fig. 6.2a**) shows the formation of agglomerates of ~ 5 µm sized particles of $Ce/TiZrO_4@SO_4^{2-}$ in irregular geometries. The EDX analysis of $Ce/TiZrO_4@SO_4^{2-}$ indicates the presence of Ti/Zr in a ratio of 1.78, along with 5.53 % sulphur and 1.46 % cerium (Table 6.1) to support sulphate and cerium impregnation over the matrix.

Table 6.1. Comparison of EDX analysis of $Ti(OH)_4$-$Zr(OH)_4$ and $Ce/TiZrO_4@SO_4^{2-}$.

Catalyst	O (wt%)	Ti (wt%)	Zr (wt%)	S (wt%)	Ce (wt%)
$Ti(OH)_4$-$Zr(OH)_4$	79.09	13.39	7.52	-	-
$Ce/TiZrO_4@SO_4^{2-}$	74.28	11.45	7.27	5.53	1.46

The TEM image of the catalyst (**Fig. 6.2b**) also indicates the formation of agglomerates consisting of spherical or oval shape particles of about 16 nm size. The particle size calculated from TEM imaging is almost similar to the crystallite size (15 nm) calculated from XRD data. The SAED pattern demonstrates the well-resolved lattice fringes (**Fig. 6.2c**), which allows an accurate measurement of crystallographic spacing and identification of the observed crystalline phase. The measured lattice fringe spacing of 0.19, 0.23, and 0.26 nm matches with the (**Fig. 6.2d**) 800, 120, and 002 planes corresponding to $Ce_{10}S_{14}O$, $TiZrO_2$, and TiO_2 phase, respectively.

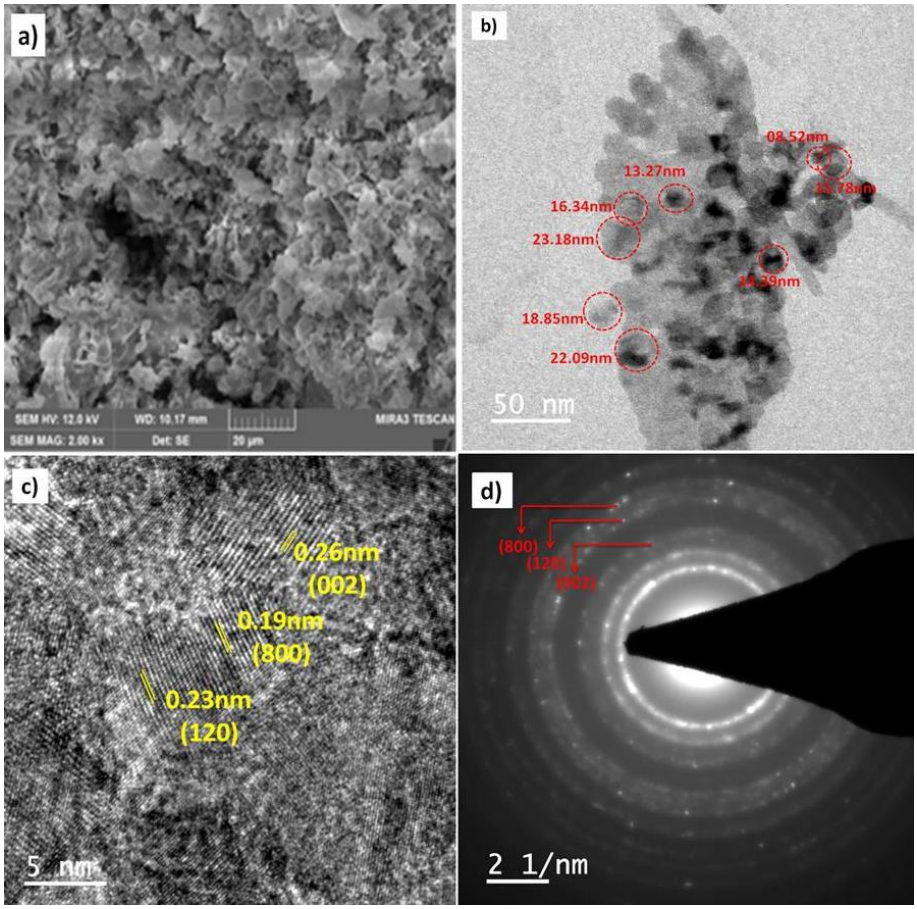

Fig. 6.2. Image of $Ce/TiZrO_4@SO_4^{2-}$ (a) FF-SEM, (b) TEM image (c) lattice fringes and (d) SAED pattern.

6.3.1.3. BET analysis

The nitrogen adsorption-desorption isotherms of the matrix $Ti(OH)_4$-$Zr(OH)_4$ and catalyst $Ce/TiZrO_4@SO_4^{2-}$ are presented in **Fig. 6.3a**. The bare matrix and supported catalyst showed H1 and H2 types of hysteresis loops, respectively, with type-IV adsorption-desorption isotherm according to the IUPAC nomenclature. The bare support showed the hysteresis loop at p/p0 = 0.7-1.0, to indicate the relatively large pore size of 16 nm as measured by the N_2 adsorption-desorption isotherm (**Fig. 6.3a**). Upon cerium and sulphate impregnation, the hysteresis loop shifts to relatively low pressure of p/p0 = 0.5-0.9, with a pore size of 11 nm. The broader shape of the catalyst hysteresis loops supports the impregnation of the catalytically active species in the pores of the matrix, which allow the slow escape of the adsorbed nitrogen molecules. H2 hysteresis loop endorses the formation of ink bottle-shaped (narrow necks and wider bodies) particles due to the accumulation of the impregnated particles within the matrix pores [11].

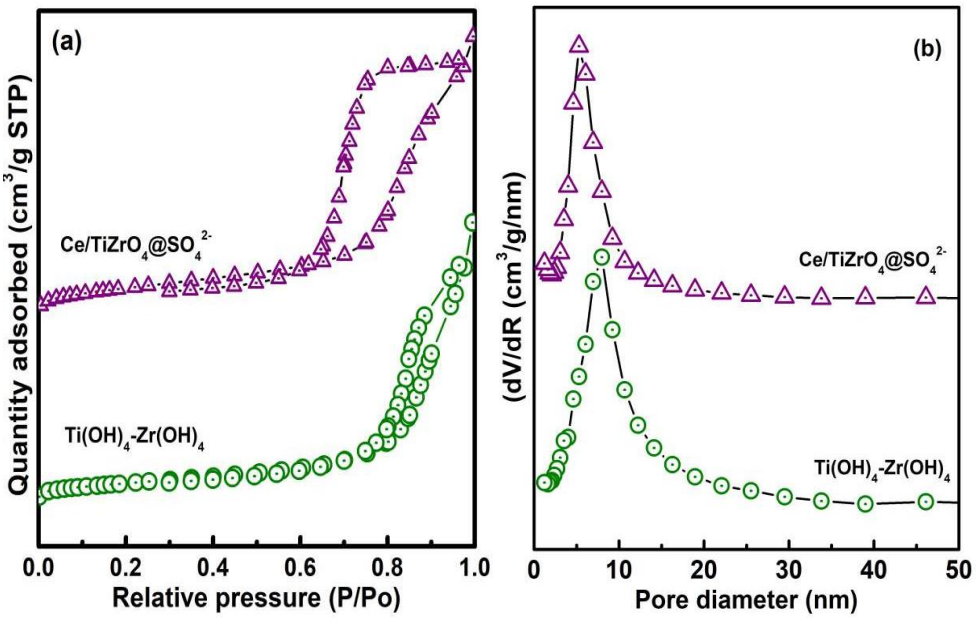

Fig. 6.3. (a) N_2 adsorption-desorption isotherms and (b) Pore size distribution of $Ti(OH)_4$-$Zr(OH)_4$ and $Ce/TiZrO_4@SO_4^{2-}$.

The quantity of adsorbed nitrogen gas also increases upon sulphate and cerium impregnation over the matrix. This may be due to the increase in surface area of the catalyst (82 m^2g^{-1}) with respect to the matrix (53 m^2g^{-1}). The rise in surface area may be due to the pore opening upon sulphate group and cerium anchoring inside the pores of the matrix. The total pore volume and pore diameter of the matrix were found to decrease due to the attachment of the catalytically active species inside the matrix pores (**Table 6.2**).

Table 6.2. Comparison of the BET specific surface area, pore volume, pore size, and total acidity of $Ti(OH)_4$-$Zr(OH)_4$ and $Ce/TiZrO_4@SO_4^{2-}$.

Catalyst	BET surface area (m^2g^{-1})	Pore volume (cm^3/g^{-1})	Pore size (nm)	Total acidity (mmol g^{-1})
$Ti(OH)_4$-$Zr(OH)_4$	53	0.26	16	0.36
$Ce/TiZrO_4@SO_4^{2-}$	82	0.23	11	8.15

6.3.1.4. NH_3-Temperature Programmed Desorption study

The strength of acidic sites over the catalyst surface and total acidity was calculated with the help of ammonia TPD analysis. The TPD profiles of the matrix ($Ti(OH)_4$-$Zr(OH)_4$), sulphated matrix without cerium ($TiZrO_4@SO_4^{2-}$) and with cerium ($Ce/TiZrO_4@SO_4^{2-}$) are compared in **Fig. 6.4a-c**. All samples showed a broad desorption peak at 229 ^oC owing to the desorption of physisorbed gases from the surface. Another desorption peak observed at 451 ^oC, is

indicating the presence of strong acidic sites. However, the maximum acidity (8.15 mmol g^{-1}) was observed when Ce and SO_4^{2-} were present together in the catalyst to support the synergy between the two species. Chene *et al*. reported that in the case of sulphated silica-zirconia, two desorption peaks during NH_3-TPD study, at 257 and 458 ^oC were observed to support the presence of weak and strong acidic sites, respectively [12]. The presence of moderate or strong acidic sites were found to be essential to carry out the GL acetylation.

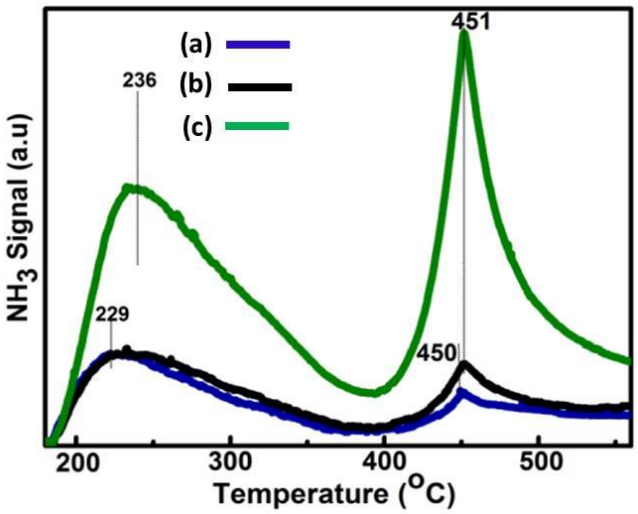

Fig. 6.4. NH_3-TPD profiles for (a) $Ti(OH)_4$-$Zr(OH)_4$, (b) $TiZrO_4@SO_4^{2-}$ and (c) $Ce/TiZrO_4@SO_4^{2-}$.

6.3.1.5. Pyridine adsorption DRIFT study

To establish the nature of acidic sites present over the catalyst, diffuse reflectance infrared fourier transform (DRIFT) spectra of pyridine saturated sample was studied. In the DRIFT spectra of pyridine saturated $Ti(OH)_4$-$Zr(OH)_4$, no peak in the region of 1400 to 1700 cm^{-1}, (**Fig. 6.5a**) was observed to rule out the presence of Brønsted acidic site over the matrix. Impregnation of the sulphate group over the matrix was found to generate Brønsted acidic sites (H^+), which upon interaction with pyridine generate the pyridinium ion. In the DRIFT spectra of $Ce/TiZrO_4@SO_4^{2-}$ weak bands at ~1638 and 1540 cm^{-1} (**fig 6.5d**) were observed to support the formation of pyridinium ion. Thus sulphate group anchoring has generated the Brønsted sites over the catalyst, which facilities the release of H^+ from the –OH of sulphate group [13]. The band corresponding to the covalently bonded pyridine with Lewis acidic cites was observed at ~1611 cm^{-1}. The presence of the Lewis acid sites in the catalyst could be ascribed to the presence of the vacant d-orbital of the matrix metal ions. The peak observed at ~1487 cm^{-1} was due to the presence of Brønsted as well as Lewis acidic sites in the catalyst

[14]. Co-immobilization of sulphate and cerium further strengthen the acidic sites as supported by the increase in band intensity corresponding to the Lewis and Brønsted sites (**Fig. 6.5c-d**). Thus, the presence of cerium was found to incorporate more number of sulphate groups over the matrix. Maximum acidic sites were found in the catalyst prepared by incorporating sulphate group in presence of 4 wt% cerium followed by calcination at 600 ^{o}C. The thermal stability of the present catalyst was also found to be higher than the reported SO_4^{2-}/TiO_2 catalyst, which decomposed at 600 ^{o}C [14]. A further increase in calcination temperature (700 ^{o}C) was found to reduce the acidic strength (**Fig. 6.5e**) of the catalyst due to the decomposition of sulphate group, as supported by the DRIFT spectra of the heat treated catalyst.

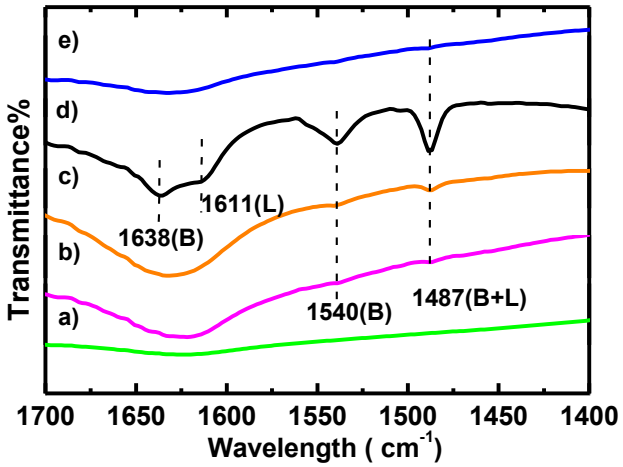

Fig. 6.5. FTIR spectra of pyridine adsorption of (a) $Ti(OH)_4$ -$Zr(OH)_4$, (b) $TiZrO_4@SO_4^{2-}$-600 (c) 2-$Ce/TiZrO_4@SO_4^{2-}$-600 (d) 4-$Ce/TiZrO_4@SO_4^{2-}$-600, (e) 4-$Ce/TiZrO_4@SO_4^{2-}$-700 °C.

6.3.1.6. XPS analysis

The X-ray photoelectron spectroscopy (XPS) technique was used to establish the electronic state of the metal ions present in the catalyst as shown in **Fig. 6.6**. The full scan XPS spectrum of the $Ce/TiZrO_4@SO_4^{2-}$ confirmed the presence of S, Zr, Ti, O, and Ce, elements over the catalyst surface as shown in **Fig. 6.6a**. The band observed at 165.6, 168.7 and 171.2 eV could be attributed to the S^{6+} $2p_{3/2}$ level, of sulphate group as shown in **Fig. 6.6b**. Observed values are very close to the reported values of 167.4 eV and 170.0 eV for S^{6+} 2p in case of SO_4^{2-}/TiO_2-ZrO_2 and SO_4^{2-}/TiO_2, respectively [15]. The presence of three peaks may be ascribed to the linkage of sulphate group with three different metal ions present in the matrix. The binding energies corresponding the Zr^{4+} $3d_{5/2}$ state was observed at 184.4 and 182.2 eV, while of that Zr^{4+} $3d_{3/2}$ were observed at 187.1, 184.9 eV (**Fig. 6.6c**) [16-17]. In case of

native ZrO_2 the binding energy of the Zr^{4+} $3d_{5/2}$ state has been reported at 182.5 eV [18]. An increase in the photoelectron peaks energy as well splitting of the peaks may be due to the formation of $TiZrO_4$ compound upon which sulphate groups were anchored during the catalyst preparation as supported by the XRD analysis of the sample. **Fig. 6.6d** depicts the binding energies of Ti^{4+} $2p_{1/2}$ state at 467.1 and 464.6 eV, and Ti^{4+} $2p_{3/2}$ state at 461.3 and 458.8 eV, which is higher than the Ti $2p_{3/2}$ line observed at 458.5 eV, for the native TiO_2 [19]. The deviation in Ti binding energy again supports the formation of $TiSO_4$ which is also observed by the XRD study. The fitting of the O^{2-} 1s region with three peaks (**Fig. 6.6e**) indicates the existence of three different types of O^{2-} *viz.*, at 530.4 eV due to the presence of lattice oxygen (Ti—O or Zr—O or Ce—O), at 532.7 due to sulphate oxygen and at 534.7 eV due to the chemically adsorbed oxygen (M—OH) over the catalyst surfaces of catalyst. The observed Ce 3d XPS spectrum (**Fig. 6.6f**) of the catalyst shows characteristic six peaks due to Ce^{4+} state. The higher binding energies observed at 897.5, 902.8, 907.4 eV could be ascribed to the Ce^{4+} $3d_{3/2}$ state while the lower binding energy peaks observed at 879.6, 884.6, 886.6 eV, could be assigned to Ce^{4+} $3d_{5/2}$ state. These values were found to be higher side in comparison to the values observed for native ceria due to the formation of cerium sulphate phase [17, 20].

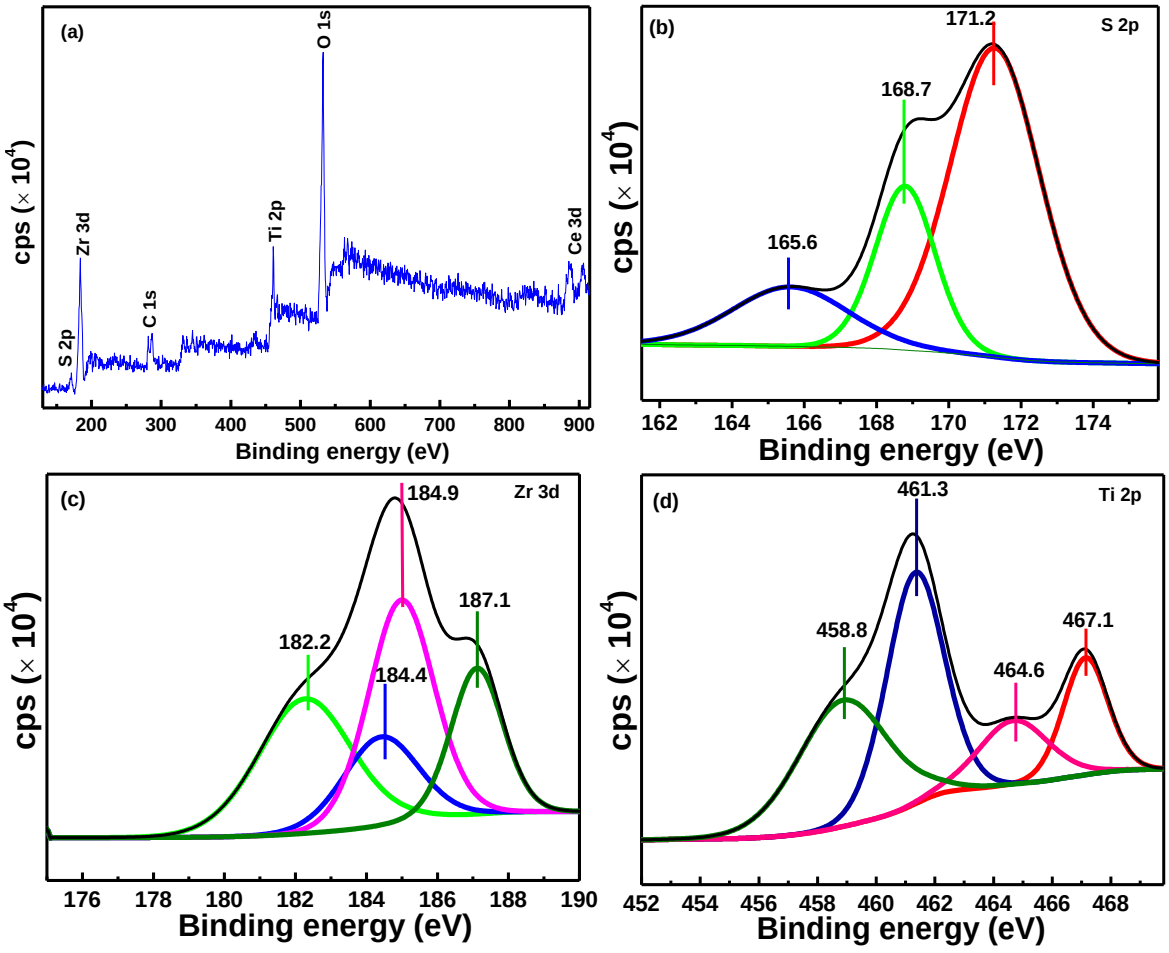

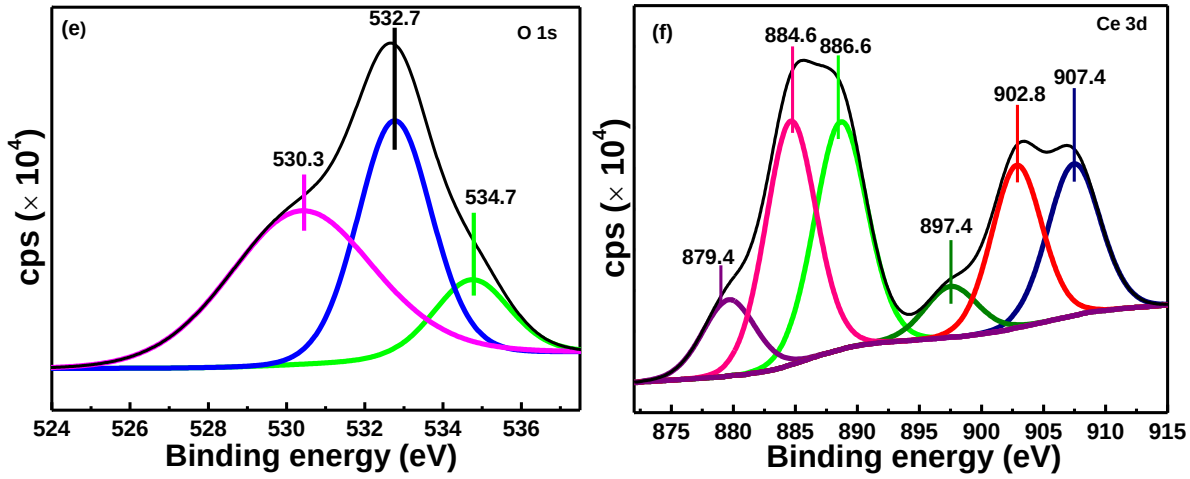

Fig. 6.6. XPS spectra of Ce/$TiZrO_4$@SO_4^{2-} catalyst (a) full scan (b) S 2p, (c) Zr 3d, (d) Ti 2p, (e) O 1s and (f) Ce 3d.

6.3.2. Product analysis

6.3.2.1. HPLC analysis

In HPLC chromatogram peak observed at 9.907 minutes was assigned to the GL (**Fig. 6.7a**). Upon GL acetylation, the product shows new peaks, at 6.394 and 6.674 min, corresponding to TA and DA, respectively as shown in **Fig. 6.7b**. The GL peak in the product mixture was not observed to confirm its complete conversion into acetins.

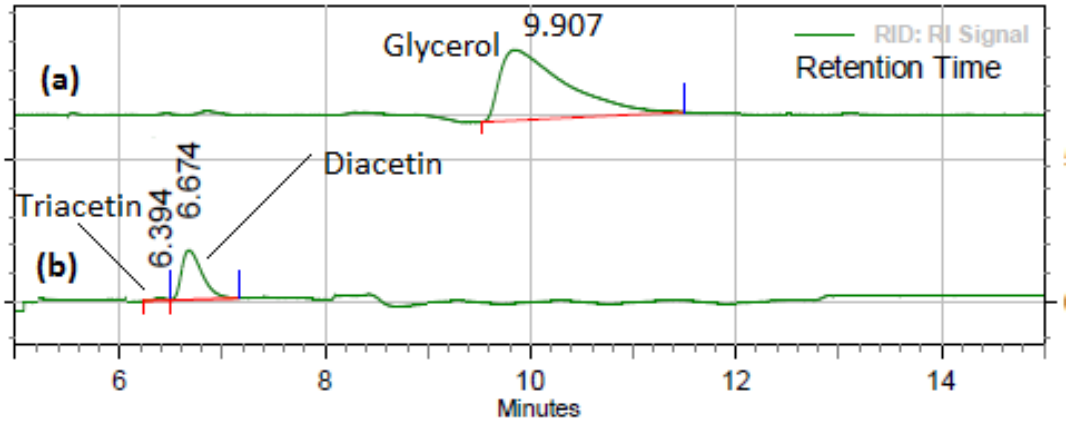

Fig. 6.7. HPLC chromatogram of (a) glycerol and (b) products formed during acetylation.

6.3.3. Catalyst Screening

In literature, sulphate species anchored over ZrO_2 or CeO_2 or Al_2O_3 or mixed metal oxides have been studied extensively for acetins synthesis [9]. However, in most of the cases either partial conversion levels of GL to DA were achieved or a mixture of product was obtained. In the present study $TiZrO_4$ matrix was employed to anchor the sulphate ions in presence of

Ce^{4+} ions. To demonstrate the necessity of each component present in the catalyst, various controls experiments have been performed as shown in **Fig. 6.8**. The matrix ($Ti(OH)_4$ - $Zr(OH)_4$) demonstrated relatively less activity in comparison to the sulphated matrix ($TiZrO_4@SO_4^{2-}$) while the cerium impregnated sulphated catalyst ($Ce\text{-}TiZrO_4@SO_4^{2-}$) shows the highest activity. In absence of Ce^{4+} ions, as shown in **Fig 6.8**, the activity was found to be minimal to underline the role of cerium ions in the catalyst activity. Moreover, the TOF calculation, supports that the $Ce/TiZrO_4@SO_4^{2-}$ catalyst showed a maximum TOF (320 h^{-1}) as compared to the $Ti(OH)\text{-}Zr(OH)_4$ (18 h^{-1}), and $TiZrO_4@SO_4^{2-}$ (22 h^{-1}) catalyst as shown in **Fig. 6.8**.

As discussed by Li *et al*. sulphate impregnation over $TiZrO_4$ matrix in presence of La^{3+} ions was found to impart more Lewis acid sites as well better interaction between the support material and sulphate ions [21]. Both the effects were found to enhance the acetylation activity as well as stability of the catalyst. In the present study, to further extend the analogy, sulphate ions were impregnated over the $TiZrO_4$ matrix in presence of Ce^{4+} and resulted catalyst was employed for the acetylation of GL with AcA to obtain the maximum DA yield. The yield and selectivity during GL acetylation not only depends on the nature of the catalyst but also on the reaction parameters. The influence of different reaction parameters, over DA yield, such as catalyst amount, AcA/GL molar ratio, reaction temperature and reaction time were studied.

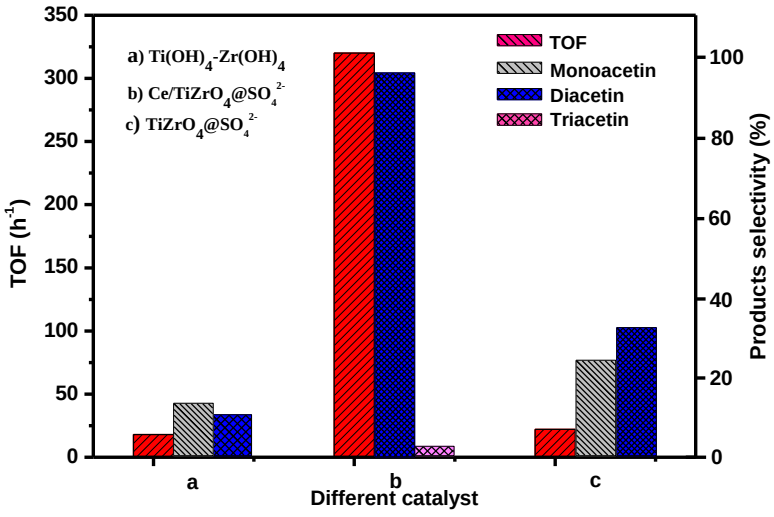

Fig. 6.8. Effect of the various catalysts over the acetylation of glycerol. [*Reaction conditions:* AcA/GLmolar ratio = 6:1, reaction time = 40 min, catalyst amount = 5 wt% (with respect to GL), and reaction temperature = 120 ^oC]

6.3.3.1. Effect of catalyst amount on product selectivity

Fig. 6.9a shows the effect of catalyst amount ($Ce/TiZrO_4@SO_4^{2-}$) on the acetylation of GL during the DA formation. The reaction was performed at 120 ^oC, employing AcA/GL molar ratio of 6:1 for a reaction duration of 60 min while catalyst amount was varied in the range of 3-7 wt% (with respect to GL). A maximum yield (96 %) of DA was obtained when 5 wt% of catalyst was employed. A further increase in the catalyst amount was not found to increase the reaction rate or product yield to the significant extent. This could be due to the fact that at a higher catalyst amount reaction mixture becomes more viscous which could repel the mass transfer in a liquid-liquid-solid system [22].

6.3.3.2. Effect of AcA/GL molar ratio on product selectivity

The effect of AcA/GL molar ratio is one of the vital factor which would influence the DA yield as well as economics of the reaction. To optimize the AcA/GL molar ratio, the reactions were carried out with 5 wt% catalyst amount at 120 ^oC for 60 min by altering the AcA/GL molar ratios from 2:1 to 6:1 as shown in **Fig. 6.9b**. The diacetin selectivity was found to increase with the amount of AcA, and reached to a maximum level of 96 % when AcA/GL molar ratio of 6:1 or higher was employed.

It literature, $SO_4^{2-}/CeO_2–ZrO_2$ catalyst was found to demonstrate the MA, DA, and TA yield of 57 % , 38 %, and 5 %, respectively, while AcA/GL molar ratio being 3:1. On increasing the molar ratio upto 6, the selectivity towards diacetin was found to increase (from 38 % to 58 %) at 120 ^oC in 1 h of reaction duration [9].

6.3.3.3. Effect of reaction temperature on product selectivity

The reaction temperature was found to affect the course of the reaction in terms of product yield and reaction duration. In order to optimize the reaction temperature, the acetylation of AcA/GL (6:1 molar ratio) was carried out in presence of 5 wt% catalyst amount and by varying the temperature 60 to 120 ^oC as shown in **Fig. 6.9c**. The DA yield was found to increase by increasing the reaction temperature (60 to 120 ^oC) and a maximum yield of 96 % was achieved at 120 ^oC. GL acetylation in literature has been reported to follow the endothermic pathway and hence, an external source of heat is essential to push the reaction in a forward direction [23]. A further rise in reaction temperature was not attempted as the boiling point of the acetic acid is 118 ^oC.

6.3.3.4. Effect of reaction time on product selectivity

To optimize the reaction duration, GL acetylation was performed with AcA/GL molar ratio of 6:1, in presence of 5 wt% catalyst, at 120 ^{o}C and varying the reaction duration from 15 to 60 min as shown in **Fig. 6.9d**. The DA yield was found to increase significantly with the increase in reaction time and attain a constant value of 96 % after 60 min of reaction duration. A further increase in reaction duration was not found to affect the product yield to a significant extent.

Studies have specified that monoacetin yield is higher during the initial phase of the acetylation reaction [24]. As the reaction duration increases, the yield of MA decreases whereas the, yield of DA and TA increases. Lingaiah *et al*. also studied the extent of GL acetylation at various time intervals employing tungstophosphoric acid as a catalyst at 120 ^{o}C utilizing 5:1 AcA/GL molar ratio. They observed 58 %, 40 % and 3 % selectivity of MA, DA, and TA, respectively, within 30 min of reaction duration [23]. However, diacetin selectivity of 58 % remains constant even after 2 h of reaction duration. Thus our study as well as literature report supported the stepwise GL acetylation and increase in DA and TA yield on increasing the reaction duration.

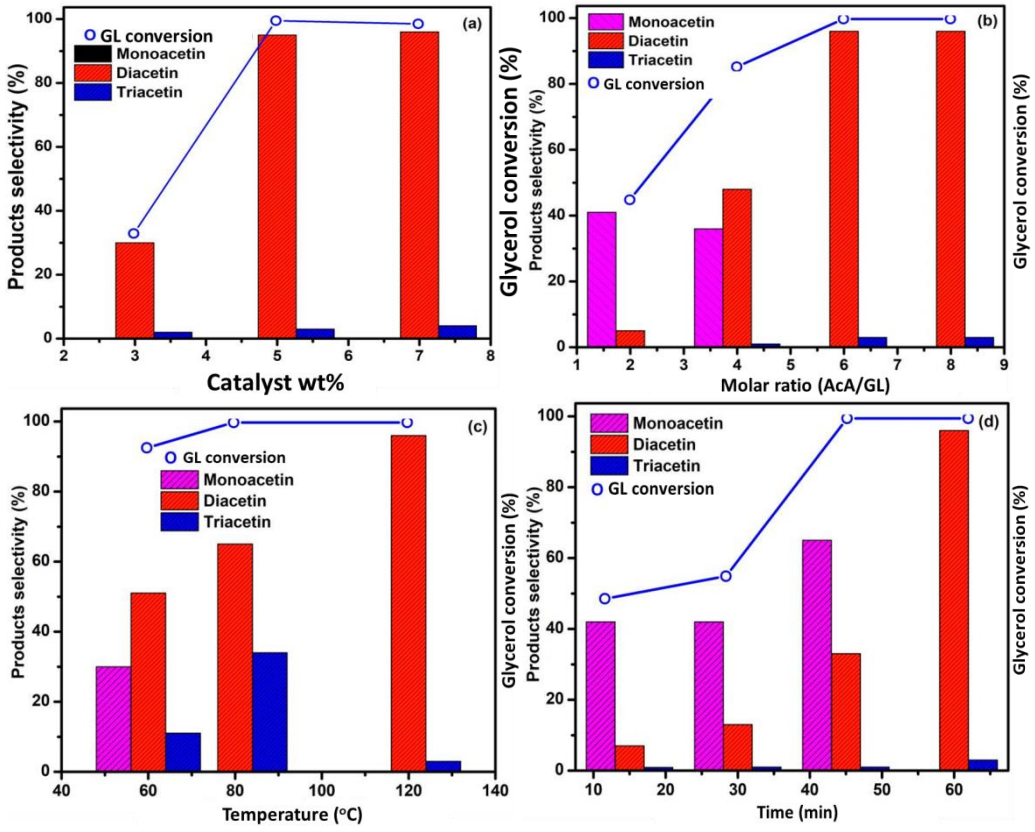

Fig. 6.9. Influence of various reaction parameters on Ce/TiZrO$_4$@SO_4^{2-} assisted glycerol acetylation (a) catalyst amount, (b) AcA/GL molar ratio, (c) reaction temperature and (d) reaction duration.

6.3.4. The reusability and stability

To test the reusability of Ce/$TiZrO_4$@SO_4^{2-}catalyst, acetylation of GL was carried out with AcA under optimized reaction parameters. After the completion of the reaction, the catalyst was recovered from the reaction mixture by centrifugation, which was washed with methanol, dried at 120 °C and finally calcined at 600 °C for 4 h. The catalyst hence regenerated was engaged during 5 successive catalytic runs under similar experimental and regeneration conditions. As shown in **Fig. 6.10**, the reused catalyst was found to capitulate > 90 % DA selectivity during 2nd and 3rd catalytic cycles while in 4th and 5th runs the diacetin selectivity was found to decreases up to 36 %. Thus a major loss in the catalyst activity was experienced which could be either due to the active sites hindrance because of the substrate adsorption, or due to the partial leaching of catalytically active species.

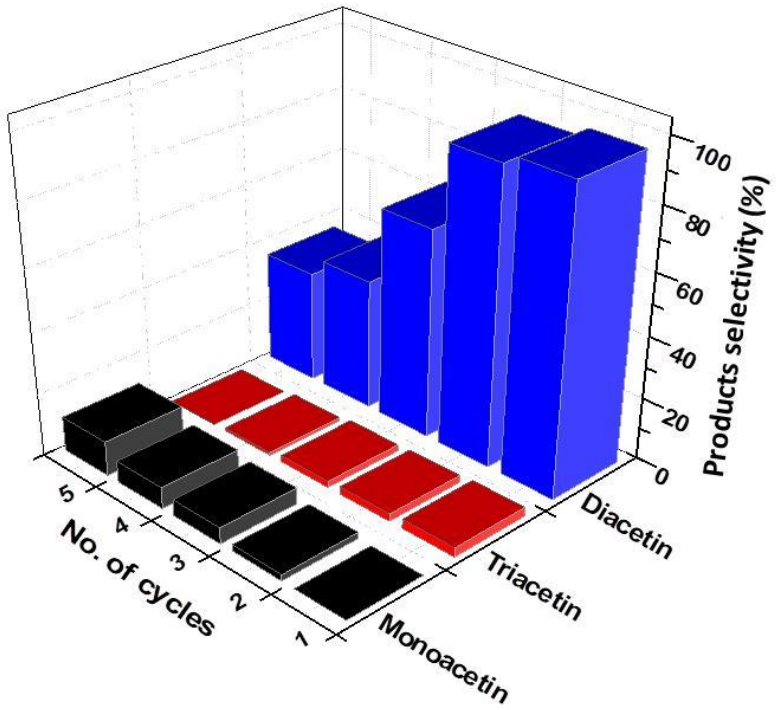

Fig. 6.10. Study of the Ce/$TiZrO_4$@SO_4^{2-} reusability during the glycerol acetylation with acetic acid.

To establish the reason(s) for the loss in catalyst efficacy, XRD patterns of the fresh and reused catalysts were compared. As revealed in **Fig. 6.11a**, additional peaks at 22° and 54.8° were observed in the diffraction pattern of the recycled catalyst due to the creation of hexagonal phase of TiO_2 (JCPDS card no. 00-84-1286). Other peaks at 33°, 40.7° and 71.8° were also observed due to the formation of an orthorhombic phase of $TiZrO_4$ (JCPDS card

no. 00-034-0415). Therefore, the XRD study supports the structural changes in the reused catalyst which might have caused the loss of catalyst activity.

An evaluation of the FTIR spectra (**Fig. 6.11b**) of fresh and recycled catalysts revealed that SO_4^{2-} moiety has partially detached from the catalyst. The comparison of EDX data of fresh and reused catalysts also indicates the decrease in sulphur content in the reused catalyst (2.73 wt%) against the fresh catalyst (5.54 wt%). No vibration band related to the DA or GL was found in the FTIR spectrum of recycled catalyst to maintain that organic molecules have not collected over the catalyst surface to obstruct the active sites.

A comparison of NH_3-TPD profiles of fresh and reused catalysts are shown in **Fig. 6.11c**. The fresh catalyst exhibited the strong acid sites at 450 ^oC, with a total acidity value of 8.15 mmol g^{-1} and the same was found to reduce to 3.46 mmol g^{-1} in the case of spent catalyst. The decrease in acidic sites is a consequence of the loss of sulphate species from the catalyst which resulted in the loss of catalytic activity.

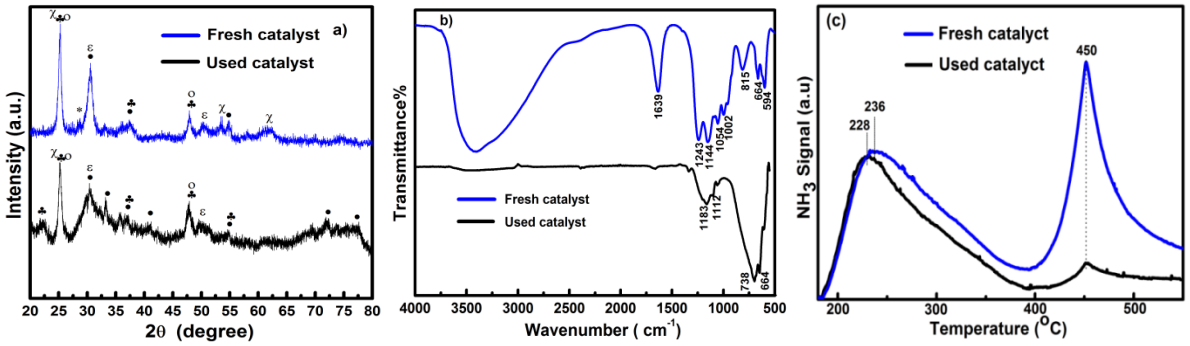

Fig. 6.11. Comparison of (a) XRD, (b) FTIR and (c) NH_3-TPD of fresh and reused catalyst.(♣- TiO_2, ●- $TiZrO_4$, ε- $Zr(SO_4)_2$, χ- $TiOSO_4$, *- Ce_7O_{12}, o- $Ce_{10}S_{14}O$ and ♦- ZrO_2)

The previous study supported the loss of sulphate ions which may remain present in the reaction blend and could catalyze the reaction analogous to a homogeneous catalyst. To measure the homogeneous contribution, the GL acetylation was performed under optimized reaction conditions. After 30 min, the catalyst was removed by filtration and the reaction was allowed to continue for an additional 30 min to evaluate the activity of the soluble species. As evident from **Fig. 6.12**, when the reaction was carried out without catalyst the MA and DA selectivity has increased to 13 and 19 %, respectively. Thus, a fractional homogeneous contribution in the catalyst activity was observed in this case, however, heterogeneous catalyst is primarily responsible for the maximum catalytic activity.

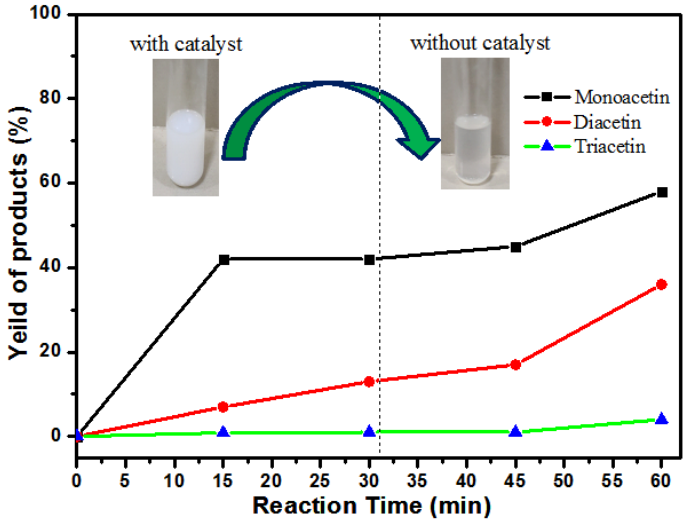

Fig. 6.12. Study of homogeneous contribution during the acetylation of glycerol with acetic acid.

6.4. Conclusions

The acetylation of glycerol with acetic acid was performed over $Ce/TiZrO_4@SO_4^{2-}$ heterogeneous acid catalyst. The reaction parameters (AcA/GL molar ratio, catalyst amount, reaction duration and reaction temperature) have been optimized to obtain the highest selectivity towards diacetin. Under the optimized reaction conditions, the catalyst was found to give a maximum diacetin selectivity of 96 %. The catalyst was reused during five catalytic cycles, however, the efficacy of the catalyst was found to reduce during the successive runs. The loss of sulphate species from the matrix, during the reusability experiments, was found to be the main reason behind the gradual loss of catalyst activity.

References

[1] Wang, S.; Wang, J.; Sun, P.; Xu, L.; Okoye, P. U.; Li, S.; Zhang, L.; Guo, A.; Zhang, J. A. Disposable baby diapers waste derived catalyst for synthesizing glycerol carbonate by the transesterification of glycerol with dimethyl carbonate. *J. Clean. Prod*. **2019**, 211, 330-341.DOI: 10.1016/j.jclepro.2018.11.196

[2] Lee, C. S.; Aroua, M. K.; Daud, W. M. A. W.; Cognet, P.; Pérès-Lucchese, Y.; Fabre, P. L.; Reynes, O.; Latapie, L. A review: Conversion of bio glycerol into 1,3-propanediol via biological and chemical method. *Renew. Sustain. Energy Rev*. **2015**, 42, 963–972. https://doi.org/10.1016/j.rser.2014.10.033

[3] Pagliaro, M.; Ciriminna, R.; Kimura, H.; Rossi, M.; Della Pina, C. From Glycerol to Value-Added Products Angewandte Chemie International Edition. **2007**, 46, 4434–4440. https://doi.org/10.1002/anie.200604694

[4] Liu, J.; Wang, Z.; Sun, Y.; Jian, R.; Jian, P.; Wang, D. Selective synthesis of triacetin from glycerol catalyzed by HZSM-5/MCM-41 micro/mesoporous molecular sieve. *Chin. J. Chem. Eng*. **2019**, 27, 1073–1078. https://doi.org/10.1016/j.cjche.2018.09.013

[5] Nebel, B.; Mittelbach, M.; Uray, G. Determination of the Composition of Acetyl glycerol Mixtures by ^{1}H NMR Followed by GC Investigation. *Anal. Chem*. **2008**, 80, 8712–8716. https://doi.org/10.1021/ac800706s

[6] Dizoğlu, G.; Sert, E. Fuel additive synthesis by acetylation of glycerol using activated carbon/UiO-66 composite materials. *Fuel* **2020**, 281, 118584. DOI:10.1016/J.fuel.2020.118584

[7] Liao, X.; Zhu, Y.; Wanga, S. G.; Chen, H.; Li, Y. Theoretical elucidation of acetylating glycerol with acetic acid and acetic anhydride. *Appl. Catal. B: Environ*. **2010**, 94, 64–70. DOI: 10.1016/j.apcatb.2009.10.021

[8] Ferreira, P.; Fonseca, I. M.; Ramos, A. M.; Vital, J.; Castanheiro, J. E. Glycerol acetylation over dodecatungstophosphoric acid immobilized into a silica matrix as catalyst. *Appl. Catal. B: Environ*. **2009**, 91, 416-422. https://doi.org/10.1016/j.apcatb.2009.06.009

[9] Reddy, P. S.; Sudarsanam, P; Raju, G.; Reddy, B. M.; Selective acetylation of glycerol over CeO_2–M and SO_4^{2-}/CeO_2–M (M = ZrO_2 and Al_2O_3) catalysts for synthesis of bioadditives. *J. Ind. Eng. Chem*. **2012**, 18, 648–654. https://doi.org/10.1016/j.jiec.2011.11.063

[10] Reddy, P. S.; Sudarsanam, P; Raju, G.; Reddy, B. M. Synthesis of bio-additives: Acetylation of glycerol over zirconia-based solid acid catalysts. *Catal. Commun*. **2020**, 11, 1224–1228. https://doi.org/10.1016/j.catcom.2010.07.006

[11] Nayak, N. B.; Nayak, B. B. Temperature-mediated phase transformation, pore geometry and pore hysteresis transformation of borohydride derived in-born porous zirconium hydroxide nanopowders. *Sci. Reports* **2016**, 6, 26404. https://doi.org/10.1038/srep26404

[12] Chen, X.; Ju, Y.; Mou, C. synthesis of Mesoporous Sulfated Silica-Zirconia Catalysts with High Catalytic Activity for Biodiesel via Esterification. *J. Phys. Chem. A*. **2007**, 111, 18731-18737. https://doi.org/10.1021/jp0749221

[13] Yang, Q.; Xie, C.; Xu, Z.; Gao, Z.; Du, Y. Synthesis of Highly Active Sulfate-Promoted Rutile Titania Nanoparticles with a Response to Visible Light. *J. Phys. Chem. B* **2005**, 109, 5554-5560. https://doi.org/10.1021/jp045676l

[14] Parvulescua, V.; Comanb, S.; Grangel, P.; Parvulescu, V. I. Preparation and characterization of sulfated zirconia catalysts obtained via various procedures. *Appl. Catal. A: Gen*. **1999**, 176, 27-43. https://doi.org/10.1016/S0926-860X(98)00219-1

[15] Reddya, B. M.; Sreekanth, P. M.; Yamadab, Y.; Xub, Q.; Kobayashi, T. Surface characterization of sulfate, molybdate, and tungstate promoted TiO_2-ZrO_2 solid acid catalysts by XPS and other techniques. *Appl. Catal. A: Gen*. **2002**, 228, 269–278. https://doi.org/10.1016/S0926-860X(01)00982-6

[16] Ardizzone, S.; Bianchi, C. L.; Signoretto, M. Zr(IV) surface chemical state and acid features of sulphated-zirconia sample. *Appl. Surf. Sci*. **1998**, 136, 213–220. https://doi.org/10.1016/S0169-4332(98)00335-3

[17] Reddya, B. M.; Chowdhury, B.; Smirniotis, P. G. An XPS study of the dispersion of MoO_3 on TiO_2–ZrO_2, TiO_2–SiO_2, TiO_2–Al_2O_3, SiO_2–ZrO_2, and SiO_2–TiO_2–ZrO_2 mixed oxides. *Appl. Catal. A: Gen*. **2001**, 211, 19–30. DOI: 10.1016/S0926-860X(00)00834-6

[18] Reddy, B. M.; Reddy, G. K.; Ganesh, I.; Ferreira, J. M. Single step synthesis of nanosized CeO_2–MxOy mixed oxides (MxOy = SiO_2, TiO_2, ZrO_2, and Al_2O_3) by microwave induced solution combustion synthesis: characterization and CO oxidation. *J. Mater. Sci*. **2009**, 44, 2743–2751. https://doi.org/10.1007/s10853-009-3358-2

[19] Ovari, L.; Kiss, J. Growth of Rh nanoclusters on TiO_2 (110): XPS and LEIS studies. *Appl. Surf. Sci*. **2006**, 252, 8624–8629. https://doi.org/10.1016/j.apsusc.2005.11.081

[20] Beche, E.; Charvin, P.; Perarnau, D.; Abanades, S.; Flamant, G. Ce $_3$d XPS investigation of cerium oxides and mixed cerium oxide (CexTiyOz). *Surf. Inter. Analysis* **2008**, 40, 264–267. https://doi.org/10.1002/sia.2686

[21] Li, Y.; Zhang, X.; Sun, L.; Zhang, J.; Xu, H. Fatty acid methyl ester synthesis catalyzed by solid superacid catalyst SO_4^{2-}/ZrO_2–TiO_2/La^{3+}. *Appl. Energy* **2010**, 87, 156–159. https://doi.org/10.1016/j.apenergy.2009.06.030

[22] Balaraju, M.; Nikhitha, P.; Jagadeeswaraiah, K.; Srilatha, K.; Sai Prasad, P. S.; Lingaiah, N. Acetylation of glycerol to synthesize bioadditives over niobic acid supported tungstophosphoric acid catalysts. *Fuel Proces. Technol*. **2010**, 91, 249–253. https://doi.org/10.1016/j.fuproc.2009.10.005

[23] Unlu, D.; Hilmioglu, N. D. Production of Fuel Bioadditive "Triacetin" Using a Phosphomolybdic-Acid-Loaded PVA Membrane in a Pervaporation Catalytic Membrane Reactor. *Energy Fuels* **2019**, 33, 2208−2218. https://doi.org/10.1021/acs.energyfuels.8b03344

Conclusions and Futuristic aspects

Overview of the chapter

The results discussed in Chapters three to six have been concluded, compared and correlated in this chapter. The future scope of work with the synthesized catalysts is also discussed.

7.1. Conclusions and correlations

In Chapter 3, sulphate incorporated siliceous zirconia heterogeneous acidic catalyst was synthesized and employed as a catalyst for the GL acetylation with acetic acid to yield 93 % triacetin within 40 min reaction duration as shown in **Table 7.1**. The heterogeneous acidic catalysts with Brønsted acidic sites was found to enhance the catalytic activity and stability. The regenerated catalyst was reused in six successive cycles while retaining 50 % triacetin selectivity in the last cycle.

In Chapter 4, sulphated silica-coated magnetic ($Fe_3O_4@SiO_2@SO_4^{2-}$) heterogeneous acidic catalyst was successfully synthesized and found to be active for the glycerol acetylation. The optimum values of the parameters to achieve 100 % triacetin selectivity with 100 % glycerol conversion were: catalyst amount of 5 wt% (concerning glycerol), acetic acid/glycerol molar ratio of 9:1 at 80 °C and 45 min reaction duration. The catalyst was reused for six consecutive reaction cycles; however, > 80 % TA selectivity was observed during the first three cycles.

In Chapter 5, niobium loaded magnetic (3-Nb@Fe_3O_4-700) catalyst was synthesized and employed for the glycerol acetylation with acetic acid to produce 92 % triacetin with 99 % glycerol conversion under optimized reaction parameters as shown in **Table 7.1**. The same catalyst was reused during seven catalytic cycles, with a reduction in the catalyst efficacy during the successive runs. The catalyst was found to be partially soluble in the reaction mixture, however, the dissolved catalyst was not found to enhance the conversion levels of the glycerol.

In Chapter 6, glycerol was esterified with acetic acid in the presence of $Ce/TiZrO_4@SO_4^{2-}$ heterogeneous acidic catalyst. Under the optimized reaction parameters highest diacetin selectivity (96 %) with 99 % of glycerol conversion level was obtained (**Table 7.1**). The same catalyst was reused during five catalytic cycles, however, the efficacy of the catalyst was found to reduce during the successive runs. The loss of sulphate species from the matrix was found to be the main reason behind the gradual loss of catalyst activity.

Table 7.1. The comparison of catalytic activity during glycerol acetylation with acetic acid.

Chapter	Catalyst	Acidic sites (mmol g^{-1})	TOF (h^{-1})	wt % (concerning GL)	AcA/GL (mol/mol)	Temp (^oC)	Time (h)	MA %	DA %	TA %	GL conversion %	Catalyst reusability (# of cycles)
3	SSZ	4.96	262	3.0	9:1	80	0.67	-	7.0	93.0	100	6
4	$SO_4^{2-}@SiO_2@Fe_3O_4$	8.63	458	5.0	6:1	80	0.6	-	-	100	100	6
5	$Nb@Fe_3O_4$	4.1	137	7.0	9:1	80	1.33	-	7.0	92	99	7
6	$Ce/TiZrO_4@SO_4^{2-}$	8.15	320	5.0	6:1	120	1.0	-	96	3	99	5

SSZ = $SO_4^{2-}/SiZrO_4$

Based on the comparison provided in **Table 7.1**, the maximum acidity, 8.63 mmol g^{-1}, was found for the $SO_4^{2-}@SiO_2@Fe_3O_4$ catalyst which could also be correlated with the highest catalyst activity based on TOF calculation. The presence of Brønsted acidic sites was found to impart the glycerol acetylation activity to the catalyst. Based on the proposed mechanism, stepwise acetylation of the glycerol –OH groups have been considered. The reaction might be initiated by the Brønsted acid-mediated acetic acid carbonyl group protonation, which reacts with the –OH of GL to form the ester group as discussed in Chapters 3 and 4. The catalyst, $Ce/TiZrO_4@SO_4^{2-}$, was found to demonstrate a maximum diacetin selectivity of 96 %, which is even higher than the purity of commercially available diacetin sample (50 %). On the other hand, the remaining three catalysts have demonstrated TA selectivity in the range of 92 -100 %.

7.2. Futuristic aspects

The work presented in the thesis demonstrated the development of the catalysts which could be utilized to produce the triacetin or diacetin molecules from glycerol in higher selectivity of 92-100%. However, similar selectivity levels for monoacetin could not be achieved in the presence of developed catalysts. Thus one of the futuristic aspects of the present study would be to develop a catalyst or establish the reaction parameters that could yield monoacetin molecule with higher selectivity (> 90 %) or as an exclusive product. The reusability study of the catalyst suggested the loss in catalyst activity upon its repeated use. Thus enhancement in catalyst stability would be another aspect to look for. The reactions were performed at the lab scale (few gram scale) during the present study. To demonstrate the commercial application of the developed catalysts, it is essential to scale up the reactions while performing the reaction in pilot plant set up.

Publications from thesis

Abida, K.; Ali, A. Sulphuric acid-functionalized siliceous zirconia as an efficient and reusable catalyst for the synthesis of glycerol triacetate. *Chem. Papers* **2020**, 74, 3627–3639. https://doi.org/10.1007/s11696-020-01189-z

Abida, K.; Chudasama, B.; Ali, A. Development and functionalization of magnetic nanoparticles as stable and reusable catalysts for triacetin synthesis†. *New J. Chem.***, 2020**, 44, 9365-9376. DOI: 10.1039/d0nj00488j

Other Publications

Kumar, S.; Thakur, N.; Abida, K.; Kumar, A.; Gupta, R. K.; Ali, A. Transesterification of triglyceride over Ni impregnated Zn/CaO nanocatalysts. *Mater. Today: Proc.* **2021**, 36(3), A1-A8. https://doi.org/10.1016/j.matpr.2020.03.215

Katiyar. M.; Abida, K.; Ali, A. Candida rugosa lipase immobilization over SBA-15 to prepare solid biocatalyst for cotton seed oil transesterification. *Mater. Today: Proc.* **2021**, 36(3), 763-768. https://doi.org/10.1016/j.matpr.2020.06.061

Kaur, A.; Bhardwaj, N.; Kaur, A.; Abida, K.; Nagaraja, T. P.; Ali, A.; Prakash, R. Proton Nuclear Magnetic Resonance-Based Method for the quantification of Epoxidized Methyl Oleate. *J. Am. Oil. Chem. Soc*. **2021**, 98: 139–147. DOI 10.1002/aocs.12439

Kumar, D.; Abida, K.; Ali, A. Aminolysis of triglycerides using nanocrystalline nickel doped CaO as an efficient solid catalyst†, RSC Adv., 2016, 6, 66822-66832. DOI: 10.1039/c6ra12114d

Manuscript under review

Abida, K.; Jindal, R.; Ali, A. Glycerol esterification for triacetin production using $Fe_3O_4@SiO_2@PO_4^{3-}$ as heterogeneous magnetic catalyst (Environmental Science and Pollution Research)

Abida, K.; Ali, A. A review on catalytic role of heterogeneous acidic catalysts during glycerol acetylation to yield acetins (Industrial & Engineering Chemistry Research)

Manuscripts under preparation

Abida, K.; Ali, A. ^{1}H NMR assisted quantification of triacetin in the mixture of tri-, di-, mono-acetin and glycerol.

Abida, K.; Kaur, A.; Ali, A. A review on different routes of glycerol carbonate production utilizing waste crude glycerol derived as a by-product of biodiesel production

Patent (in process)

Abida, K.; Ali, A. Development of acidic heterogeneous catalyst for diacetin synthesis from glycerol

Conferences, Seminar and Workshop

Abida, K; Jinda, R; Ali, A. *Glycerol esterification for triacetin production using* $Fe_3O_4@SiO_2@PO_4^{3-}$ *as heterogeneous magnetic catalyst*, International Chemical Engineering Conference 2021-100 Glorious Years of Chemical Engineering & Technology, organized by Department of Chemical Engineering, Dr. B. R. Ambedkar National Institute of Technology, Jalandhar (India). ***(Award for Best Paper)***

Participate in Indo-US Webinar and Lecture Series during June 1-9, **2021** under the aegis of SPARC Scheme of Ministry of Education, Govt. of India organized by the Department of Chemistry, Jamia Millia Islamia, New Delhi.

Abida, K.; Ali, *A. Acetylation of Glycerol to produced Triacetin from Sulfated Magnetic catalyst: Reusability and Catalyst Stability Studies*, 24th International Conference of International Academy of Physical Sciences (CONIAPS XXIV), **2019**, organized by Chaudhry Charan Singh University, Meerut (UP).

Abida, K.; Ali, A. *Phosphate Incorporated* $Fe_3O_4@SiO_2$ *Magnetic Nanoparticles for the Production of Triacetin*, National Conference on Advanced Functional Materials (NCAFM), **2019**, organized by Department of Chemistry, Jamia Millia Islamia, New Delhi**.** ***(Award for Best Poster)***

Abida, K.; Ali, A. *Mixed Metal Oxides as heterogeneous catalysts for the triacetin synthesis*, "10th National Conference on Chemical and Environmental Sciences: Innovations and Advances-2018, CES: IA-**2018**, organized by Panjabi University, Patiala, Punjab.

Abida, K.; Ali, A. *Production of triacetin via Acetic acid by Esterification of Glycerol in Presence of Heterogeneous Sulphated Catalyst*, 10th National Conference on Achievements of Women in Science and Technology: Current Scenario and Future Prospects-**2017**, organized by Panjab University Chandigarh, Punjab.

Abida, K.; Ali, A. *Sulphate and Cerium impregnated* Ti/ZrO_2 *as heterogeneous catalyst for glycerol esterification*. National Seminar on New Paradigm in Chemical Sciences: Synthetic and Analytical Perspectives-**2016**, organized by Panjabi University, Patiala, Punjab.

Participate in National Seminar on Society of Chemists for the Promotion of Research and Education-2016, organized by Thapar University, Patiala, Punjab.

Participate in National Workshop on X-ray Powder Diffraction, Dynamic Light Scattering, Scanning- and Transmission Electron Microscopies (NXDST) **2016**, organized by Panjab University, Chandigarh, Punjab.

Abida, K.; Ali. A. *Esterification of glycerol using Sulphate and Cerium impregnated* Ti/SiO_2 *as heterogeneous catalyst*, International Conference on Frontiers at the Chemistry-Allied Sciences Interface- **2016**, organized by University of Rajasthan, Jaipur.

Kaur, A.; Abida, K.; Ali. A. *Sodium Impregnated Zirconia as a Solid Base Catalyst for the Transesterification of Waste Cotton Seed Oil*, National Seminar on Synergistic Aspects of Chemical and Other Sciences-**2015**, organized by Panjabi University, Patiala, Punjab.

Participate in National Seminar on Society of Chemists for the Promotion of Research and Education-**2015**, organized by Thapar University, Patiala.

Participate in National workshop on Advance Materials and Characterization Techniques-**2015** organized by N. I. T. University, Jalandhar, Punjab.

Participate in National Workshop on advance techniques for surface characterization-**2015** organized by Thapar University, Patiala, Punjab.